FRANCE - JAPAN COOPERATION ON GEOLOGICAL HAZARDS

GeoHazards –2004 Workshop

東海大学
Tokai University

Shizuoka University
静岡大学

Shizuoka Prefecture

MEXT

静岡新聞
SBS

Liberté • Égalité • Fraternité
RÉPUBLIQUE FRANÇAISE
Ambassade de France au Japon
在日フランス大使館

CNRS
CENTRE NATIONAL DE LA RECHERCHE SCIENTIFIQUE

ministère éducation nationale enseignement supérieur recherche

cnes
CENTRE NATIONAL D'ETUDES SPATIALES

Seismology, Volcanology, Geomorphology and Hydrogeology

December 1 - 4 , 2004
Shizuoka, Japan

ABSTRACTS

February 28, 1873 earthquake in Guadeloupe

Supporting Organizations

Japan

TOKAI UNIVERSITY

SHIZUOKA UNIVERSITY

MINISTRY OF EDUCATION, CULTURE, SPORTS, SCIENCE AND TECHNOLOGY (MEXT)

PREFECTORAL GOVERNMENT OF SHIZUOKA

INOUE FOUNDATION FOR SCIENCE

SHIZUOKA SHIMBUN AND SHIZUOKA BROADCASTING SYSTEM

France

FRENCH MINISTRY OF FOREIGN AFFAIRS, SERVICE FOR SCIENCE AND TECHNOLOGY, EMBASSY OF FRANCE IN JAPAN (MAE)

FRENCH NATIONAL CENTER FOR SCIENTIFIC RESEARCH (CNRS)

FRENCH MINISTRY OF EDUCATION AND RESEARCH (MENESR)

NATIONAL CENTER FOR SPATIAL RESEARCHES (CNES)

GeoHazards 2004

Japan is a country which suffers many different types of geological risks. Earthquakes, volcanic eruptions, floods and landslides belong to the daily life of the Japanese population. As example Kobe Earthquake which killed 6432 people in 1995 is still fresh in our memory. Furthermore, an extensive avalanche hit Minamata city in Kyushu Island in 2003.

Geological hazards are also real in France. Some active and dangerous volcanoes are located on the French territory; Mount Pelée in Martinique island killed about 30,000 inhabitants in 1902 while about 50,000 people were evacuated for several months from Soufrière of Guadeloupe during the 1976-1977 volcanic crisis. Medium seismicity occurs too in France, mainly in the South-East, South-West and East regions. And the number of floods and landslides has significantly increased over the last years.

Geological hazards are thus a common important issue both in France and Japan.

Research activities on these topics are very powerful in Japan and in France as well, and many laboratories and teams are considered as outstanding level institutions in these domains.

In natural hazards bilateral cooperation has been set in the past between several laboratories and teams. These collaborations have given an advanced knowledge about the genesis of these hazards and the way to monitor and mitigate them.

GeoHazards 2004 will be a multi-disciplinary forum on the issues of geological hazards from which new developments will be set up.

Both young and senior scientists will be involved in the workshop in order to enhance already existing cooperation and impulse new common researches.

About forty scientists from Japan and France will contribute to this workshop.

The workshop will be held in Shizuoka prefecture, located at the foot of Mount Fuji, between the 1st and the 4th of December 2004.

CONTENT

French Organizing Committee

Organizing committee

John LUDDEN, Directeur Adjoint
Département des Sciences de la Terre et de l'Univers ; CNRS
Email : john.ludden@cnrs-dir.fr
Tel : 33- 6 75 51 80 61

Professeur Laurent DEVER
Laboratoire de géochimie et d'hydrologie isotopique
Université Paris-Sud
Mission Scientifique, Technique et Pédagogique
Ministère de la Jeunesse, de l'Education Nationale et de la Recherche
Email : laurent.dever@recherche.gouv.fr
Tel : 33- 1 55 55 89 11

Serge HAGEGE
Attaché scientifique,
Service pour la Science et la Technologie
Ambassade de France au Japon
Email : spi@mc.rosenet.ne.jp
Tel : 81- 3 5420 88 82

Professeur Robert FARHI
Attaché scientifique,
Service pour la Science et la Technologie
Ambassade de France au Japon
Email : farhi@ma.rosenet.ne.jp

Dr Jacques ZLOTNICKI
Laboratoire Magmas et Volcans (CNRS OPGC-UMR 6524)
et Université Blaise Pascal, Clermont-Ferrand, France
Email: jacques.zlotnicki@opgc.univ-bpclermont.fr
Tel : 33- 4 73 40 73 70 // 33- 6 08 77 91 08; Fax : 33- 4 73 40 78 85

Olivier GEORGEL
Volontaire International
Service pour la Science et la Technologie
Ambassade de France au Japon
Email: olivier.georgel@diplomatie.gouv.fr

General secretary

Dr Jacques ZLOTNICKI
Laboratoire Magmas et Volcans (CNRS OPGC-UMR 6524)
et Université Blaise Pascal, Clermont-Ferrand

JAPANESE ORGANIZING COMMITTEE

President :

Professor Seiya UYEDA
Professor of Tokai University, Professor emeritus of Tokyo University,
Member of the Japan Academy, Foreign members of Russian Academy of Science and Greece Academy of Science
Email : suyeda@st.rim.or.jp

General secretary:

Professor Toshiyasu NAGAO
Director, Earthquake Prediction Research Center,
Institute of Oceanic Research and Development
Tokai University
Email : nagao@scc.u-tokai.ac.jp
Tel : 81-543 36 28 62
Fax : 81- 543 36 0920

Organizing committee

Keizo Sayanagi
Associate Professor, Tokai University
Institute of Oceanic Research & Development

Prof. Mikio Satomura
Faculty of Science, Shizuoka University

Prof. Satoshi Tsuchiya
Faculty of Agriculture, Shizuoka University

Prof. Masato Koyama
Faculty of Education, Shizuoka University

Prof. Masahiro Chigira
Disaster Prevention Research Institute, Kyoto University

Dr. Masashi Kamogawa
Assistant Professor, Tokyo Gakugei University

Dr. Naoji Koizumi
Tectono-Hydrology Research Group (Group Leader)
National Institute of Advanced Industrial Science and Technology (AIST)

Prof. Yoichi SASAI
Disaster Prevention Specialist (Chief)
The Disaster Prevention Division, Tokyo Metropolitan Government

FIELD TRIP

Izu peninsula and Shizuoka prefecture are among the most active seismic regions in Japan, with a subduction zone of 10 km depth compared with the 40 km depth around Tokyo area.

The Tokai region, which includes Shizuoka prefecture, is one of the most sensitive areas in Japan as far as geological survey and seismic hazards are concerned.

The excursion at Mount Fuji, close to the conference center, will allow participants to discover the beauty of the region and the volcanic activity.

Schedule:

1) Shizuoka Prefectural Earthquake Preparedness Education Center
http://www.e-quakes.pref.shizuoka.jp/english/index.htm

2) Typical land slide site on the way to Mount Fuji (Yui District)

3) Mount Fuji and its vicinity

4) Tanna Fault (which moved in 1930 earthquake with M7.3)

5) Hakone Volcano (Ohwaku-dani)
http://volcano.und.nodak.edu/vwdocs/volc_images/north_asia/hakone.html

6) Kanagawa Prefectural Museum of Natural History
http://nh.kanagawa-museum.jp/info/indexen.html

GeoHazards 2004

Scientific programme

Wed. 1st , December		**Session**	**Talk**	**Title**
AM	9h30-10h00	**Opening Ceremony**		
	10h00-10h30	**Session 1 Seismology**	Keynote 1 Megumi MIZOUE	Mitigating and Responding to the Tokai Earthquake
	10h30-11h00		Keynote 2 Pascale ULTRE-GUERARD	Current and future CNES space missions relevant to geohazards
	11h00-11h30	Pause		
	11h30-12h00		Keynote 3 Kimiro MEGURO	Lessons learned from recent earthquakes and efficient countermeasures for earthquake disaster reduction
	12h00-12h30		Keynote 4 Pierre HENRY	Deformation processes and earthquakes in Nankai
	12h30-14h00	Lunch		
PM	14h00-14h25		Talk 5 Philippe LOGNONNE	Detection and modeling of ionospheric signals associated to seismic surface waves and tsunamis
	14h25-14h50		Talk 6 Toshiyasu NAGAO	The new view of the short-term earthquake prediction research by using electromagnetic methods
	14h50-15h15		Talk 7 Michel PARROT	The micro-satellite Demeter
	15h15-15h40		Talk 8 Yoshiko YAMANAKA	Asperity map along the subduction zone in northeastern Japan inferred from regional seismic data
	15h40-16h10	Pause		
	16h10-16h35		Talk 9 Christophe VOISIN	Seismic risk: from earthquake physics to social seismology
	16h35-17h00		Talk 10 Naoji KOIZUMI	Strategical roles of hydrological methods in earthquake prediction research
	17h00-17h25		Talk 11 Bertrand MEYER	Active faulting and earthquake hazard in the Marmara sea region

Thur. 2 , December		Session	Talk	Title
AM	09h45-10h15	**Session 2 Volcanology**	Keynote 1 Hidefumi WATANABE	Recent major two volcanic activities in Japan. Mount Usu and Miyake eruptions in 2000
	10h15-10h45		Keynote 2 Georges BOUDON	The French volcanic observatories and the volcano monitoring
	10h45-11h15	Pause		
	11h15-11h40		Talk 3 Kazuhiro ISHIHARA	Living with an active volcano, Sakurajima, Japan
	11h40-12h05		Talk 4 Philippe JOUSSET	Volcanic risk assessment and geophysical information: examples from Indonesia, Japan, Montserrat and Cameroun
	12h05-12h30		Talk 5 Hiromu OKADA	Comparative study on scientists' hazard mitigation efforts before, during and after the 4 eruptive episodes of Mt. Usu in the 20th century
	12h30-14h00	Lunch		
PM	14h00-14h25		Talk 6 Christophe DELACOURT	Remote sensing techniques for multiscale surface displacement mapping
	14h25-14h50		Talk 7 Masato KOYAMA	Hazard map of Fuji Volcano: how did we make and how should we use it?
	14h50-15h15		Talk 8 Jacques ZLOTNICKI	How electromagnetic phenomena can contribute to mitigate the volcanic risk?
	15h15-15h40		Talk 9 Yoichi SASAI	The use of volcanic hazard information by Tokyo Metropolitan Government
	15h40-16h10	Pause		
	16h10-16h40	**Sesion 3 Geomorphology**	Keynote 1 Haruo YAMAZAKI	Reconstruction of recent behavior of active faults in the plate convergence zone, central Japan: Application of the off-fault paleoseismology to estimate the recurrence interval and the last event age
	16h40-17h10		Keynote 2 Stéphane GARAMBOIS	Ground Penetrating Radar measurements and developments for fracture imaging and characterization in limestone cliffs
	17h10-17h40		Keynote 3 Masahiro CHIGIRA	Shallow landslide mechanism and its susceptibility evaluation from geological view point
	19h30-21h30	Party		

Fri. 3, December		Session	Talk	
AM	9h30-10h00	**Session 3 Geomorphology**	Keynote 4 Yves GUGLIELMI	Multi-scale rock slope failure mechanisms: An attempt to generalize results from multi-parametric field and modeling studies conducted on the Upper-Tinee valley (French Alps) over the past 10 years.
	10h00-10h30		Keynote 5 Satoshi TSUCHIYA	Some large-scale earthquake induced landslides and debris transport in Shizuoka prefecture, Japan
	10h30-11h00		Keynote 6 Olivier MAQUAIRE	Long-term behaviour and assessment of the hazard associated to slow-moving earth flows in clay-shales
	11h00-11h30	Pause		
	11h30-12h00	**Session 4 Hydrology**	Keynote 1 Kaoru TAKARA	Hydrological modelling and forecasting -application of geospatial information systems
	12h00-12h30		Keynote 2 Laurent DEVER	Isotopic groundwater dating as indicators of the change of groundwater environment : examples under natural and anthropogenic conditions
	12h30-14h00	Lunch		
PM	14h00-14h30		Keynote 3 Tomochika TOKUNAGA	Evolution of human-induced "natural hazards" in urban geosphere due to the change of groundwater environment -an example from Tokyo Metropolitan Area
	14h30-15h00		Keynote 4 Marine RIFFARD	Cemagref's flood forecasting methodologies in the french flood alert system
	15h00-15h25		Talk 5 Mio TAKEUCHI	Groundwater pollution and role of organisms
	15h25-15h50		Talk 6 Daizo TSUTSUMI	Preferential flow through fractures in weathered bedrock and slope stability: Numerical modeling
	15h50-16h20	Pause		
	16h20-17h20	**Round table**		
	17h20-17h30	**Closing Ceremony**		
	18h30		Outreach program	

Sat. 4, December			
		Field excursion	

SEISMOLOGY

Mitigating and Responding to the Tokai Earthquake

Megumi Mizoue(1), Noriko Kamaya (2) and Hidemi Ito (2)

(1) Professor Emeritus, the University of Tokyo amd Chair of the Earthquake Assessment Committee,
(2) Japan Meteorological Agency

ABSTRACT

In the region where the Philippine Sea Plate is subducting beneath the Eurasian Plate along the Suruga and Nankai troughs, large-scale inter-plate earthquakes have repeatedly occurred periodically with an interval of 100 – 150 years. Approximately 150 years have elapsed since the previous earthquake in the Tokai region along the Suruga trough. In addition to the historical evidence, the recent precise multi-parameter measurements, mainly by seismometer, strainmeter and GPS network system, have clarified several anomalous changes attributable to a weakening of a mechanical coupling of the plate boundary. Thus, the possibility of a large-scale earthquake occurring near future is considered to be getting higher. This is what we refer to as "the Tokai Earthquake".

Continuous Monitoring System

A comprehensive, continuous and real-time monitoring system has been operated in the Tokai region. The monitoring is available for the detection of the anomalous small signals caused by the pre-slip on the plate boundary along the limited portion of the fault of the Tokai earthquake. Based on the experimental, theoretical and observational research and examinations of the dynamical behavior of plate boundary, the pre-slip movement will be accelerated and eventually resulted in a catastrophic failure along the entire fault plane of the Tokai earthquake. Borehole type strainmeter network is available for the most sensitive and reliable instrument for the detection of the pre-slip on the possible earliest stage just before the Tokai earthquake occurs.

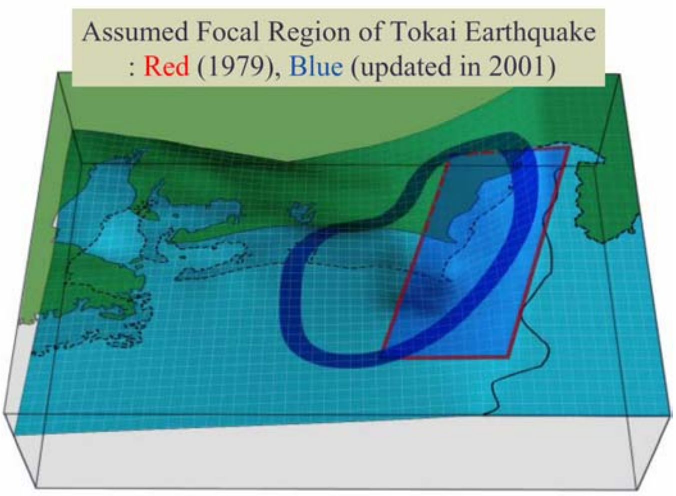

Warning Information System

Judging from the continuous real-time base observations, any anomalous signals detected by borehole type strainmeter are immediately analyzed to test whether the signals indicate any possibility with pre-slip origination. Depending on the numbers of the anomalous strainmeter data and their physical evidence in relation to the imminence of the Tokai earthquake, JMA issues the information of the pre-slip observation and sends messages with the three step timings.

When the anomaly is observed at one, two and three stations stepwise way, "Tokai Earthquake Report", "Tokai Earthquake Advisory" and "Tokai Earthquake Warning" are issued by JMA. In the case of "Tokai Earthquake Warning", Director-General of JMA sends the message urgently to Prime Minister asking the declaration of "Warning Statement", which automatically linked the establishment of Government Headquarters for Earthquake Disaster Prevention.

Earthquake Disaster Management Measures

The monitoring system for the Tokai Earthquake has been prepared and any small or local anomalous signals are carefully watched with 24 hours system. The monitoring system is conducted with real-time processing of the observation data which is believed to be effective for detecting the pre-slip signals about 24 hours before the Tokai earthquake occurs.

Futhremore, in areas subject to intensified measures against earthquake disasters (263 municipalities, 8 prefectures), as designated under the Large-Scale Earthquake Countermeasures Special Act established in June 1978. The preparation of evacuation site, evacuation routes, firefighting pumps, wells for fighting fires and other equipment falls under special stipulations in the tax system based on the Special Measures for National Finance Concerning Urgent Earthquake Measure Improvement for Areas Requiring Intensified Measurement to Prevent Earthquake Disasters, enacted in May 1980.

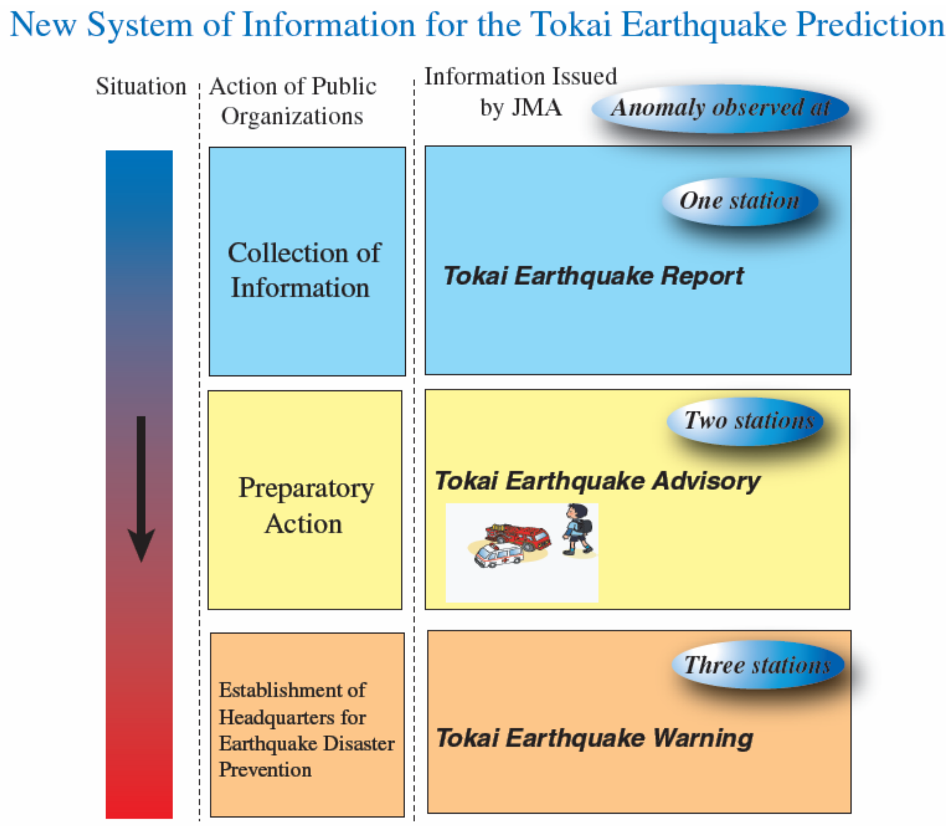

Megumi Mizoue
C/O Seismological and Volcanological Department,
Japan Meteorological Agency
Otemachi 1-3-4, Chiyoda-ku, Tokyo 100-8122, JAPAN

Current and Future Space Missions Relevant to Geohazards

Pascale Ultré-Guérard [(1)]

(1) CNES: French Space Agency, Paris

ABSTRACT

The Cnes Earth Observation Program relevant to geohazards is presented. This presentation includes operational programs: Earth observing satellites SPOT, radar satellites of ESA, future plans with the ORFEO program and also initiatives like the International Charter "Space and Major Disasters" and like the GMES and GEOSS process; it also includes research missions like DEMETER and future plans which could be of potential interest for geohazards studies.

KEYWORDS: space program, remote sensing, geohazards, volcanology, seismology

INTRODUCTION

The Cnes (and, to some extent, ESA) Earth Observation Program relevant to geohazards is presented. The presentation separates operational programs and research programs because their decision process and their implementation logic are not exactly the same. However, notice that the research community uses all these data indifferently.

OPERATIONAL PROGRAMS

The SPOT Program

For operational programs, Cnes has a long tradition in optical Earth observation missions with the SPOT series: SPOT 1 launched in 1986 to SPOT 5 (Figure 1) launched in 2002. SPOT 3 is no more operating and SPOT 1 has been put on a lower orbit in order to respect the new rules of cleaning space after use! SPOT 5, the most recent satellite of the series, has a resolution of 5 m in panchromatic mode, 10 m in spectral mode and 2,5 m in panchromatic mode through processing. It is also equipped with the High-Resolution Stereoscopic camera which allows to get precise DEM (~5m in Z). SPOT5 is then an interesting tool for the geohazard studies. Two initiatives ISIS & OASIS (founded by EU/FP6) give access to the SPOT data at a lower cost for the European scientific community.

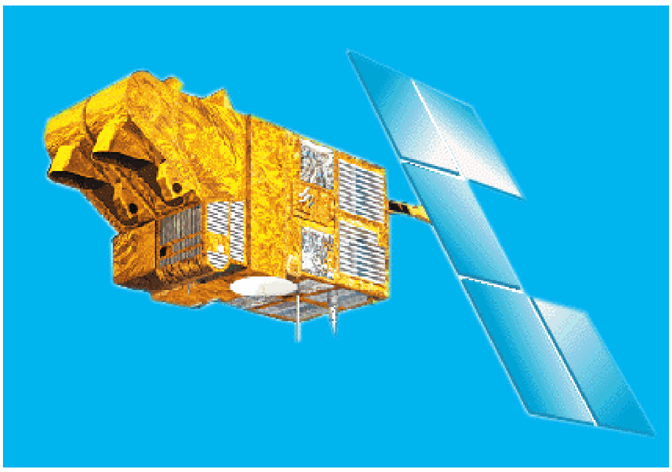

Figure 1. The SPOT 5 Satellite (artist view).

Radar Program

Concerning the radar observing capability, ESA has launched a series of satellites equipped (among other instruments) with C band SAR: ERS 1&2 and Envisat. An innovative method of data analysis, the SAR interferometry, has been developed by scientists and proven to be very useful to study the Earth surface displacement with a very high precision: a few cms in the direction of the satellite. This method is particularly used to study the surface deformation associated to earthquakes, volcanic eruptions, landslides, subsidences…

International Charter "Space and Major Disasters"

Following the UNISPACE III conference held in Vienna, Austria in July 1999, the European and French space agencies (ESA and CNES) initiated the International Charter "Space and Major Disasters", with the Canadian Space Agency (CSA) signing the Charter on October 20, 2000. In September of 2001, the National Oceanic and Atmospheric Administration (NOAA) and the Indian Space Research Organization (ISRO) also became members of the Charter. The Argentine Space Agency (CONAE) became a member in July 2003. JAXA intends to join the Charter after the launch of ALOS (2005). The International Charter aims at providing a unified system of space data acquisition and delivery to those affected by natural or man-made disasters through authorized users. Each member agency has committed resources to support the provisions of the Charter and thus is helping to mitigate the effects of disasters on human life and property. The International Charter was declared formally operational on November 1, 2000. An authorized user can now call a single number to request the mobilization of the space and associated ground resources (RADARSAT, ERS, SPOT, ENVISAT, IRS, SAC-C, NOAA…) of the agencies to obtain data and information on a disaster occurrence. A 24-hour on-duty operator receives the call, checks the identity of the requestor and verifies that the User Request form sent by the Authorized User is correctly filled up. The operator passes the information to an emergency on-call officer who analyzes the request and the scope of the disaster with the User, and prepares an archive and acquisition plan using available space resources. Data acquisition and delivery takes place on an emergency basis, and a project manager, who is qualified in data ordering, handling and application, assists the user throughout the process. Since its implementation, the International Charter was triggered 61 times over a period of 47 months as of September 30, 2004: for flooding, earthquakes, forest fires, volcanic eruptions, oil spills, hurricanes, landslides, hazardous material. CNES has also established a protocol with French scientists in order to make them involved as experts when the Charter is triggered for geohazards and when Cnes is involved (CIEST). Two examples of what has been done are shown: for the Niyragongo eruption in 2002 and the Bam earthquake in 2003.

Future plans

For the future, the ORFEO program, which is a cooperation between Cnes Pléiades project and ASI (Italian Space Agency) Cosmo-Skymed project, will also play an important role for the survey of geohazards and for the disaster management. The Pléiades system is composed with two satellites with high-resolution optical capability (1m, swath 20km) and is due to be launched in 2008-2009. The Cosmo-Skymed system is composed with four satellites equipped with X band radar and is due to be launched from 2005. In order to prepare the programmation of the system and the data utilization, an ORFEO preparatory program has been implemented. It consists in different thematic groups (Sea and coastal area, Risks, Cartography, Geology, Hydrology, forest, agriculture and defense) in charge of the definition of their needs. For instance, the survey of the most dangerous volcanoes of the world, which was the objective of a previous European project called Space Volcano Observatory, will be now included in the ORFEO Program.

Other systems like high spatial resolution (~10m) geostationary observation systems are also under study and could be essential in the disaster prevention and management in the future.

Two new components are now part of the landscape and will play a very important role in the future: the GEOSS (Global Earth Observation System of systems) program which is a worldwide initiative for the coordination of Earth Observing systems and the European program GMES (Global Monitoring for Environment and Security) which can be seen as the European contribution to GEOSS. GMES is a joint EU (European Union) and ESA initiative. The first step of GMES is the preparation of service elements (including space and ground infrastructures and the value-added products) and is financed by the FP6 and by the Earth Watch program of ESA. Risk management is one of the priorities of GMES. ESA has proposed to study 6 satellites « sentinels » in order to insure the continuity of observation and to guaranty the services in the following domains: SAR, superspectral imagery, ocean survey (altimetry and ocean color), geostationary survey of atmosphere chemical and pollution, low orbit survey of air composition. The next step will be the operational implementation of the services, which will have proven to be useful and mature.

RESEARCH MISSIONS

The DEMETER mission

In the category of research missions, Cnes has developed and launched the Demeter microsatellite (Figure 2). Demeter is devoted to the study of electromagnetic emissions associated to geodynamic events at the Earth surface (over land: earthquake, volcanic eruption and over ocean: tsunamis) and to the human activity. There are also some technological experiments on board Demeter.

Figure 2. The DEMETER satellite (artist view).© CNES November 2003, ill. D. Ducros

A Scientific Advisory Committee has selected Demeter in 1998. It is the first mission of the Cnes Myriad microsatellite series; the next missions are Parasol to study the Earth radiation budget, Microscope to test the equivalence principia. Demeter has been developed in 5 years. A lot of attention has been paid to the magnetic cleanness of the satellite (see M. Parrot paper). It has been launched the 29th of June 2004 by a DNEPR rocket from Baïkonour. The booms have been deployed and the instruments have been turned on nominally during the first days. The satellite commissioning has been performed in one month. Apart some small technical problems, Demeter is doing well and the instruments have the expected behavior. An International Call for Research Proposal has been released by Cnes end of 2003 in order to have a Demeter International Science Team. Three categories of users have been identified: Category 0 is for the Demeter Experimenters, Category 1 is for the guest investigators who have other data to propose which can be of interest for Demeter (data comparison or assimilation) and Category 2 is for other scientists who have interesting research projects with Demeter data. 37 proposals or letters of interest have been submitted from various countries. An ad hoc group of experts have assessed the proposals: 15 proposals have been selected for category 1, 14 for category 2 and 8 have been rejected because they were not acceptable. The rules for Category 1 of users are reminded. The guest investigators have to:
- Participate to the validation of Demeter data by providing other data or information (ground based experiments, TEC, numerical models…);
- Make these data or information available for the Category 1 group of users;
- Keep the main Investigators of Demeter informed of their work and publication of results.

In order to limit the quantity of data, all the Demeter data users have to select their data with attention (by instruments, events…). More information can be found at: http://demeter.cnrs-orleans.fr.

Cnes also supports other scientific activities related to Demeter: EM ground based stations have been installed in the Corinth Gulf and on the Piton de la Fournaise volcano, Island Reunion and can be used to compare space and ground data in case of seismic or volcanic events (leader OPGC). Dense networks of GPS stations over California and Japan are used to model the TEC (Total Electron Content) and study co-seismic effects in the ionosphere in order to complete the Demeter approach (leader IPGP).

Future plans

For the future, Cnes have studied an innovative and interesting concept: the Interferometric Cartwheel. The Interferometric Cartwheel is a formation flight of 3 microsatellites flying in the vicinity of a radar satellite, L or C band nominally (Figure 3). These microsatellites are equipped with receiving antennae and are moving along an ellipse. The vertical and horizontal baselines between two microsatellites can be used for interferometry and the potential products are the topography or the horizontal displacement (for instance sea currents). A phase A has been performed and has demonstrated the feasibility of the project. But due to the high cost of this project, the hard competition between projects and some open questions that are related to the physics of the measure, Cnes has decided to mandate a Working Group on DEM before to go further with the Interferometric Cartwheel. This working group is in charge to analyze what exits (techniques, images, data, and tools) and what is really needed in terms of DEM.

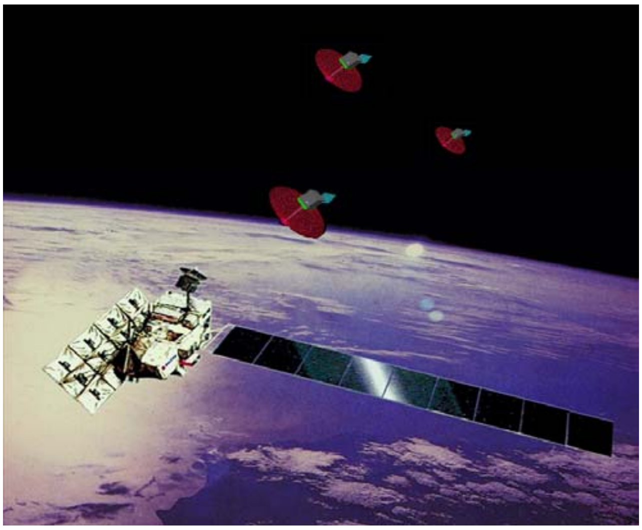

Figure 3. The interferometric cartwheel (artist view) represented with the Japanese ALOS satellite (this scenario has been studied by Cnes and Nasda before the interruption of the IC project).

CONCLUSION

The space systems are already highly involved in the geohazards study. But this activity is always evolving: the system and the techniques improve gradually and so does the data analysis. Some emergent research fields with high potential returns for geohazards understandings and prevention could or should benefit of this progress. For instance, the interest of GPS, and the future European system Galileo, for tectonics and seismic studies is proven and still under progress; the potential of radar interferometry to understand the inter-seismic cycle has to be further examined; the interest of Demeter-like missions has to be estimated… For the future, new dedicated systems have to be invented. Some emergent ideas like doing seismology from space could be of high interest for the Earth science and geohazards communities…

Pascale Ultré-Guérard
CNES (French Space Agency)
2 Place Maurice Quentin
75039 PARIS Cedex 01
FRANCE, email: pascale.ultre-guerard@cnes.fr

Lessons Learned from Recent Earthquakes and Efficient Countermeasures for Earthquake Disaster Reduction

*Kimiro Meguro

International Center for Urban Safety Engineering, Industrial Science, The University of Tokyo

ABSTRACT

Japan is an earthquake-prone country and it is currently facing a period of high seismic activity. Within the coming 30 to 40 years, several huge earthquakes with a magnitude 8 or higher will strike major parts of Japan. Including magnitude 7 class events, such as the 1995 Kobe earthquake, which will happen before and after these huge earthquakes, the number of disastrous earthquakes increases several times. The total losses estimated will be over 300 trillion yen, which is 60% of the Japanese Gross Domestic Product.

No matter how many excellent non-structural measures, such as a quick response and rescue system, and recovery and reconstruction strategy, are implemented, if we do not ensure that the structures will survive, we can not reduce the number of victims. This becomes an essential cause of various problems appearing after the quake. In the case of the Kobe earthquake, 92 % of the victims in Kobe city were killed within the first 15 minutes, and 95 % were affected by structural damage. In spite of this, the number of retrofitted wooden houses, the most seismically vulnerable, is still very limited.

The retrofitting cost for one house is equivalent to that of a very simple car. Retrofitting our houses is more a matter of decision than a matter of money. If we plan the retrofitting work together with other restoration of the house, the cost will be drastically decreased. Why don't we use this opportunity to reduce the probability that our loved ones will die and that our important possessions will be lost during an earthquake? We are not yet aware of the urgency and necessity of retrofitting our houses.

In order to become more earthquake disaster conscious, we should develop our thinking about disaster. What will happen and how life will be affected when a big earthquake strikes? With this developed capability, we can understand the gaps between the current and ideal situations and then take steps to prevent and reduce the damage or react better during the disaster.

In this paper, I will introduce some methods and systems to promote retrofitting low earthquake resistant houses and to increase disaster imagination capability to decrease earthquake disaster in future.

KEYWORDS: earthquake, disaster reduction, retrofitting, imagination

1. INTRODUCTION

Earthquakes are caused by sudden fault motion. It has long been known that the global distribution of earthquakes is far from uniform, as shown in Fig. 1. While mid-oceanic ridges are characterized by linear distribution of relatively small earthquakes, large earthquakes occur mainly in the circum-Pacific belt and in the wide zone between Eurasia and the southern continents. The reason why they are distributed in this manner is explained by plate tectonics (e. g., [1]); large earthquakes occur due to plate interactions at convergent and transform plate boundaries. Convergent plate boundaries consist of subduction and collision zones. Statistical properties of earthquake occurrences in these seismic zones are well-known thanks to many decades of seismic observations around the globe, and many seismic hazard maps have been compiled both globally and regionally (e. g., [2]).

Plate tectonics has shown with reasonable certainty that plate motions have been essentially steady for the time-scales of a few millions of years, although they have changed over much longer time scales during the earth's history (e.g., [3]; [4]). However, the seismicity of the globe also displays variation on finer time-scales of tens of years, as shown in the upper panel of Fig. 2. The detailed mechanisms for these short-term secular changes are not clear, but it seems plausible that there can be fluctuations even under steady global plate motions. It seems significant that the variations in the loss of life shown in the lower panel of Fig. 2 are very different from variations of seismicity. The reason for this is quite clear. Earthquakes in densely populated regions cause greater disasters ([5]). For instance, the two largest giant earthquakes, the 1960 M9.5 Chilean and 1964 M9.2 Alaskan earthquakes, caused much less loss of life compared to the much smaller 1923 M7.9 Kanto and 1976 M7.8 Tangshan earthquakes. (Hereafter, M stands for the magnitude of an earthquake).

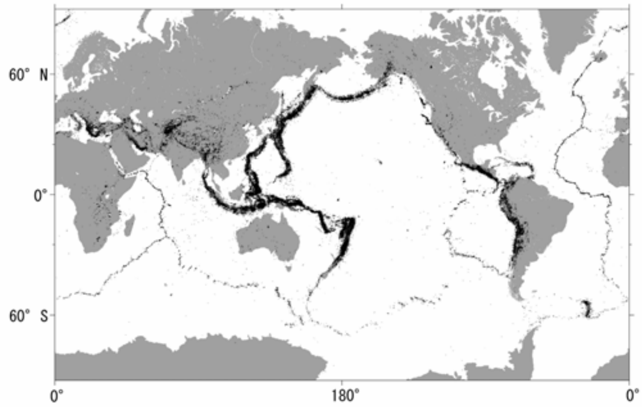

Figure 1. Epicenter distribution of the world for magnitude greater than 4.0 in 1980-2000, after USGS PDE.

Here we review briefly the state of the art on seismic hazard and present personal views on the priority items related to earthquake hazard mitigation. Specific matters taken up in the text are focused on Japan. However, it is anticipated that what we present will be generally applicable to all earthquake-prone regions of the world.

As well as loss of life, earthquakes cause disasters of all kinds. In terms of monetary loss, this can amount to a substantial fraction of the Gross Domestic Product (GDP) of a nation. For the 1995 Kobe earthquake, monetary loss was estimated at 10 billion US dollars and for the Tonankai-Nankai event, which is a major anticipated future earthquake, it may amount to at least 80 billion US dollars, which would be more than 15% of the GDP according to the Central Disaster Management Council of Japan. Since buildings in Japan are now more seismic resistant than in the past, loss of life in large cities may be less than those in the past. However, huge damage of complicated life-lines and infra-structures can still be expected in modern mega-cities when they are hit by major quakes. Further many mega-cities in the developing world do not have good adherence to building codes and so there can be huge loss of life as illustrated by the 2004 Bam earthquake in Iran. Seismic risk rapidly escalates with population growth and the disasters come when the last experience is "forgotten".

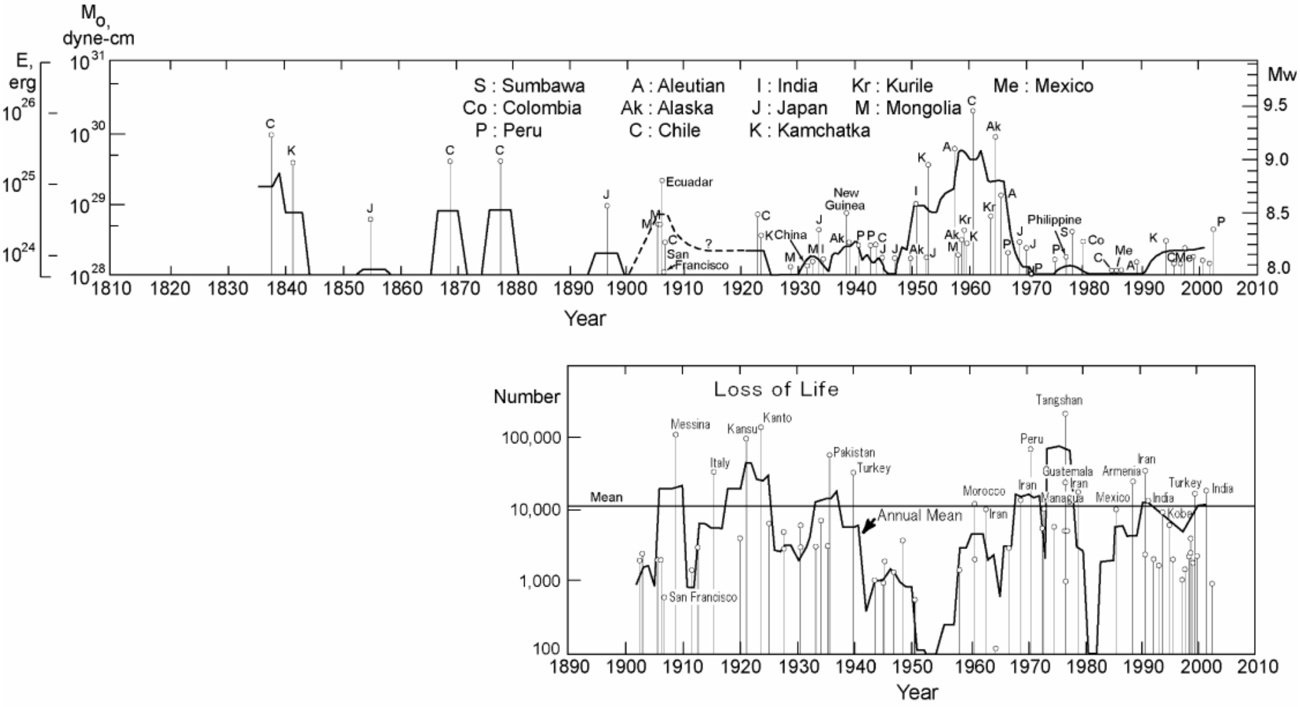

Figure 2. Secular variations of seismic energy release (upper panel) and human loss (lower panel). Ordinate of the upper panel represents the size of earthquakes in seismic moment M0, seismic energy E and the moment magnitude Mw. Ordinate of the lower panel shows the number of victims. In both panels, the vertical bars are for individual event and the solid curve shows the annual average (unlagged 5-year running average) (after H. Kanamori, private communication).

2. FIRST PRIORITY IS THE REINFORCE MENT OF OUR HOUSES

Many problems arise at and after a disastrous earthquake ([6]), including:

1) Loss of life at the time of the main shock,
2) Further victims due to fires,
3) Psychological instability of people in the affected areas,
4) Disruption of the community,
5) Building refugee camps for large number of displaced people,
6) Demolition of damaged structures and related environmental effects,
7) Economic, business and societal disruption.

At the time of the main shock, rapid delivery of information on ground motions and damages to the authorities and public are critically important for rescue activity. Thanks to major advances in information technology, there is an emerging new category of hazard mitigation; real-time seismology that has been developed in several areas, including Japan, Mexico, California and Taiwan [e. g., [7]; [8]; [9]; [10]). The Seismic Alert System in Mexico made use of the gap of the arrival times of the P- and S-waves. The authorities were able to issue timely alarms so that the subways in the Mexico City were stopped 50 seconds before the arrival of the destructive S-waves from the 1995 M7.3 Guerrero earthquake located at the Pacific coast. However, many of the problems listed above will last for a long time after the event. To cope with the evolution of disaster situations in hours, days, weeks and even months, innovative engineering strategies will be needed. A new kind of strategy can be called the real-time earthquake engineering. After the main shock, continuing data collection of structure damage distribution, rescue activities, lifeline interruptions, debris removal, refugee camps, and power demand fluctuations and other parameters will be critical because of the utmost importance for disaster relief agencies and local and national governments to allocate resources in the most prompt and efficient manner ([11]).

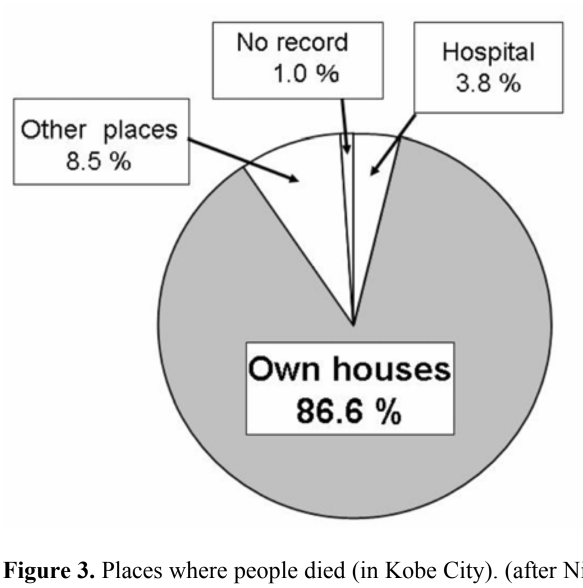

Figure 3. Places where people died (in Kobe City). (after Nishimura et al., 1997b)

We now focus items 1) and 2) in the above list, namely on how to save human life. Experiences all over the world show that, almost without exception, the majority of victims are killed by the collapse of buildings right at the moment of the main shock (Plate 1, a & b). An example is shown in Fig. 3 for the 1995 M7.3 Hyogoken Nanbu Earthquake, which took over 5,500 human lives. (This earthquake is commonly called the Kobe earthquake after the name of the city, where the damage was most intense.) Almost 90 % of the victims were killed in their own houses. Moreover, medical examinations indicate that 92 % of casualties were killed within less than 15 minutes after the quake before any organized rescue operation had started ([12]; [13]).

Plate 1 Damage to low earthquake resistant structures is major cause of casualties and many problems generated after the earthquake in the world *(photo by K. Meguro)* (a) Damage to old timber houses due to the Kobe earthquake (M7.3), 1995 in Japan (b) Damage to masonry houses due to the Qayen earthquake (M7.1), 1997 in Northeast Iran.

Many of victims of earthquakes can be killed by fires. Although fires can be caused by shaking, most of big fires start from collapsed houses. Fires that started in non-collapsed houses were commonly extinguished by the residents, while those that started in collapsed houses were not. Residents under debris could not fight the fires and the first priority of outside rescuers was to get them out from the fallen houses. Furthermore, roads were often blocked to fire engines by collapsed houses. In Kobe, the Fire Department had a capacity to handle only three to four fires at a time. When many tens of fires started simultaneously, they were completely overwhelmed. To prevent fires from developing to uncontrollable size, the best way is to prevent houses from collapsing.

If the government of Japan were to fund 10 billion US dollars annually, all the necessary reinforcement of houses in Japan would be completed in ten years ([14]). In order to implement the house reinforcement program effectively, the following system, called the Retrofitting Promotion System, has been proposed ([6]). The main concept of this system is that the government guarantees to pay a portion of the repair and reconstruction expenses of damaged houses provided that proper retrofitting had been implemented by the owners before the earthquake. With such a system, the overall financial burden of both government and residents can be greatly reduced. The feasibility of this system has been verified for cases in which the retrofitting cost is 10 to 15% of the new construction cost, as is the case in Japan. However, for countries like Turkey, where the retrofitting cost amounts to approximately 75% of the new construction cost, the system is not viable. In such cases, efficient and economic techniques for retrofitting are needed, especially for masonry structures, using locally available and inexpensive materials ([15]). If the structural damage is reduced, loss of human life is reduced. Thus, the most effective and highest priority countermeasure against the loss of human life, and all kinds of related seismic hazards and consequences, is the structural issue. In the recent December 26, 2003, M6.7 Bam Earthquake in Iran, there were more than 30,000 casualties due to the collapse of adobe and brick structures which lacked reinforcement. After the disaster, international and local agencies rushed to the affected sites trying to rescue survivors. Although these were valuable efforts, only a few people survived and were rescued, again highlighting the quality of buildings as a key issue.

REFERENCES

[1] Stein, S. and E. Klosko, Earthquake mechanisms and plate tectonics, in *" International Handbook of Earthquake and Engineering Seismology"* (W. H. K. Lee, H. Kanamori, P. C. Jennings and C. Kisslinger (Eds.), Academic Press, 69-78, 2002.

[2] Giardini, D. (Ed.), The Global Seismic Hazard Assessment Program (GSHAP), *Annali di Geofisica*, **42**, No.6, 1999.

[3] Kumazawa, M. and S. Maruyama, Whole Earth tectonics, *J. Geol. Soc. Japan*, **100**, 81-102, 1994.

[4] Uyeda, S., Continental drift, sea-floor spreading and plate tectonics/Plume tectonics, in *"International Handbook of Earthquake and Engineering Seismology"* (W. H. K. Lee, H. Kanamori, P. C. Jennings and C. Kisslinger (Eds.), Academic Press, 51-67, 2002.

[5] Utsu, T., A list of deadly earthquakes in the world: 1500 – 2000, in *"International Handbook of Earthquake and Engineering Seismology"* (W. H. K. Lee, H. Kanamori, P. C. Jennings and C. Kisslinger (Eds.), Academic Press, 691-717, 2002.

[6] Meguro, K., and T. Takahashi, System for promotion of retrofitting of existing pre code-revision weak structures, *J. Social Safety Science,* **3**, 81-86, 2001. (In Japanese with English abstract)

[7] Nakamura, Y., On the urgent earthquake detection and alarm system (UrEDAS), *Proc. Ninth World Conf. Earthq. Engineering*, **17**, 673-678, 1988.

[8] Aranda, E. et al., Mexico City seismic alert system, *Seimol. Res. Lett*., **66**, 42-53, 1995.

[9] Kanamori, H., E. Hauksson and T. Heaton, Real-time seismology and earthquake hazard mitigation, *Nature*, **390**, 461-464, 1997.

[10] Shin, T. C., K. W. Kuo et al., A preliminary report on the 1999 Chi-Chi (Taiwan) earthquake, *Seismol. Res. Lett*., **71**, 24-30, 2000.

[11] Hada, Y. and K. Meguro, Application of Power Demand Changes to Evaluate Building and Dwelling Damages due to Earthquake, *Bulletin of Earthquake Resistant Structure Research Center - Institute of Industrial Science*, **35**, 135-144, 2002.

[12] Nishimura, A., Y. Ueno, S. Fujiwara, I. Ijiri, T. Fukunaga, S. Hishida, K. Hatake, A. Tanegashima, H. Kinoshita, Y. Mizoi, and Y. Tatsuno, Medical examination report on the Great Hanshin Earthquake, *J. Advance in Legal Medicine,* **3**, 234-238, 1997a.

[13] Nishimura, A., Y. Ueno, S. Fujiwara, I. Ijiri, T. Fukunaga, S. Hishida, K. Hatake, A. Tanegashima, H. Kinoshita, Y. Mizoi, and Y. Tatsuno, Statistical Report on Casualty of the Great Hanshin Earthquake, *J. Advance in Legal Medicine,* **3**, 346-349, 1997b.

[14] Ohtake, M., Reinforcement is urgently needed for wooden houses, *Japan Society for Disaster Information Studies News Letter*, No. 13, 1, 2003 (in Japanese)

[15] Mayorca, P., and K., Meguro, Proposal of a new economic retrofitting method for masonry structures, *Proc. 27th Earthquake Engineering Symposium*, CD-ROM, Japan Soc. Civil Engineers, 2003.

Kimiro Meguro
International Center for Urban Safety Engineering, Industrial Science, The University of Tokyo,
4-6-1, Komaba, Meguro-ku, Tokyo 153-8505 JAPAN
email: meguro@iis.u-tokyo.ac.jp

Deformation processes and earthquakes in Nankai

Pierre Henry (1), Stephane Operto (2), Siegfried Lallemant(3), Jean-Xavier Dessa(2), Victor Martin (4), Mark Noble (4), Hidekasu Tokuyama(5), Shuichi Kodaira (6), Shin'ichi Kuramoto(7), Masataka Kinoshita (8)

(1) CNRS-College de France, Aix-en-Provence; (2) Géosciences Azur (CNRS), Villefranche sur mer; (3) Université de Cergy Pontoise; (4) Centre de Géophysique, Ecole des Mines de Paris, Fontainebleau; (5) ORI, U. of Tokyo; (6) IFREE, Jamstec, Yokohama; (7) CEDEX, Jamstec, Yokosuka; (8) Deep Sea Research, Jamstec, Yokosuka

ABSTRACT

Studying the Japanese Trenches, and particularly the Nankai subduction has been one objective of French-Japanese bilateral cooperation for nearly 20 years, notably within the Kaiko (and SFJ) projects. Work done within this framework has contributed to our understanding of deformation processes in subduction zones. Deep riser drilling of the subduction seismogenic zone is now a major objective for the international scientific community, undertaken within the framework of IODP. The Nankai subduction zone is among the primary targets (NanTroSEIZE Complex Drilling Proposal). We wish to pursue bilateral cooperation as a component of the NanTroSEIZE international project.

KEYWORDS: seismogenic zone, subduction.

1. INTRODUCTION

One important incentive for geoscience studies in subduction trenches is to understand processes occurring within the seismogenic zone. The societal importance of this scientific objective is well understood as great subduction earthquakes present a major natural hazard for many cities (notably Tokyo). While earthquake prediction may still be considered as an ultimate goal, our understanding of the physical processes involved is currently insufficient, even though precursors are detectable before some earthquakes. New seismological and geodetic observations, fault geology, laboratory experiment and theory have lead to significant progress in understanding the mechanics of earthquake and fault slip. Progress in drilling and borehole monitoring technologies have also opened a new approach of seismically active faults, by in situ sampling and monitoring. One major difficulty is that the part of fault zones where earthquakes nucleate can only be reached at several kilometers depths within the crust, corresponding to temperatures of more than 150°C. However, this objective is considered achievable in the near future and several projets onshore within ICDP (e.g. SAFOD) and offshore within IODP (e.g. NanTroSEIZE) have this aim. Drilling the updip limit of the seismogenic zone of a subduction thrust is the objective of the SEIZE (SEIsmogennic Zone Experiment) initiative and the Nankai subduction is one possible target. However, the subduction plane is not the only fault that may cause large earthquakes and tsunamis in Nankai. For example, we will show here that the earthquakes southeast of Kii which occurred this year (September 5, 2004) are caused by intraplate deformation within the downgoing plate.

2. HISTORY

Studies of the Nankai margin by geoscientists accumulated a great wealth of data. These include margin scale geophysics such as multibeam bathymetry, OBS, 2D and 3D MCS as well as more detailed studies of fault outcrops and fluid seepage sites, using deep towed seismics, side scan sonars, manned and unmanned submersibles. Investigation by drilling was also performed as part of the ODP project, or as part of Japanese projects (lead by MITI and JNOC). In the early days of the Kaiko project (starting around 1985), French-Japanese bilateral cooperation has been a strong component of this data acquisition process. For instance, the first multibeam bathymetric maps of the Japanese Trenches and the first submersible dives (leading to the discovery of cold seeps on active fault outcrops) took place within this framework. The main objectives of the following phases (Kaiko-Nankai and Kaiko-Tokai) were to understand the tectonics around the Izu collision, and notably within the Tokai segment of the Nankai subduction. Results relevant for hazard assessment include a detailed active fault map of the off Tokai region [1]. These studies showed that the subduction plane is not the only fault that may slip during large earthquakes. Should also be considered: a compressive intraplate system South of the subduction trough (Zenisu ridge) [2], splay faults at the updip limit of the seismogenic zone (which presumably slip during large subduction earthquakes), and strike-slip faults resulting from shear partitioning within the Tokai margin [3]. Furthermore, the subduction of a large basement ridge (named Paleo-Zenisu) beneath the Tokai margin was inferred from tectonic and geophysical observations [4-6]. This ridge may influence the distribution of coseismic slip during large earthquakes [7].

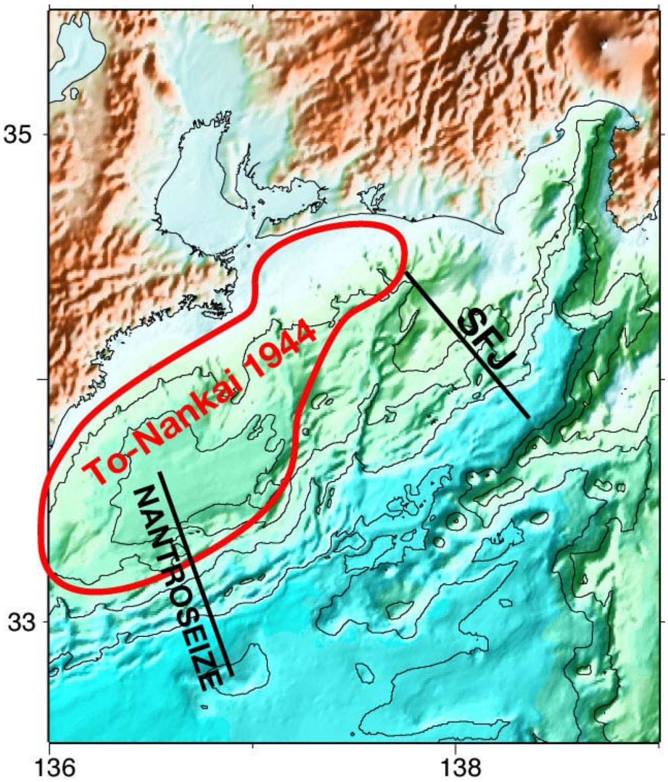

Figure 1. Map of Eastern Nankai showing the slip zone of the To-Nankai (1944) earthquake, the location of the SFJ transect (Figure 2) and the location of the Nantroseize transect (figure 3)

We will here summarize activities and results of the latest phase of Kaiko (SFJ for Seize Franco-Japonais), which primary goal was to image the splay faults and the subduction seismogenic zone in the TOKAI area. We will then present an outline of recent ODP activites in Nankai, and of the Nantroseize project, which goal is to drill, sample and instrument the Nankai seismogenic zone using Chikyu riser drilling vessel. Finally, we will discuss the implications of the recent earthquake sequence Southeast of Kii for earthquake hazard assessment in this area.

3. SFJ

The core of the SFJ project was a combination of 2D and 3D MCS (Nadir cruise in 2000) and dense OBS array (JAMSTEC cruise in 2001) on the same profile located at the eastern end of Nankai Trough (Fig. 1). Processing of the dense OBS array has been done in collaboration by JAMSTEC and CNRS (Geosciences Azur at Villefranche sur Mer). Velocity inversion by travel time tomography confirmed that at least one oceanic basement ridge, similar to Zenisu is subducting beneath the Tokai margin [8-9]. Cyclic subduction of ridges extending westward from the Izu-Bonin arc is the likely cause of forearc basin uplift and shortening in the Tokai area [6].

Images have been obtained by pre-stack migration of MCS data and OBS data (Figure 2). 2-D full waveform inversion has also been applied to the OBS data set to obtain a refined velocity model [10]. All these images found a series of landward dipping reflectors correlated with low velocity zones below the fore-arc basin. This structure suggests large scale stacking of thrust sheets. However, the correlation of the shallower part (upper 5 km) of the MCS image with the deep structure is unclear. According to our interpretation (Figure 2) the deep structures and the currently active splay faults correspond to two generations of structures. MITI/JNOC drilling results suggest the deep structures are within the Pre-Miocene (Shimanto) accretionary complex [. They only experienced minor Post-Miocene reactivations.

Confrontation of velocity models acquired over the years on Nankai margin with the geological framework suggests a general relationship between the extent of the forearc basin domain and velocities exceeding 5 km/s within the margin [12]. In the Tokai segment as well as in the East off Kii (ToNankai segment) active splay faults localize in the transition between the forearc basin and, likely, mark the updip limit of the seismogenic zone [13].

4. ODP AND IODP

Drilling of the Quaternary accretionary wedge and trough was performed as part of the DSDP and ODP program (Legs 57, 87A, 131, 190 and 196). One essential objective of ODP drilling was the study of deformation and fluid flow processes associated with decollement initiation. Drillholes were located near the trench where the decollement level could be reached at less than 1 km below seafloor [14-15]. They are thus located in the aseismic domain seaward of the seismogenic zone. Studies of rock physical properties and Logging While Drilling provided insight on deformation mechanisms and fluid-mechanic coupling in the decollement zone. Decollement initiation results from a combination of factors: low intrinsic friction coefficient [16], removal of grain contact cement [17] and pore pressure cycling [18-21]. Multiple level pore pressure monitoring is going on in two holes equiped with ACORKs (Advanced Circulation Obviation Retrofit Kit) [15, 22].

NanTroSEIZE is an integrated program of geophysical and geologic studies, non-riser drilling, and riser drilling designed to investigate the aseismic to seismic transition of the megathrust system and the processes of earthquake and tsunami generation at the Nankai Trough subduction zone. Our fundamental goal is the creation of a distributed observatory spanning the up-dip limit of seismogenic and tsunamigenic behavior. The area chosen is off the Kii Peninsula, where the plate interface and active mega-splay faults – implicated in tsunamigenesis – are accessible to drilling within the region of coseismic rupture in the 1944 Tonankai M8 great earthquake (figure 1). One cornerstone of NanTroSEIZE strategy is to document the evolution of fault zone properties by trading time for space along the dipping plate boundary (figure 3).

Three distinct phased IODP drilling efforts are proposed: Phase 1 – Inputs to the seismogenic zone system, investigating variations in the sediments, oceanic crust, and fluids input to the plate boundary system; Phase 2 – Mega-splay (OOST) fault drilling to sample and instrument thrusts which splay from the basal décollement up through the forearc, in order to characterize fault properties transecting the aseismic to seismic transition from 1 to 3.5 km depth shallow; and Phase 3 – Sampling and instrumenting the plate interface (décollement) at ~ 6 km below seafloor, in a region predicted to be within both the zone capable of generating seismogenic behavior and in the zone of co-seismic slip in the 1944 great earthquake. Long-term monitoring of a wide range of phenomena will be a major part of the effort, to detect signals of fault zone processes in the near-field. In addition, ongoing seismological and geodetic arrays in the vicinity as well as in the deep boreholes, geologic studies, laboratory and modeling efforts are all integral components of the NanTroSEIZE project.

The construction by the Japanese of the Chikyu drilling vessel is a unique opportunity for scientists all other the world. By the nature of IODP, participation to drilling cruises will be open to scientists from all participating countries, and this includes France. Currently, contributions of French scientists to the NanTroSEIZE project are considered within the framework of French-Japanese bilateral cooperation, and as a prolongation of SFJ. These include contributions to site survey data processing and expertise in seismotectonics. The full waveform inversion program developed by J.X. Dessa and S. Operto (Geosciences Azur) has just been installed on the Earth Simulator (at JAMSTEC) and will be used for processing new OBS data. At the earliest, non-riser drilling could start in 2006, and riser drilling in late 2007. Future contributions should be thus planned in the long term. These could involve contributions to laboratories studies of samples (e.g. at EOPG, Strasbourg) and to borehole measurements (e.g. with IPG, Paris).

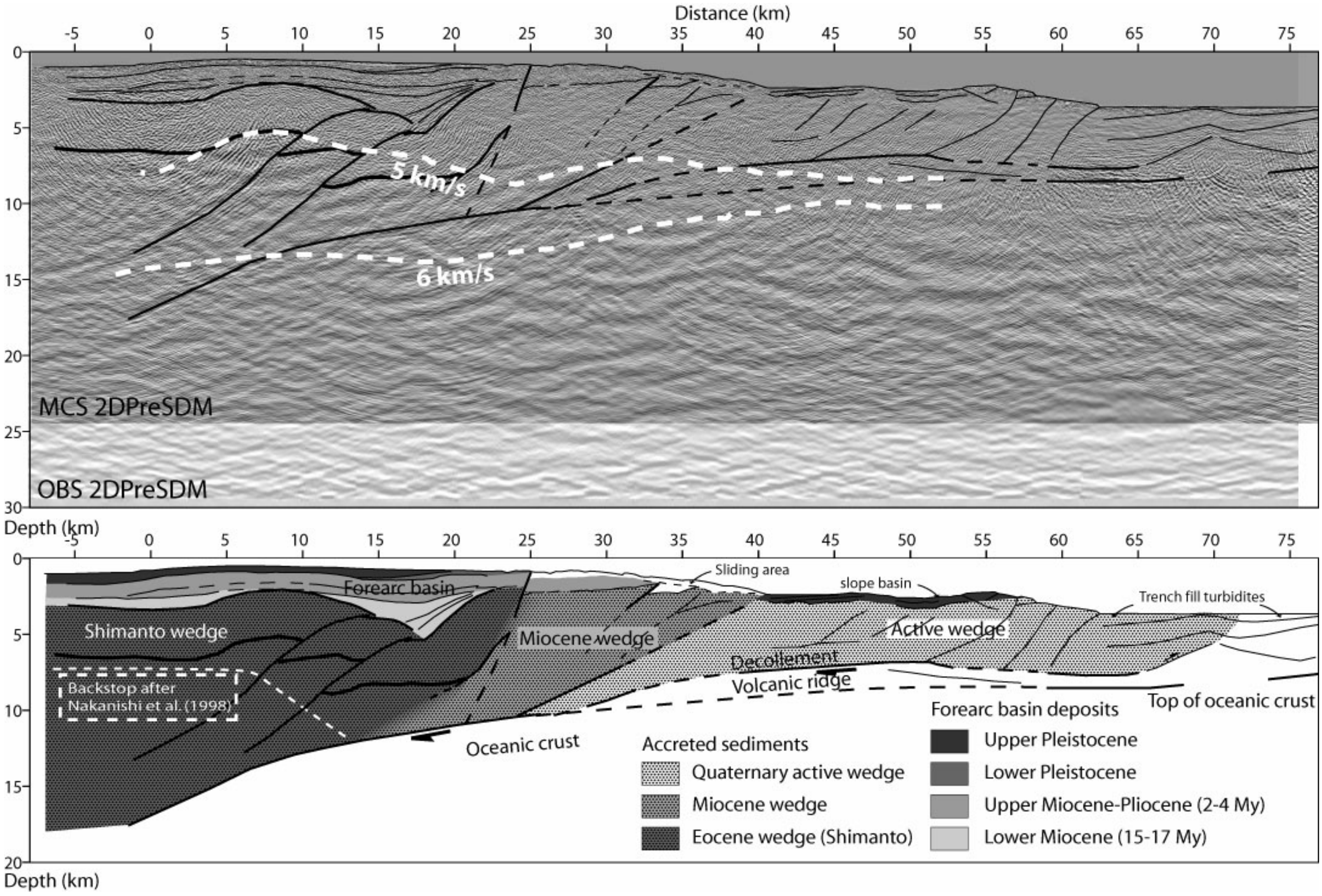

Figure 2: Combined MCS and OBS pre-stack depth migration images (top) and structural interpretation (bottom). Accreted material is dot-filled, sedimentary cover is plain. 5 km/s and 6km/s velocity contours from travel time tomography are also shown.

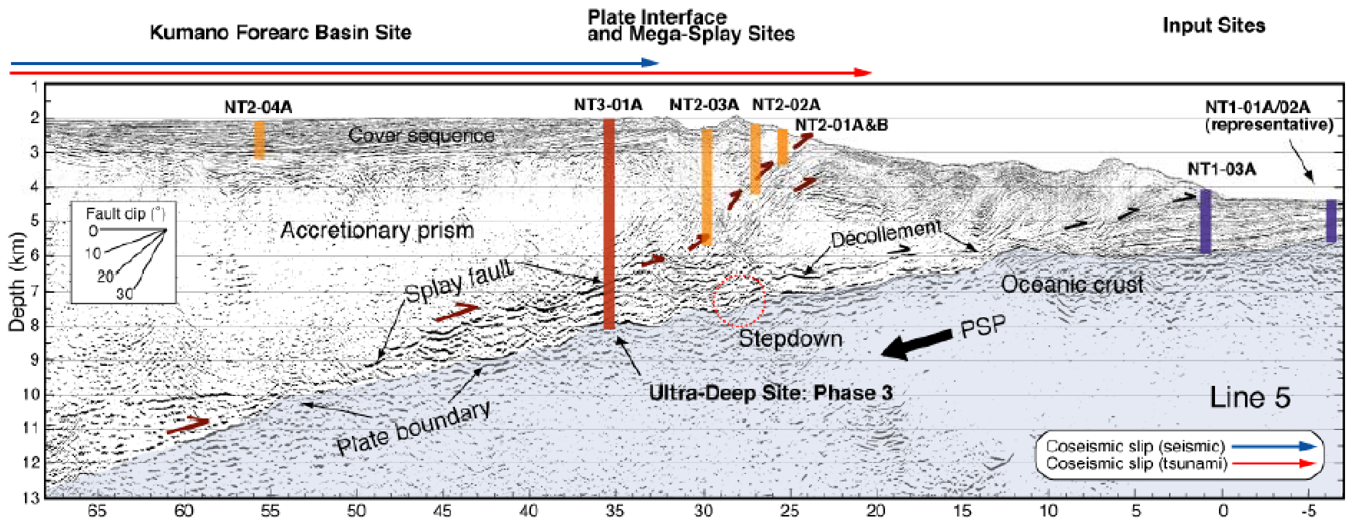

Figure 3. Poststack depth-migrated MCS profile showing the Kii/Kumano plate interface, accretionary prism, Kumano basin, and prominent splay fault system [12]. See Figure 1 for profile location. The seaward distribution of the 1944 Tonankai coseismic slip estimated from tsunami (red line) and seismic (blue line) inversions is projected over the profile. Location of the décollement stepdown to the top of the oceanic basement is marked with orange dotted circle. Phase 1 is in purple, Phase 2 in orange, and Phase 3 in red.

5. RECENT OFF KII EARTHQUAKES

An earthquake sequence in Nankai Trough, South of Kii Penninsula, started September 5, 2004 with an earthquake of magnitude Mw=7.2 at 10:07 (UT), followed by a magnitude Mw=7.5 at 14:57 (UT). The largest aftershock occurred at 23:29 (UT) on September 6, with Mw=6.5. Although the focal mechanisms are compressive, these earthquake do not seem to correspond with subduction earthquakes because of their location (too close to the trench) and because the N-S compression does not correspond to the N310° direction of subduction. These earthquakes are instead well understood as intraplate deformation within the Philipine Sea Plate, in the westward prolongation of the Zenisu

Ridge. Kinematic models bases on the assumption of rigid platelets were constrained combining tectonic and seismological observations offshore with GPS data from GEONET (Geographic Survey of Japan permanent GPS network) on land, and predict about 10 mm/yr north-south compression in this area (Figure 4) [5, 23, 24]. This is remarkably consistent with the focal mechanisms of the three main shocks.

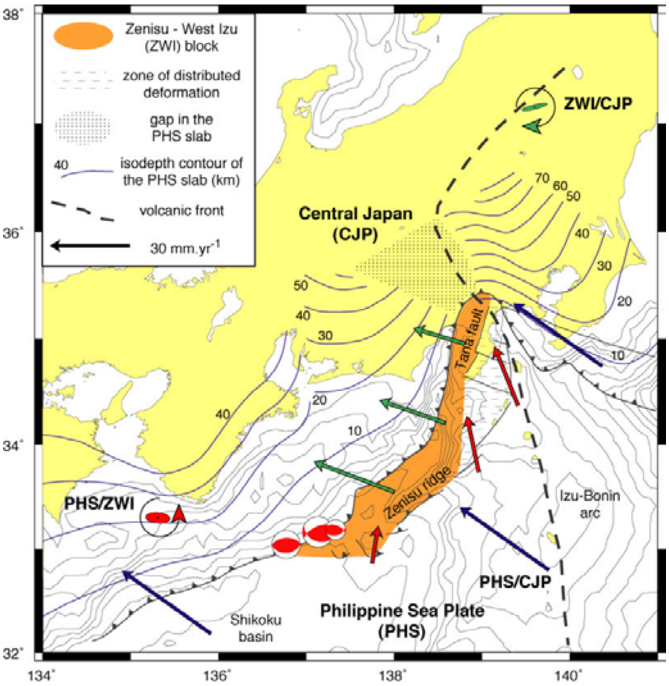

Figure 4: Kinematic model for Eastern Nankai showing how the Philippine Sea Plate - Central Japan motion (blue arrows) is partitioned between the subduction trough (green arrows) and the Izu-Zenisu intraplate deformation zone (red arrows) [23]. Focal mechanisms (here shown as determined by NIED) indicate north-south compression. These focal mechanisms are consistent with relative motion in the Izu-Zenisu deformation zone, but not with the subduction velocity.

In these kinematic models, convergence in the Eastern Nankai Trough and Suruga Trough is less that the Philippine Sea Plate/Japan convergence (by about 30%). This may explain the longer interval of subduction earthquake recurrence in the Tokai segment compared with the adjacent ones [24]. It is also possible that the next large earthquake in this area occurs on Zenisu ridge rather than on the subduction megathrust. An earthquake on Zenisu Ridge may cause limited damage from ground shaking as it is further away from the coast, but has the potential to produce a large tsunami if the major thrust along the southern side of Zenisu slips during one event. Furthermore, stress change caused by the recent earthquakes likely modifies the probablity of occurrences of earthquakes in Eastern Nankai. Obviously, these earthquakes have reduced the load on the subduction megathrust off Kii Penninsula (i.e.: the slip zone of the To-Nankai 1944 event) and increased the load on thrusts of the Zenisu system. Further assessment of stress change and its consequences, notably on the Tokai-Suruga segment of the subduction (which did not rupture during the 1944 event [25]), would require modeling of elastic stress transfer and Coulomb stresses.

6. CONCLUSION

Current efforts to understand earthquake processes in subduction zones rely on an integrated approach, of which NanTroSEIZE is an example. In situ sampling and monitoring of the seismogenic zone is one essential aspect, which will be made possible by the construction by the Japanese of the Chikyu riser drilling vessel. However, the deep holes should be understood as part of a broader data acquisition program which will include the deployment of an array of instrumented boreholes. For the purpose of hazard assessment, one must also keep in mind that the subduction megathrust is not the only active fault that may cause large earthquakes in the Eastern Nankai area.

REFERENCES

[1] Tokuyama, H., J. Ashi, W. Soh, S. Kuramoto, and Y. Ikeda, Active submarine faults off Tokai: Results from the Japan-France Kaiko-Tokai Project, 151 (in Japanese) pp., Univ. Tokyo Press., Tokyo, 1999.

[2] Lallemant, S.J., N. Chamot-Rooke, X. Le Pichon, and C. Rangin, Zenisu Ridge: a deep intraoceanic thrust related to subduction, off Southwest Japan, Tectonophys., 1, 151-174, 1989.

[3] Huchon, P., H. Tokuyama, S.J. Lallemant, A. Taira, P. Henry, S. Mazzotti, X. Le Pichon, and the Kaiko-Tokai Scientific Party. Pervasive dextral strike-slip faulting within the backstop of the eastern Nankai wedge confirmed by deep-towed seismic data (Kaiko-Tokai496 cruise), C. R. Acad. Sci., 326, 869-876, 1998.

[4] Lallemand, S.E., J. Malavieille, and S. Calassou, Effects of oceanic ridge subduction on accretionary wedges: experimental modeling and marine observations, Tectonics, 11, 1301-1313, 1992.

[5] Le Pichon, X., S.J. Lallemant, H. Tokuyama, F. Thoue, and P. Henry, Structure and evolution of the backstop in the Eastern Nankai trough area (Japan): implications for the soon to come Tokai earthquake, The Island Arc, 5, 440-454, 1996.

[6] Mazzotti, S., S.J. Lallemant, P. Henry, X. Le Pichon, H. Tokuyama, and N. Takahashi, Intraplate shortening and underthrusting of a large basement ridge in the eastern Nankai subduction zone. Japan-France Kaiko-Tokai Project; tectonics of subduction in the Nankai Trough, Mar. Geol., 187 (1-2), 63-88, 2002.

[7] Park, J.-O., G.F. Moore, T. Tsuru, S. Kodaira, and Y. Kaneda, A subducted oceanic ridge influencing the Nankai megathrust earthquake rupture, Earth Planet. Sc. Lett., in press, 2003.

[8] Kodaira, S., A. Nakanishi, J.-O. Park, A. Ito, T. Tsuru, and Y. Kaneda, Cyclic ridge subduction at an inter-plate locked zone off central Japan, Geophys. Res. Lett., 30, 1339, doi:10.102ç/2002GL016595.

[9] Dessa, J.-X., S. Operto, S. Kodaira, A. Nakanishi, G. Pascal, K. Uhira, and Y. Kaneda, Deep seismic imaging of the eastern Nankai trough, Japan, Form multifold ocean bottom seismometer data by combined travel time tomography and prestack depth migration, J. Geophys. Res., 109, B02111, doi:10.1029/2003JB002689, 2004.

[10] Dessa, J.-K., S. Operto, S. Kodaira, A. Nakanishi, G. Pascal, J. Virieux, and Y. Kaneda, Multiscale seismic imagin of the eastern Nankai trough by full waveform inversion, Geophys. Res. Lett., 31, L18606, doi:10.1029/2004GL020453, 2004.

[11] Nakanishi, A., S. Kodaira, J.-O. Park, and Y. Kaneda, Deformable backstop as seaward end of coseismic slip in the Nankai Trough seismogenic zone, Earth Planet. Sc. Lett., 203 (1), 255-263, 2002.

[12] Park, J.-O., T. Tsuru, S. Kodaira, P.R. Cummins, and Y. Kaneda, Splay fault branching along the Nankai subduction zone, Science, 297 (5584), 1157-1160, 2002.

[13] Tokuyama, H., E. Honza, M. Kimura, S. Kuramoto, J. Ashi, Y. Okamura, H. Arato, Y. Itoh, W. Soh, R. Hino, T. Nohara, H. Abe, S. Sakai, and K. Mukaiyama, Quaternary structural map in Japanese waters (Map and CD), 2001.

[14] Moore, G.F., Taira, A., Klaus, A., et al., 2001. Proc. ODP, Init. Repts., 190 [Online]. Available from World Wide Web: http://www-odp.tamu.edu/publications/190_IR/190ir.ht

[15] Mikada, H., Becker, K., Moore, J.C., Klaus, A., et al., 2002. Proc. ODP, Init. Repts., 196 [Online]. Available from World Wide Web: http://www-odp.tamu.edu/publications/196_IR/196ir.htm

[16] Kopf, A., and Brown, K.M., 2003. Friction experiments on saturated sediments and their implications for the stress state of the Nankai and Barbados subduction thrusts. Mar. Geol., 202:193-21
[17] Morgan J.K., and Ask, M.V.S., 2004. Consolidation state and strength of underthrust sediments and evolution of the décollement at the Nankai accretionary margin: results of uniaxial reconsolidation experiments. J. Geophys. Res., 109:10.1029/2002JB002335.
[18] Ujiie, K., Hisamitsu, T., and Taira, A., 2003. Deformation and fluid pressure variation during initiation and evolution of the plate boundary décollement zone in the Nankai Accretionary Prism. J. Geophys. Res., 108:10.1029/2002JB002314.
[19] Henry, P., Jouniaux, L., Screaton, E.J., Hunze, S., and Saffer, D.M., 2003. Anistropy of electrical conductivity record of initial strain at the toe of the Nankai Accretionary Wedge. J. Geophys. Res., 108:10.1029/2002JB002287.
[20] Bourlange, S., Henry, P., Moore, J.C., Mikada H., and Klaus, A., 2003. Fracture porosity in the décollement zone of Nankai accretionary wedge using Logging While Drilling resistivity data. Earth Planet. Sci. Lett., 209:103-112.
[21] McNeill, L.C., Ienaga, M., Tobin, H., Saito, S., Goldberg, D., Moore, J.C., and Mikada, H., 2004. Deformation and in situ stress in the Nankai Accretionary Prism from resistivity-at-bit images, ODP Leg 196. Geophys. Res. Lett., 31:10.1029/2003GL01879
[22] Davis, E.E., and Becker, K., 2001. Using ODP boreholes for studying sub-seafloor hydrogeology: results from the first decade of CORK observations. Geoscience Canada, 28:171-1.
[23] Mazzotti, S., P. Henry, X.L. Pichon, and T. Sagiya, Strain partitioning in the zone of transition from Nankai subduction to Izu-Bonin collision (Central Japan): implication for extensional tear within the subducting slab, Earth Planet. Sc. Lett., 172, 1-10, 1999.
[24] Mazzotti, S., P. Henry, and X.L. Pichon, Transient and permanent deformation of central Japan estimated by GPS. 2; Strain partitioning and arc-arc collision, Earth Planet. Sc. Lett., 184, 443-453, 2001.
[25] Ando, M., Source mpechanisms and tectonic significantce of historical earthquakes along the Nankai Trough, Japan, Tectonophys., 27, 119-140, 1975.

Pierre Henry
College de France, chaire de Geodynamique, Europole de l'Arbois
BP 80, 13545 Aix en Provence Cedex 04, FRANCE
email: henry@cdf.u-3mrs.fr

Detection and modeling of ionospheric signals associated to seismic surface waves and tsunamis

Philippe Lognonné (1), Raphael Garcia (1), François Crespon(1), Giovani Occhipinti(1) Juliette Artru(2) and Makoto Murakami (3)

(1) Département de Géophysique Spatiale et Planétaire, Institut de Physique du Globe de Paris, Saint Maur des Fossés, France (2) Seismological Laboratory, California Institut of Technology, Pasadena, California, USA (3) The Geographic Survey Institute, Tsukuba, Ibaraki, Japan

ABSTRACT

We present several examples of post-seismic ionospheric signals. These signals are associated either to Rayleigh surface waves, to acoustic waves generated in the near field or to tsunami waves. The use of GPS dense network allow to image the associated perturbations at altitudes between 200 and 400 km typically, leading then to the determination of the velocity of these waves, while Doppler sounding can provide observations of the waves at lower altitudes, below 200 km. These observations can be performed for all major earthquakes, with magnitude greater than 7.5. We show several examples and present the theory necessary to understand these signals.

KEYWORDS: Surface waves, tsunamis, Doppler sounder, Global Positioning System, remote sensing.

1. Introduction

After a quake, the surface of a planet is vibrating horizontally and vertically. By continuity of the vertical displacement, the atmosphere is therefore forced to move with a vertical velocity equal to the surface vertical velocity, and this vibration is then propagating upward. Such atmospheric vibrations are producing adiabatic pressure and temperature variations, which propagate up to the ionosphere, as shown on Fig 1.

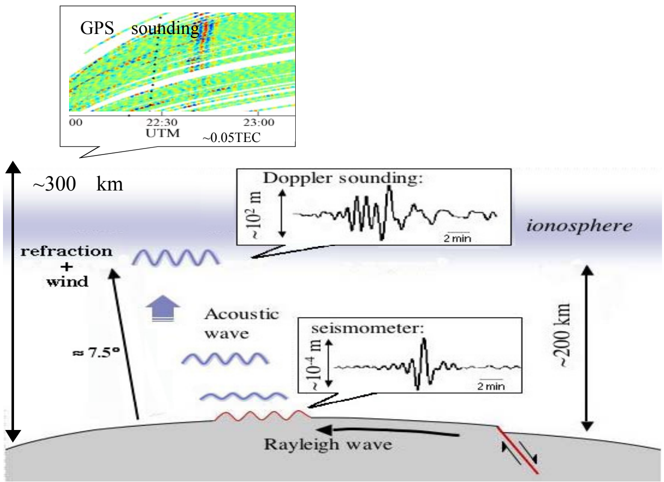

Figure 1: Examples of observation of ionospheric seismic signals. Observation at altitude of 150-200 km are performed with HF Doppler sounder for quakes of magnitude greater than 6.5 whereas observations at higher altitude, performed by GPS networks, can be done only for large quakes with M>8.

Near field seismic waves, Rayleigh surface waves and tsunamis are therefore producing vertical oscillations of the earth surface propagating upward up to the ionosphere. These waves are detected by Doppler sounders and dense GPS networks, such as those of Japan and California. We show in this paper several examples of ionospheric detections, develop the theory and present perspectives

2. THEORY

Theory is detailed in *[1,2]*, the latter paper taking into account the viscosity of the atmosphere. The atmosphere of the Earth changes the boundary conditions of the elasto-dynamic operator. The atmosphere is indeed such that no specific boundary can be defined, due to the exponential decay of the density. However, acoustic waves are not reflected when propagating upward at high altitude, and loose their energy due to viscosity and non-linear effects. These effects can be modeled by using a radiative boundary condition instead of the usual free surface boundary condition.

Normal modes for such boundary condition are computed with a variational method, which uses a basis of test functions found by mapping the normal modes with free surface toward functions verifying explicitly the radiative boundary conditions. All normal modes of the Solid Earth-Ocean-Atmosphere coupled system are then found (Spheroidal Solid Earth Normal modes, Acoustic, Gravity and Lamb atmospheric modes, Gravity-Tsunami gravity modes).

The main perturbation, for the spheroidal normal modes are found in the amplitude of normal modes rather than in the frequency or quality coefficient perturbations, which appears too small to be detected. Two regimes for the fundamental spheroidal modes are found: below 3.68 mHz (the exact frequency depending on the model), the atmospheric part of the mode is trapped and decay exponentially with altitude. At higher frequency in contrary, the energy propagates upward [Figure 2].

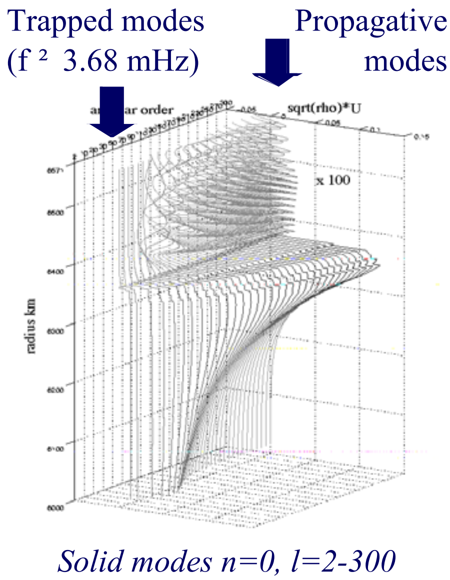

Figure 2: Amplitude of the Solid spheroidal normal modes in the upper mantle and atmosphere

2. DOPPLER DETECTION

We presents first data of ionospheric oscillations recorded in France by an ionospheric sounder developed by CEA/DASE. This instrument performs the measurement of the Doppler shift between a HF EM wave emitted from the ground and its counterpart reflected by ionospheric F layer and provides a direct measurement of the vertical velocity of the ionosphere. 3 receivers are located 50-100 km apart from the emitter, located in Francourville, France. Detail on the instruments and on observations can be found in [3].

The network has been working continuously since August 1999, most of M>6.5 earthquakes have been observed. We present the comparison of synthetics with these data [Figure 3]. Significant differences in amplitude are found, mainly associated to the effect of lateral variations of the Earth on seismic waves. Even if non-linear effects are not taken into account here, they should represent about 10% of the signal at 150km and can be neglected in first approximation. In contrary, we found that attenuation due to viscosity is important above 100 km height and strongly constraints the attenuation of waves: our data can therefore be used to constrain the relatively poorly known profiles of the atmospheric viscosity.

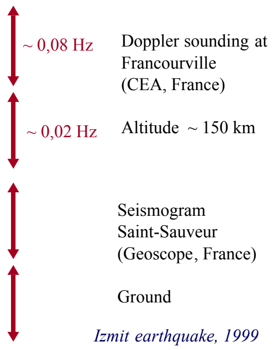

Figure 3 *Observation of ionograms at Francourville and seismograms at the nearby Geoscope SSB station, with their synthetics for the PREM model with US standard atmospheric model.*

2. GPS DETECTION

GPS networks can also image the ionospheric TEC variations every 30 sec at high altitude (250-350km), and in some case at higher rates (1 Hz). Depending on the number of stations, either the 2D ionospheric TEC maps or the 3D ionospheric structure can be reconstructed by the processing. Several signals were observed, either for near field observations, such as those of the Hokkaido, 2003 and San Simeon, 2003, earthquakes, or in far field, for Rayleigh waves generated by the Alaska, Denali, 2003 event or for the tsunami generated by the Peru, 2001, earthquake. In the case of the Hokkaido event, all waves are observed and a 3D analysis is necessary to separate the waves.

The November 3, 2002 Alaska earthquake (M_s=7.9) gave us the first opportunity to perform such successful remote sensing of Rayleigh waves. A band-pass filter between 150 sec and 350 sec corresponding to a central period of 225 sec close to the Airy phase of Rayleigh waves was applied. Data are here plotted as a function of time and epicentral distance, the latter of which changes with time as a result of the satellites orbital motion [Figure 4a]. We observed a signal two to three times larger than the noise level, arriving about 660-670 sec after the arrival time of Rayleigh waves at the ground. The amplitude of the perturbation varies from satellite to satellite, but the signals are consistent and were observed on 6 others satellites in visibility. The total electron content (about 60 TECU at this local time) is fund to be perturbed by about 0.1% (0.05 TECU peak to peak). We were able to determine, by cross-correlation, the altitude where the signal maximized and to extract from these signals the first group velocity measurement of Rayleigh waves obtained with ground-space measurement techniques, fitting well with the value obtained by tomographic models [4]. Further analysis have been done [5], enabling a 3D tomographic picture of the signals. Movies of the signal can be downloaded [6].

The Hokkaido Tokacho-Oki earthquake of September 25, 2003, gave us another opportunity and spectacular ionospheric waves have been observed. In contrary to the Alaska earthquake observations, these signals are associated to the near-seismic waves and especially to infrasonic waves generated near the source and propagating in the atmospheric wave-guide. (Figure 4b).

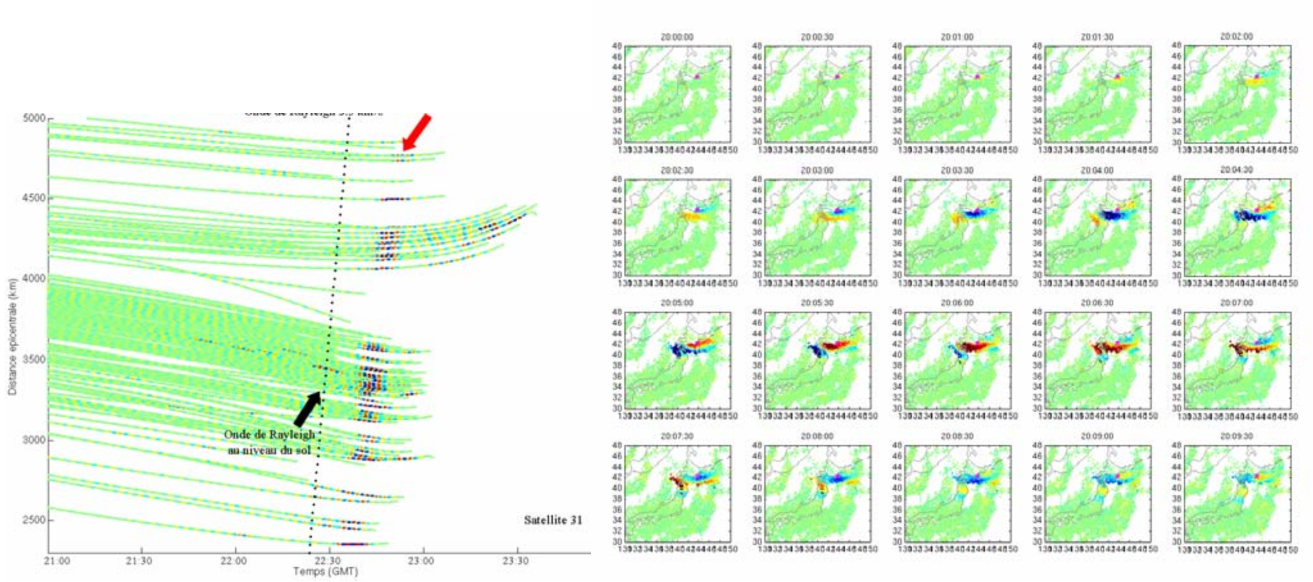

Figure 4: (a) TEC observation of the Denali Surface waves for the records from satellite 31. Each trace is corresponding to a GPS station and the epicentral distance at a given time is the epicentral distance of the sub-ionospheric point. The black arrow shows the arrival time at the ground while the red arrow shows the arrival time at the maximum of ionization. (b) Map of the ionospheric perturbations over Japan after the Hokkaido earthquake. Each map is performed every 30 sec. A spectacular ionospheric perturbation is observed, corresponding mainly to acoustic waves generated by the quake and appears approximately 10 minutes after. The earthquake occurred at 19h50 UT while the first map is at 20h00 UT

5.TSUNAMI DETECTIONS

Tsunami waves propagating across long distances in the open-ocean can induce atmospheric gravity waves by dynamic coupling at the surface. In the period range 10 to 20 minutes, both have very similar horizontal velocities, while the gravity wave propagates obliquely upward with a vertical velocity of the order of 50 m/s, and reaches the ionosphere after a few hours.

We use ionospheric sounding technique from Global Positioning System to image a perturbation possibly associated with a tsunami-gravity wave. The tsunami was produced after the Mw =8.2 earthquake in Peru on June 23rd, 2001 with run-up reaching locally 2–5 m. The tsunami propagated across the Pacific Ocean and was detected on tide gauge measurements along the coast of Japan (International Tsunami Information Center 2001). Numerical simulation predicts a first peak arrival there approximately 21–23 hours after the event (*i.e.* 17:30-19:30 GMT on June 24th), with open-ocean amplitudes between 1 and 2 cm in the Northern Pacific. The tsunami wave was detected on tide gauges in Japan with amplitudes between 10 and 40 cm, 20 to 22 hours after the earthquake. We used data from the GEONET network in Japan to image small-scale perturbations of the Total Electron Content above Japan and up to 400 km off shore [7]. We observed a short-scale ionospheric perturbation that presents the expected characteristics of a coupled tsunami-gravity wave [Figure 5]. This first detection opens new opportunities for the application of ionospheric imaging to offshore detection of tsunamis.

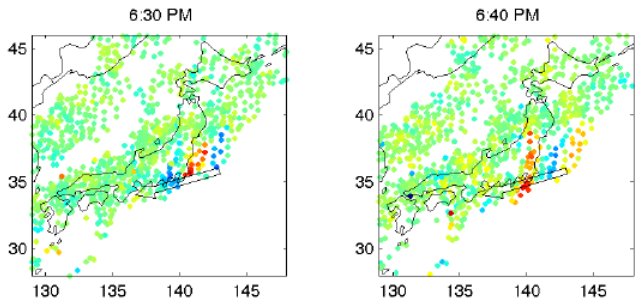

Figure 5. Observed signal: TEC variations plotted at the ionospheric piercing points. A wave-like disturbance is propagating towards the coast of Honshu. This perturbation presents the expected characteristics of a tsunami induced gravity waves, and arrives approximately at the same time as the tsunami wave itself. Peak to peak amplitudes are about 1TECU

3. PERSPECTIVES

These ionospheric signals can be used for several scientific investigations. The first are dealing with ionospheric science and wave propagations. Even if further efforts in the neutral/ionospheric waves coupling modeling remain to be done, the major features of the signals can however be explained by solid earth/atmospheric coupling theories. Another application is related to the early warning of tsunami, in addition with other tsunami warning techniques. The last application can be found for tomographic studies of the lithosphere with surface waves. While the ionosphere is an amplifier for the detection of surface waves, it is indeed not affecting the horizontal propagation of these waves, which depend on the lithospheric seismic velocities at a depth depending on their frequency (about 100 km for 100 sec waves). The determination of the horizontal propagation velocity of the seismic waves can therefore be helpful for lithospheric tomographic studies, especially in Earth's area without dense broadband seismic networks, such as oceans. Such a goal is the objective of a consortium built between the Département de Géophysique Spatiale et Planétaire, at the Institut de Physique du Globe de Paris, the company Noveltis a French scientific engineering company, NOVELTIS and now the Departement Electromagnétique et Radar, at ONERA. This consortium plans to run two major projects. The first project, already operational, is the SPECTRE service based on the processing tools developed for the scientific investigations [8]. SPECTRE will generate the ionospheric products required by the scientific teams. Initially implemented over Europe, SPECTRE will be extended to other regions, its capabilities broaden to troposphere sounding and its products will find many other applications: precise positioning, landslide studies, meteorology. The second project is based on a new concept of detection of seismic waves, based on the Nostradamus overhorizon radar. Based on a mono-static surface array, this radar allows an azimuth coverage of 360° and will map the ionosphere over most of Europe with a resolution of a few m/s in vertical ionospheric velocity and a lateral resolution of less than 10 km This will be a new jump and will allow the possibility to image the seismic waves in the ionosphere. TEC measurements will support this instrument and will provide detailed models of the ionosphere, enabling a better modeling of the radar beams.

Future improvements of the project are foreseen. The first will be achieved by the development of dense network in Japan, USA and hopefully Europe and by the Galileo mission. But dedicated space missions will be necessary for recording these signals over oceans, where the acquisition of seismic signals is the most difficult, especially for short period surface waves (10 s < T < 100s). This is the goal of the ISIS project (Ionospheric Seismic Imaging Satellite), which feasibility is studied by the consortium, together with other French Industries and Europeans partners.

ACKNOWLEDGMENT

This works was funded by the French Ministry of Research (RTE SPECTRE), by ESA under a Space weather pilot project activity and by CNES. We thank CEA/DASE, GSI and the California GPS Networks (SCIGN+BARD+IGS) for providing us with the data. We thank V.Bazin, G.Auffray and S. Saillant from ONERA Nostradamus team and E. Jeansou, J. Helbert from NOVELTIS Co for fruitful discussions.

REFERENCES

[1] Lognonné, P., C. Clévédé and H. Kanamori, Normal mode summation of seismograms and barograms in an spherical Earth with realistic atmosphere, Geophys. J. Int., *Geophys. J. Int.*, **135**, 388-406,1998.

[2] Artru J., P. Lognonné et E. Blanc, Normal modes modeling of post-seismic ionospheric oscillations, *Geophysical Res. Lett.,* **28**, 697-700, 2001.

[3] J. Artru, T. Farges, P. Lognonné, Acoustic waves generated from seismic surface waves: propagation properties determined from Doppler sounding observation and normal-modes modeling. *Geophys. J. Int*., **158**, 1067–1077, 2004.

[4] V.Ducic, J. Artru and P. Lognonné, Ionospheric remote sensing of the Denali Earthquake Rayleigh surface waves, Geophys. Res. Lett., **30(18)**, 1951, 2003

[5] Garcia, R., F. Crespon, V.Ducic, P. Lognonné, 3D ionospheric tomography of the Denali seismo-acoustic waves over California, Geophys. Journal Int., submitted, 2004.

[6]http://ganymede.ipgp.jussieu.fr/~garcia/Denali.Vcut.Az2.movie.mpg.gz

[7] J. Artru,V. Ducic, H.Kanamori, P. Lognonné and M. Murakami , Ionospheric detection of gravity waves induced by tsunamis, submitted to Geophy. J. Int, 2004,

[8] http://ganymede.ipgp.jussieu.fr/projets/spectre/

Philippe Lognonné
DGSP/IPGP, 4 Avenue de Neptune, 94100 Saint Maur des Fossés, France, email: lognonne@ipgp.jussieu.fr

The new view of the short-term earthquake prediction research by using electromagnetic methods

Toshiyasu Nagao

Earthquake Prediction Research Center, Tokai University

ABSTRACT

Despite its extreme importance and decades of efforts, practical short-term earthquake prediction still remains to be achieved in future. However, the electromagnetic research has been demonstrating some promises. This paper reviews the recent progress of what we call "seismo-electromagnetics", mainly referring to Japanese studies.

The electromagnetic studies will play an important role in not only earthquake prediction but also in understanding the physical processes of earthquake generation.

KEYWORDS: earthquake prediction, electromagnetism, volcanic eruption, ULF, electrokinetic, direction finding

Introduciton

To promote the seismo-electromagnetics, the devastating 1995 Kobe earthquake (EQ) was a big impact, because pre-seismic electromagnetic (EM) anomalous changes in different frequency ranges were detected by scientists who were largely working on the problem independently. It was probably the first case where multiple methods detected possible precursors for one EQ (Nagao et al., 2002).

After the Kobe event, former Science and Technology Agency (STA, now MEXT) decided to initiate five year programs of RIKEN International Frontier Research Project on Earthquakes and NASDA Earthquake Remote Sensing Frontier Research Project addressed to the short-term earthquake prediction research by using the electromagnetic methods. The objectives of these projects were to attain comprehensive understanding of the EM phenomena related to EQs, thereby contributing to the establishment of science of their prediction. To verify the validity of the geoelectric potential method, including the so-called Greek VAN method, was one of the specific targets of the RIKEN project. It was also intended to explore other possibilities related with wider frequency EM phenomena. Recently some special issues appeared to focus in this subject (Hayakawa et al. eds., 2004, Hayakawa and Molchanov, eds,., 2002, Hayakawa ed., 2002, Uyeda and Park eds., 2002). One of the important issues raised in the recent years is the possible existence of the ionospheric/tropospheric anomalies before/during/after the major shallow earthquakes (e.g. Fujiwara et al., 2004, Molchanov and Hayakawa, 1998).

In this paper, we would like to introduce the latest progress in this field, mainly referring to the achievements of the both RIKEN and NASDA projects.

1995 Kobe Earthquake

City of Kobe was struck by the M7.3 Hyogo-ken Nanbu earthquake (Kobe EQ) of January 17, 1995. Some possible precursory phenomena have been claimed through post factum analyses of mainly seismicity and hydro-geochemical data (e.g., Tsunogai and Wakita, 1996). Concerning the seismicity change, Huang et al. (2001) demonstrated the existence of a pre-seismic quiescence by applying the RTL algorithm, which disappeared after the EQ.

At the time of Kobe EQ, several groups of scientists were independently engaged with monitoring of electromagnetic field at various frequencies at various sites in Japan. Here, we try to integrate these independent electromagnetic observations by placing them in a common time frame (Nagao et al., 2002).

At the event, a lot of anomalous electromagnetic anomalies possibly related with this EQ were observed. Among these anomalies, the most amazing one was anomalous transmission of man-made electromagnetic waves. This was amazing because some transient disturbances in the ionosphere/troposphere above the focal region would be needed to cause such a transmission anomaly. This subject is now called "Lithosphere-Atmosphere-Ionosphere Coupling problem" and constitutes an up-to-date topic in the URSI (International Union of Radio Science) and other related academic communities. It has shown that this phenomenon is statistically significant (Fujiwara et al., 2004).

On the very day, there are numerous reports on radio/TV noise, lights and other macroscopic anomalies that happened at about the same time. The gist of witness documented through interviewing a truck driver, as an example, is as follows. "Early morning of Jan, 17, Mr. J. Takahashi, who was also a licensed radio engineer, was driving his truck toward Kobe from the west listening to Radio Kansai (558 kHz) as usual. At about 05 o'clock passing Higashi Kakogawa about 30 km west of Kobe, he first noticed unusual noise which increased as approaching Kobe. He tried five other available stations (550 kHz to 1. 6 MHz), but none of them were audible due to noise until he had to abandon his truck at the fierce shock that destroyed the highway he was on. When he returned to the truck after finding out what had happened about 10-20 minutes later, the radio was announcing about the earthquake. There was no strong noise."

All these indicate us that there are still so many factors that are unknown to us, that careful accumulation of more data and enhanced theoretical investigation are needed. The detailed description was made by the author's group (Nagao et al., 2002).

Seismo-Electriomagnetic Phenomena in ULF range

As we mentioned earlier, one of the main objectives of the RIKEN's project was to verify Greek VAN method (e.g., Uyeda, 1996). VAN method is defined as the multi-component ULF electric field measurements (geoelectric potential difference measurement, GPD). VAN method seems to work well in Greece in some extent (e.g., Nagao et al., 1996).

Actually, during the project period (1996-2001), we were able to observe Greek type SES. The main result of GPD was published by Uyeda et al., (2000) and Nagao et al., (2000).

ULF emission before and after large EQs was almost simultaneously discovered in Russia and America on the occasions of 1988 M6.9 Spitak EQ and 1989 M7.1 Loma Prieta EQ (e.g. Frather-Smith et al., 1990). In August 1993, a very large EQ (M8.0) occurred near Guam Island. Hayakawa et al., (1996) found precursory emission of ~ 0.1 nT in 0.02-0.05 Hz band at Guam Island about 60 km from the epicenter. They demonstrated that the use of the ratio (S_Z/S_H), called polarization, is of essential importance in discriminating the seismic emissions from space plasma waves. Here S_Z and S_H indicate the spectral intensities of vertical and horizontal components.

The RIKEN and NASDA projects embarked on three-component ULF magnetic monitoring. As explained below, we have confirmed the existence of ULF changes before EQs mainly through the use of the polarization.

A small L-shaped array has been set with inter-station distance of 5 km in each of the western part of Izu Peninsula and the southern part of Boso Peninsula.

Figure 1 is the global summary of the investigation on the pre-seismic ULF magnetic changes, showing the empirical relationship between M of EQ and epicentral distance of ULF stations. White and black marks show the EQ with ULF anomalies and without ULF anomalies, respectively. The solid line indicates the threshold for appearance of ULF signals. Pre-seismic ULF emissions would be detected for M>5 EQs which roughly satisfy the relationship of R<40(M – 4.5), where R is epicentral distance in km. During the RIKEN and NASDA's study period, there have been 9 EQs which are reasonably expected to show pre-seismic signatures. Out of these, 8 EQs actually showed the anomalies.

It should be emphasized here that pre-seismic anomalies are generally too weak to recognize by looking at raw data and some elaborate data processing is needed. We have found several methods, including polarization analysis, principal component analysis and direction finding technique, are quite useful for this purpose. We have found also that the frequency range of around 0.01 Hz is significant for monitoring crustal activity.

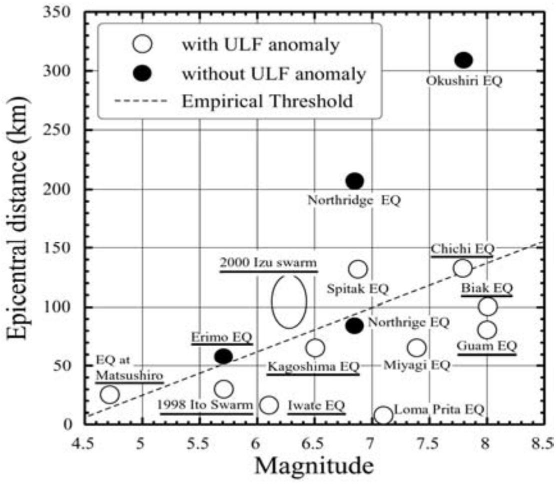

Fig. 1
The relation between magnitude and ULF magnetic anomaly. Dashed line shows an empirical relationship of delectability of ULF anomaly. Underlined EQs are analyzed through the RIKEN/NASDA's projects.

Electric and Magnetic Anomalies Associated with the 2000 Izu Volcanic-seismic Activity, Japan

A swarm seismic activity started on June 26, 2000, simultaneously with the volcanic activity of Miyake-jima Island. Within the three month period of activity, more than 10,000 earthquakes, including some magnitude 6 class EQs, were recorded (Fig. 2).

Through the event, very clear anomalous changes in the ULF range (~ 0.01 Hz) were observed in both geoelectric and geomagnetic fields (Uyeda et al., 2002). The spectral intensity of geoelectric potential difference between some electrodes on Niijima Island and the third principal component of geomagnetic field variations at an array network in Izu Peninsula started to increase from a few months before the onset of the volcano-seismic activity, culminating immediately before nearby magnitude 6 class earthquakes. Appearance of similar changes in two different measurements conducted at two far apart sites seems to provide information supporting the reality of preseismic electromagnetic signals. We would like to explain both records more detail.

Concerning the geoelectric potential changes, usually Niijima Island is electrically almost noise free. From about two months prior to the onset of the activity on June 26, the electric field started to show visually clear innumerable unusual changes, consisting of semi-box shape changes and one to a few minutes oscillations.

The upper part of the Fig. 3a is the three-year records of daily spectral intensity at 0.01-0.0003 Hz band of the GPD measurement.

Concerning the magnetic field changes, there were tripartite geomagnetic differential array networks in both Izu and Boso Peninsulas (Figs. 2 and 5). The spacing between stations was 5-10 km. Each station was equipped with a three-component magnetometer. Extraction of possible seismo-ULF emissions from the array data was made through the principal component analysis (PCA). The north-south component data for the whole period of tripartite observation were used to differentiate the variations due to different sources.

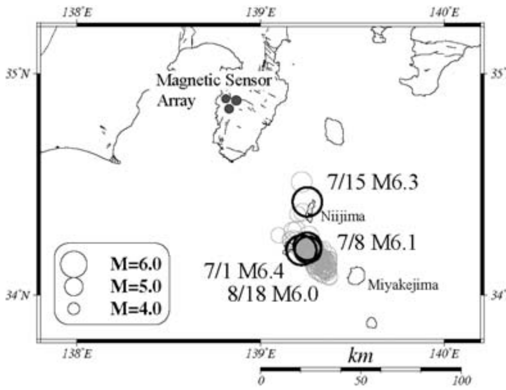

Fig, 2
ULF magnetometer array in Izu Peninsula and Niijima Island, where GPD station had been operated. Some notable seismic activities were also shown.

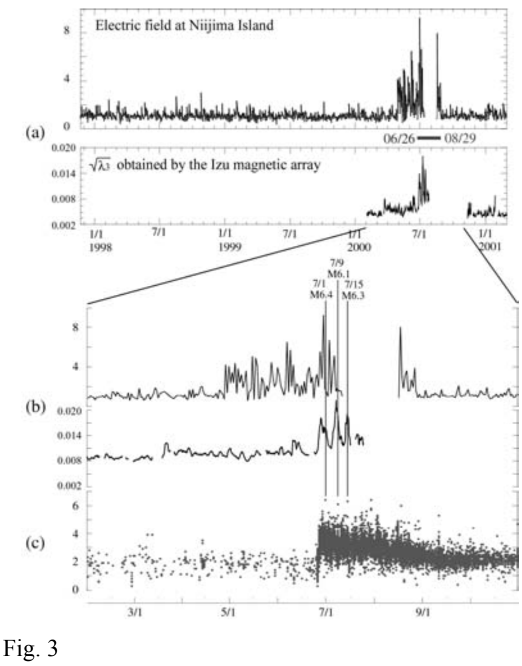

Fig. 3
Time change of the 0.01 Hz spectral intensity ratio of geoelectric potential difference at Niijima Island, and that of the third principal component (λ3) at 0.01 Hz of the geomagnetic field at Izu Peninsula array station. The gap in data was caused by system failure in July and August.
a) For 3-year period records.
b) For January through October, 2000. Three M>6 earthquakes in July are indicated by vertical lines.
c) Seismicity of the Izu Island region by JMA.

After the PCA analysis, the time variation of the first principal component (eigenvalue) is likely solar activity. The change of the second principal component showed very interesting feature, which had a regular daily variation (Fig. 4a) probably related to human activities. During weekdays, there is a lunch-time effect (Fig. 4b), while there is no such effect on Sundays (Fig. 4c). The third principal component is the variation due to causes other than the previous two, possibly including seismo-ULF emission if it exists. Both lower part of the Figs 4b and 4c illustrate the time change of the third principal component.

About three months before the beginning of the swarm activity, the level of the third eigenvalue was slightly enhanced. Correspondingly, the pattern of eigenvector direction in the signal subspace was changed simultaneously and recovered to the original position after the swarm (Hattori, et al., 2004).

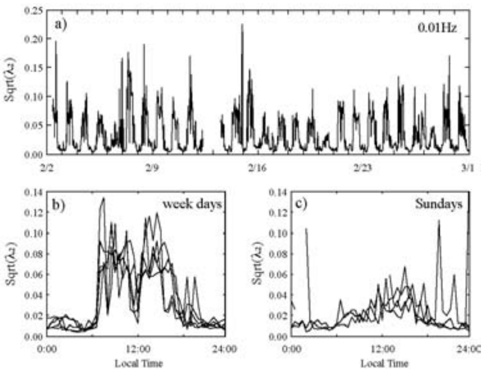

Fig. 4

a) Time change of the second principal component ($\lambda 2$) during 1 month data (February 2000).
b) The diurnal variation of $\lambda 2$ on weekdays. Clear lunch-time effects can be seen.
c) The diurnal variation of $\lambda 2$ on Sundays.

Furthermore, using these array data, two direction finding techniques were developed (Fig. 5; gradient vector method, phase velocity method, e.g. Hattori, 2004). This is basically important, because these techniques are corresponding to hypocenter determination of seismology. Old fashioned what we call “precursory study” only showed temporal relationship.

In summary, we observed that distinct anomalous changes started a few months before the outbreak of the 2000 swarm activity in Izu Island region in both electric and magnetic fields measured at far apart stations. Three component geomagnetic monitoring was conducted by array networks in west Izu Peninsula and south Boso Peninsula, each array consisting of three closely spaced (~5 km) stations with identical sensors. The signals received in the summer of 2000 were coming from the direction of the swarm activity. We think that the observed features are very likely correlated with the swarm.

Other new approaches

In the LF-VLF ranges, almost all past reports only showed temporal correlation between “precursors” and impending EQs.

However, the nature of such signals is still not clear due to insufficient observation data. One reason is that in most cases the waveform is not recorded. Asada et al., (2001) adopted signals in the frequency range from 1 kHz to 10 kHz and recorded waveforms of each signal. It is well known that most of these frequency signals are determined to be atmospherics. Therefore one of the fundamental problems is how to establish the method of delineating signals that are related to EQs from those that are not related to them. One idea is that the location of the source of atmospherics generally changes with time due to the movement of thunderstorm clouds, while signals possibly associated with an EQ appear to be generated in a definite area close to its epicenter. This feature, if established, would be very useful in distinguishing signals related to an EQ from atmospherics.

According to Asada et al. (2001), signals are recorded digitally in waveforms, and the direction of approach is calculated for each signal. They have obtained the results which showed that signals were generated in areas close to the epicenters several days prior to EQ occurrences., i.e., very clear, sharp and the specific waveform emissions came from the future epicentral direction. They also claimed that detectable magnitude was about 5 and depths of EQs were up to 40 km, and the epicentral distances from our recording networks were less than 100 km. EQs which occurred in the ocean floor, smaller EQs (M<4), deeper EQs (D> 50km) and distant EQs (more than 100km) did not generate any clear signals.

In the VLF range, Tsutsui (2002) observed an anomalous signal using the newly designed underground antenna just before the Chi-Chi EQ of Taiwan probably traveled in the underground wave guide for the first time, which was mentioned theoretically more than thirty years ago.

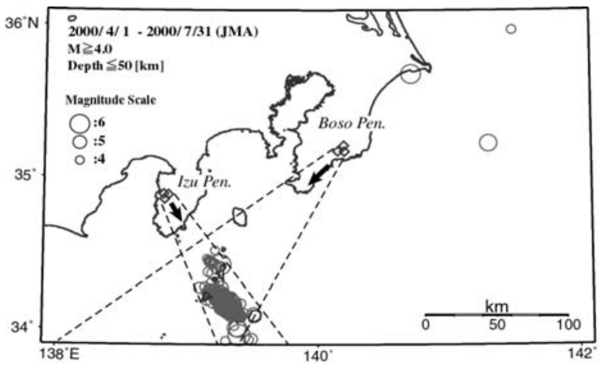

Fig. 5

Location of magnetic array stations and epicenters. Black arrows are the direction of magnetic gradient vectors defined in the frequency ranges of around 0.05 Hz during the period of seismic activity. Dashed lines are gradient cones of the ULF EM source location a few davs before the swarm.

Lithosphere-Atmosphere-Ionosphere (LAI) Coupling

In this section, it is rather unfamiliar and sound curios for ordinal seismologists. However, the author considers it may be a really new category of multidisciplinary science. Last two decades, many reports related to earthquakes and ionosphere disturbances not only before but also during/after large earthquakes (e.g., Gufeld et al., 1994, Molchanov and Hayakawa, 1998).

The coupling includes microfracturing, gas and water diffusion, heat flux and tectonic deformation inside ground media, followed by gas exhalation, changes, in tropospheric conductivity and acoustic-gravity turbulence in atmosphere.

The researches of the anomalous propagation of ionosphere related to earthquakes is energetically doing in the LF, VLF and VHF ranges. They are producing the new concept called LAI (Lithosphere – Atmosphere - Ionosphere) coupling hypothesis. This subject was one of the main scientific themes of NASDA’s frontier project. Recently, a book was published on this subject (Hayakawa and Molcbanov, eds., 2002). Nowadays, the existence of the Lithosphere – Atmosphere - Ionosphere (LAI) Coupling were recognized both observationally and theoretically among the radio science communities (e.g., Pulinets et al., 2003, Pulinets, 2004)).
The ionosphere is affected by many external factors, including solar activity and meteor streams. Their mechanisms are well investigated. On the other hand, the mechanism of seismic ionospheric disturbance is not clear. Researchers have suggested three types of mechanism. They are "Chemical Effects", "Mechanical Effects", and "EM Effects". "Chemical Effects" by anomalous radon emission associated with EQs (e.g. Heincke et al., 1995) assume that the emitted radon molecules arrive at the ionosphere by diffusion and enhance the ionization. In the "Mechanical Effects", it was suggested that weak atmospheric oscillations on the ground surface before the main shocks might

affect the ionosphere. As to the "EM Effects", there are research groups that proposed the existence of the relationship between the static electric field and the localized ionospheric disturbance. Considering all theses possible mechanisms, it seems important to check if there is really a charge at the ground surface before EQs.

EM signal generation mechanisms

This issue is quite important to justify seismo-EM phenomena to the society. In this section, we just introduce recent experiments and theories.

There have been many laboratory studies on electric signals from rock specimens associated with fracture, which suggested that the electric signals are produced by the piezoelectric effect of quartz (e.g., Yoshida et al., 1997), point defects (e.g., Varotsos and Alexopoulos, 1986; Hadjicontis and Mavromatou, 1994), emission of electrons and related models (e.g., Enomoto and Hashimoto, 1990, Fruend, 2002). Besides these mechanisms, the electrokinetic effect has been studied as another plausible origin.

Mizutani et al. (1976) first proposed a model in which during the dilatancy stage, pore pressure in the dilatant region decreases and water flows into this region, generating electric and magnetic precursors to earthquakes due to electrokinetic effects. Since then, many models have been proposed.

Byerlee (1993) proposed a model of a fault zone with a high-pressure fluid, assuming that impermeable seals hydrologically isolate the fault zone from the surrounding country rock. On the basis of Byerlee's model, Fenoglio et al. (1995) evaluated the electric and magnetic fields generated during fault failures and showed that the calculated signals from an appropriate fault length were comparable in magnitude to the magnetic signals observed by Fraser-Smith et al. (1990) prior to the M7.1 Loma Prieta earthquake of 1989.

In laboratory experiments, recently, some data have become available on electric signals due to electrokinetic effects during rock deformation up to failure using triaxial apparatus (e.g. Yoshida et al., 1998). For example, they measured electric potential during rock deformation and found electric potential changes prior to dynamic rupture in saturated rocks, including basalt for which they did not detect precursory signals in a dry situation. They inferred that the signal in saturated rock is caused by accelerating evolution of dilatancy as cracks grow in the rock before rupture, resulting in water flow into the dilatant region with an electric current produced concurrently. In their experiment, however, they did not measure dilatancy itself.

Recently, convection electric current at rock rupture was studied with a specially designed triaxial apparatus with extremely slow strain rate (10^{-10}/s). It has been demonstrated that the convection current flowed before the main fracture, showing good correlation with the dilatancy rate and the water flow rate. The current density was about 1 mA/m2 indicating that the electric current is caused by an electrokinetic effect due to the water flow associated with accelerating evolution of dilatancy before the fracture (Yoshida, 2001).

Summary of this section

We consider that the RIKEN project succeeded to demonstrate the existence of SES even in Japan. However, the only SES data cannot predict impending EQs in a practical sense at least in Japan too. We think that multi-component data acquisition and comparison are the most important.

Last decade, seismo-electromagnetic research has made notable progress not only in Japan. Integration with other disciplines, such as seismology, geodesy, and hydrogeochemistry, will also be the key to the success of seimo- electromagnetrics. Almost explosive rise of seismo-EM is not limited in Japan. Internationally too, the research has made rapid progress. China, France, Greece, Italy, Mexico, Russia, Taiwan and USA are especially active in this field. In France, a satellite called DEMETER (Detection of Electro-Magnetic Emissions Transmitted from Earthquake Region) was launched in June, 2004 for global seismo-EM monitoring. Recognizing this trend, International Union of Geodesy and Geophysics (IUGG) established an Inter-association Working Group on Electro Magnetic Study on Earthquakes and Volcanoes (EMSEV) in 2002.

To establish seismo-EM phenomena, we still need continued efforts to collect and accumulate more data since EQ phenomena are so diverse. In doing so, it will be needed to seek continuously the better way through positive feed back with laboratory and field experiments, theory, and modeling. Simultaneous observation by methods which deal with different frequency phenomena will be essential for making the results more convincing.

Especially to solve physics of DC to ULF/ELF signal generation/transmission now appears more or less tractable, but emergence of VLF to VHF emission from focal zone through conducting earth remains a puzzling question.

Furthermore, role of water in the seismogenic process is also an important issue and EM investigation may be particularly useful in detecting the movement of water in the earth.

Another essential point will be to integrate seismo-EM findings with those of other equally rapidly advancing disciplines, notably seismology, geodesy, hydrology and geochemistry. Only through this approach, seismo-EM will be able to contribute to the understanding of physics of seismicity as a critical phenomenon and gain full credibility from the wide geoscience community and society at large.

Conclusion

This paper introduces the recent progress of the electromagnetic approaches.

Through the past forty years' efforts, we now know “earthquakes” much better than before and also realize that “earthquake” phenomena are exceedingly complex. Recent progress of the digital technology has brought about a lot of progresses in dealing the complex phenomena in many ways. For instance, in seismology, the discovery of non-volcanic tremor in the deep subduction zone is really a product of continuous digital recording of the seismic networks established after the Kobe earthquake. Establishment of the asperity theory is also a very important progress in clarifying the source process of the major interplate earthquakes. .

Concerning the electromagnetic researches, the progress of digital technology is also the key issues. We now know about precursory electromagnetic changes are very small. Therefore, we need sophisticated data processing techniques to discriminate the “real” signal from all kinds of noise contained in the records. Data are gathered in a wide frequency range from DC to VHF and the increasing capacity of a hard disc is the key issue in all these efforts. Now we are able to use giga-bytes of physical memory very easily, which was almost impossible ten years ago. Now it appears that the earthquake prediction study is entering a really new era.

REFERENCES

Asada, T., H. Baba, M. Kawazoe, and M. Sugiura, An attempt to delineate very low frequency electromangnetic signals associated with earthquakes, Earth Planets Space, 53, 55-62, 2001.

Byerlee, J., Model for episodic flow of high-pressure water in fault zones before earthquake, *Geology,* **21**, 303-306, 1993.

Enomoto, Y. and H. Hashimoto, Emission of charged particles from indentation fracture of rocks. *Nature, 346,* 641-643, 1990.

Fenoglio, M. A., M. J. S. Johnston, and J. D. Byerlee, Magnetic and electric fields associated with changes in high pore pressure in fault zones: Application to the Loma Prieta ULF emissions, *J. Geophys. Res.*, *100*, 12,951-12,958, 1995.

Fraser-Smith, A. C., A. Bernardi, P. R. McGill, M. E. Ladd, R. A. Helliwell, and O. G. Villard, Jr., Low-frequency magnetic field measurements near the epicenter of the Ms 7.1 Loma Prieta earthquake, Geophys. Res. Lett., 17, 1465-1468. 1990.

Freund, F., Charge generation and propagation in igneous rocks, J. Geodynamics, 33, 543-570, 2002.

Fujiwara, H., M. Kamogawa, M. Ikeda, J. Y. Liu, H. Sakata, Y. I. Chen, H. Ofuruton, S. Muramatsu, Y. J. Chuo, and Y. H. Ohtsuki, Atmospheric anomalies observed during earthquake occurrences, Geophysical Research Letters, Vol. 31, L17110, doi:10.1029/2004GL019865, 2004

Gufeld, I., Gusev, G., and Molchanov, O., Is the prediction of earthquake dates possible by the VLF radio wave monitoring methods, in *Electromagnetic Phenomena Related to Earthquake Prediction*, Eds. Hayakawa M. and Fujinawa Y., 381-389, Terra Scientific Pub. Co. Ltd., Tokyo, 1994.

Hadjicontis, V. and C. Mavromatou, Transient electric signals prior to rock failure under uniaxial compression. *Geophys. Res. Lett.,* **21**, 1687-1690, 1994.

Hattori, K., A. Serita, K. Gotoh, C. Yoshino, M. Harada, N. Isezaki, and M. Hayakawa, ULF Geomagnetic Anomaly Associated with 2000 Izu Islands Earthquake Swarm, Japan, *Journal of Physics and Chemistry of the Earth*, 29, 425-436, 2004.

Hattori, K., ULF geomagnetic changes associated with large earthquakes, Terrestrial, Atmospheric and Ocean Sciences (TAO), 15, 3, 329-360, 2004.

Hayakawa, M., R. Kawate, O.A. Molchanov, and K. Yumoto, Results of ulutra-low-frequency magnetic field measurements during the Guam earthquake of 8 August 1993, *Geophys. Res. Lett.*, **23**, 241-244. 1996

Hayakawa, M. and O. A. Molchanov, eds., *Seismo Electromagnetics Lithosphere – Atmosphere - Ionosphere Coupling*, TERRAPUB, Tokyo 477pp., 2002.

Hayakawa, H. ed., Seismo Electromagnetics. *Journal of Atmospheric Electricity*, **22, 3** 300pp., 2002.

Hayakawa et al., eds., Physics and Chemistry of the Earth, Vol. 29, issues 4-9, 2004

Heinicke, J., U., Koch and G. Martinelli, CO2 and Radon measurements in the Vogtland area (Germany)- a contribution to earthquake prediction research, *Geophys. Res. Lett.*, **22**, 7, 771-774, 1995.

Mizutani, H., and T. Ishido, T. Yokokura, and S. Ohnishi, 1976 , Electrokinetic phenomena associated with earthquakes, *Geophys. Res. Lett.,* **3**, 365-368.

Molchanov, O. A. and M., Hayakawa, Subionospheric VLF perturbations possibly related to earthquakes, *J. Geophys. Res.,* **103,** A8, 17489-17504, 1998.

Nagao, T., M. Uyeshima, and S. Uyeda, An independent check of VAN's criteria for signal recognition, *Geophys. Res. Lett.* **23,** 1441-1444, 1996.

Nagao, T., Y., Orihara, T. Ymaguchi, I. Takahashi, K. Hattori, Y. Noda, K. Sayanagi, and S. Uyeda, Co-seismic geoelectric potential changes observed in Japan, *Geophysical Research Letters,* **27, 20,** 1535-1538, May, 2000.

Nagao, T., Y. Enomoto, Y. Fujinawa, M. Hata, M. Hayakawa, Q. Huang, J. Izutsu, Y. Kushida, K. Maeda, K. Oike, S. Uyeda, T. Yoshino, Electromagnetic anomalies associated with 1995 KOBE earthquake, *J. Geodynamics*, **33**, 401-411, 2002.

Pulinets, S.A., A. D. Legen'ka, T. V. Gaivoronskaya, V. Kh. Depuev, Main phenomenological features of ionospheric precursors of strong earthquakes, *J. Atmospheric and Solar-Terrestrial Physics*, **65**, 1337-1347, 2003.

Pulinets, S., Ionospheric Precursors of Earthquakes, 316pp., Springer, ISBN: 3-540-20839-9, 2004

Tsunogai, U. and H. Wakita, Anomalous changes in groundwater chemistry, *J. Phys. Earth,* **44,** 381-390, 1996.

Tsutsui, M., Detection of earth-origin selectric pulses, *GRL,* **29,** 8, 10.1029/2001GL013713, 35, 2002.

Uyeda, S., Introduction to the VAN method of earthquake prediction , *A critical review of VAN, World Scientific, London, Singapore,* 3-28, 1996.

Uyeda, S., T. Nagao, Y. Orihara, T. Yamaguchi, and I. Takahashi, Geoelectric Potential Changes : Possible Precursors to Earthquakes, *The proceeding of the National Academy of Sciences, USA (PNAS),* **97, 9,** 4561-4566, April 2000.

Uyeda, S., M. Hayakawa, T. Nagao, O. Molchanov, K. Hattori, Y. Orihara, K. Gotoh, Y. Akinaga, and H. Tanaka, Electric and magnetic phenomena observed before the volcano-seismic activity 2000 in the Izu Island Region, Japan, *The proceeding of the National Academy of Sciences, USA (PNAS),* **vol. 99, No. 11,** 7352-7355, 2002.

Uyeda, S. and S. Park eds., Recent investigations of electromagnetic variations related to earthquakes, Journal of Geodynamics, 33, 4-5, 570pp., 2002.

Varotsos, P. and K. Alexopoulos, *Thermodynamics of point defects and their relation with bulk properties*, 474pp., North-Holland, Amsterdam, 1986.

Yoshida, S., M. Uyeshima and M. Nakatani, Electric potential changes associated with slip failure of granite: Preseismic and coseismic signals, *J. Geophys. Res.,* **102,** 14,883-14,897, 1997.

Yoshida, S., O. C. Clint, and P. R., Sammonds, Electric potential changes prior to shear fracture in dry and saturated rocks, *Geophys. Res. Lett.,* **25,** 1577-1580, 1998 .

Yoshida, S., Convection current generated prior to rupture in saturated rocks, *J. Geophys. Res.*, **106**, B2, 2103-2120, 2001.

Toshiyasu Nagao
Earthquake Prediction Research Center, Tokai University,
3-20-1, Shimizu-Orido, Shizuoka, Shizuoka, 424-8610 JAPAN,
email: nagao@scc.u-tokai.ac.jp

The Micro-Satellite DEMETER

Michel Parrot (1), and the DEMETER experimenters

(1) LPCE/CNRS, Orléans, France

ABSTRACT

DEMETER is a micro-satellite (130 kg) with a low-altitude (710 km) and a nearly polar orbit. The launch by CNES (French National Space Agency) was in June 2004, and the duration of the mission is 2 years. This paper describes the scientific objectives of the mission and the scientific payload. First results are shown.

KEYWORDS: seismo-electromagnetic effects, ionosphere, wave propagation

SCIENTIFIC OBJECTIVES

The experiment onboard the DEMETER micro-satellite is proposed by a group of scientists involved in external and internal geophysics. The list is given in Table 1.

Institutes	Experimenters
LPCE (France)	D. Lagoutte, F. Lefeuvre, M. Parrot, B. Poirier, J.L. Pinçon
CESR (France)	J.-A. Sauvaud, A. Cros
CETP (France)	J.J. Berthelier, M. Menvielle
IPGP (France)	J. Artru, P. Bernard, Y. Cohen, G. Hulot, J.F. Karcewzski, J.L. Le Mouël, P. Lognonné, J.P. Montagner
DESPA (France)	M.Maksimovic
LDG/CEA (France)	E. Blanc, J.L. Plantet
OPGC (France)	J. Zlotnicki
LPSH (France)	A. Kerdraon
Univ. of Electro-Comm. (Japan)	M. Hayakawa
SSD/ESTEC (ESA)	J.P. Lebreton
CBK (Poland)	J. Blecki, J. Juchniewicz

TABLE 1. List of DEMETER experimenters.

The main scientific objectives of the DEMETER experiment are to study the disturbances of the ionosphere due to the seismo-electromagnetic effects, and due to anthropogenic activities (Power Line Harmonic Radiation, VLF transmitters, HF broadcasting stations).

The seismo-electromagnetic effects are the electric and magnetic perturbations caused by natural geophysical activity such as earthquakes and volcanic eruptions. It includes: electromagnetic emissions in a large frequency range, perturbations of ionospheric layers, anomalies on the records of VLF transmitter signals, particle precipitation, and night airglow observations. Such phenomena are of great interest, because they start a few hours before the shock and can be considered as short-term precursors. Electromagnetic emissions in the ULF/ELF/VLF range that are related to seismic or volcanic activity are known since a long time but their generation mechanisms are not well understood. Many papers have presented ground observations of wave emissions during seismic events.

Two types of emissions can be considered:

- First, precursor emissions occur between a few days and a few hours before earthquakes, in a large frequency range from one hundredth Hertz up to several MHz.
- Second emissions observed after the shock generally are attributed to the propagation of acoustic-gravity waves. However, all hypotheses concerning the generation mechanism of precursor emissions are also valid after the shock, when the Earth's crust returns to an equilibrium state.

The emissions can propagate up to the ionosphere, and observations made with low-altitude satellites have shown increases of ULF/ELF/VLF waves above seismic regions. In contrast to ground experiments, satellite experiments cover most seismic zones of the Earth, and statistical studies become meaningful because of the much larger number of recorded events. A simple simulation has shown that, in two years, a polar satellite can fly over 400 earthquakes of magnitude larger than 5, with a track less than 5° in latitude and in longitude from the epicentre and within a time interval between 0 and 5 hours before the shock.

SCIENTIFIC PAYLOAD

The payload of the DEMETER microsatellite allows measuring these waves and also some important plasma parameters (ion composition, electron density and temperature, energetic particles). The scientific payload is composed of several sensors: - Three Electric and three magnetic sensors (6 components of the electromagnetic field to investigate from DC up to 3.5 MHz), - A Langmuir probe, - An ion spectrometer, and, - An energetic particle analyzer. The experiment capabilities are given in Table 2. There are two modes of operation: (i) a survey mode to record low bit rate data, and (ii) a burst mode to record high bit rate data above seismic regions (see Figure 1). In the survey mode the telemetry is of the order of 950 Mb/day, and in burst mode, it is larger than 1 Gb/orbit.

Frequency range, B	10 Hz - 17 kHz
Frequency range, E	DC – 3.5 MHz
Sensibility B :	$2\ 10^{-5}$ nT $Hz^{-1/2}$ at 1 kHz
Sensibility E :	0.2 μV $Hz^{-1/2}$ at 500 kHz
Particles: electrons	30 keV - 10 MeV
Particles: ions	90 keV - 300 MeV
Ionic density:	$5\ 10^{2}$ - $5\ 10^{6}$ ions/cm^{3}
Ionic temperature:	1000 K - 5000 K
Ionic composition:	H^+, He^+, O^+, NO^+
Electron density:	10^{2} - $5\ 10^{6}$ cm^{-3}
Electron temperature:	500 K - 3000 K

TABLE 2. Experiment capabilities.

For the wave experiment the following data will be recorded:

During the Burst mode

- Waveforms of 3 electric components up to 15 Hz,
- Waveforms of the 6 components of the EM field up to 1 kHz,
- Waveforms of 2 components (1B + 1E) up to 17 kHz,
- Spectrum of one electric component up to 3.5 MHz
- Waveform of one electric component up to 3.5 MHz (snapshots).

During the Survey mode

- Waveforms of 3 electric components up to 15 Hz,
- Spectra of 2 components (1B + 1E) up to 17 kHz,
- Spectrum of one electric component up to 3.5 MHz,
- Results of a neurone network to detect whistlers and sferics.

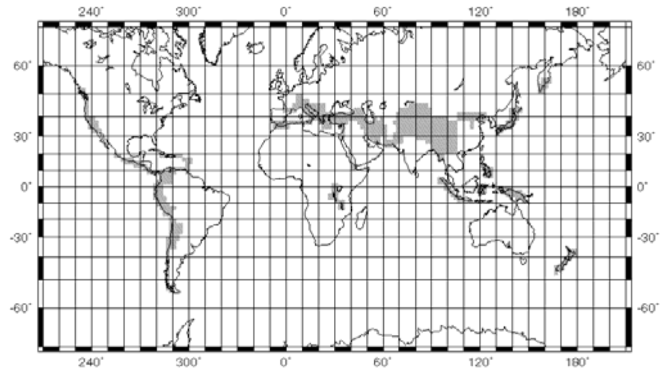

Figure 1: Map of the Earth where locations of the Burst mode are indicated in grey (from Pascal Bernard, IPGP).

For the other experiments, the difference between the Burst and the Survey modes only concerns the time resolution of the data. The number of telecommands is estimated to be of the order of 600 octets/3 days.

The secondary mission of DEMETER is technological. The purpose is to perform in flight validation of

i) an advanced system of payload telemetry incorporating a solid state mass memory of 8 Gbits and an X band transmitter at 16,8 Mbits/s,
ii) a system of autonomous orbit control relying on a GPS receiver and an integrated navigator,
iii) pyro device firing by laser, and
iv) thermal protections performance.

CONSTRAINTS

EMC Constraints

The high level of electro magnetic sensibility required by the payload brought specific constraints on DEMETER:

- Sensors mounted at end of boom, bringing high inertia and low natural modes of the satellite: AOCS laws had to be optimized,
- Equipotentality of the external surface of the satellite: MLI are covered with specific conductive black painting. The solar generator is protected by ITO (Indium Tin Oxyde), coverglasses are interconnected, and any current loop is compensated in order to reduce any generation of magnetic field
- Magnetic shielding of equipment. The reaction wheels are placed in double shells made of µ metal. The electronic box of the star tracker was wrapped in a single sheet of µ metal. Finally local shielding of the OBC was developed.
- Magneto-torquers activation limited to orbital period free from scientific measurements (terrestrial high invariant latitudes > 65° and <-65°)
- Solar generator rotation is stopped when the scientific instruments perform measurement, which is at invariant latitude < 65 °.

Constraints on the mission

DEMETER records data all around the Earth and normally all the time. But it exists some restrictions. Data are not recorded in the auroral zones (invariant latitude > 65°) because the seismic activity is low (except in Alaska), and the large level of the natural noise could be prevent the observations of signal due to seismic activity. Then it is a zone which is reserved for the attitude control of the satellite because magneto-torquers activation perturbs magnetic measurements.

DATA PROCESSING

The data are stored in the large onboard memory which is downloaded when the satellite is above Toulouse (two times per day). Then, the data is sent to the DEMETER mission center in Orléans where various data processing are done. Data and plots are available through a web server (http://demeter.cnrs-orleans.fr). Experimenters and guest investigators have access to the facility of this server in order to download or to display online selected data.

GUEST INVESTIGATOR PROGRAM

Guest investigators have been selected by CNES following an announcement of opportunity. They are meanly performing ground-based experiments and intend to compare their data with the DEMETER data when the satellite flies over the places of these experiments. Other guest investigators intend to realize active experiments (ionospheric heating). Then, the burst zones of DEMETER are extended to allow the data registration when these active experiments are running. The tools for correlation between the epicentres of earthquakes and the orbit of DEMETER which are implemented on the mission center will be presented. We perform correlation with seismic activity using data from the GEOSCOPE network. Quick-Looks of the data are in public access on a WEB site dedicated to the experiment (see Figure 2). Access to full resolution data will be only given to experimenters and "Guest investigators". The data processing center will be also in relation with ground-based experiments. It is expected to have close collaboration with ground-based experimenters performing measurements of DC fields, electromagnetic noise in various frequency bands, ionospheric parameters, optical parameters,.... In Europe, special attention has been paid to Greece and dedicated ground stations have been installed in the Corinth Gulf by IPGP (Institut de Physique du Globe de Paris) and close to La Réunion volcano by OPGC (Observatoire de Physique du Globe de Clermont-Ferrand). The satellite data will give an overview of the ionospheric parameters above the regions where these ground-based measurements are performed. Mutual comparison of all parameters (ground-based and satellite recorded) will allow to understand the generation mechanism of the EM perturbations registered during seismic activity.

RESULTS

Figure 2 is an example of quick-look relative to data recorded on August 23, 2004 between 00.12 and 00.48 UT. Each quick-look corresponds to a half-orbit. From top to bottom, the first line indicates if the experiments are in “burst” mode or in “survey” mode; the three first panels are related to the ICE experiment and represent data in the HF, VLF, and ULF ranges respectively; the fourth panel is devoted to the VLF data of the IMSC experiment, the fifth panel presents data from the neural network, the sixth panel is related to the IDP experiment, the two following panels present data of the IAP experiment whereas the two other panels are devoted to the ISL experiment. The last panel is related to the correlation between the seismic activity and the orbit of DEMETER.

Figure 3 shows data recorded by the micro-satellite DEMETER two days before a M=6 earthquake (09/15/2004 – 19:10:50, Lat = 14.25, Long = 120.42). From top to bottom, the first panel shows an ELF spectrogram of an electric component, the three others represent data from the Langmuir probe: the electron density, the electron temperature, and the ion density respectively, and the last panel displays distances between the satellite and earthquakes occurring along the orbit. The full red triangle indicates the closest approach and perturbations can observed on data recorded by the Langmuir probe and on the electric field at frequency lower than 100 Hz. Due to the curvature of the magnetic field lines which can guide waves, the perturbations are also detected at lower latitudes.

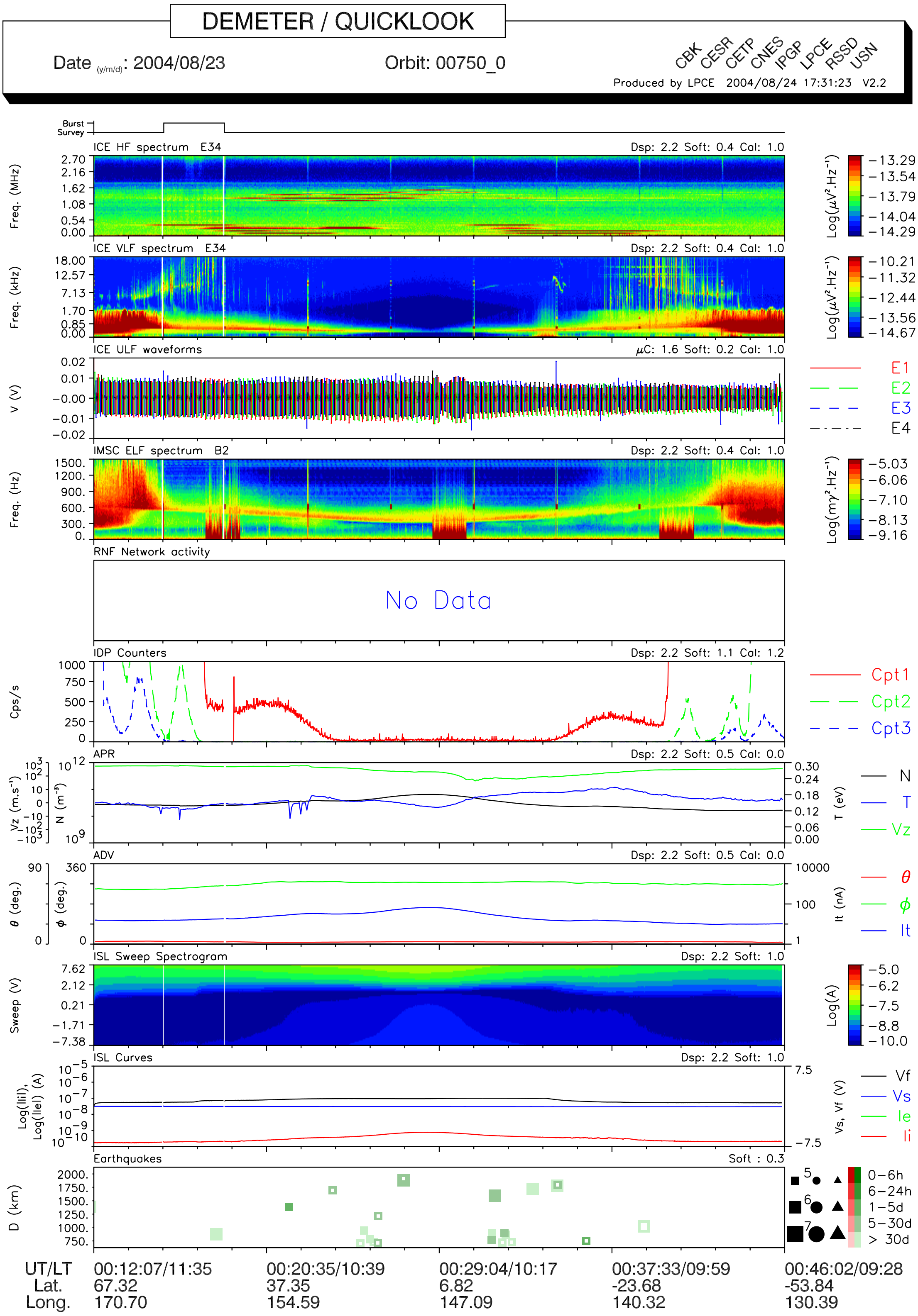

Figure 2. Example of Quick-look showing data recorded by DEMETER. Effects of the wheel desaturation for the control of the attitude of the satellite are clearly seen on the spectrogram of the magnetic components. This has been fortunately suppressed in mid-october.

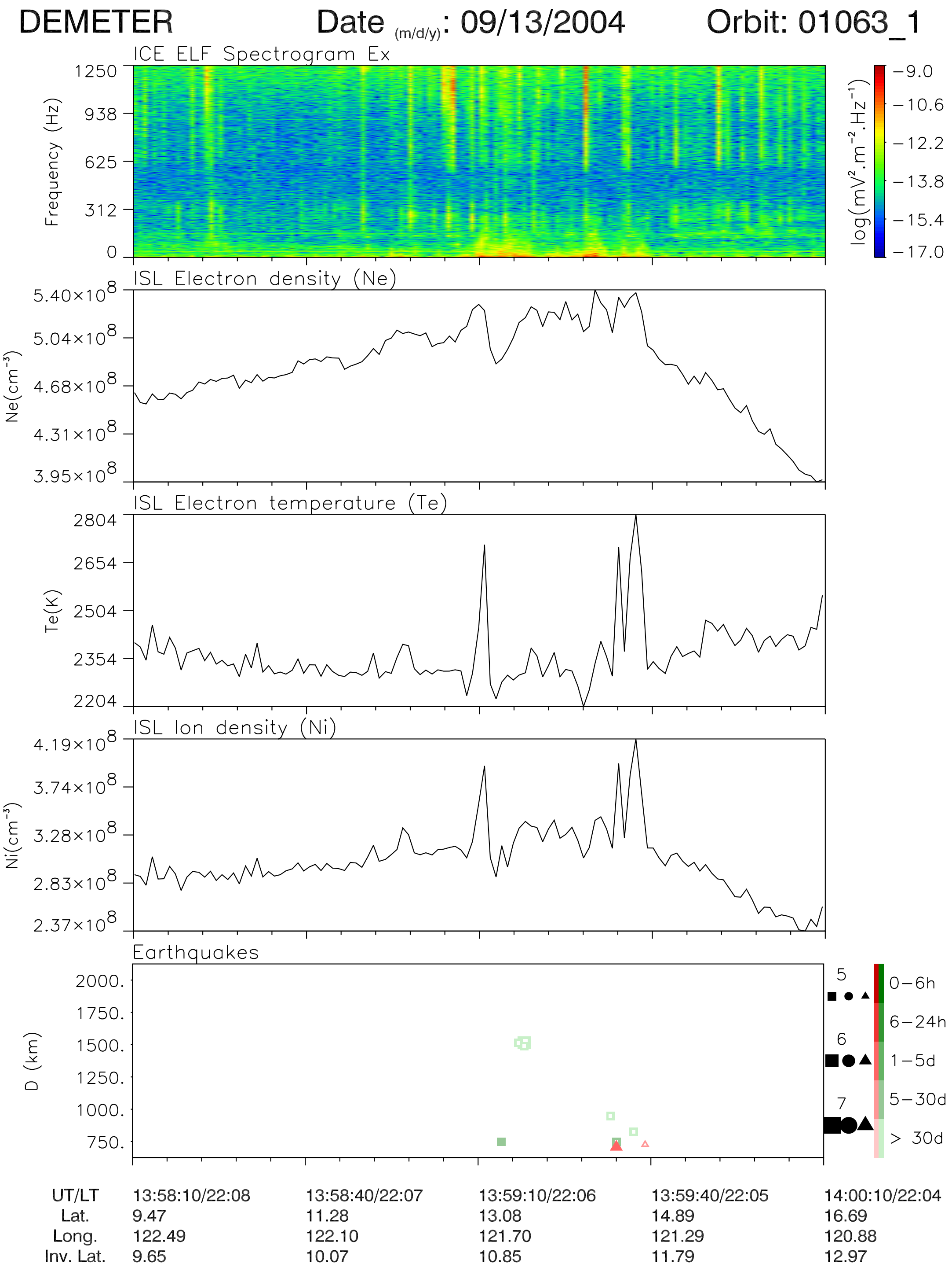

Figure 3. Data recorded by the micro-satellite DEMETER two days before a M=6 earthquake (09/15/2004 – 19:10:50, Lat = 14.25, Long = 120.42). See text for explanations.

CONCLUSIONS

The study of the seismo-electromagnetic effect is the main scientific objective of DEMETER. It is too much earlier to present conclusions because many events are needed to perform a statistic. However, the first data have shown that they are of good quality and usable for scientific analysis.

ACKNOWLEDGMENT

The authors are grateful to Thibery Cussac the DEMETER project manager, and to the numerous people in CNES who worked on DEMETER. They wish to thank Bernard Poirier who was the project manager of the scientific payload before his retirement and Jan Slominski, Witold Nowosielski, and Roman Wronowski (CBK) for their participation to the mission.

Michel Parrot
LPCE/CNRS, 3A Avenue de la Recherche, 45071 Orléans cedex 2, France, email: mparrot@cnrs-orleans.fr

Asperity map along the subduction zone in northeastern Japan inferred from regional seismic data

Yoshiko YAMANAKA

Earthquake Research Institute, the University of Tokyo

ABSTRACT

In an attempt to examine the characteristic behavior of asperities, we studied the source processes of large interplate earthquakes offshore of the Tohoku district, northeastern Japan, over the past 70 years. In this area, earthquakes of M7 class have a recurrence interval of about 30 years. Seismic observation using a strong-motion seismometer has been carried out by the Japan Meteorological Agency since the beginning of the 1900's. We collected these seismograms in order to make a waveform inversion. Based on the derived heterogeneous fault slip, we identified large slip areas (asperities) for eight earthquakes which occurred after 1930, and we constructed an asperity map. The typical size of individual asperities in northeastern Japan is M7 class, and an M8 class earthquake can be caused when several asperities are synchronized. We propose that the patterns of asperity distribution beneath offshore Tohoku fall into three different categories. In the northern part (40°N-41.3°N), the seismic coupling in the asperity is almost 100%, and the size is large. In the central part (39°N-40°N), little seismic moment has been released by large earthquakes, and the asperity size is small. In the southern part (37.8°N-39°N), the seismic coupling is medium. The weak seismic coupling may be related to submarine topographical features and to the sediment and water along the subducting plate. Our results also suggest a general tendency for the asperities to be located away from the hypocenters (initial break), with aftershocks occurring in the area surrounding the asperity.

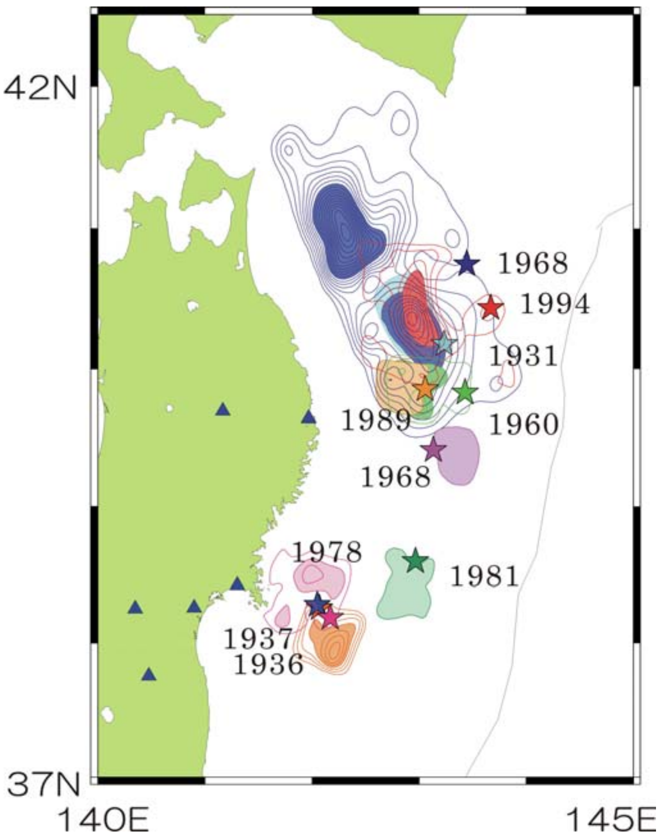

Asperity map along the subduction zone in northeastern Japan. Stars show the mainshock epicenters. Contour lines show the moment release distribution. The interval of the contour lines is 0.5m. Each earthquake is distinguished by color. We painted the area within the value of half the maximum slip as an asperity.

Yoshiko Yamanaka
Earthquake Research Institute, the University of Tokyo.
1-1-1, Yayoi, Bunkyo-ku, Tokyo 113-0032, JAPAN,
email: sanchu@eri.u-tokyo.ac.jp

Strategical Roles of Hydrological Methods in Earthquake Prediction Research

*Naoji Koizumi and Norio Matsumoto

Tectono-Hydrology Research Group, Geological Survey of Japan, Nationnal Institute of Advanced Industrial Science and Technology (AIST)

ABSTRACT

For earthquake prediction, we should strategically use several methods. The hydrological method has not yet given a suitable theory which can adequately explain hydrological precursors of earthquakes. Therefore it is important to clarify the mechanism of earthquake-related hydrological changes and turn the hydrological information into the one which can be easily understood by seismologists. From this point of view, we propose four strategical roles of hydrological methods for earthquake prediction. At present, only the one role, i.e., providing crustal deformation data converted from hydrological changes, can be applied to the practical earthquake prediction. Therefore Geological Survey of Japan (GSJ), Nationnal Institute of Advanced Industrial Science and Technology (AIST), which is responsible for the Tokai earthquake prediction project in the field of hydrology, is investigating hydrologidal changes together with crustal deformation. As the examples, we show the simulation of groundwater level before the Tokai earthquake and groundwater level changes related to the earthquake swarms off the east coast of the Izu Peninsula.

KEYWORDS: earthquake prediction, groundwater, Tokai earthquake, hydrological methods, crustal deformation, strain, groundwater level

1. INTRODUCTION

In order to predict earthquakes, we should strategically use several methods. The hydrological method has recently developed and not yet given a suitable theory which connects preseismic hydrological changes to earthquake occurrences [1]. Therefore it is important to clarify the mechanism of earthquake-related hydrological changes and turn the hydrological information into the one which can be easily understood by seismologists.

From this point of view, we propose following four strategic roles of hydrological methods for earthquake prediction;

(1)Providing crustal deformation data, which is mainly volumetric strain changes, converted from hydrological changes: It is usually useful for the short-term prediction.

(2) Providing information related to temporal changes in permeability in and around active faults: It contributes much to understanding the earthquake-cycle in the active faults and the long-term prediction as a result [2, 3].

(3) Providing information related to displacements of surface caused by groundwater level changes: Since it contributes to improving S/N ratio in the geodetic measurement such as GPS observation, it is

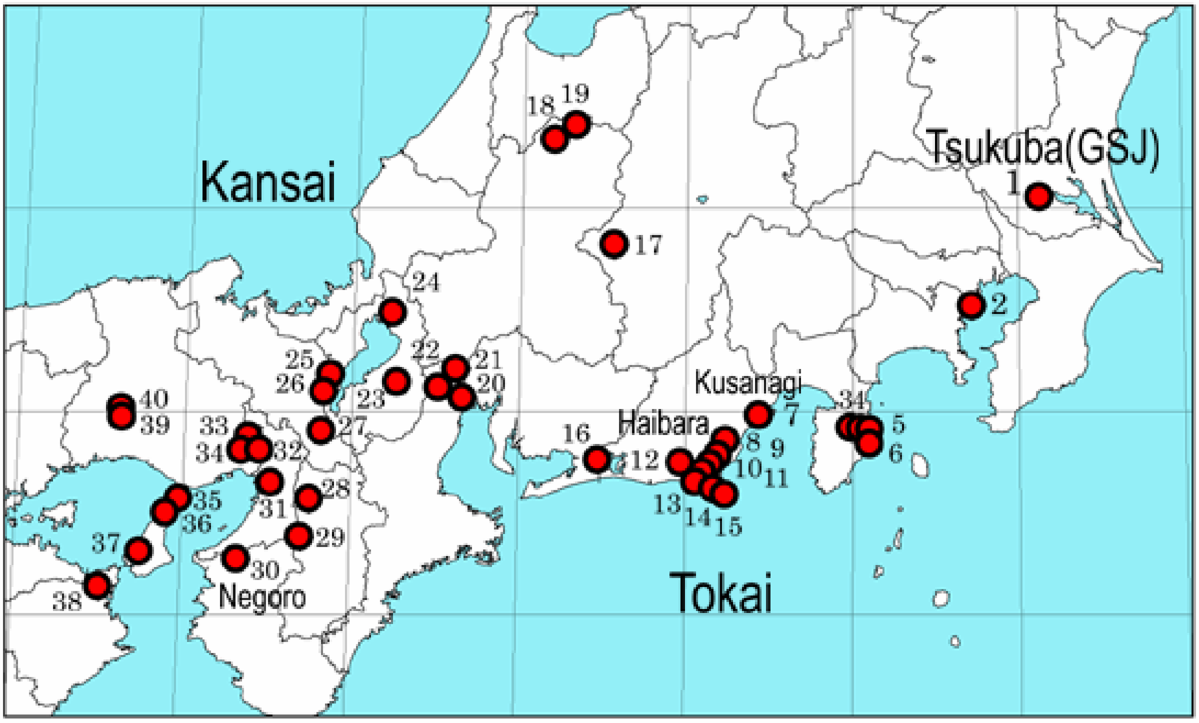

Figure 1. Distribution of the observation wells of Geological Survey of Japan, AIST.

useful for the mid-term or long-term prediction. Quantitative evaluation of changes in relative heights caused by shallow groundwater level changes induced by non-tectonic reason was preliminary carried out by Matsumoto (1996)[4] and Ohtani et al.(2000) [5]. This has been recently investigated by Geographical Survey Institute, which is officially responsible for GPS observation in Japan [6]. It has also been popular to research the relationship between post-seismic crustal deformation and pore-pressure changes [7].

(4) Providing the information of pore-pressure changes in the deep place: Although the depths of observation wells or observable groundwaters are usually smaller than 1 km, those of seismic regions are larger than a few kilometers. Therefore it has not been well developed to estimate pore-pressure in the seismic region by direct observation of groundwater. Hydrological researches in the thermal regions, where shallow seismicity is often active and the information of deep groundwaters or thermal waters is usually rich, may make some progress in this field [8].

At present, only the first one can be quantitatively discussed related to earthquake fault models based on poro-elastic theory [9] and applied to the practical earthquake prediction such as a national project of the Tokai earthquake prediction. Therefore we will discuss mainly about the first role in this paper related to the hydrological research of Geological Survey of Japan (GSJ), AIST, which has a groundwater observation network composed of about 40 stations in the Tokai, Kansai and surrounding areas (Figure 1). Only GSJ is responsible for the Tokai earthquake prediction project in the field of hydrology.

2. MODELS

At present there are 2 possible models which can explain hydrological precursors. One is a 'strain model',and the other is a 'crack model'.

We think a simple confined aquifer model. A water-saturated porous elastic medium, which is the confined aquifer, is sandwiched between two impermeable layers (Figure 2). Based on this configuration, we will introduce the above two models.

2.1 Strain model

When the aquifer is stressed, it is deformed or strained and the pore pressure in it is changed. As a result, groundwater level (sometimes groundwater discharge) will be changed (Figure 2). When the volumetric strain is increased or decreased, the groundwater level falls or rises. So the sense of the changes in water level is opposite to the changes in strain. Therefore strain sensitivity of the groundwater level is usually expressed as a negative value.

In some sensitive wells, stresses from earth tides and atmospheric loading can change groundwater levels. So in such wells we can estimate the strain sensitivity. Ignoring the frequency dependence of the goundwater's response to volumetric strain changes, 10^{-8} in volumetric strain change corresponds to 0 - 10 mm in water level changes. Both poroelastic theory [9] and observational results support this sensitivity. In this way quantitative estimation can be easily made in this model.

2.2 Crack model

The second model is a ' crack model' (Figure 3). When the aquifer is stressed, it is also possible that new cracks are generated or present cracks are open or closed. It will cause changes in the physical properties of the aquifer such as permeability, porosity and so on, which will next change the groundwater level or discharge. This crack generation also enables the groundwater to enter or leave the aquifer (Figure 3). Therefore this model can explain not only changes in groundwater level or discharge but also those in groundwater temperature or chemistry more easily than the strain model. But quantitative estimation in this model is difficult because usual stress sources like the atmospheric loading and earth tides are not thought to generate cracks. Since changes in the physical properties of the aquifer should affect the strain sensitivity of the groundwater, it is also important to compare the groundwater changes with the crustal strain changes in view of developing the crack model.

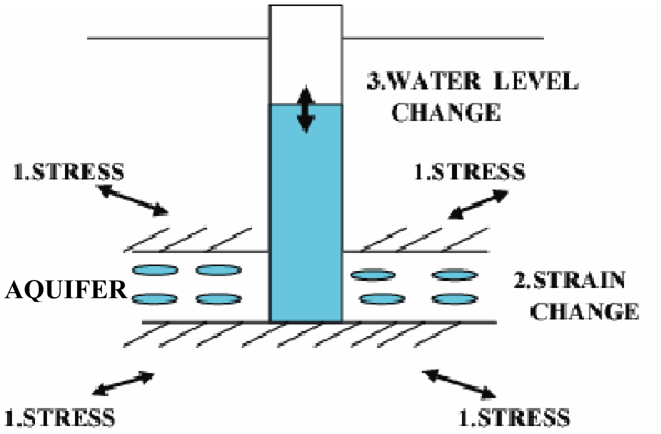

Figure 2. Strain model.

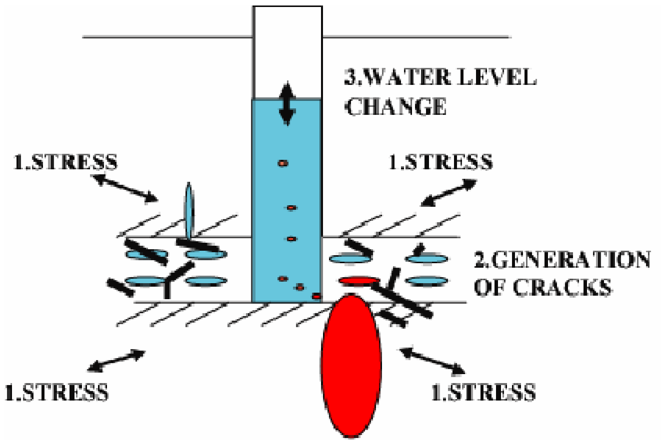

Figure 3. Crack model.

3. OBSERVATION

The Geological Survey of Japan (GSJ) has a groundwater observation network composed of about 40 stations as mentioned above (Figure1). The depths of them are 130m-1000m and those of the screens are 100m-800m. It is the best groundwater observation network for earthquake prediction research in Japan. All of the wells have water level meters and some of them also have water temperature meters , borehole-type strain meters, GPS receivers and gas monitoring systems and the observational data are telemetered to GSJ in Tsukuba (Figure1) and exibited in http://gxwell.aist.go.jp/ GSJ_E/.

The 10 stations in and around the Tokai area, whose numbers in Fig.1 are from 7 to 16, were established mainly for prediction research for the impending Tokai Earthquake [4]. The 4 stations, whose numbers are from 3 to 6, are motivated by the seismic activity in and around the Izu Peninsula, especially the earthquake swarms. Some of these 14 stations were established more than 20 years ago. The other 24 stations mainly in and around the Kansai area, whose numbers are from 17 to 40, are situated along active faults and made for prediction research for inland shallow earthquakes. They were installed after the 1995 Kobe earthquake.

4. RESULTS

As mentioned above, only the strain model can quantitatively deal with earthquake-related groundwater level changes now. Therefore we would like to introduce the estimated groundwater level change related to the Tokai earthquake based on the strain model. After that we will also introduce the results of the groundwater level change related to the earthquake swarms off the east coast of the Izu Peninsula [10, 11]. It is an actual example which can be explained by the strain model

.

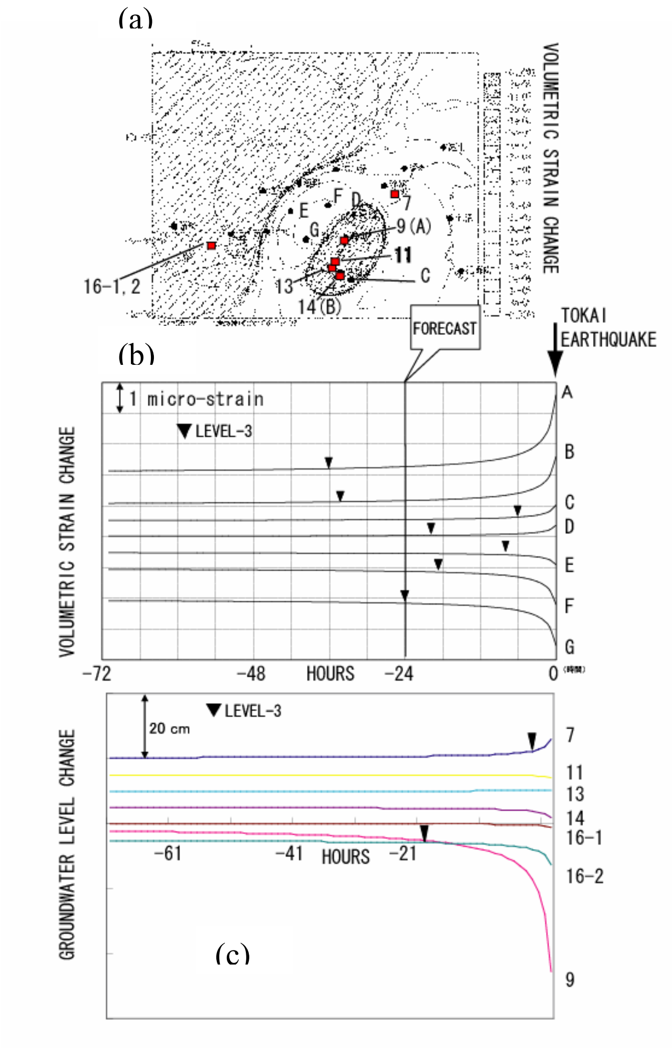

Figure 4 (a) Location of the observation station (● : JMA strain station; ■ : GSJ groundwater station) , (b) simulated volumetric strain changes and (c) well-water level changes corresponding to the assumed pre-slip of a magnitude of 6.5 just under the No.9 well or Haibara well where the volumetric strain meter of JMA(Japan Meteorological Agency) is also set. In this case the pre-slip is assumed to start 3 days before the Tokai earthquake. ▼ means that the changes in the volumetric strain and well-water level exceed twice the usual noise levels. It is called the change of "level-3". Figures (a) and (b) are modified from JMA (2003)[12].

4.1 Estimated groundwater level changes before the Tokai earthquake

At present, the most hopeful precursor of earthquake is the small crustal deformation caused by a pre-slip or aseismic slip near the focal region just before the earthquake. Japan Meteorological Agency (JMA), which is responsible for prediction of the Tokai earthquake, recently developed the method to estimate and detect the crustal deformation that will be caused by the pre-slip for the Tokai earthquake using the data of JMA's volumetric strain meters in and around the Tokai area (Figure.4).

Based on the strain model, the well-water level changes can be regarded as the volumetric strain changes if the strain sensitivity is large enough and the well-water level changes caused by the other factors are adequately eliminated. Therefore we can analyze these well-water level data by the same method as JMA's and estimate and detect precursory well-water level changes [13]. Figure 4 shows that some strain-sensitive wells of GSJ have enough ability to detect the pre-slip.

4. 2 Preseismic changes in groundwater level and volumetric strain associated with earthquake swarms

The Izu Peninsula is situated at a collision zone among the Eurasian, Philippine Sea and North American plates (Figure 5). Earthquake swarms have often occurred off the east coast of the Izu Peninsula since 1978. These swarms are inferred to be caused by magma intrusion [14]. Because of the frequent seismic activities and tectonic importance of this area, many kinds of observations have been conducted by various institutions [15].

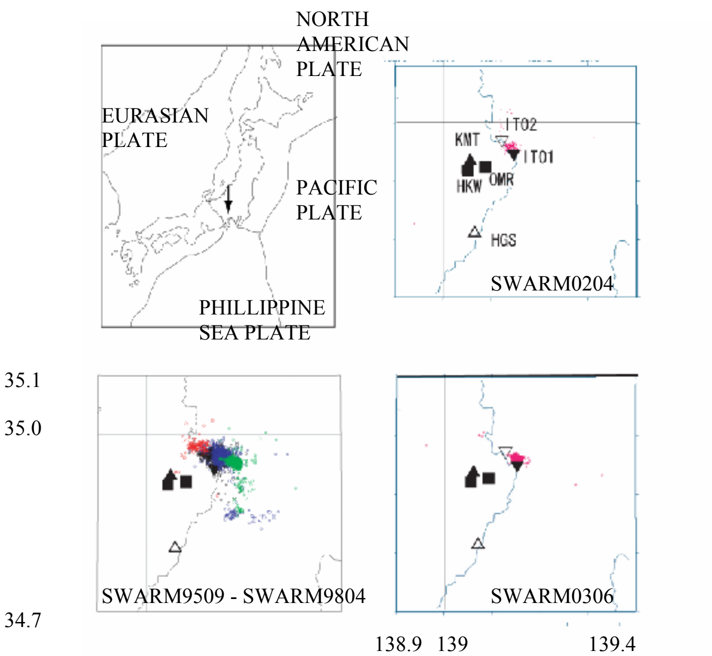

Figure 5 Location of observation stations and epicenter distribution of the six earthquake swarms off the east coast of Izu Peninsula, Japan (Table 1). Depths of the earthquakes are 30 km or shallower.■(OMR): No.5 well in Fig.1, ■(HKW): No.4 well in Fig.1, ▲(KMT): Kamata seismic station of JMA, △(HGS): Higashi-Izu strain station of JMA, ▼(Ito 1): Tilt station of National Research Institute for Earth Science and Disaster Prevention, ▽(Ito 2): Strain and tilt station of Earthquake Research Institute, University of Tokyo.

GSJ has observed groundwater at several wells on the Izu-Peninsula since 1976. Observations at OMR, which were initiated in October 1994, are the nearest to the earthquake swarm regions among the GSJ observation wells. The strain sensitivity of groundwater level at OMR is about - 0.3 cm/10^{-8}strain calculated from its tidal fluctuations. KMT is the nearest permanent seismic

Table 1 Six major earthquake swarms* off the east coast of the Izu Peninsula since October 1994

Date Start	Date End	No. of Events	Strain change** (micro-strain)	Name
Sep.29,1995	Oct.28,1995	9,078	-0.8	SWARM 9509
Oct.15,1996	Nov.10,1996	6,005	-0.5	SWARM 9610
Mar.3,1997	Mar.26,1997	9,334	-0.6	SWARM 9703
Apr.20,1998	Jun.2,1998	11,033	-1.0	SWARM 9804
May 8,2002	May 15,2002	399	-0.2	SWARM 0205
Jun.13,2003	Jun.21,2003	641	-0.1	SWARM 0306

* Events of the six swarms, which were observed at KMT in Figure 5, were greater than 500 or absolute value of related volumetric strain changes at HGS was 0.2 micro-strain or greater.
** Volumetric strain change at HGS in Figure5.

stations of JMA and HGS is also one of the nearest strain stations of JMA, where a borehole-type volumetric strain meter is set.

Since October 1994 there have been six relatively large earthquake swarms (Table 1). We have found four preseismic groundwater level changes at OMR together with corresponding volumetric strain changes at HGS [11].

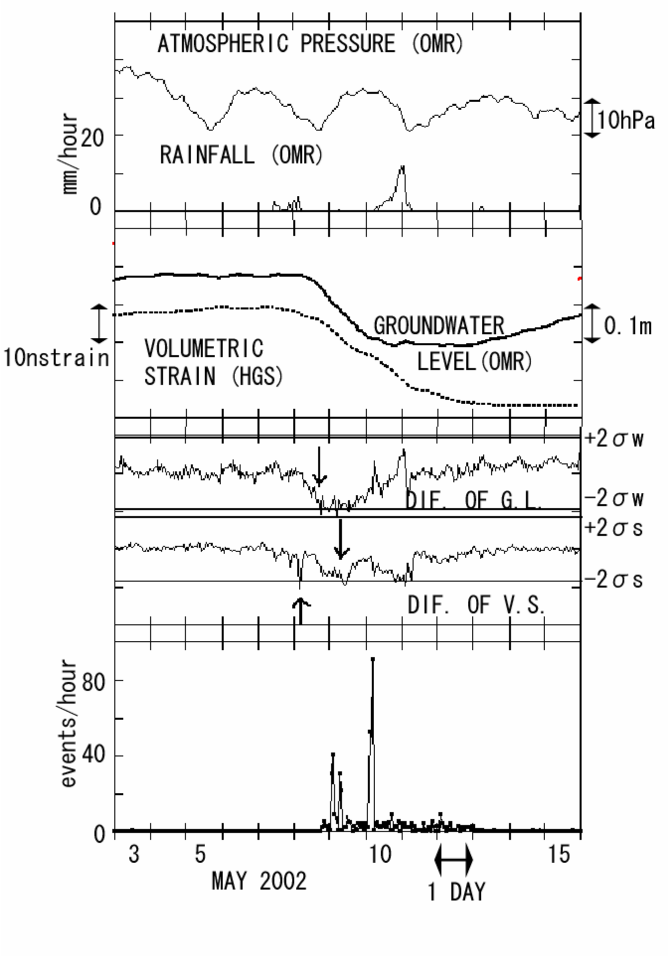

Figure 6 Observation results before and during Swarm 0205 as typical examples. The tidal and barometric effects are eliminated in the groundwater level at OMR and volumetric strain at HGS. The short-term rainfall effects are also eliminated in the groundwater level at OMR. 'nstrain ' means 10^{-9} strain. 'DIF. OF G.L.' and 'DIF. OF V.S.' mean hourly difference values of the groundwater level at OMR and volumetric strain at HGS, respectively. As to the volumetric strain data at HGS, linear trend was removed. The downward arrows indicate the first occurrences when the earthquake-related changes in the difference reached twice the standard deviation (σw,σs). The upward arrow indicates rainfall's effect on the volumetric strain data.

Figure 6 , which is the result before and after the earthquake swarms in May 2002 named Swarm 0205 shows the typical result of the preseismic changes at OMR. Groundwater level drops exceeded twice the standard deviation a few hours before the earthquake swarms started. We four times detected such preseismic groundwater level drops in the 6 earthquake swarms. In the other 2 cases, we could not detect preseismic changes due to large rainfall-induced groundwater level changes or to insufficient magnitude of the swarms.

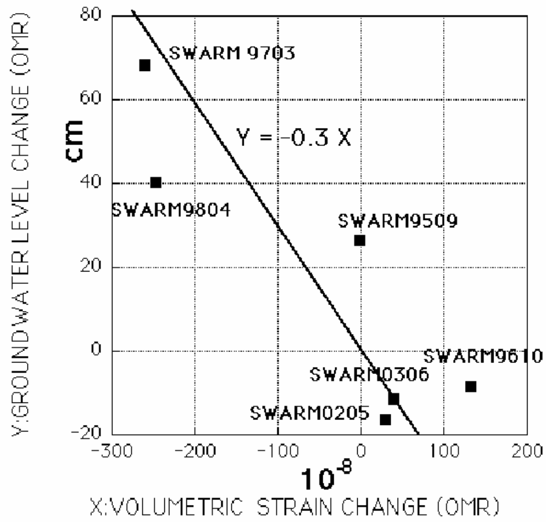

Figure 7 Comparison of the total theoretical volumetric strain changes to the total observed earthquake-related groundwater level changes at OMR. The straight line shows the strain sensitivity of the groundwater level at OMR estimated from the tidal fluctuations.

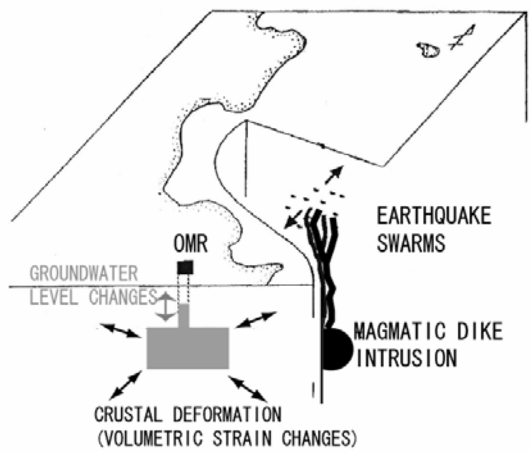

Figure 8 Schematic figure of the mechanism of the earthquake swarms, related crustal deformation and groundwater change.

Figure 7 compares the total earthquake-related groundwater level changes to the volumetric strain changes at OMR calculated from the fault models which were mainly estimated from the geodetic data such as GPS, which are independent of the groundwater level data at OMR. The total earthquake-related groundwater level change at OMR is estimated by subtracting the observed value just before the start of the preseismic or coseismic changes from the value when the swarm ended. The earthquake-related groundwater level changes seem to relate well to the theoretical volumetric strain changes at OMR and can be explained by the strain sensitivity of - 0.3 cm/10^{-8} strain.

The earthquake swarms off the east coast of the Izu Peninsula have been considered to be caused by magmatic dike intrusions as mentioned above. These dike intrusions are inferred to start generating the earthquake swarms after they come up to about 10 km depth. Therefore the dike intrusions at deeper places should cause only crustal deformation[15], which can next induce groundwater anomalies. We think that if a dike were large and close enough to OMR it could cause detectable changes in the groundwater level at OMR (Figure 8). This is supported by the fact that the crustal deformation before these earthquake swarms was also observed at Ito1 and Ito2 (Figure 5) [15,16].

These preseismic groundwater level changes in relation to earthquake swarms off the east coast of the Izu Peninsula probably represent the first case in the world that can be quantitatively explained by the strain model. It also gives some hope for general earthquake prediction by hydrological methods based on the strain model.

5.CONCLUSION

At present, providing crustal deformation data converted from hydrological changes is strategically important for hydrological research for earthquake prediction.: Using the strain model, we can turn volumetric strain changes into groundwater level changes or groundwater level changes into volumetric strain changes on the contrary. The examples are the simulation of groundwater level before the Tokai earthquake and the groundwater level changes related to the earthquake swarms off the east coast of the Izu Peninsula Therefore investigating hydrologidal changes together with crustal deformation is very important.

REFERENCES

[1] Koizumi, N., Review of geochemical research for earthquake prediction (In Japanese with English abstract, J.Jap.Soc.Natural Disas.Sci., 16, pp.41-60（1997）

[2] Kitagawa, Y., K.Fujimori and N.Koizumi, Tempral change in permiability of the rock estimated from repeated water injection experiments near the Nojima Fault in Awaji Island, Japan, Geophys.Res.Lett., 29, 10, pp.121-1 - 121-4, 2002.

[3] Sato, T., R. Sakai, K. Furuya and T. Kodama, Coseismic spring flow changes associated with the 1995 Kobe earthquake, Geophys. Res. Lett., 27, pp.1219-1221, 2000.

[4] Matsumoto, N., Groundwater level changes in Tokai region- Comparison to earthquake and crustal deformation- (In Japanese), Chikyu Monthly, Special Issue No.14, pp.33-41, 1996．

[5]Ohtani, R., N. Koizumi, N. Matsumoto and E. Tsukuda, Preliminary results from permanent GPS array by the Geological Survey of Japan in conjunction with groundwater-level observations, Earth Planets Space, 52, pp.663-668, 2000.

[6]Munekane, H., M.Tobita and K.Takashima, Groundwater-induced vertical movements observed in Tsukubva, Japan, Geophys. Res.Lett., 31, L12608, doi:10.1029/2004GL020158, 2004.

[7]Jonsson, S., P.Segall, R.Pedersen and G.Bjomsson, Post-earthquake ground movements correlated to pore-pressure transients, Nature, 424, pp.179-183, 2003..

[8]Roeloffs, E., M.Sneed, D.L.Galloway, M.L.Sorey, C.D.Farrar, J.F.Howle and J.Hughes, Water-level changes induced by local and distant earthquakes at Long Valley caldera, California, J.Volc.Geotherm.Res.,127, pp.269-303, 2003.

[9]Roeloffs, E., Poroelastic techniques in the study of earthquake-related hydrologic phenomena, in Advances in Geophysics, edited by R.Dmowska, Academic ,San Diego, Calif., pp.135-195, 1996.

[10]Koizumi, N., E. Tsukuda, O. Kamigaichi, N. Matsumoto, M. Takahashi and T. Sato, Preseismic changes in groundwater level and volumetric strain associated with earthquake swarms off the east coast of the Izu Peninsula, Geophys.Res.Lett., 26, pp.3509-3511, 1999.

[11]Koizumi N., Y. Kitagawai, N. Matsumoto, M. Takahashi, T. Sato, O. Kamigaich and K. Nakamura, Pre-seismic groundwater level changes induced by crustal deformations related to earthquake swarms off the east coast of Izu Peninsula, Japan, Geophys.Res.Lett., 31, L10606, doi:10.1029/2004GL019557, 2004.

[12]Japan Meteorological Agency, New system for forecast of the Tokai earthquake (in Japanese), http://www.jma.go.jp/JMA_HP/jma/press/0307/28a/20030728tokai.pdf, 2003.

[13]Matsumoto, N., M.Takahashi, Y. Kitagawa and N.Koizumi, Detectability of slow slip before the anticipated Tokai earthquake by groundwater level monitoring network of GSJ, AIST, Programme and Abstracts of the Seism.Soc.Jap. 2003, Fall Meeting, P129, 2003.

[14]Shimazaki, K., Dyke intrusion hypothesis at east off Izu Peninsula (abstract in Japanese), Programme and abstracts of the Seismol. Soc. Jpn. 1988 Spring Meeting, No.1, 220, 1988.

[15]Okada,Y., E. Yamamoto and T. Ohkubo, Coswarm and preswarm crustal deformation in the eastern Izu Peninsula, central Japan, J.Geophys.Res., 681-692, 2000.

[16]Ishii, H., S. Nakao, S. Matsumoto and Y. Hirata, Precursory variation of Ito earthquake swarms observed by multi-component borehole instrument (in Japanese), paper presented at the symposium of continuous observation of crustal deformation in the deep place, Chiba, Japan, Oct. 17 to Oct. 18, 1998.

Naoji Koizumi
Tectono-Hydrology Research Group, Geological Survey of Japan, AIST,
Site C-7, 1-1-1Tsukuba Ibaraki, 305-8567, JAPAN,
email: koizumi-n@aist.go.jp

Active faulting and earthquake hazard in the Marmara Sea region: A summary

B. Meyer* (1), R. Armijo (2)

(1) Laboratoire de Tectonique, Université Pierre et Marie Curie, Paris, France
(2) Laboratoire de Tectonique, Institut de Physique du Globe, Paris, France

The Sea of Marmara is a major feature of the North Anatolian Fault (NAF) system (Figure 1). However, its present kinematics and the mechanisms responsible for its formation remain debated. Three different classes of models have been proposed. The recent structures in the Sea of Marmara result mainly from (1) distributed Aegean extension (Parke et al., 2002), (2) strike-slip along a single throughgoing fault (e.g., Le Pichon et al., 2001, 2003) or (3) pull-apart extension across a step-over of the NAF (Armijo et al., 1999, 2002). Assessment of seismic hazard in the city of Istanbul, which is located close to the Northern shore of the Maramara Sea, is not independent issue. The contrasting models seem partly to reflect disagreement about the observations needed to retrieve the first-order kinematics.

Geological and morphological features are critical to determine the overall kinematics of the Marmara Sea region. On land, they provide evidence for long-lived localized deformation and for the step-over geometry of the Marmara fault system. Unambiguous geological right-lateral offsets constrain the amount of finite displacement across Marmara (Figure 2, Armijo et al., 1999). Offshore, seismic sections demonstrate long-lived extensional subsidence across deep sedimentary basins in the step-over. The offset submarine morphology provides the detailed geometry of the active fault system, shows pull-aparts at a range of scales (Figure 3) and implies a kinematics similar to that required over the long-term. Microbathymetric surveys of the submarine faults highlight recent breaks consistent with the morphology and the fault kinematics.

Both the short- and the long-term kinematics prove consistent with the broader motion of Anatolia extrusion as derived from space geodesy (McClusky et al., 2000), but require asymmetric slip partitioning within the Sea of Marmara (Flérit et al., 2003). Such an asymmetry seems to have persisted throughout the formation of the pull-apart and can be used to model the details of the GPS data. Aegean extension is not required to reconstruct the geology, nor to model the GPS. A throughgoing strike-slip fault may locally explain the GPS data but is inconsistent with the extensional Marmara stepover.

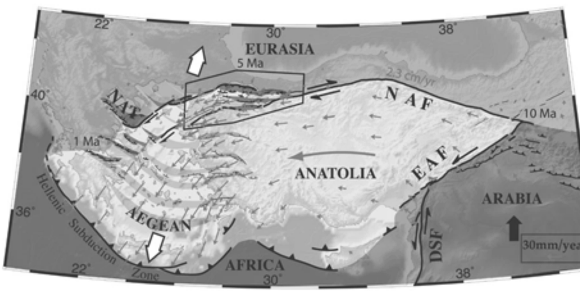

Figure 1. Tectonic setting of continental extrusion in eastern Mediterranean, modified from Armijo et al (1999). Anatolia-Aegea block escapes westward from the Arabia-Eurasia collision zone, toward Hellenic subduction zone. EAF - East Anatolian fault, DSF - Dead Sea fault, NAT – North Aegean Trough. GPS vectors are from MacClusky et al. (2000). In western Turkey, the North Anatolian Fault (NAF) splays westward into two main branches 100 km apart that form a large extensional step-over. Box locates the Northern Sea of Marmara detailed in Figure 2.

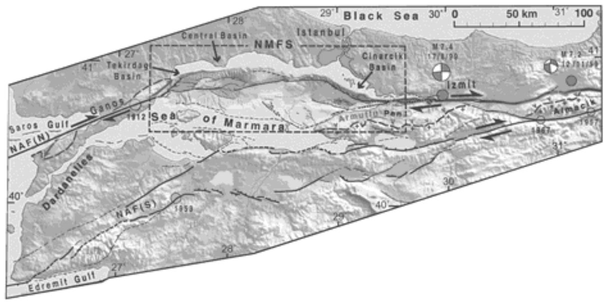

Figure 2. The Sea of Marmara pull-apart system form Armijo et al. (2002). Whithin the large extensional step-over delineated by the Northern and southern branches, a smaller pull-apart called North Marmara Fault System (NMFS) interconnects deep basins with the Ganos and Izmit strike-slip faults onland. Offset geologic markers are indicated east (contact between eocene volcanites and basement) and west (Dardanelles folds) of the NMFS. Box locates Figure3

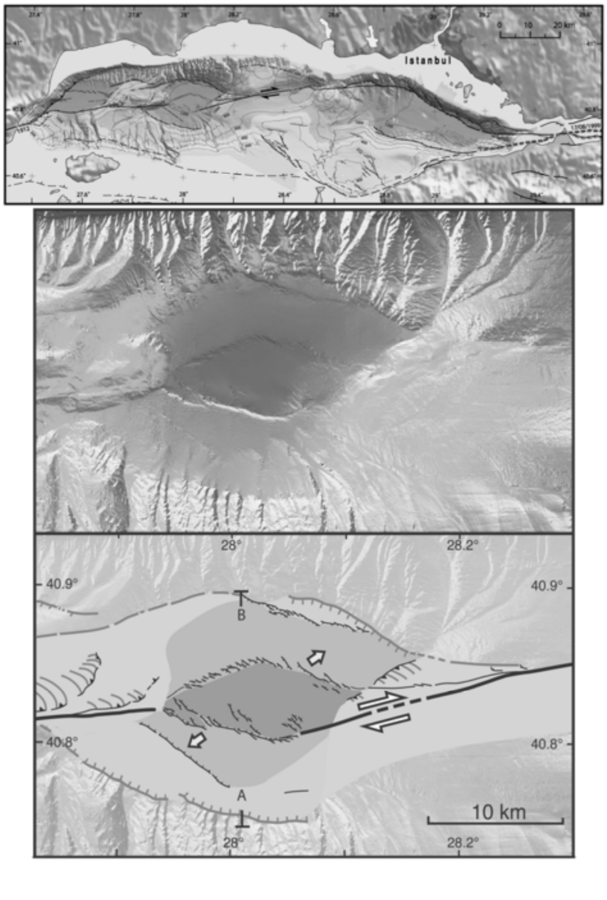

Figure 3. Pull-apart features in the Northern Maramara Sea modified from Armijo et al. (2002). Top, bathymetric Map of the North Marmara Fault System (NMFS). Contours in metres. The fault system involves oblique extension across pull-apart features at a range of scales. Several faults segments with different strike and kinematics appear capable to generate destructive earthquakes. They are separated by step-over and/or sharp bend that may be able to arrest earthquake ruptures. Bathymetry (middle) and sketch map (bottom) of the central basin provides an example of such a step-over. An internal pull-apart has formed within the larger pull-apart structure.

REFERENCES

Armijo, R., Meyer, B., Hubert, A. & Barka, A., 1999. Westward propagation of the North Anatolian fault into the northern Aegean: Timing and kinematics, *Geology,* 27, 267-270.

Armijo, R., Meyer, B., Navarro, S., King, G. & Barka, A., 2002. Asymetric slip partitioning in the Sea of Marmara pull-apart: A clue to propagation processes of the North Anatolian Fault, *Terra Nova,* 14, 80-86.

Flerit, F., Armijo, R., King, G.C.P., Meyer, B. & Barka, A., 2003. Slip partitioning in the Sea of Marmara Pull-Apart determined from GPS velocity vectors, *Geophys. J. Int.,* 154, 1-7.

Le Pichon, X., Sengor, A.M.C., Demirbag, E., Rangin, C., Imren, C., Armijo, R., Görür, N., Cagatay, N., Mercier de Lépinay, B., Meyer, B., Saatçilar, R. & Tok, B., 2001. The active main Marmara fault, *Earth Planet. Sci. Lett.,* 192, 595-616.

Le Pichon, X., Chamot-Rooke, N., Rangin, C. & Sengor, A.M.C., 2003. The North Anatolian Fault in the Sea of Marmara, *J. Geophys. Res.,* 108, 10.1029/2002JB001862.

McClusky, S., Balassanian, S., Barka, A., Demir, C., Ergintav, S., Georgiev, I., Gurkan, O., Hamburger, M., Hurst, K., Kahle, H., Kastens, K., Kekelidze, G., King, R., Kotzev, V., Lenk, O., Mahmoud, S., Mishin, A., Nadariya, M., Ouzounis, A., Paradissis, D., Peter, Y., Prilepin, M., Reilinger, R., Sanli, I., Seeger, H., Tealeb, A., Toksöz, N. & Veis, G., 2000. Global Positioning System constraints on the plate kinematics and dynamics in the eastern Mediterranean and Caucasus, *J. Geophys. Res.,* 105, 5695-5719.

Parke, J.R., White, N.J., McKenzie, D., Minshull, T.A., Bull, J.M., Kuscu, I., Görür, N. & Sengor, A.M.C., 2002. Interaction between faulting and sedimentation in the Sea of Marmara, western Turkey, *J. Geophys .Res.,* 107 (B11), doi:10.1029/2001JB000450.

Bertrand Meyer
Laboratoire de Géologie Structurale, Université Paris VI
4 place Jussieu, 75252 Paris cedex 05.
email: bertrand.meyer@lgs.jussieu.fr

VOLCANOLOGY

Recent major two volcanic activities in Japan: Mt. Usu and Miyake-jima eruptions in 2000

Hidefumi Watanabe

Earthquake Research Institute, University of Tokyo

ABSTRACT

In this report, we review prediction researches on the recent major eruptions at Usu and Miyakejima volcanoes, based on three points of view: 1) basic understanding of magma-plumbing system, 2) detection of magma accumulation processes, 3) detection of magma movements by extensive observations.

Each volcano showed contrasting long-term precursors. Usu volcano showed no remarkable inflation before the eruption, while Miyakejima showed quasi-continuous inflation. Before both eruptions, we could clearly detect remarkable precursors and contributed to dispatch actual warnings leading to quick evacuation of inhabitants. After the beginning of the eruption, however, it was difficult to predict the time developments of the activities, especially in case of Miyakejima volcano where a caldera collapse was accompanied by repeated explosive hydromagmatic eruptions, and followed by a huge amount of continuous degassing.

In order to make a successful long-term prediction or to predict a scale, style and time developments of volcanic eruption, we further need to elucidate magma-plumbing system and to understand particular processes operating in magma.

KEYWORDS: eruption prediction, volcanic eruption, precursors, magma, Usu, Miyake-jima

1. INTRODUCTION

There are five important elements of eruption prediction: time, place, scale, style, and time-developments. By accumulation of observation research, we can now grasp the state of volcanic activity and can perform the short-term prediction of eruption time, a place, and transition to some extent, if suitable observation is made. However, mid- and long-term prediction of eruption time and prediction of a scale, a style, and transition are still difficult subjects.

For realizing the five elements of eruption prediction, there are three strategic research subjects: understanding of a magma supply system (magma reservoir and conduit, magma mixing, change of magma composition, etc.), grasp of precursory processes (a style of magma supply and accumulation of volatiles etc.), and exact grasp of magma movement. The 2000 eruptions of Usu and Miyake-jima volcanoes are the second major eruptions, respectively, after the National Project for Prediction of Volcanic Eruption was initiated in 1974. Below, we report the observation results and problems viewed from the above-mentioned three research subjects.

2. THE 2000 ERUPTION OF USU VOLCANO

2.1 Magma supply system

Previous petrological research suggests that two (dacite and basalt) magma reservoirs are located at the depths of 4-6km and 10km, respectively, and that the same magma supply system is used after the 1663 eruption.

2.2 Detection of magma accumulation processes

The annual number of earthquakes, which occurred at the summit and northern foot of the volcano, was in an increasing trend from 1995. The rise of fumarole temperature was also observed on the Meiji new mountain at the northern foot. However, we observed no remarkable inflation of the volcano until the beginning of seismic swarm activity.

2.3 Detection of magma movements

Swarm earthquakes started at the northwest part of the summit on March 27, and an inflation centering on the northwest summit was detected by GPS observation and elevation angle measurements (the depth of the source being estimated to be 2km). Based on these observation results, information about volcanic activity and the possible scenarios of pyroclastic flow eruption from the northwest summit or the hydromagmatic explosion at the northwestern foot were shown, and residents around the dangerous area could evacuate quickly.

The first eruption occurred at the northwestern foot on March 31, and petrological analyses revealed that a half of ejecta was essential including pumice and disrupted at a depth of about 2-3km. After the eruption started, the initial inflation centering on the northwest summit stopped, while a remarkable inflation around the eruption sites continued, and phreatic explosions occurred repeatedly. The upheaval rate at the northwestern foot decreased exponentially after April, and stopped after the end of July. Moreover, a regional GPS observation network detected the wide-area contraction around Usu volcano, and suggested the rise of magma from the deeper storage zone at a depth10km. Furthermore, a 3-dimensional tomographic study revealed the low velocity zone at a depth of 6km beneath the volcano.

Integrating the results of observation and analyses, we could suppose that magma started to rise up from the deep source and intruded to the shallow depth beneath the northwest summit, and then migrated to the northwestern foot. Future important research subjects include a detailed tomographic study to detect the subsurface shallow/deep magma storage zones, and to clarify the physico-chemical precursory processes in the shallower magma reservoir.

3. The 2000 ERUPTION OF MIYAKE-JIMA VOLCANO

3.1 Detection of magma accumulation processes

The Miyake-jima volcano has repeated the flank fissure eruption every several tens of years since 1469, and the eruption interval in recent years was about 20 years. The repeated precise leveling surveys revealed that the southwest part of the volcano, which subsided in the last 1983 eruption, was continuing upheaval after 1983. The repeated GPS observation also indicated a remarkable inflation of the volcano during the period of 1990-1995. The results of leveling and GPS observation clearly indicated, for the first time, the continuing accumulation of magma beneath Miyake-jima volcano. Moreover, the geomagnetic total force observation detected a systematic elevation of the subsurface temperature beneath the southern slope of the volcano after 1996.

3. 2 Detection of magma movements

Shallow seismic swarm activity started beneath the south slope of the volcano on June 26. Then, the hypocenters of earthquakes moved to the west of Miyake-jima, and the results of GPS and tilt observation also indicated a dyke intrusion to the west. In fact, a small-scale submarine eruption occurred in the west offshore area of Miyake-jima on the morning of the 27th, and the seismicity in the volcano also decreased. After July 3, however, shallow earthquakes beneath the summit began to occur, and the summit collapsed on the 8th, producing a small amount of ash. Although we could detect magma movements quite well by extensive observation till this point in time, subsequent developments were unexpected.

The collapse of the summit continued till the end of August, and finally the caldera with a diameter of 1.6km was formed. During the caldera collapse, phreatic and phreatomagmatic explosions occurred repeatedly. Since the largest phreatomagmatic explosion occurred on August 18 and a low-temperature pyroclastic flow event was also generated on August 29, the Coordinating Committee for Prediction of Volcanic Eruption (Izu subcommittee) released the view that the eruption accompanied by a larger scale of pyroclastic flow might also occur from now on. In response to this view, evacuation of all residents from the Miyake-jima island was carried out at the beginning of September. Discharge of sulfur dioxide gas became noticeable late in August, and it increased rapidly after the middle of September, and amounted to a peak of 40,000 t/day in October. The discharge of sulfur dioxide gas with an amount of several thousand ton/day is also continuing as of November 2004.

One of the most important observation results is that we could obtain much information on the close relation between the magma movements from Miyake-jima volcano and the gigantic seismic swarm activity caused by a large scale of tensile opening of the crust beneath the west offshore area. Moreover, a submarine earthquake observation group installed ocean bottom seismometers to obtain the precise hypocenter distribution of swarm earthquakes in the west offshore area and to explore the subsurface velocity structure. They could obtain a vertical plate-shaped hypocenter distribution that suggests the dyke intrusion.

We may say that we could detect the magma accumulation processes to some extent for prediction of the 2000 Miyake-jima eruption. However, we could not perform sufficient prediction about the style of an eruption and its time development: an outflow out of magma from Miyake-jima, formation of caldera, large-scale phreatomagmatic explosions, etc. This is largely because the present eruption prediction only refers to the historic eruption events, and we obtained no evidence on the existence of huge magma reservoir beneath the volcano before the eruption. For this reason, we were inadequate to examine unexpected phenomena from many sides. It is also an obstacle that detailed information about a position and a size of the magma reservoir is not acquired when predicting time development of the huge degassing activity.

4. CONCLUSION

In the eruption of Usu volcano, we could detect short-term precursors steadily and contributed to performing useful information dispatch for the quick evacuation of residents before beginning of the first eruption. We could also detect eruption precursors and magma movements in the initial stage of activity of Miyake-jima volcano. We owe these successful results to the continued establishment of observation network, development of prediction techniques, etc. since the start of the National Project for Prediction of Volcanic Eruption.

However, it has also become clear that several problems are left behind on prediction of time developments after the start of eruption. Moreover, continuous discharge of a huge amount of volcanic gas, which followed the formation of collapsed caldera at the summit of Miyake-jima volcano, is the activity style experienced for the first time in the history of observation research of our country, and shows anew that a comparative study with foreign volcanic activity is also important. We are needed to conduct more fundamental observation research with a wide view in time and space, in order to solve difficult subjects, such as mid- and long-term prediction of an eruption, and prediction of a style and time developments of activity.

Although the 2000 eruptions of Usu and Miyake-jima volcanoes were the volcanic events where cooperation was strengthened among observation research, monitoring by disaster prevention organization, and disaster prevention by administration, an important problem was also raised about the situation of research observation at the time of an eruption. There were some cases where observation researchers were not able to perform investigation in a required zone, just because it took the danger of volcanic activity into consideration. It is necessary to advance examination about investigation in a regulation zone, the principle of safe reservation, etc.

Hidefumi Watanabe
Earthquake Research Institute, University of Tokyo,
1-1- 1, Yayoi, Bunkyo-ku, Tokyo, 113-0032 JAPAN,
email: watanabe@eri.u-tokyo.ac.jp

The monitoring of the French active volcanoes: More than 30 years of experience

*Georges Boudon[(1)] and Jean Louis Cheminée[(1)]

(1) Institut de Physique du Globe de Paris, Observatoires Volcanologiques, Boîte 89, 4 place Jussieu, 75252 Paris Cedex 05, France

ABSTRACT

From all the volcanoes of France, only those located in the french overseas territories are active: Piton de la Fournaise on La Réunion island, Soufrière in Guadeloupe and Montagne Pelée in Martinique. Piton de la Fournaise volcano, which is located on a hotspot, is one of the most active volcanoes of the world, with more than 50 eruptions in the last 6 years, the last one occurring in May 2004. Each of the two subduction volcanoes of the Lesser Antilles arc have experienced two eruptive events during the last century: phreatic eruptions (1956 et 1976-77) on Soufrière of Guadeloupe and magmatic dome-forming eruptions (1902-1905 and 1929-1932) for Montagne Pelée in Martinique. The 1902-1905 eruption is sadly famous because of the destruction of the two towns of Saint-Pierre and Morne Rouge and the death of 30 000 persons. Extensive monitoring of these volcanoes necessary to avoid future similar catastrophic events was implemented at different times for both volcanoes. Second in the world after Vesuvius volcano, the Montagne Pelée volcanological observatory was installed as early as 1902. The evolution of the monitoring networks during the last 30 last years make these volcanoes among the best monitored in the world. The monitoring is based on different geophysical and geochimical methods: seismic stations, ground deformation measurements (tiltmeters, automatic EDM measurements, extensometry, GPS), magnetic and electric stations, ^{222}Radon measurements, geochemistry of hot springs and fumaroles - mainly on Soufrière of Guadeloupe). The time over which the volcanoes show an increase of activity prior an eruption is very different between the volcanoes of the Lesser Antilles arc and that of La Réunion. Since becoming operational in 1979, the Piton de la Fournaise volcano observatory has gained a long experience in monitoring numerous eruptions that allow the identification of clear pre-eruption indicators in time to warm the autorities in charge of the civil protection. This experience will be useful to follow the next volcanic crisis on the lesser Antilles volcanoes, even if the eruptions are of different styles

KEYWORDS: Volcanic observatories, active volcanoes, monitoring and predictability

---

Georges Boudon
de Physique du Globe de Paris, Observatoires Volcanologiques,
Boîte 89, 4 place Jussieu, 75252 Paris Cedex 05, France
Email : boudon@ipgp.jussieu.fr

Living with an active volcano, Sakurajima, Japan: Strategy of mitigation of volcanic hazards

Kazuhiro Ishihara

Sakurajima Volcano Research Center, Disaster Prevention Research Institute, Kyoto University

ABSTRACT

Sakurajima volcano has caused serous damage on people around it in 20th century. Local and national governments and residents have struggled with the volcano how to live under the volcano. On the other hand, scientists and the Meteorological Agency have made efforts how to monitor volcanic activity precisely and how to issue reliable volcanic information to public. The Kagoshima International Conference on Volcanoes in 1988 seemed to activate mutual communication among administration, scientists and citizens. Volcanic hazards map was made as common concepts for disaster expected in future eruption among them, and volcanic information was improved. The basic strategy of mitigation of volcanic hazards is almost completed.

KEYWORDS: volcanic hazards, volcanic eruption, evacuation, volcanic information, communication

1. Introduction

1.1 Volcanic activity and hazards

Sakurajima volcano is an andesitic stratovolcano of approximately 10 km in radius, located in Kagoshima bay, southern Kyushu, Japan. The volcano was born about 20,000 ago and has grew up by repeated eruptions at the southern edge of the Aira caldera, which was formed by the biggest eruption [1]. Historical activity is characterized by big flank eruptions and by summit eruptions. Big flank eruptions which ejected more than 1 cubic kilometers of magma from both the flank occurred in 1471-1476, 1779-1781 and 1914. Many villages were buried by lava flows and pumice, and many people were killed. In 1946, the volcano extruded 0.18 cubic kilometers of lava, and two villages were buried.

Since 1955, the volcano has repeated explosive eruptions of a vulcanian type, and emitted more than 200 millions tons of volcanic ash. People more than a half million around the volcano has been suffered from volcanic ash, and, inhabitants of Sakurajima have been threatened with suffered from volcanic bombs and mud flows. People, local and national governments and agencies around Sakurajima has struggle with volcano to keep life and houses safety and to keep living by agriculture, fishery and so on.

Many volcanologists have also studied Sakurajima volcano since the 1914 eruption, and clarified that magma has been supplied continuously from deeper portion over several hundreds years, and stored in a magma chamber 10 km beneath the Aira caldera, and that Sakurajima eruption has been generated by injection of magma from the caldera, as illustrated in Figure 1[2]. Sakurajima will cause big eruption in future.

1.2 Lesson from the 1914 eruption

The 1914 Sakurajima Eruption is the largest eruption of 20th century in Japan. On 12 January 1914, eruption started at eastern and western flanks and 2 km^3 of lava and pumice were ejected. At Sakurajima, 25 persons were killed or missed, and more than 15,000 people lost houses buried by lava flows and burnt by pyroclastic flows (Figure 2). Precursory earthquake swarm started a few days before the eruption and significant abnormal phenomena recognized by inhabitants. One day before eruption (11 January, Sunday), most of inhabitants were afraid of eruption and began to escape by ships, but village headmen held back them due to the reply from

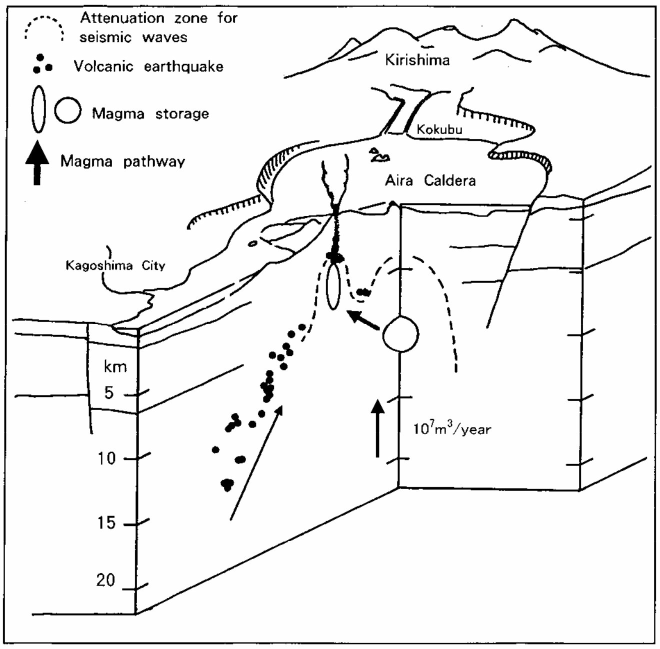

Figure 1. Image on subsurface structure of Sakurajima volcano

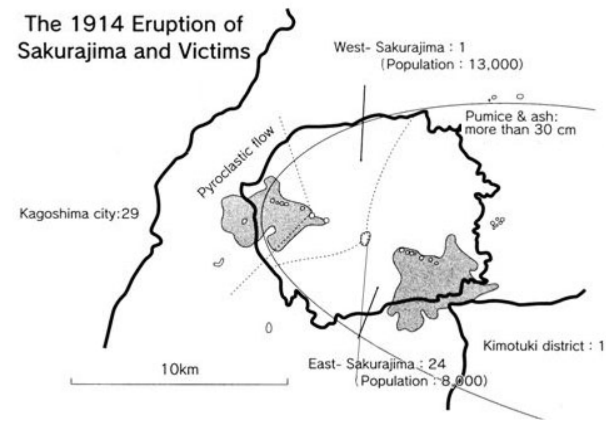

Figure 2. The 1914 eruption and victims

Kagoshima Weather Station:" Location of earthquakes is out of Sakurajima".

The chief of the weather station had also struggled to analyze seismic record of a low-magnification seismograph with a few staff and contacted police to get additional information. However, the response of police was very slow, and there was no activity at Kagoshima prefecture government until eruption started on 12 January. The governor stated later:" I felt earthquakes one day before, but I did not expect any eruption".

The experience of the 1914 Sakurajima eruption suggests what are important in volcano crisis and for mitigation of volcanic disaster. (1) the leadership of local governors and police who have authority to public, (2) volcano monitoring and volcanic information by authorized agency, and (3) joint ownership of knowledge and information on volcanic activity and hazard between them.

The most important for mitigation of volcanic disaster is, however, mutual communication among local governments, volcanologists, residents and mass media. In 1988, Kagoshima Prefectural Government held 'Kagoshima International Conference on Volcanoes' and the main theme was 'Better coexistence between human beings and volcanoes'. Many citizens joined the conference and exhibitions, and learned many of volcanoes directly from foreign volcanologists. This was the first international conference on volcanoes organized by local governments. Since then, mutual communication among local government, volcanologists, residents and mass media, and international cooperation was activated and some of fruits for mitigation of volcanic hazards were produced.

2. Strategy of mitigation of volcanic hazards

In 1973, Act on special measure for active volcanoes was enacted, and volcanic disaster countermeasures have much improved; shelters, harbors and roads for evacuation, radio communication network, countermeasures for damages for agricultural products, countermeasures for volcanic ashfall and for mudflows. Recently, 'software' for mitigation of volcanic hazards has been improved.

2.1 Volcanic hazard map and evacuation drill

In 1992, Kagoshima local government organized a committee to make volcanic hazards map of Sakurajima. The members are experts in Volcanology, Social science and Sabo engineering, representatives of autonomies and agencies, including Japan Meteorological Agency (JMA). The committee made three categories of maps: volcanological hazard map, hazards map for administration and volcanic hazard information map for residents. Volcanic hazard information map and guidebook were distributed to all the families in Sakurajima. The maps may be rather radical, because it indicates that in Sakurajima there are no spaces safe from big eruption. However, all the member and residents accepted them.

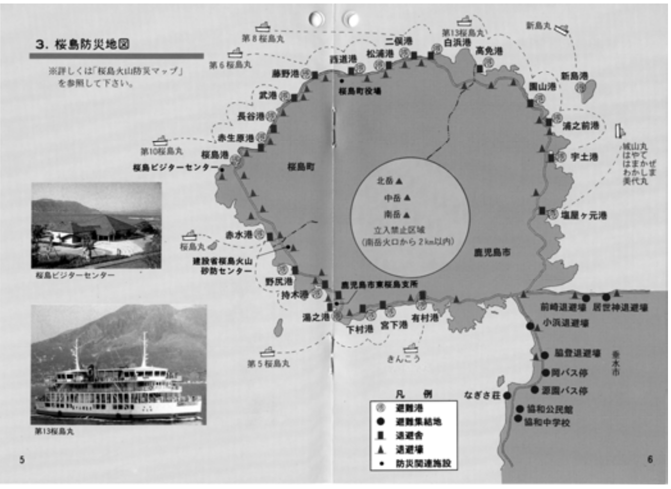

Figure 3. Disaster prevention map of Sakurajima in the guidebook. Location of harbors and ships for evacuation is indicated for each community.

These maps were authorized administratively by the local plan for volcanic disaster prevention, which described the detail plan in crisis and indicates roles of each organization (totally about 40). Every year, a few thousands people, residents and staffs of local government and related organizations have carried evacuation drill on January 12, the memorial day of the 1914 eruption. The drill is started by volcanic information from Kagoshima Meteorological Observatory, JMA. The local plan for volcanic disaster prevention defined 5-level of response to volcanic activity and volcanic information: (1) off-limit near the crater, (2) off-limit zone 2 km from the summit crater, (3) preparation of evacuation from Sakurajima, (4) evacuation counsel: gather to evacuation harbor and (5) order of evacuation. At Sakurajima, the area 2 km from the summit has been asigned as off-limit zone during the past 45 years.

2.2 Improvement in volcano monitoring and information

Kagoshima Meteorological Observatory (KMO) has monitored Sakurajima for half a century, and now various kinds of method are applied: seismic, infrasonic, tilt, TV-camera, GPS and so on. Some of additional data, automated warning system for summit eruption, has been provided in real time to KMO and the office of sabo engineering from a university observatory [4].

Volcanic information issued by JMA is classified into 3: 'Volcanic alert', 'Volcanic advisory' and 'Volcanic observation report'. Volcanic alert is the highest issued when volcanic activity becomes extremely high and urgent response to prevent damage to human lives is required. The information has issued just when increase in volcanic activity is observed, but it is not clear or local governments and residents what kind of response is required and how long the response should be continued.

In November 2003, JMA introduced 'Level of volcanic activity' to Sakurajima and other 4 volcanoes. That is basically the same concept as used by Volcanological Survey of Indonesia. The level at each volcano is defined considering eruption style and social situation, e.g. distance between the volcano and human beings. . At Sakurajima, there are no houses within 2.5 km from the summit, and levels are defined as follows:

Level 0: no sign of activity
Level 1: low volcanic activity
Level 2: intermittently small eruptions
Level 3: repeated explosive eruptions which cause heavy ash-fall
Level 4: large explosive eruption which induce serious damage, e.g. by volcanic bombs, in a part of resident zone
Level 5: big eruption which induces serious damage in wide area l

The level of volcanic activity since 1955 ranges 2 to 4. The level of activity has been kept at 2 since 2003, as volcanic ash ejected each month is less than 10,000 tons and there are few data which suggest increase in volcanic activity.

3. Concluding remarks

The strategy of mitigation of volcanic hazards at Sakurajima is basically completed. However, we have some of problem, e.g. how to evaluate damage out of the volcano and how to design the regional mitigation plan for people living out of the volcano.

REFERENCES

[1] S. Aramaki, Formation of the Aira caldera, southern Kyushu, -22,000 years ago. *J.Geoph. Res.*, **89**, pp. 8485-8501, 1984.

[2] K. Kamo, A dialogue with Sakurajima volcano. *Proc. Kagoshima International Conference on Volcanoes 1988*, pp.3-13, 1988.

[3] K. Kamo and K. Ishihara, A preliminary experiment on automated judgment of the stages of eruptive activity using tiltmeter records at Sakurajima, Japan. *IAVCEI Proceedings in Volcanology,* 1, Springer-Verlag, Berlin Heiderberg, pp.585-598, 1989.

[4] K.Kamo, K. Ishihara and M. Tahira, Infrasonic and seismic detection of explosive eruption at Sakurajima Volcano, Japan, USGS. Bull. 2047, pp. 357-365, 1994.

Kazuhiro Ishihara
Sakurajima Volcano Research Center, Disaster Prevention Research Institute, Kyoto University,
Sakurajima-Yokoyama, Kagoshima, Kagoshima, 891-1419 JAPAN, 3-20-1, email: ishi-svo@svo.dpri.kyoto-u..ac.jp

Volcanic risk assessment and geophysical information: examples from Indonesia, Japan and Montserrat

Philippe Jousset [(1)]

(1) BRGM, ARN, Development Planning and Natural Risks Division, 3 avenue Claude Guillemin , 45060 Orléans Cedex 2, France

ABSTRACT

Volcanic risk assessment is based on the analysis of the interface between volcanic hazard and vulnerabity of human beings, constructions and activities located around volcanoes. Assessment of vulnerabilities is probably one of the most complex studies to be done. Hazard estimation is usually obtained from geological and historical studies. I review in this paper geophysical studies, initially aimed at a better scientific knowledge of magmatic processes, and reinterpret them with objectives of hazard assessment in mind. Examples of scientific studies on deformation and microgravity studies at Merapi Volcano (Indonesia) and Usu Volcano (Japan), seismological modelling at Soufrière Hills (Montserrat) give insights in the magma processes, but also may help to improve hazard assessment. By doing so, I suggest that geophysical monitoring and observations give complementary information to geological studies for a more accurate assessment of volcanic hazard, and provide further keys for decision-makers.

KEYWORDS: volcano, risk, hazard, microgravity, deformation, seismology, modelling, inversion

INTRODUCTION

Volcanoes provide fertile soils, mineral riches, hydrothermal power, touristic attraction due to the fascination they produce on man's imagination. However, an erupting volcano may be, at best, a cause of disruption to normal human activities or a cause of massive loss of lives, destruction to rural and urban infrastructures and economies of to the destruction of entire communities or civilizations (Marinatos, 1939 [1], McCoy and Heiken, 2000 [2]). Scientists and policy makers and disaster/emergency planners and the public have become aware of the dangers that volcanoes may pose, after eruptions at Montagne Pelée (1902), Mount St Helens (1980), Nevado del Ruiz (1986), Unzen, (1991), Merapi (1994), Montserrat (1997).

The theoretical framework of hazard, vulnerability and risk is explored by Alexander (2000) [3]. According to definitions given by the UNESCO within the International Decade for Natural Disaster Reduction (IDNDR), the risk is the expected losses of lives, injuries, property damaged and economic disruption due to a particular hazard. It is the interface between hazard (the probability of occurrence of a potentially damaging phenomenon with a given intensity within a given time period and area) and vulnerability (the susceptibility of the human and biophysical systems to a hazardous event).

The vast majority of volcano-related published work has been concerned with "pure research rooted in Earth Sciences" (Dominey-Howes and Minos-Minopoulos, 2004 [4]). A shift paradigm (Chester et al, 2002 [5]), however, occurred in the perception of risk assessment, due to significant changes in the social theory of natural hazards and the work done by the IDNDR. Much efforts is made on human vulnerability, the potential for marginalization of disadvantaged individuals and social groups, and the requirement to make applied volcanology sensitive to the characteristics of local demography, economy, culture and politics. In recent years, interest has increased in undertaking risk assessments and in determining vulnerability of populations, in order to reduce them. For example, Stieltjes, 2001 [6] proposed a methodology to evaluate the volcanic risk at Montagne Pelée, which we describe shortly in the first section of this paper. From this research (Alexander, 2000 [3]; Chester et al., 2002 [5]; Dominey-Howes and Minos-Minopoulos, 2004 [4]), it has been realized that volcanic risk is increasing (1) as a consequence of the attractiveness of volcanoes and the draw of people to their environs, and more importantly, (2) as a results of cultural, economic and social factors at work within individual countries' growth and development programs (civil protection, public education and health programs). Catastrophic events prevent development (Masure, 1996 [6bis])

Volcano-related emergencies demonstrate that there is a clear relation-ship between the success in dealing with an emergency and the degree to which policies focused on vulnerability reduction were already in place prior to that emergency (Paton et al., 1998 [7]; Caristan et al., 2001 [8]; Kokelaar, 2002 [9]). When faced with managing an environmental problem, such as natural hazards related to volcanic activity, decision-makers such as government officials, operations managers, hazard scientists, land-owners and environmental groups, use formal or informal models to assess the likely outcomes of different scenarios and management options. Because a decision has to be made, somebody will select a model, choose or collect data to use with the model and produce and interpret results. Given limited resources, time and expertise, a series of pragmatic choices will be made so that there are some results on which to base a decision. This process operates most effectively if there is a clear understanding of how model assumptions and data accuracy at each step influence the final assessment and decision-making (Collins et al., 2000 [10]). Practical decision-making in civil protection based on predicting volcano hazards increasingly involves using process models linked with Geographical Information Systems (Radke, 2000 [11]). Optimum use of these techniques for such decision-support requires careful and coordinated consideration of process, data and model scales and their related uncertainties. Renschler (in press) [12] draw the basement of a scaling theory, as a response to the pressing need for a scientific and functional framework within which to examine implementation and use of geo-spatial assessment tools.

Volcanology, however, is a science which differs from most others in one crucial respect: crises may arise from time to time which require (scientific) volcanologists to make immediate recommendations to decision-makers that affect public safety (Aspinall et al., 2003 [13]). Their training generally follows the scientific tradition of making observations of Nature, conducting experiments, and developing models. Where significant uncertainty exist, further research is understaken to reduce it. But the time scale for such research in volcanology can be very protracted, being dependent on the occasional occurrence of future events (not to mention fundings…). Aspinall et al., 2003 [13] describe an original approach to hazard analysis approach in which such scientific data are available during a volcanic crisis, albeit inevitably incomplete, insufficient and uncertain, and can be used most logically and effectively for assessing and stating hazard levels. In addition, the use of this probabilistic approach helps also in dealing with uncertainties.

To summarize, many published studies have been focussing on the mechanisms within active volcanoes, aiming at a better understanding of magmatic and volcanic phenomena for the need of pure science, and less amount of work has been published on the vulnerability approaches and the social aspects. Both are however fundamental for a successful emergency management (Tilling and Lipman, 1993 [14]). The aim of this paper is to review some scientific results obtained by geophysical research, and reinterpret them in the light of hazard assessment and emergency response requirements. By doing so, keys arise that may help "rooted geophysicists" to contribute to reduce the gap between fundamental science and applied volcanology.

After a short description of the methodology used at BRGM for risk analysis (Stieltjes, 2001 [6]), I review three geophysical techniques (deformation, microgravity and seismology) using results at 3 andesitic volcanoes (Merapi, Usu, Komagatake and Montserrat volcanoes).

ASSESSMENT AND MITIGATION OF RISK: THE BRGM METHODOLOGY

Introduction

The quantitative estimation of volcanic risk presented here is based on the original work by Laurent Stieltjes (2001) [6]. The aim is to give efficient tools for decision makers facing questions like:

- When, where and how will occur the next eruption?
- Which nature will be the next eruption?
- Who is at risk?
- Which amount of risk?
- How to protect human systems from the effects of eruptions?

In order to help decision-makers to answer these questions, Stieltjes (2001) [6] proposes a methodology, with 5 main steps 1) quantitative evaluation of hazard; 2) complete listing of exposed elements (elements at risk, IDRDN); 3) qualitative and quantitative evaluation of vulnerability of the exposed elements; 4) quantification of importance of all exposed elements within the society at various stage of a potential eruption (before, during and after the eruption) 5) risk analysis on the basis of the interface between hazard and vulnerability. The risk summarizes in the formula:

$$\text{Risk} = \text{Hazard} * \text{expected damages} = \text{Hazard} * (\text{vulnerability} * \text{value}) \text{ of exposed elements} \quad (1)$$

This methodology allows us to reproduce and compare the analysis of various scenarii, with respect to disruption and damages, and then to quantify the vulnerability and the risk.

Hazard assessment

To evaluate the hazard, three fundamental parameters are defined for each volcanic event: its extension, its frequency of occurrence and its intensity. A quantitative protocol has been defined, from the analysis of past eruptions, for the Montagne Pelée, Martinique. To quantify hazards, Stieltjes introduced several key parameters, among which we find a reference period of the geological history of the volcano; a listing of known eruptions for the reference period; among the previous events, a selection of the most representative ones; a reference eruption, a selection of hazardous volcanic events (lava flow, pyroclastic flows, aerial fall, gaz, lahars, landslides and tsunamis); a selection of secondary volcanic dangerous events (blasts, acid rains, ash); definitions of damage mechanisms; a scale of frequency occurrence, based of the return period for the events; an exposition index.

Listing of exposed elements (elements at risk)

Maps of systematic human activities are to be mapped at that stage, including population, houses, social buildings, like heath care buildings, hospitals, educational facilities, …, and economic centers for agriculture, industry, finance, … These elements are then classified according to their value, with respect to not only their cost (financial value), but also their importance within the human systems (fonctional value, cultural value, …

Vulnerability description

Vulnerability may be analysed qualitatively, by describing factors of vulnerabilities for human lives and for buildings and constructions (technical and physical factors; functional factors, institutional factors and social and cultural factors). We may classify vulnerabilities in 3 groups, according to the impact the eruption has on exposed elements: 1. short term impact: human, physical and fonctional vulnerabilities; 2. short and medium-term impact: social and economocal vulnerabilities, and 3. Medium and long term impact: patrimonial and ecological vulnerabilities.

Vulnerability quantification

The quantification of vulnerability has the following objectives: 1. Estimation of the amplitude of possible dammages; evaluation of the susceptibility of elements to eruption; evaluate and classify the weaknesses of the regional network. The three fundamentals notions are "exposed elements", the "possible exposed area" and "reference eruptive scenario". Basic tools for the evaluation of the vulnerability are 1) the definition of a specific scale, which gives a quantification of possible damage on exposed elements, 2) the definition of areas potentially affected by one damage type, for each exposed element, and 3) damage matrix, which quantify explicitely vulnerabilities, for each exposed element and each hazard. For instance, human vulnerability is defined by types and seriousness of wounds: death, wounds, illness, for ash fall, pyroclastic flows, and so on…

Risk assessment

Risk evaluation is carried out in giving hints on how to reduce impacts of a possible future eruption. The objective is to give a series of tools to help decision-makers to prepare human systems before the occurrence of en emergency, to manage properly a possible emergency, to recover efficiently from possible damage due to an emergency, so that the crisis is reduced to a period of time as short as possible. By doing such preventive planing, risk is theoretically reduced.

The theoretical evaluation of risk is however not realistic: it would consist of trying to add numbers that have nothing to do one with another, like number of dead, disruption of trains, and so on. The analysis of risk is carried out efficiently in practice by the classification of the components, using 1. hazard mapping; 2. classification of the exposed elements by the relative importance within the human systems, and 3. interfacing hazard maps and vulnerability maps.

Summary

The methodology developed at BRGM consists in 5 steps.

1. Description of volcanic activity in the past (geology and historical records), which gives hazard map;
2. Description of the regional environment (systematic analysis of elements, and evaluation and classification);
3. Evaluation of the hazard mapping, which gives the degree by which each element is exposed;
4. Vulnerability analysis of the exposed elements, by a classification of the relative importance of human systems, which highlight weaknesses of the human systems, in normal conditions before an emergency,
5. Risk analysis which measures the impact of eruption on human systems, and which allows us to define preventing measures to reduce risk.

Hazard assessment in mainly done from the analysis of the past eruptions given by geological studies. In the following, results of fundamental research in geophysics applied to volcanology are reviewed, and tentative new interpretations are tentatively drawn.

MICROGRAVITY AND DEFORMATION OBSERVATIONS, MODELLING AND INVERSION

Methodology

Volcanic eruptions are related to complex magmatic processes, the understanding of which requires both monitoring and modelling of physical and chemical aspects of these systems. Distinguishing between these processes is not straightforward. For example, the intrusion of new magma or the exsolution of gas within magma both imply an increase in the volume of the magma chamber, which may lead to the same pattern of ground deformation at surface. Models have been built (e.g., Mogi, 1958 [15], Okada, 1985 [16]), but they do not allow these cases to be distinguished. Yet, these processes could lead to different eruption styles, putting (or not) at risk human activities around the volcano. One variable that can allow us to discriminate between processes is density. In addition, density variations may be in some cases the only suitable parameter to detect internal processes (like magma emplacement without seismicity, Rymer et al., 1993 [17]).

Gravity and microgravity techniques give information about the underground density distribution and its variation with time. The Bouguer anomaly gives information on the internal density distribution and thus leads to the inner structure of the volcano (e.g., Rymer and Brown, 1986 [18]; Deplus et al., 1995[19]). Temporal microgravity studies consist of monitoring and interpreting temporal variations of the gravity field and simultaneous vertical elevation change. Considering that data reduction removes both instrumental and tidal effects, the remaining temporal gravity changes on volcanoes are caused by the elevation changes, mass redistribution and change of density, acting in concert (Fig. 1).

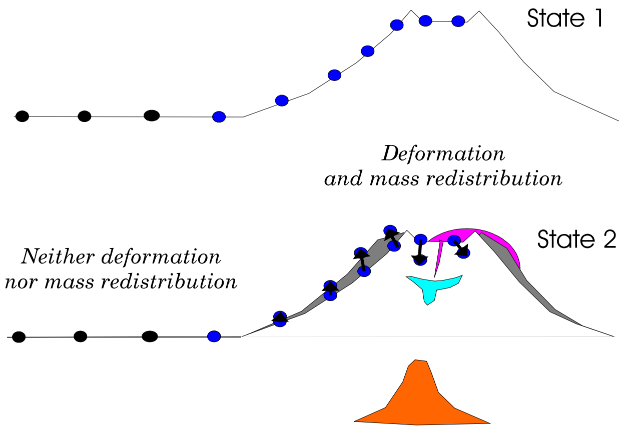

Figure 1. Schematic temporal evolution of an active volcano. Possibilities to produce gravity changes are reported on the figure. From an initial state (state 1), where black dots represents the location of measurements point, the gravity variation at the second state (state 2) may change due to the surface movement (which involves free-air elevation change and volume change of the volcano), mass redistribution of the topography at surface (extrusions) and internal mass redistribution.

This is summarised in the equation:

$$\Delta g_{observed} = \Delta g_{Topography\ change} + \Delta g_{Free\text{-}air\ deformation} + \Delta g_{Volume\ change} + \Delta g_{Density\ change} \quad (1)$$

with:

$\Delta g_{Topography\ change}$: Gravity effect of the mass added/removed on the ground surface due to extrusion/collapse of material in the surroundings of the points.

$\Delta g_{Free\text{-}air\ deformation}$: Gravity effect of elevation changes of the observation point.

$\Delta g_{Volume\ change}$: Gravity effect of the global volume variation, at the observation point, generated by an increase/decrease of the volume of the volcano from an internal process, excluding added/removed mass at surface.

$\Delta g_{Density\ change}$: Gravity effect due to the change of global mass inside the edifice: internal density change (e.g., groundwater level change, volcanic process) or inner mass displacement.

Two methods may be used to investigate the volcanic processes disturbing the gravity field with time:

1) Measurements are repeated at different times at many points. The repetition network should extend from areas where the gravity field is expected to vary to areas where it is expected to be constant (Fig. 1).

2) Continuous recording of the gravity field over a long period of time; idealy, at least two continuously-recording stations are needed in order to obtain differential measures.

Previous studies have shown that microgravity changes are detectable before, during or after volcanic crises (see e.g., Jachens and Eaton, 1980 [20]; Yokoyama, 1989 [21]; Brown et al., 1987 [22]). These changes may or may not be associated with height variations and volcanic eruptions with their amplitude varying from a few to several hundred microgal (1 μGal = 10^{-8} ms^{-2}).

Usu volcano, Hokkaido, Japan

Within the framework of a 2-year postdoctoral position supported by the Japanese Society for the Promotion of Science, I carried out several microgravity and GPS surveys at Usu and Komagatake volcanoes, in order to contribute to the knowledge of the volcanic behaviour of those volcanoes (Jousset & Okada, 1999 [23]; Jousset et al., 2000 [24]; 2003 [25]) and contribute to the intense monitoring effort carried by the Usu Volcano Observatory, Hokkaido University. I focus here on results obtained at Usu volcano.

Located on the northern part of the Japanese subduction arc, Mt. Usu (Latitude 42° 32 N; Longitude 140° 05 E; elevation 700 m) is a truncated stratovolcano built on the southern rim of the Toya Caldera. Toya volcano ejected 120 km^3 of rhyolitic pyroclastic fall and flow (Ikeda, 1985 [26]; Katsui et al., 1992 [27]). The resulting 10 km diameter caldera (late Pleistocene, Okumura and Sangawa, 1984 [28]; Machida et al., 1987 [29]) is now filled by a 180 m deep lake. Mt. Usu is composed of a large somma lava (Soya et al., 1981 [30]), built from basalt and mafic andesite (early Holocene). About 7000 or 8000 years ago, its summit was disrupted by a violent explosion accompanied by the Zenkoji debris avalanche which reached the south-western coast, more than 5 km away, from the crater rim. The destruction of the summit resulted in the formation of a somma, the main crater being about 2 km in diameter and 500 m in elevation at the rim (Yokoyama et al., 1973 [31]; Katsui et al., 1992 [27]). After a quiescence of several thousand years, it has erupted 7 times since 1663 (in 1663, 1769, 1822, 1853, 1910, 1943-45 and 1977-1978, sometimes with pyroclastic flows, surges and volcanic mudflows). Each eruption resulted in the formation of a dome or crypto-dome located on the main fractures of the upper somma volcano (Katsui et al., 1985 [32]). With time, the decreasing silica content of the dacite magma (from 74 % in 1663 to 69 % in 1977) has become interpretable as in terms of a compositionaly zoned magma chamber (Katsui et al., 1978 [33]; Oba et al., 1983 [34]).

After 23 years of dormancy, Usu Volcano erupted on 31st of March, 2000. Many observations (seismicity, deformation rates, gravity observations, groundwater level monitoring) show that the period of intense activity was short, starting abruptly, and continuing for ca. 5 months with a decreasing rate. Uplift was observed at two successive and separate locations at the time of the eruption.

Because the characteristics of Usu Volcano are unique, and due to the successful crisis management by the Japanese authorities, the French Comité Supérieur de l'Evaluation des Risques Volcaniques (Ministère de l'Environnement) decided to carry out a scientific, social and crisis management survey in Japan (Caristan et al., 2001 [8]).

Within this framework, we obtained new GPS and microgravity observations on the prior network set up by Jousset & Okada (1999) [23]. The study of Jousset & Okada (1999) [23] provides a good baseline for comparing gravity and deformation measurements to the new data, because data were collected every 2 to 4 months and because the volcanic activity was very low between October 1996 and June 1997. No changes greater than 8 cm/year and 80 microgal/year were detected at the time. The changes were interpreted to be due to subsidence and contraction as part of the post-eruptive behavior of the Usu-Shinzan 1977-1982 crypto-dome. We collected additional data between June 1997 and July 1998. With the addition of new GPS and gravity data from November 2000, our complete GPS and gravity data set covers a period which is able to measure the total budget of the two-stage 2000 eruption of Usu Volcano, gives insights in volcanic processes associated with this eruption, and confirms that the coupling of gravity and deformation is a fundamental monitoring tool for improving hazard assessment. By analysing and inverting this GPS and gravity data set, we contribute to a better understanding of dacitic volcanism.

Figure 2. Measuring GPS (left) and gravity (right) on repeated network at Usu volcano.

Between July 1998 and November 2000, the displacements and gravity variations are among the largest ever recorded on an active volcano in association with an eruption.

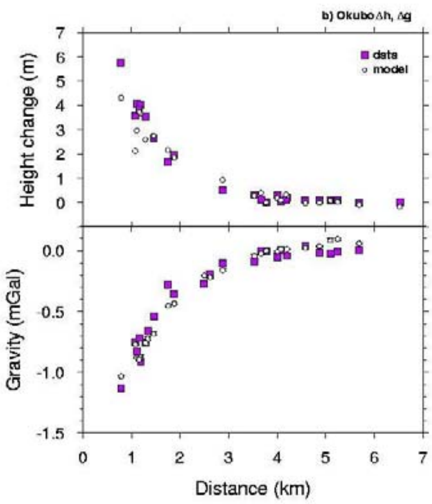

Figure 3. Results from inverting vertical displacmeents and gravity data using Okubo's model (Okubo, 1985 [35]). Observed (coloured squares) and modelled (white circles) vertical displacements (top) and gravity variations(bottom) as a function of the radial distance from the 'epicenter' of the source with the smallest misfit.

We review three different elastic models commonly used in volcano-geodesy (sphere, fault system, fissure zone) and invert the high quality data using each of these models. The combined inversion of GPS and microgravity data leads to the best solution in the least-squares sense. It is compatible with the intrusion of approximately $5X10^{11}$ kg of new magma into the western part of Usu Volcano. This appears to have occurred in a subvertical fracture zone (about 2.4 km length, 0.1 km width) aligned in the East-West direction. The fracture zone is between 0.4 and 3.3 km depth with an extension of about 30 m. The fractures are likely to be filled with material having a density slightly higher than the density of old products of Mount Usu, i.e., about 2400 kg m^{-3}. This model is consistent with the locations and magnitudes of the earthquakes recorded during the period of the intense seismic activity in April and May 2000. These earthquakes correspond to the boundaries of the intruded magma body. The model suggests that the two locations of uplift are not independent.

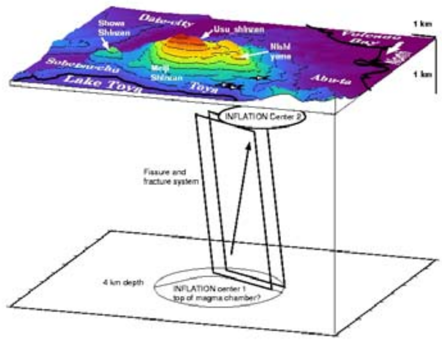

Figure 4. 3-D model for the Usu 2000 eruption. Two inflation centers were recognised at the time of the eruption, the first one at 4 km depth and the second one at 400 m depth. The deep source could correspond to the magma chamber, while the upper inflation center would correspond to the expansion of magma from decompression. The fissure zone modelled here would have allowed the magma to transit from depth toward the surface.

At Usu Volcano, the characteristics of the volcanic cycle (magma intrusion, eruption and repose) are well known and have been described in detail. The scenario of the eruption in 2000 followed this cycle again. As a consequence, short-term forecasting of eruptions at Mount Usu, mainly based on seismic activity, is much easier than at other volcanoes, where the cycle is longer or unknown. In March 2000, the interval between the initial precursory earthquakes and the first eruption was about 4 days, allowing a safe and successful evacuation before the first explosion.

Toyako-onsen is a famous tourist resort in Japan, visited by millions of tourists per year. The 2000 eruption of Mount Usu disrupted this industry: the northernmost crater erupted a few hundred meters from the main tourist center. Local authorities have been working together with the local scientists for a long time. They were fully aware of the possibility that a new eruption might occur at any time, and had an evacuation plan prepared for the next crisis. At the time of the crisis, the Japan Meteorological Agency, Tokyo, was in charge of the multidisciplinary integration of monitoring observations, but data were also sent to the local authorities. Thanks to the efficient communication between central and local authorities and the scientists, the local authorities took appropriate action, evacuating the population soon after the begining of the crisis. Nearly 16,000 people were evacuated 2 days before the onset of the eruption. Neither casualties nor injuries were reported, making this crisis one of the most successfully managed in Japan and in the world.

Merapi volcano, Central Java, Indonesia

Merapi volcano is one of the andesitic volcanoes of the Sunda arc, which extends 3000 km from North Sumatra to the Sunda islands of East Indonesia. This subduction arc results from convergence between the Indian plate and the Asian plate (Lee and Lawver, 1995 [36]). In Java, the convergence is frontal with a speed of 6.5 cm/year (De Mets et al., 1990 [37]), although speed and direction vary along the arc (Zen Jr., 1993 [38]). The Sunda arc is located in an area where subduction has been going on since Upper Paleozoic (Katili, 1974 [39]). Merapi is located about 300 km from the trench and the depth of the Benioff zone is around 170 km (Hutchison, 1976 [40]). The history of the Merapi volcano is rather complex (Berthommier, 1990 [41]; Camus et al., 2000 [42]; Newhall et al., 2000 [43]). Three main divisions are seen. “Ancient Merapi” (more than 60000 to 8000 years b.p.) is the basement of the edifice, made principaly of various andesitic breccias. “Middle Aged Merapi” (from 8000 to 2000 years b.p.) involved alternating andesitic lava flows and breccia deposits. A Mount St. Helens-type edifice collapse (Christiansen and Peterson, 1981 [44]) probably occurred during this period. “Recent Merapi” (from 2000 to 600 years b.p.) is made of three main kinds of deposits: large andesite flows, nuées ardentes deposits, and deposits from phreato-sub-plinian and sub-plinian eruptions.

Merapi volcano is at present one of the most active and dangerous volcanoes in the world. The present main threat from the volcano is the collapse of an andesite dome growing at the 3000 m high summit, in a 200 m wide horse shoe-crater open towards the southwest. Collapse of the domes produces nuées ardentes (McDonald, 1972 [45]; Young et al., 1994 [46]), such as those of the November, 22, 1994 eruption (Sukhyar, 1995), in which about 64 people died.

Merapi volcano is located at 30 km North of Yogyakarta, where more than one million inhabitants are living. Its persistent activity, its achetypal dome growth and subsequent collapses generating "nuées ardentes” of the so-called Merapi-type have been described and tentatively explained since the pioneering days of modern volcanology. Its almost continuous activity between few paroxyms, and the relative ease of access to its buldging dome, makes it a special case among andesitic volcanoes. As a result, Merapi volcano gradually became in the late 60^{th} (much before IAVCEI classified it as one of the Decade Volcano), the focus of several bilateral or international cooperative programs within the locally field of Indonesian volcanology. Locally, the increasing awareness of the potential for volcanic disaster at Merapi volcano led to the implementation of a network of observational posts, together with the development of hazard mapping, risk prepared-ness, and volcanic emergency management. These mitigation policies, including sabo-works (erosion and volcanic control engineering) and early warning systems, significantly limited the death toll and property loss in the wake of outburts at Merapi.

Within this framework, a cooperation between the Volcanological Survey of Indonesia and the French Ministry of Environment officially began in the late 80^{th}, with Indonesian students getting their PhD in France and French civil servant learning about field work and volcano crisis management. The Laboratoire of Gravimétrie and Géodynamique (Institut de Physique du Globe de Paris) started in 1993 a scientific collaboration with VSI in order to observe, quantify and model temporal gravity variations due to the volcanic activity (Jousset, 1996 [48]).

Gravity signals were recorded during volcanic activity of Merapi volcano between 1993 and 1995. First we repeated measurements of gravity (with Scintrex CG3-M) and of elevation (with GPS receivers) on a network. Within this period, we observed little deformation (less than 5 cm), but significant gravity changes (up to almost +400 μGal and -270 μGal). The growth of the dome explains most of the gravity signal. However, a residual gravity change is interpreted as an increase of $4*10^8$ kg of the volcano mass, under the northwestern part of the summit. We consider and discuss several models, including non-volcanic effects (e.g. water table level change), and magmatic processes, such as the intrusion of magma, or the effect of crystallisation of implaced magma. Secondly, we installed a gravity meter in Babadan observatory, located at 4 km from the summit, which has been recording continuously since 1993. The analysis of these records leads to a precise Earth tide model for the Merapi area with an accuracy of 1.3 μGal for M_2. We consider both the continuous monitoring of the mass movement within the volcano and the response of the volcano to the tidal potential. A correlation exists between residual drift and seismic and volcanic activity. For example, a decrease of the residual drift corresponds to intensive seismic activity (LF event) and the occurrence of nuées ardentes, whereas no remarkable activity is associated with increases of the residual drift. The admittance variations, a combination of the meter sensitivity (which is tilt-dependent) and the mechanical response of the ground to tidal forces, are also correlated to volcanic events. We propose that during 1993-1995, oscillations of the internal pressure (a few MPa) due to crystallisation and degassing magma lead to direct summit activity (Jousset et al., 2000 [49]).

Conclusions

These results confirms that repetition networks (deformation and gravity) and continuous gravity recording are promising techniques for studying and monitoring volcanoes. There may be a hope for possible forecasting of nuées ardentes, dome collapse, from the variations of the continuous gravity monitoring.

SEISMIC WAVES ANALYSIS AND MODELLING: EXAMPLE OF MONTSERRAT

Introduction

The eruptive behaviour is dependent on many parameters, amongst which the rheology of the magma plays an important role (Dingwell, 1989 [50], Barmin, 2002 [51]). In particular, the transition in the properties of the melt phase from a liquid-like to a solid-like response in a cooling magma (glass transition), is one of the most fundamental phenomena which influences the eruptive style of volcanic rocks (Dingwell 1989 [50], Stevenson, 1995 [52]). Similar to many volcanoes around the world, Soufrière Hills volcano, Montserrat presents a variety of eruption styles ranging from dome grows and collapses (Young, 1998 [53]) to Vulcanian explosions.

The observation and modelling of seismic waves is one of several different ways to study volcanoes, aiming at a better understanding of volcanic processes. Long-period earthquakes and tremor are important waveforms in volcano-seismology (Chouet, 1996 [54]), as they have been observed at many active volcanoes. At Montserrat, a continuum exists between long-period and hybrid events, the latter having an additional high frequency content Neuberg (2000) [55]. Throughout this section we refer to both types as low-frequency earthquakes (Jousset et al., 2003 [56]). Low-frequency earthquakes, whose frequency content ranges from 0.2 to 5 Hz, last several tens of seconds and often occur in swarms of multiplets. Their characteristics are very similar both in time and frequency domain, suggesting that the processes generating these events are the same.

In recent years, good progress has been made in the understanding of the generation of the associated wave-field. Most models rely on the excitation of normal modes in fluid-solid systems (Biot, 1952 [57]; Chouet 1985 [58]; Ferrazzini 1987 [59]). Neuberg (1998) [60] and Neuberg & O’Gorman (2002) [61] propose a model where a source of seismic waves is triggered inside the volcanic conduit filled with a gas-melt mixture with depth dependent properties. The resulting synthetic wavefield matches well the characteristics of observed low-frequency events at Montserrat. The seismic energy which forms a resonance by propagating as interface waves up and down the conduit boundaries, is released at the ends of the conduit at regular time intervals, interacts with the free-surface and travels as surface waves along the topography to the seismic stations (Jousset et al., 2003 [56]). Using realistic magma properties (Sturton & Neuberg, 2003 [62]), this model explains also the frequency properties of those earthquakes in swarms: their time-dependence is observed as gliding spectral lines (Jousset et al., 2003 [56]). Magma properties are fundamental to explain the volcanic eruption style as well as the generation and propagation of seismic waves. A second study (Jousset et al., 2004 [63]) focusses on magma properties and rheology and their impact on low-frequency volcanic earthquakes.

We present these two studies below.

Time-dependent frequency content of low frequency volcanic earthquakes

Low-frequency volcanic earthquakes and tremor have been observed on seismic networks at a number of volcanoes, including Soufrière Hills volcano on Montserrat. Single events have well known characteristics, including a long duration (several seconds) and harmonic spectral peaks (0.2 to 5 Hz). They are commonly observed in swarms, and can be highly repetitive both in waveforms and amplitude spectra. As the time delay between them decreases, they merge into tremor, often preceding critical volcanic events like dome collapses or explosions. Observed amplitude spectrograms of long-period volcanic earthquake swarms may display gliding lines which reflect a time-dependence in the frequency content. Using a magma-filled dyke embedded in a solid homogeneous half-space as a simplified volcanic structure, Jousset et al. (2003) [56] employ a 2D finite-difference method to compute the propagation of seismic waves in the conduit and its vicinity.

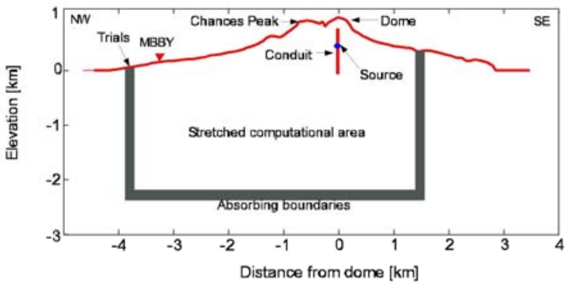

Figure 5. Model used in the finite difference scheme.

We successfully replicate the seismic wavefield of a single low-frequency event, as well as their occurrence in swarms, their highly repetitive characteristics, and the time-dependence of their spectral content. We use our model to demonstrate that there are two modes of conduit resonance leading to two types of interfaces waves which are recorded at the free surface as surface waves. We also demonstrate that reflections from the top and the bottom of a conduit act as secondary sources that are recorded at the surface as repetitive low-frequency events with similar waveforms. We further expand our modelling to account for gradients in physical properties across the magma-solid interface. We also expand it to account for time-dependence of magma properties, which we implement by changing physical properties within the conduit during numerical computation of wave propagation. We use our expanded model to investigate the amplitude and time-scales required for modelling gliding lines, and show that changes in magma properties, particularly changes in the bubble nucleation level, provide a plausible mechanism for the frequency variation in amplitude spectrograms.

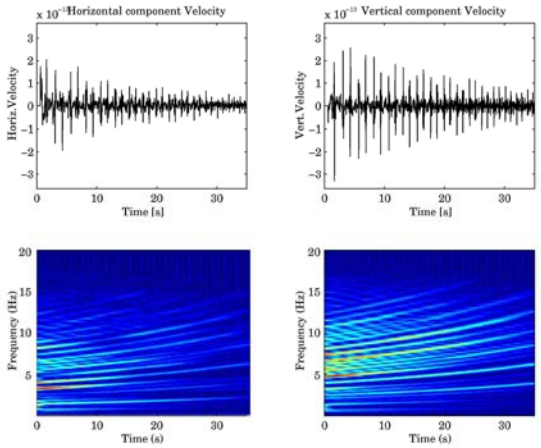

Figure 6. Bubble nucleation level change. Seismogram and spectrogram in the case where the nucleation level rises from a depth of 1100 m at constant level speed of 10 m s^{-1}. The initial conduit length is 1100 m. After 10 s the length of the conduit is reduced to 900 m. This speed is certainly too large for real cases, but the amplitudes of frequency peaks shift several Hz, in accordance with observations at Montserrat.

Influence of attenuation and topography on low frequency volcanic earthquakes

We investigate the effects of anelasticity and topography on the amplitudes and spectra of synthetic low-frequency earthquakes. Using a 2D finite difference scheme, we model the propagation of seismic energy initiated in a fluid-filled conduit embedded in a homogeneous viscoelastic medium with topography. We model intrinsic attenuation by linear viscoelastic theory and we show that volcanic media can be approximated by a standard linear solid for seismic frequencies above 2 Hz. Results demonstrate that attenuation modifies both amplitudes and dispersive characteristics of low-frequency earthquakes. Low frequency volcanic earthquakes are dispersive by nature; however, if attenuation is introduced, their dispersion characteristics will be altered. The topography modifies the amplitudes, depending on the position of the seismographs at the surface. This study shows that we need to take into account attenuation and topography to interpret correctely observed low-frequency volcanic earthquakes. It also suggests that the rheological properties of magmas may be constrained by the analysis of low-frequency seismograms.

The analysis of low-frequency event has to be to considered for the evaluation of hazard for at least two reasons:

1. The occurrence of gliding lines in spectrograms may indicate a bubble level change within the volcano conduit. This contributes to indicate the need for a change in the warning level at a volcano at the time of their occurrence.

2. Rheology of magma is one important parameter that determine eruption style. It can be accessed by the low-frequency analysis

Low frequency events therefore contribute to refine hazard assessment.

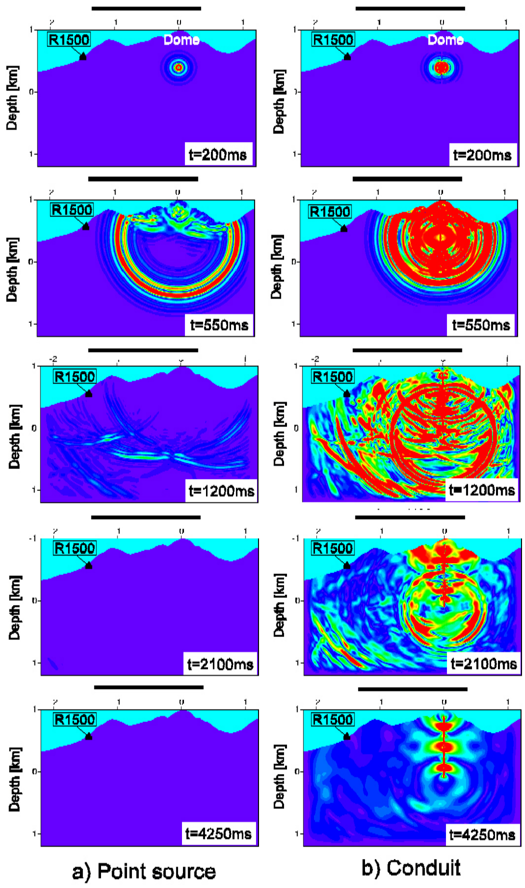

Figure 7.Series of snapshots of the velocity wave field produced by (a) an explosive point source in the homogeneous medium and (b) the resonance of the conduit (Q=20 in the conduit). In both examples, the topography crosses the dome along a NE-SE profile. R1500 is the location for seismograms modelled in Jousset et al., 2004 [

CONCLUSIONS

Risk assessment is based on the interface knowledge of hazard and vulnerabilities. Earth science studies may contribute to both by 1. improving the knowledge of structure and magmatic mechanisms of volcanoes; 2. assessment of volcanic hazard using past information.

The review of geophysical results with the view of hazard assessment allowed to draw tentative suggestions: geophysical studies in deformation, gravity and seismology contribute to 1. A better knowledge of the internal mechanisms within volcanoes, which is the aim of research, and 2. a better knowledge of hazard assessment, via the monitoring, because they give the state of a volcano at a given time. When the state of the volcano changes hazard is modified, because the probability of an eruption becomes more (or less) likely.

Repetitive measurements indicate long term behaviour of a volcano, giving time to a better preparation in case of an emergency. Continuous observations allow us to get short-term evolution of a volcano, which help the triggering of alert level. Specifically, gravity variations indicate the amount of magma to erupt, i.e., hints on the power of the future eruption, and the analysis of low-frequency events indicate rheology and bubble status, i.e., possible eruption style and intensity of possible explosion. These information are provided with long-term and short-term monitoring, implemented for hazard assessment.

ACKNOWLEDGMENT

Many people and institutions are involved in this work, among which the Laboratoire de Gravimétrie et Géodynamique, Institut de Physique du Globe de Paris, the Volcanological Survey of Indonesia, Usu Volcano Observatory, Hokkaido University, The University of Leeds, Montserrat Volcano Observatory. Many thanks to the French Embassy in Tokyo (Ministère des Affaires Etrangères), the Japan Society for the Promotion of Science and the Centre National de la Recherche Scientifique, France. I would like to thank Thierry Winter and Philippe Masure for their comments or the first draft.

REFERENCES

[[1] Marinatos S., 1939. The volcanic destruction of Minoan Crete. *Antiquity*, **13**, 425-439.
[2] McCoy F.W. and G. Heiken, 2000. The Late-Bronze age explosive eruption of Thera (Santorini), Greece: regional and local effects. *Geology of America Special paper,* **345,** 43-70.
[3] Alexander, 2000. Confronting Catastrophe. *Terra Publishing, Huxfordshire,* 282 pp.
[4] Dominey-Howes D. and D. Minos-Minospoulos, 2004. Perceptions of hazard and risk on Santorini. J. Volcanol. Geotherm. Res., **137**, 285-310.
[5] Chester D.K., Dibben C.J.L. and Duncan A.M., 2002. Volcanic hazard assessment in W. Europe. *J. Volc. Geoth. Res.*, **115**, 411-435.
[6] Stieltjes L., 2001. Evaluation et prévention du risque volcanique à la Martinique. *Rapport BRGM R 40492*, 510 pp.
[6bis] Masure P., 1996. Preventive planning, condition for the sustainable development of cities. Methodological bases for the GEMITIS programmes. DHA News, N° 18, April-May 1996.
[7] Paton D., Johnson D. and Houghton B.F., 1998. Organisational response to a volcanic eruption. *Disaster Prevention and Management,* **7**, (1), 5-13.
[8] Caristan Y, R.M. Chevrier, R. D'Ercole, P. Jousset and B. Massinon, 2001. Mission d'expertise du Comité Supérieur de l'Evaluation des Risques Volcaniques sur le Mont Usu (Japon), *CSERV, Ministère de l'Environnement*, 4th report, 77 pp.
[9] Kookelaar B.P. 2002. Setting, chronology and consequences of the eruption of Soufrière Hills Volcano, Montserrat (1995-1999). In: Druit T.H., Kookelaar B.P. (Ed.), The eruption of Soufrière Hills Volcano, Montserrat, from 1995 to 1999. *Geological Society, London, Memoirs,* **21**, 1-43.
[10] Collins G., J. N. Kremer and I. Valiela, 2000. Assessing uncertainty in estimates of nitrogen loading to estuaries for research, planning and risk assessment. Environ. Manag., **25**, 6, 635-645.
[11] Radke J., T. Corva, M.J. Sheridan, A. Troy, M. Lan and R. Johnson, 2000. Application challenges for geographical information science: implications for research, education and policy for emergency preparedness and response. *URISA J.*, **12**, 2, 15-30.
[12] Renschler , in press. Scales and uncertainties in using models and GIS for volcano hazard prediction. *J. Volcanol. Geotherm. Res.*
[13] Aspinall W.P. and G. Woo and B. Voight and PJ. Baxter, 2003. Evidence-based volcanology: application to volcanic crises. J. Volcanol. Geotherm. Res., **128**, 273-285.
[14] Tilling R. and R. W. Lipman, 1993. Lessons in reducing volcanic risk. *Nature,* **364**, 277-280.
[15] Mogi, K. 1958. Relations between the eruptions of various volcanoes and the deformations of the ground surfaces around them. *Bull. Earth. Res. Inst. Tokyo.* **36**, 99-134.
[16] Okada Y, 1985. Surface deformation due to shear and tensile faults in half-space. *Bull. Seism. Soc. Am.* **75**, 1135-1154.
[17] Rymer H., Murray J., Brown G., Ferruci F. and McGuire W., 1993. Mechanisms of magma eruption and emplacement at Mount Etna between 1989 and 1992. *Nature*, **361**, 439-441.
[18] Rymer H and G. Brown, 1986. Gravity fields and the interpretation of volcanic structures: geological discrimination And temporal evolution. *J. Volcanol. Geotherm. Res.*, **27**, 229-254.
[19] Deplus C., S. Bonvalot, D. Dahrin, M. Diament, H. Harjono and J. Dubois, 1995. Inner structure of the Krakatau Volcanic Complex (Indonesia) from gravity and bathymetric data. *J. Volcanol. Geotherm. Res.*, **64**, 23-52.

[20] Jachens R. C. and G. P. Eaton, 1980. Geophysical observations of Kilauea volcano, Hawaii, 1. Temporal gravity variations related to the 29 November, 1975, M=7.2 Earthquake and associated summit collapse. *J. Volcanol. Geotherm. Res*., **7**, 225-240.
[21] Yokoyama, I., 1989. Microgravity and height changes caused by volcanic activity: four Japanese examples. *Bull. Volcanol.*, **51**, 333-345.
[22] Brown, G.C., Rymer, H. and Thorpe, R.S., 1987. The evolution of andesite volcano structures: new evidence from gravity studies in Costa Rica. *Earth. Plan. Sc. Lett.*, **82**, 323-334.
[23] Jousset P. and H. Okada, 1999. Post-eruptive volcanic dome evolution as revealed by deformation and microgravity at Usu Volcano (Hokkaido, Japan), . *J. Volcanol. Geoth. Res*., **89**, 255-275.
[24] Jousset P., H. Mori and H. Okada, 2000. Possible magma intrusion revealed by temporal gravity, ground deformation and ground temperature observations at Mount Komagatake (Hokkaido) during the 1996-1998 crisis. *Geophys. J. Int*., **143**: 557-574.
[25] Jousset P., H. Mori and H. Okada, 2003. Elastic models for the magma intrusion associated with the 2000 eruption at Usu Volcano, Hokkaido, Japan. *J. Volcanol. Geotherm. Res.,* **125**, 81-106.
[26] Ikeda, T., 1985. Volcanological study of Toya pyroclastic deposits. *Master thesis of Hokkaido University* (in Japanese).
[27] Katsui, Y., Yamagishi, H., Soya, T., Watanabe, Y. and Nakagawa, M., 1992. Cenozoic volcanism in southwestern Hokkaido. *29th IGC field trip guidebook*, A03: 1-28.
[28] Okumura K., and Sangawa A., 1984. Age and distribution of Toya pyroclastic flow. *Bull. Volcanol. Soc. Japan*, Ser. 2, **29**, 338.
[29] Machida, H., Arai., F., Miyauchi, T., and Okumura, K., 1987. Toya ash - a widespread lat Quaternary time-marker in northern Japan. *Quaternary Research*, **26**, 129-145.
[30] Soya, T., Katsui, Y., Niida, K. and Sakai., K., 1981. Geologic map of Usu volcano, scale 1:25000. *Geol. Surv. Japan*.
[31] Yokoyama, I., Katsui, Y., Oba, Y. and Ehara, S., 1973. Usu-zan, its volcanic geology, history of euption, present state of activity and prevention of disasters. Comitee for Prevention of Disasters of Hokkaido, Sapporo, 254 pp (in Japanese).
[32] Katsui Y., Komuro H., and Uda T., 1985. Development of fault and growth of Usu-Shinsan crypto-dome in 1977-1978 at Usu volcano, N. Japan. J. Fac. Sci. Hokkaido Univ., Ser. 4**, 21**, 339-362.
[33] Katsui, Y., Oba, Y. and Soya, T., 1978. Types of historic eruptions and nature of magma in northern Japan. In: Thera and the Agean World I, London, 171-182.
[34] Oba, Y., Katsui, Y. Kusarawa, H. Ikeda, Y. and Uda, T. 1983. Petrology of historic rhyolite and dacite from Usu volcano, north Japan. *J. Fac. Sci. Hokkaido Univ.*, Ser. 4, **20**, 275-290.
[35] Okubo, S. and Watanabe, H., 1989. Gravity change caused by a fissure eruption. *Geophys. Res. Letters*, **16**, 5, 445-448.
[36] Lee, T.Y. and Lawver, L.A., 1995. Cenozoic plate reconstruction of southeast Asia. *Tectonophys.* , **251**, 85-138.
[37] De Mets, C., Gordon, R.G., Argus, D.F. and Stein, 1990. Current plate motion. *Geophys. J. Int.*, **101**, 425-478.
[38] Zen Jr, M.T., 1993. Déformation de l'avant-arc en réponse à une subduction à convergence oblique. Exemple de Sumatra. *Thesis, Univ. Paris VII,* 253 pp.
[39] Katili, J.A., 1974. Volcanism and plate tectonics in the Indonesian Islands arc. *Tectonophys.*, **26**, 165-188.
[40] Hutchison C., 1976. Indonesian active volcanic arc: K, Sr, and Rb variation with depth to the Benioff zone. *Geology*, **4**, 407-408.
[41] Berthommier, P., Camus, G., Condomines, M. and Vincent, P., 1990. Le Merapi (Centre-Java): Elements de chronologie d'un strato-volcan andésitique. *C. R. Acad. Sci.,* **311**, II: 213-218.
[42] Camus G., Gourgaud A., P.C. Mossand-Bethommier and P.M. Vincent, 2000. Merapi (Central Java, Indonesia): an outline of the structural and magmatological evolution, with a special emphasis to the major pyroclastics events. *J. Volcanol. Geotherm. Res.,* **100**, 139-163.
[43] Newhall C., Bronto S., Alloway B.V., Andeastuti S., Banks NG, Bahar I., Del Marmol M.A., Hadisantono R.D., Holcomb R.T., McGeehin J., Miksic J.N., Rubien M., Sayudi S.D., Sukhyar R. Tilling R.I, Torley R., Trimble D., Wirakusumah A.D., 2000. 10000 years of explosive eruptions at Merapi Volcano, Central Java: archeological and modern implications. *J. Volcanol. Geotherm. Res.,* **100**, 9-50.
[44] Christiansen R.L. and Peterson D.W., 1981. Chronology of the 1980 eruptive activity, in: The 1980 eruptions of Mount St Helens, Washington, D.C., *U.S. Geol. Surv., Prof. Pap.* **1250**, 525-540.
[45] McDonald G. 1972. Volcanoes. Prentice-Hall Inc. New Jersey.
[46] Young, K.D., Voight, B., Marso, J., Subandrio, Sajiman, Miswanto, Paijo, Suharno and Bronto, S., 1994. Tilt monitoring, lava dome growth and pyroclastic flow generation at Merapi volcano, Java, Indonesia. *Geol. Soc. Am. Abstr. Prog*, **26**, 7, A-483.
[47] Sukhyar, J., 1995. Learning from the November 22, 1994 Merapi Eruption. *Merapi Decade Volcano International Workshop*. Oct, 5-9, 1995, Yogyakarta.
[48] Jousset P. 1996. Microgravimétrie et Gravimétrie en volcanologie : méthodologie et application au volcan Merapi, Java, Indonésie. Thèse 3ieme cycle, Université Paris VII, 325 pp.
[49] Jousset P., Dwipa S., Beauducel F., T. Duquesnoy and M. Diament, 2000. Temporal gravity at Merapi Volcano during the 1993-1995 crisis: an insight into the dynamical behaviour of volcanoes. *J. Volcanol. Geotherm. Res.,* **100**, 289-320.
[50] Dingwell D. & S. Webb, 1989. Relaxation in silicate melts: some applications. *Phys. Chem. Mineral.*, **116**, 508-516.
[51] Barmin A., O. Melnik and S. Sparks, 2002. Periodic behaviour in lava dome eruptions, *Earth planet. Sci. Lett.,* **199**, 173-184.
[52] Stevenson, R.J., D. Dingwell, S. Webb and N. Bagdassarov 1995, The equivalence of enthalpy and shear stress relaxation in rhyolitic obsidians and quantification of the liquid-glass transition in volcanic processes. *J. Volcanol. Geotherm. Res.,* **68**, 297-306.
[53] Young S., S. Sparks, W.P. Aspinall, L.L. Lynch, A.D. Miller, R.E.A Robertson and J. Shepperd, 1998. Overview of the eruption of Soufrière Hills volcano, Montserrat, 18 July 1995 to December 1997, *Geophys. R. Lett.,* **25** (18), 3389-3392.
[54] Chouet B., 1996. New methods and future trends in seismological volcano monitoring, in *Monitoring and Mitigation of Volcano Hazards,* pp. 23-97, eds Scarpa, R & Tilling R.I., Springer-Verlag, Berlin.
[55] Neuberg J., 2000. Characteristics and causes of shallow seismicity in andesite volcanoes. *Phil. Trans. R. Soc. Lond.,* **358,** 1533-1546.
[56] Jousset P., J. Neuberg and S. Sturton, 2003. Modelling the time-dependent frequency content of low-frequency volcanic earthquakes. *J. Volcanol. Geotherm. Res.,* **128**, 201-223.
[57] Biot, 1952. Propagation of elastic waves in a cylindrical bore containing a fluid. *J. Appl. Phys.*, **23**, 997-1005.
[58] Chouet B. 1985. Excitation of a buried magmatic pipe: a seismic source model for volcanic tremor. *J. Geophys. Res.*, **90**, 1881-1893.
[59] Ferrazini V. and K. Aki, 1987. Slow waves trapped in fluid-filled infinite-crack: implication for volcanic tremor. *J. Geophys. Res.*, **92** (B9), 9215-9223.
[60] Neuberg J., B. Baptie, R. Luckett and R. Stewart, 1998. Results from the broad-band seismic network on Montserrat. *Geophys. Res. Lett.*, **25**(19), 3661-3664.
[61] Neuberg J. and O'Gorman, 2002. A model of the seismic wavefield in gas-charged magma: application to Soufrière Hills volcano, Montserrat. *Geol. Soc., London,* Memoir, **21**, 603-609.
[62] Sturton S. and J. Neuberg, 2003. The effects of a decompression on seismic parameter profiles in a gas-charged magma. *J. Volcanol. Geotherm. Res.,* **128**, 187-199.
[63] Jousset P., J. Neuberg and A. Jolly, 2004. Modelling low-frequency earthquakes in a viscoelastic medium with topography. *Geophys. J. Int.*, **159**, 776-802.

Dr. Philippe Jousset - Bureau Recherche Géologique et Minière, Development Planning and Natural Risks Division,
3 Avenue Claude Guillemin , BP 6009, 45060 Orléans Cedex 2, FRANCE. email: p.jousset@brgm.fr

Remote sensing techniques for multiscale surface displacement mapping

*Christophe Delacourt [(1)] and Pascal Allemand [(2)]

(1) Laboratoire de Sciences de la Terre, UMR5570, UCBL & ENS Lyon, 2 Rue Dubois, 69622 Villeurbanne Cedex, France

ABSTRACT

Geohazards driven directly by geological processes, (seismic cycle, volcanoes, gravitating phenomena), involve ground displacements. Remote sensing imagery is a powerful tool for monitoring unstable areas because it offers a synoptic view that can be repeated at different time intervals. Combination of optical correlation with Differential SAR interferometry (DINSAR) is a promising method for the study of surface instabilities. Limitation of DINSAR (limited data archive starting in 1991, geometrical constraint, loss of coherence due to vegetation and atmospheric artifact) can be overcome using optical correlation. The large temporal archive of aerial images (since 1950 in France), high spatial resolution (better than 1 meter) and launch of new very high resolution optical satellites (QuickBird, Ikonos, SPOT5) can supply images that allow detailed monitoring and observation of surface displacements. DINSAR detects displacement in the range of the radar wavelength (at centimeter level), optical correlation detects displacement from the pixel size up to 100 times the pixel size.

KEYWORDS: Differential SAR interferometry, optical correlation, surface displacement, landslides, volcanoes

INTRODUCTION

Geohazards driven directly by geological processes, (seismic cycle, volcanoes, gravitating motions), involve ground displacements. For each geological process, information on the displacement acquired both actually and for past periods is a key point for better understanding its dynamics. However, as shown on Figure 1, time and distance scales of the ground deformations range on several orders of magnitude.

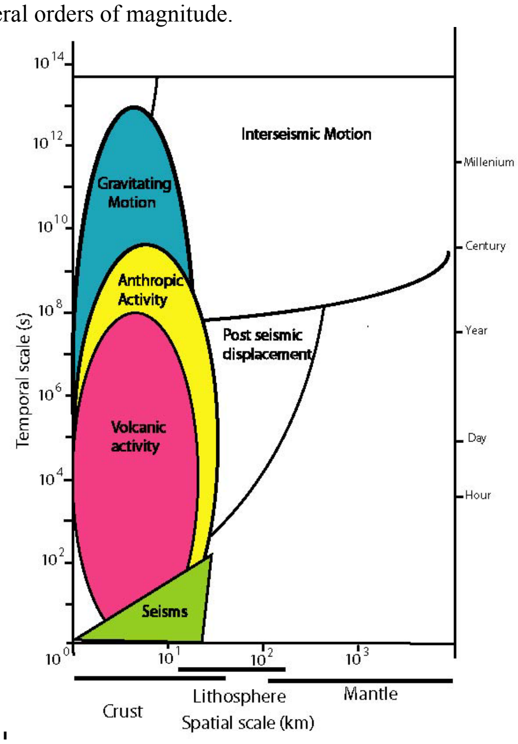

Figure 1: Earth surface motion classification.

Then, none unique technique can efficiently records motion associated to all the geological processes. Combination of several techniques is required. Presently, most of the techniques for acquiring ground displacement values are derived from measurements of reference stations. Conventional geodetic techniques (triangulation, tacheometry, leveling) and extensometry techniques remain to be the most commonly used. GPS measurements can be an alternative. However, the database of movement provided by these techniques is available only for major sites for a time span not exceeding 20 years for laser measurements and less than 15 years for GPS. Moreover, due to spatial and temporal heterogeneities of the displacements, such ground based measurements are not sufficient to describe fully the velocity field. Remote sensing imagery is a powerful tool for monitoring unstable areas because it offers a synoptic view that can be repeated at different time intervals. Two main remote sensing techniques can be combined: differential SAR Interferometry (DINSAR) and optical image correlation.

DIFFERENTIAL SAR INTERFEROMETREY (DINSAR)

The differential SAR interferometry (DINSAR) gives access to the change in distance between the ground and the sensor. The technique is based on the comparison of the phases of two SAR acquisitions (see for example [1]). As the SAR phase is proportional to the distance between the sensor and the target, altimetric information can be derived from radar interferometry. Once taken into account the different components (topographic and orbital components), the interferometric phase can be used to derive the displacement of the ground occurred between the two acquisitions with a centimeter accuracy and a decameter resolution. However, this technique is affected by several limitations

Geometrical constraints

Due to the side looking acquisition of the SAR, areas affected with severe slopes cannot be imaged by DINSAR. This is critical if observations are realized on medium and high mountainous areas as for landslides study. One way to partly overcome this limitation is to combine both ascending and descending orbits (Fig. 2).

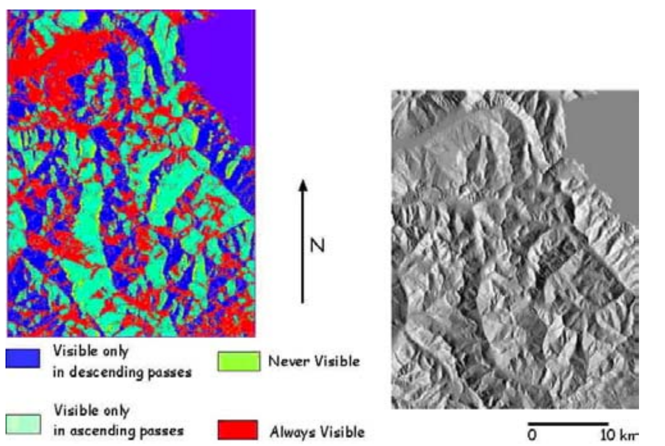

Figure 2: Geometrical visibility of the French South Alps by ERS 1 satellite in ascending and descending pass

Loss of coherence

The change in physical and geometric characteristics of the targets produces loss of coherence on interférograms [2]. In that case, the displacement signal cannot be recovered. This point is critical in vegetated area where the loss of coherence occurs only after several days. One way to overcome this limitation is to use radar satellite with low frequency (L band for example instead of C band, Fig. 3). Unfortunately, presently no L band satellite data are available.

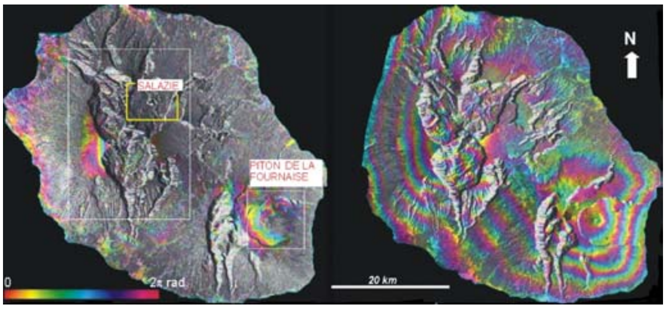

Figure 3: Potential of L band SAR interferometry in vegetated areas. Example of the "La Réunion Isle"; Left: Radarsat interferogram (C band - 2001/05/15 - 2001/11/23); Right : JERS interferogram (L band 1997/01/02 – 1997/05/14)

Atmospheric effects

Variations in atmospheric conditions in the lower part of the atmosphere (troposphere) between the 2 acquisitions dates of the images change the radar signal time delay ([3], Fig 4). This change produces a rotation of the phase which could mask part of the displacement signal. Two types of atmospheric artifacts could occur. First a global change of the atmosphere will produce low frequency artifact, correlated with topography. This artifact is very important for volcanic application, because part of the displacement observed on volcano before and during an eruption is correlated with topography. In that case, removing atmospheric artifact signal to exhibit displacement signal requires either a statistical approach or the modeling of the atmosphere [4, 5].

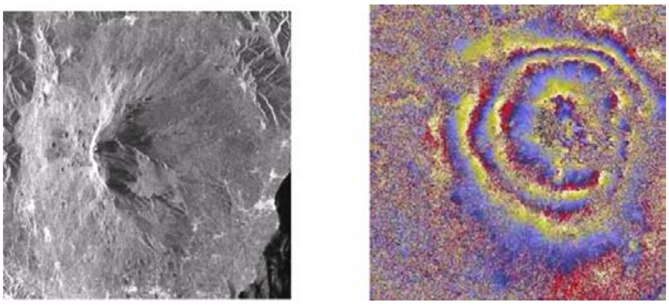

Figure 4: Example of tropospheric artifact observed on a 1 day ERS differential SAR interferogram over Etna Volcano.

The second artifact is due to local heterogeneities of the atmosphere. Those high frequency artifacts cannot be removed on a single interferogram. We can see on figure 5, on a 1 day differential SAR interferogram calculated on the French Alps, that due to the size of the heterogeneities (few tens of meter to kilometers), the artifacts can be interpreted as local motion signature (landslides for example). In that case, the only way to detect this artifact is to use various independent interférograms. Indeed these artifacts are not correlated with time.

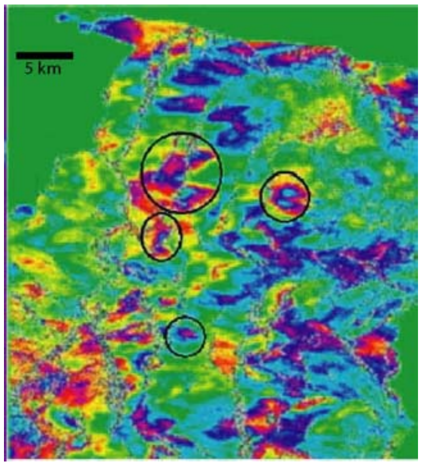

Figure 5: Example of local atmospheric artifacts on the South French Alps

Despite those severe limitations, DINSAR is a power full tool for seismic, volcanic and gravitating motions.

For example, for volcanic applications, a large scale deflation of the ETNA volcano associated with the large 1991-1993 eruption was detected in data covering the second half of the eruption [4, 5]. At local scale, we showed that the local deformation fields located in Valle del Bove (East of the volcano) where associated with the compaction of the 1986-1987 and 1989 lava fields and also partly with a subsidence of the surrounding terrain in response to the load of the new deposited material. Other local deformation fields have been identified, corresponding to the 1983, 1981 and 1971 lava fields. [6]. The DINSAR technique is now frequently used for volcanic studies.

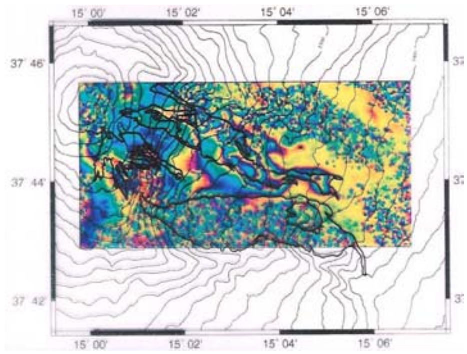

Figure 6: Displacement field associated to the 1989 lava flow on Etna observed on a one year differential ERS interferogram

Regarding gravitating motions, the "la Valette" landslide located in the Ubaye valley (France) has been investigated by 15 differential interferograms realized from ERS-1 and ERS-2 images acquired between 1991 and 1999 both in 3 days cycle and TANDEM phase (1 day). Velocity maps of "La Valette" landslide have been established (Fig. 7). Four domains characterized by their own velocity field have been detected. Three of them can be distinguished from aerial photographs and field analysis. Slow velocity of a resistive bar located near the top of the landslide has been detected on SAR interferograms. Between 1991 and 1996, evolution of the limits of the landslide has been observed both in the upper and in the lower part, by a back erosion corresponding with the main scarp and a progress of the main body of the landslide. The average velocity of the landslide between 1991 and 1999 decreased from 1cm/day to 0.2cm/day in agreement with ground based measurements [7].

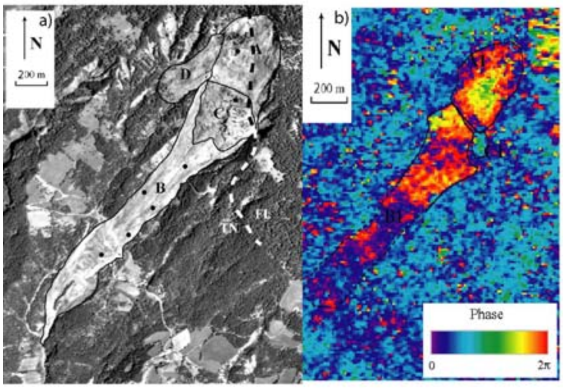

Figure 7: Left: Aerial photograph of the “La Valette” landslide on which the main tectonic features have been represented. In black are outlined the 4 zones having different morphological features mapped; Right**:** One day differential SAR interferogram dated 22-23 October 1995. In black, the three areas mapped from SAR interferometric analysis. A full phase rotation (2π) is corresponding to 2.8 cm of displacement along the line of sight.

However, for those applications, 3 limitations of DINSAR could be mentioned: the limited archive available (1991 to 2000 for ERS), the monodirectionnal component of the displacement, and the spatial resolution (around 10 meters). Aerial images and new high resolution satellite (QuickBird, Ikonos, SPOT5) could overcome those limitations.

OPTICAL IMAGES CORRELATION

A new technique based on the correlation of images acquired by optical sensor (aerial or satellite) on the same area at two different times can be applied for deriving surface displacement maps occurring between two acquisitions.

To find the ground displacement, a local window of a fixed number of pixels width is defined on the oldest image. Then, the corresponding window is searched on the recent image by maximizing a correlation function [8, 9]. The starting point of the search is the expected position of the window if no displacement had occurred between the two acquisitions. The measured shift is directly related to the ground displacement between the two acquisitions. The main parameters of the process are the size of the local window and the maximum expected displacement between the images. This process is repeated for each pixel of the oldest image. The result is composed by 3 arrays which have the size of the correlated images. The first one contains the shift in lines for each pixel, the second one contains the shift in columns and the third indicates the quality of the correlation. Such information is complementary to the DINSAR method in terms of displacement detection. DINSAR detects displacement in the range of the radar wavelength (at centimeter level), optical correlation detects displacement from the pixel size up to 100 times the pixel size.

Those techniques have been successfully applied to the measurement of coseismic deformation [10] using decametric optical satellite imagery (SPOT 1-4, LANDSAT). However, those resolutions are not suitable for small extension objects (landslides). We then apply this technique on 6 aerial images acquired on “La Clapiere landslide” (located in the French South Alps) in 1974, 1983, 1988, 1991, 1995 and 1999. Displacements maps (composed of both velocity and direction of movements) exhibiting temporal and spatial evolution of the landslide have been generated (Fig 8-9-10).

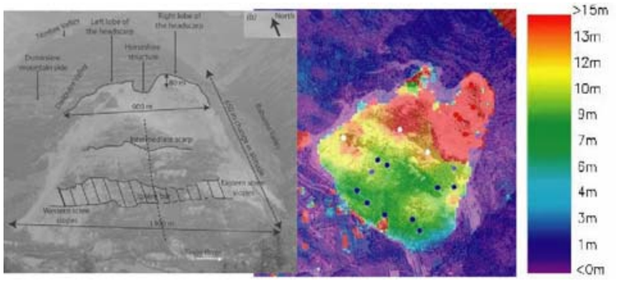

Figure 8: Left “La Clapière Landslide”; Right: velocity map calculated from 2 aerial images (1995-199)

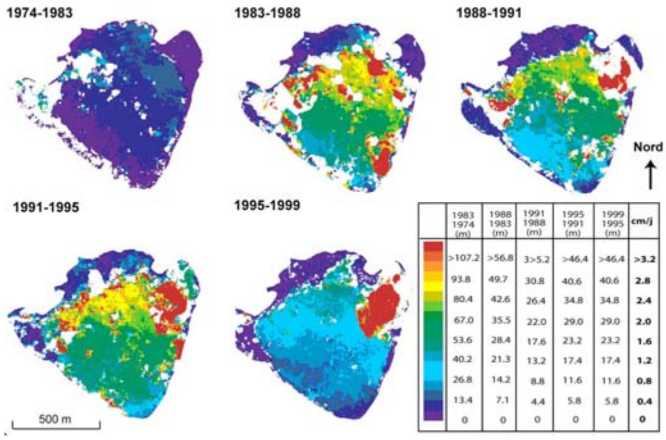

Figure 9: Velocity maps of the “ La Clapière” landslide between 1974 and 1999

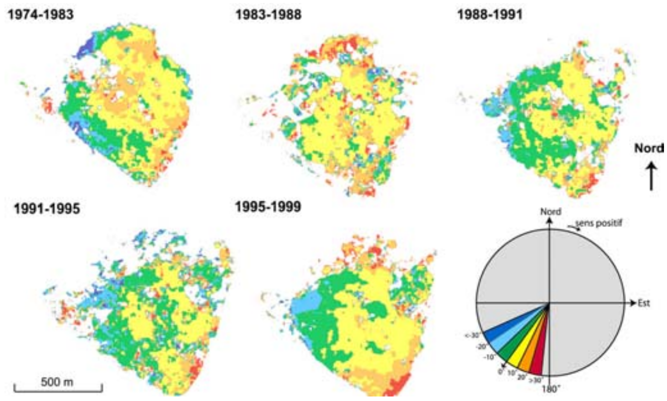

Figure 10: Maps of the direction of the displacement of the “ La Clapière” landslide between 1974 and 1999

Furthermore, in order to improve the temporal resolution of the measurements, it is possible to apply image correlation by combining optical images acquired by various sensors. A velocity map calculated from aerial and QuickBird image is presented on Figure 11 [11].

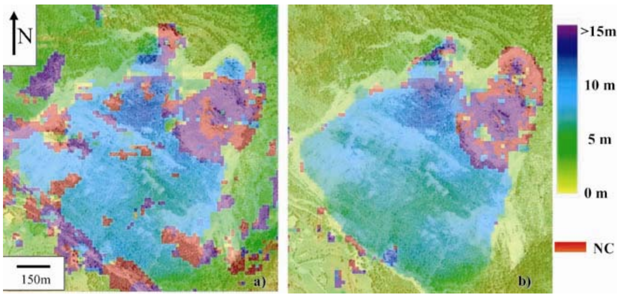

Figure 11: North-south deformation map a) between 1999 and 2003 from aerial and QuickBird image b) between 1995 and 1999 from aerial images. NC corresponds to no significant displacement areas because of poor quality correlation values.

Finally by combining, planimetric motion derived by correlation technique and Differential Digital Elevation Models (DEMs) calculated from the stereoscopic aerial images, the 3D velocity map can be obtained. These data have been used to characterize qualitatively the geometry of the slip surface of the “la Clapière landslide”. Ratios of vertical displacements to horizontal ones and distribution of differential data are in accordance with a curved slip surface characterizing a preferential rotational behaviour of this landslide. On the other hand, a spatial evolution of the geometry of the slip surface after 1988 is pointed out. Indeed, a propagation of the slip surface under the Iglière bar in the W part of the landslide is suspected and linked to the acceleration of the landslide in 1987. [12]

CONCLUSION

Combination of optical correlation with Differential SAR interferometry (DINSAR) is a promising method for the study of surface instabilities. Limitation of DINSAR (limited data archive starting in 1991, geometrical constraint, loss of coherence due to vegetation and atmospheric artifact) can be overcome using optical correlation. The large temporal archive of aerial images (since 1950 in France), high spatial resolution (better than 1 meter) and launch of new very high resolution optical satellites (QuickBird, Ikonos, SPOT5) can supply images that allow detailed monitoring and observation of surface displacements. DINSAR detects displacement in the range of the radar wavelength (at centimeter level), optical correlation detects displacement from the pixel size up to 100 times the pixel size.

REFERENCES

[1] Massonnet D. & Feigl K., (1998) Radar interferometry and its application to changes in the earth's surface, *Reviews of geophysics*, 4 , 441 - 500

[2] Zebker, H. A., and Villasenor, J., Decorrelation in interferometric radar echoes, *I.E.E.E. Transactions on geoscience and remote sensing*, 30, pp. 950-959, 1992.

[3] Tarayre, H., and Massonnet, D., Atmospheric propagation heterogeneities revealed by ERS-1 interferometry,*Geophysical Research Letters*, 23,(9), pp. 989-992, 1996.

[4] Beauducel, F., Briole, P., and J.L., Froger, Volcano-wide fringes in ERS synthétic aperture radar interferograms of Etna (1992-1998): Deformation or Tropospheric effect ?, *Journal of Geophysical Research*., 10516,391, 16402

[5] Delacourt, C., Briole, P., and Achache, J., (1998), Tropospheric corrections of SAR interferogramms with strong topography. Application to Etna, *Geophysical Research Letters*, 25, pp. 2849-2852.

[6] Briole, P., Massonnet, D., and Delacourt, C., (1997), “Post-eruptive deformation associated with the 1986-87 and 1989 lava flows of Etna.”, *Geophysical Research Letters*, 24, pp. 37-40..

[7] Squarzoni C., Delacourt, C., and Allemand P. (2003), Nine years of spatial and temporal evolution of the la valette landslide observed by SAR interferometry. *Eng. Geology,* 68-1-2, pp 53-*66*

[8] Vadon, H. et Massonnet, D., (2002). Earthquake displacement fields mapped by very precise correlation. Complementarity with radar interferometry. IGARSS proc.: 1-4.

[9]Van Puymbroeck, N., Michel, R., Binet, R., Avouac, J.P. et Taboury, J., (2000), Measuring earthquakes from optical satellite images. Apll. Optic, 39: 3486-3494.

[10] Michel, R. et Avouac, J.P., (2002). Deformation due to the 17 August 1999 Izmit, Turkey, earthquake measured from SPOT images. *Journal of Geophysical Research*, 107.

[11] Delacourt, C., Allemand, P., Casson, B., Vadon, H., (2004), Velocity field of the "La Clapière" landslide measured by the correlation of aerial and QuickBird images, Geophysical Research Letter, 31,L15619

[12] Casson, B., Delacourt, C., Allemand,P., (2004), Qualitative slip surface characterization using surface data derived from DEMs and ortho-rectified images, submitted to *Eng. Geology*

Christophe Delacourt
Laboratoire de Sciences de la Terre, UMR5570, UCBL & ENS Lyon, 2 Rue Dubois, 69622 Villeurbanne, France, email: christophe.delacourt@univ-lyon1.fr

Hazard map of Fuji Volcano: how did we make and how should we use it?

Masato Koyama

Department of Integrated Sciences and Technology, Faculty of Education, Shizuoka University

ABSTRACT

Fuji Volcano, which is located 100km to the southwest of Tokyo and has the highest summit (3,776m above sea level) in Japan, is one of the largest stratovolcanoes in the world. The Volcano has erupted at least 500km^3 of mostly basaltic lava and tephra since 100,000 years ago and is still active, because 10 reliable records of eruption are known in historical documents, which were written during the past 1,300 years. The latest "Hoei" eruption occurred in AD1707. The eruption, which lasted 16 days, is one of the most voluminous and explosive eruptions in the whole eruptive history and discharged 0.7km^3 magma, most of which was deposited as fallout scoria. During the last 20 years of the 20th century, the activity of volcanic earthquake was low and no geothermal signal was observed on its surface.

Sudden increase of low-frequency earthquakes in two periods (October, 2000-January, 2001 and May-June, 2001) 10-20 km beneath the Volcano has given a shock to the Japanese society and caused the establishment of the National Commission for Disaster Mitigation of Mount Fuji (NCDMF), which consists of prefecture governors, mayors of local government, and cabinet officials concerned. NCDMF established the Committee for Hazard Maps of Fuji Volcano (CHMF), which is managed mainly by the Cabinet Office, Government of Japan, and delegated CHMF to create hazard maps and overall mitigation planning for future eruptions of Fuji Volcano. This became the first case in Japan that the mitigation programs against volcanic disasters were done on the national level. CHMF consists of specialists, which include volcanologists, social scientists, journalists, and civil defense officers.

CHMF published its final report including a series of hazard maps on June 29, 2004. The report deals with eruptive history, assessment of future eruptions (vent position, discharge volume of magma, and mode of eruption), numerical simulation of various types of eruptions, and social damage assessment in case of a major pyroclastic (plinian) eruption. A series of discussion and assessment was made concerning the eruption forecasting and social correspondence, and crisis management during and after eruption. Model plans for disaster mitigations, both on regional and local basis, were suggested to help individual local government to make their own action plans.

The author mainly introduce how CHMF assessed the future eruptions and draw the hazard maps, and also discuss how the local communities should use the hazard maps especially during a dormant period of the volcano.

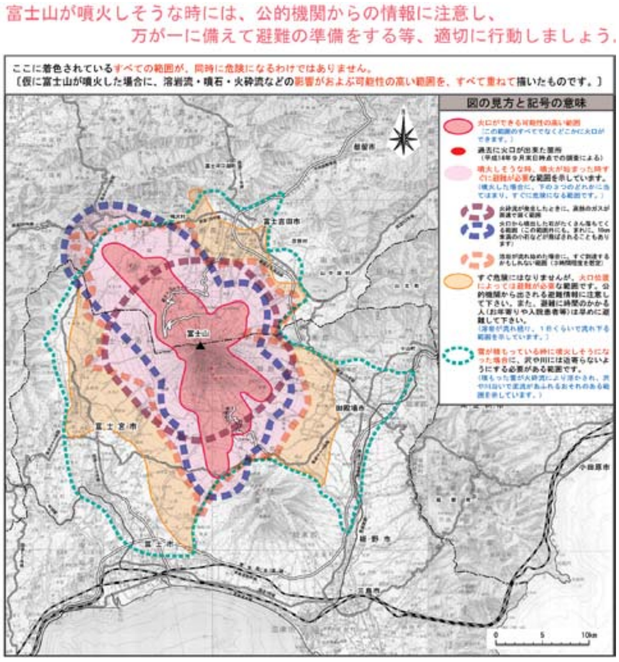

Figure: An example of the CHMF hazard maps of Fuji Volcano. This map shows zoning, which is divided by the difference of preferable actions of local residents.

Masato Koyama
Department of Integrated Sciences and Technology, Faculty of Education, Shizuoka University
836 Oya, Shizuoka, 422-8529 JAPAN,
email: edmkoya@ipc.shizuoka.ac.jp

How electromagnetic phenomena can contribute to the volcanic risk mitigation

*Jacques Zlotnicki(1), Jean Louis Le Mouël(2), Yoichi Sasai(3), G. Vargemezis(4), Paul Yvetot(1), Philippe Menny(1), and Fréderic Fauquet(1)

(1) National Scientific Research Center, OPGC-UMR6524, Clermont-Ferrand, France ; (2) Institut de Physique du Globe de Paris, France ; (3) The Disaster Prevention Specialist, Tokyo Metropolitan Government; (4) Thessaloniki University, Greece.

ABSTRACT

Millions of inhabitants are living on volcanoes or along active faults and civil infrastructures are progressively developing there. The economy also requires use of these soils for agriculture, and for urban development. But earthquake or volcanic eruption regularly occur and destroy the social tissue for a long time. The XXI century will have to use and manage this potential wealth and reduce the loss of life, to administrate the enhanced risks of land degradation, to reduce the costs of destructions and the long-term economic disruption.

For a number of decades a range of geophysical and geophysical effects associated with the volcanic activity have been monitored, including seismicity, ground deformation, gas emission, and variations of temperature, gravity, electricity and magnetism.

Among these, the study of volcano-magnetic, -electric and -electromagnetic phenomena is relatively young. These methods become more and more powerful and the integration of several complementary techniques can now give valuable information either on the volcanic structures and their regional setting or on the processes which lead to a surface activity. Electromagnetic studies have now reached the level to efficiently contribute to the volcanic risk mitigation.

We will present two complementary aspects of electromagnetic studies on volcanoes.

First, the investigations which are carried out to better understand the structure and the plumbing system and, the consequences which have to be deduced on the dynamism and the mechanical stability of volcanic edifices.

Second, the monitoring of volcanic activity which now combines several techniques for identifying the involved physical mechanisms and, the sources which are triggered.

We will illustrate the imaging of volcanoes with La Soufrière of Guadeloupe, which is located in the French West Indies. We will describe the EM monitoring of volcanoes through Miyake-jima example.

KEYWORDS: Volcano imaging, electromagnetic monitoring,

IMAGING VOLCANIC STRUCTURE

Methods

The dynamism of a volcano is controlled by the nature of its plumbing system as well as by the structure in which the magma has to find a path toward the ground surface. It is now well accepted that pre-existing faults, caldera walls, flank failure rims have to be taken into account in the risk assessment.

On some volcanoes existing aquifers and ground water flows stand in the upper part of the edifices and mineralisation processes strongly change the mechanical cohesion of the rocks and the thermo dynamical equilibrium. Such a case can imply phreatic activity before a possible magmatic eruption.

In EM investigations several techniques can be used to identify the overall and deep structure as well as the details of first kilometres depth. VLF, Self-potential (SP), DC- resistivity soundings and magnetic surveys contribute to evidence local heterogeneities. SP mappings identify hydrothermal systems and ground water channelling. Audio-MagnetoTelluric (AMT) soundings give valuable information on the first tens kilometres of depth and low MT soundings are able to prospect the structure till several tens of kilometres depth.

Soufrière of Guadeloupe

La Soufrière (1467 m) is the active island arc volcano of Guadeloupe. Magmatic activity took place prehistorically and the last event is dated 1440 AD. The two last 1956 and 1976-77 phreatic/phreato magmatic eruptions were preceded by several decades of quietness. During these quiet periods, hydrothermalisation and argillization are expanding due to high tropical rainfalls (8 to 9 m/y). Sealing of fractures yields more and more difficult the release of thermal stresses developed by a non well-known magmatic body. Overpressures are increasing in confined superficial water tables. Renew of seismic activity started in May 1992. Old outcrops began to flow again and temperature of some thermal sources smoothly increased. Since 1992 the seismic activity occurs sporadically.

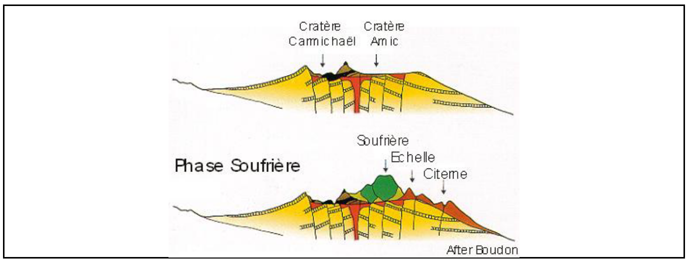

Figure 1: Scheme of the volcanic setting (after Boudon, 1987).

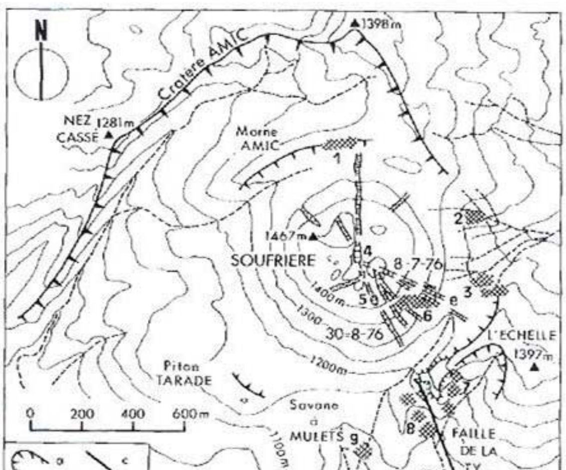

Figure 2: Detailed description of Soufrière dome. Locations of hot springs (underlined figures) and some structures (underlined letters). 1 : Bains-Jaunes; 2 : Tarade; 3 : Galion; 4 : Savane à Mûlets well ;

5 : Col de l'Echelle well ; 6 : Carbet-Echelle ; 7 : Ravine Marchand. A : South crater ; B : Morne Mitan ; C : Col de l'Echelle ; D : Chaudières-Souffleur ; E : Colardeau Fumarolic area. Cartoon : Locations of main faults. 1 : August 30, 1976; 2 : Lacroix ; 3 : 1956 ; 4 : July 8 ; 5 : North-East ; 6 : North ; 7 : North-West ; 8 : Faujas.

Audio-magnetotelluric soundings

We started to study the hydrothermal system and its activity in 1987 by developing repeated SP mappings, audiomagnetotelluric soundings and we recently made VLF surveys to get information on the superficial structure and the ground water channeling.

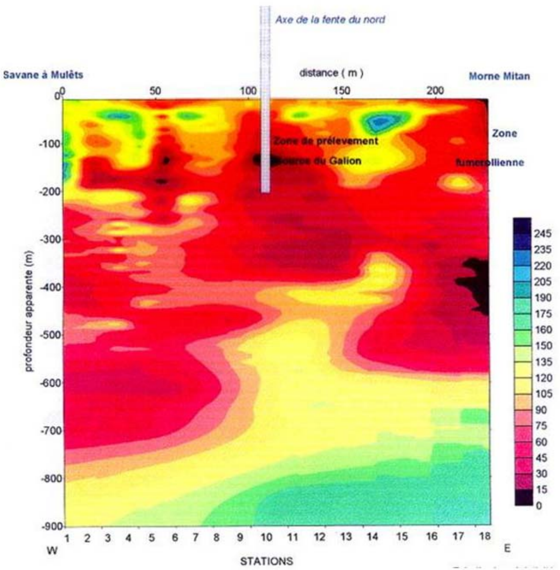

Figure 3: Apparent resistivity on the South flank of Soufrière dome showing the strong mineralisation of the dome which is set on crater Amic floor.

Self-potential mappings and hydrothermal activity

The comparison of SP mappings between 1987 (Pham et al., 1990), 1992 (Zlotnicki et al., 1994), 1994 and 2000 shows (i) smooth positive anomalies which do not exceed 350 mV, (ii) a slow spreading of the positive anomalies from the West dome flank in 1987, to the South in 1992, to the South West in 1994 and to the volcano itself in 2000, and (iii) the disappearance of local anomalies right above the faults cutting the dome. In 2000 the variations of SP anomalies, in space and time, are well-correlated with a slow increase of surface activity since 1992 expressed by a more dense fumarolic activity in the main summit crater (temperature ≤ 110°C) and sporadic, low magnitude, seismic crises. This interpretation is based on the fact that, after 1998, hydrothermal activity extended beyond the prevailing and existing water channel as faults or craters rims. The thermal equilibrium source of the steady state hydrothermal activity observed after the 1976-77 seismo-volcanic crisis is now upset, and we actually observe a slow increase of sub surface activity.

Figure 4 presented in the next column: Time changes of SP mappings on Soufrière, Guadeloupe.). D : in 1994. E : in 2000. R is the reference station. These mappings show the increase of the hydrothermal activity after 1992 when some small surface activity (gases and vapour emissions) started accompanying by sporadic seismic swarms.

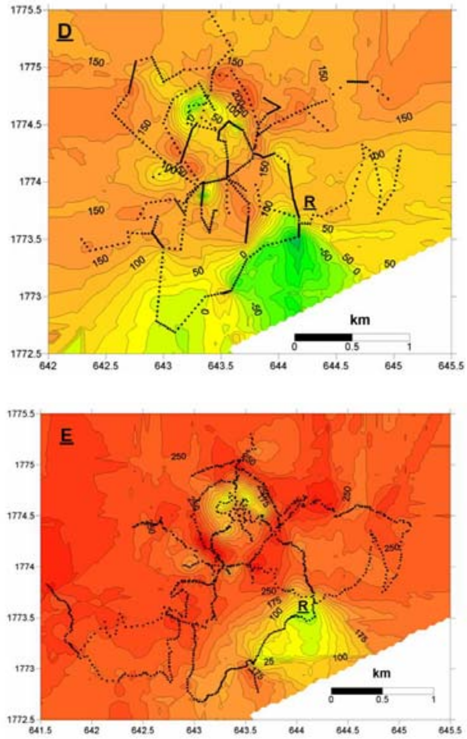

Ground water channeling and faults systems inferred by VLF surveys

In order to recognize the superficial electrical resistive and conductive zones (less than 100 m depth) as well as the cavities on Soufrière volcano, Very Low Frequency (VLF) surveys were made in 2000 (Zlotnicki et al., 2004). Electrical conductive zones are clearly associated with major radial faults starting from the summit in which the hydrothermal activity takes place. In the continuation of these active hydrothermal fractures hot springs are located down slope. Conversely some of the resistive zones are associated with inactive clayed and sealed or opened faults.

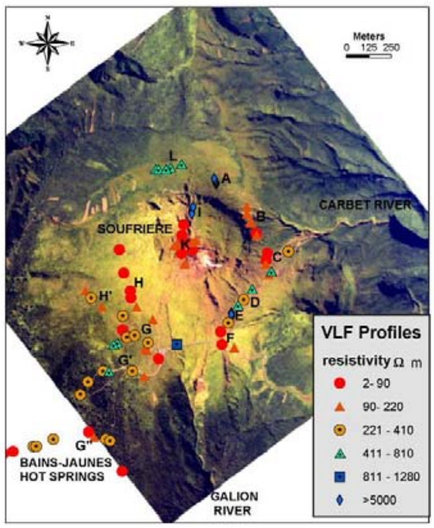

Figure 5: Main VLF anomalies on La Soufriere volcano and associated resistivity.

The 2000 VLF surveys clearly identify the active faults which are the prevailing radial drains for ground water channelling. These faults isolate the different sectors of Soufrière dome which differently interact with the renew of activity since 1992. These vertical clayed zones break up the mechanical cohesion of the dome itself (c.g. 1956 and July 8, 1976 faults). Soufrière dome has now to be considered as constituted of more or less blocks joined side by side lying on an hydrothermally crater floor which can only slacken a possible sector collapse.

Flank collapse or new eruption?

The main results are the following. The hydrothermal activity smoothly enlarged after 1992 (or before) and increased sharply after 1998. The hydrothermal activity which was more or less surrounded to the dome is now extending outside crater Amic. Superficial ground water flows along specific fractures or drains. The most powerful circulation starts from the dome and flows in the South-West direction. Due to rainfalls and hot gas or fluids issued from the magma body, the strong argillization occurs everywhere inside crater Amic and the thermal energy release is becoming more and more difficult.

Therefore two hypotheses can be suspected for the next future: (i) If the thermal source remains constant the overpressure will increase in the superficial structure until some threshold and will generate a new phreatic eruption, or (ii) the hydrothermally-altered clay rich basis surface of Amic crater could act as a slippage discontinuity and could initiate, only by gravity effect, the collapse of a part of the dome and a possible rapid decompression of the upper part of the volcano leading to an eruption.

MONITORING HE VOLCANIC ACTIVITY

The first method commonly used to monitor the volcanic activity was based on the total magnetic field recording. Between about 1940 and 1990 the networks using scalar magnetometers which were not drifting with time were developed in several countries as in Japan (Oshima) New Zealand (Ruapehu), USA (Kilauea), France (Soufrière) and Italy (Etna)…

It is only in 1986 on Oshima volcano that continuous resistivity measurements were carried out to monitor resistivity with depth due to the magma migration towards the ground surface (Yukutake et al., 1990).

Progressively new methods completed the existing permanent monitoring systems using the three components of the magnetic field, the electric field, and the audiomagnetotellurics soundings.

In 1995 a new step was done by combining and integrating EM methods on Miyake-jima volcano (Japan) which was expected to erupt in the next ten years. Such studies were made through a bilateral Japan-French cooperation (PICS 470).

Miyake-jima volcano

Miyake-jima is one of the seven volcanic islands belonging to Izu-Bonin arc in Japan. Two major caldera forming eruptions took place during the building of the volcano. Following the 7,000 yBP eruption a several kilometres large caldera, called Kuwanoki-Taira, was formed. The second produced a 1.5 km in diameter caldera, called Hatcho-Taira, and is dated around 2,500 yBP (Tsukui et al., 1998). Summit eruptions and flank fissure eruptions have occurred since.

The 2000 eruption

No noticeable volcanic seismicity was recorded between the last eruption in 1983 and June 26, 2000 when seismic swarms began to occur beneath the volcano summit. These volcanic events quickly disappeared and strong seismic swarms moved to the West of the island towards Kozushima and Nii-jima islands (JMA, 2000). From this time ground deformations appeared (Kaidzu et al., 2000). In early July new earthquakes again appeared beneath the summit. Gravimetric surveys done a few days before the eruption showed the formation of a void beneath the volcano summit (Furaya et al., 2001). During the July 8, eruption although no strong volcanic earthquakes were recorded, a new crater encompassing O-Ana and O-Yama craters and a part of Hatcho-Taira caldera occurred within 4 minutes. This crater, of about 1 km in diameter and 250 m depth, continued to enlarge during the next months. The volcanic activity became sporadic during July and was accompanied by a progressive enlargement of the newly formed caldera. The largest event was a hydro-magmatic explosion on August 18, generating an ash plume of more than 8 km height. The ash falls covered the island. Hereafter the activity receded although large SO2 emission continued. In September 2000 the size of the newly formed caldera was as large as Hatcho-Taira caldera : 1.4 km in diameter.

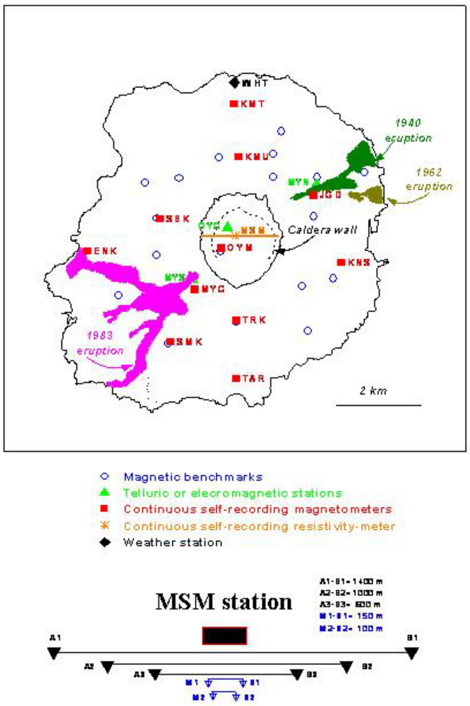

Figure 6: Stetch of Miyake-jima volcano. EM Networks.

Electromagnetic studies

The more or less regular pattern of Miyake-jima activity led us to start electromagnetic studies on the volcano in 1995. Continuous magnetic monitoring (Sasai et al., 1997, 2001, 2002), telluric field monitoring, long-baseline Self-Potential (SP) measurements, as well as SP surveys (Nishida et al., 1996), audio magnetotelluric and resistivity soundings were progressively implemented on the volcano (Zlotnicki et al., 2003).

In this paper we will focus on results obtained by audio-magnetotelluric (AMT) soundings implemented during the inter-crises 1983-2000 period, by DC resistivity soundings made during the year preceding the collapse of the summit as well as by SP surveys and by a permanent 1 km long SP line crossing Hatcho-Taira caldera.

Appearance of a deep thermal source evidenced by the magnetic changes

Eight proton magnetometers were installed on the volcano in 1995. After 1996, simultaneous opposite changes appeared in two stations located on the volcano summit (OYM) and on the southern flank (TRK)(Sasai et al., 2001). In 1998, the amplitudes reached 10 and -5 nT at OYM and TRK, respectively. These long-term precursory volcano-magnetic signals were attributed to a thermally demagnetized area caused by a vent shifting from the source of the 1983 eruption and located at about 4 km below the summit along the southern rim of Hatcho-Taira caldera (Sasai et al., 2001).

Hydrothermal system imaging by audio-magnetotelluric (AMT) soundings

In 1997 and 1998 AMT soundings were performed inside Hatcho-Taira caldera and in its vicinity. An antenna of 400 Am^2 was used in the frequency band 70 kHz-1 kHz to generate an artificial electromagnetic field in two orthogonal directions. From 1 kHz to 0.1 Hz only the natural field was used for soundings.

The campaigns clearly identified the existence of a low resistive medium beneath the 1940 cone. It most probably corresponded to the emplacement of the superficial active hydrothermal system evidenced by the SP surveys and mapping (Zlotnicki et al., 2003). It took its origin at several hundreds metres deep, below the sea level, where hot gas coming from a deep magma chamber could be mixed with fresh ground water through porous rocks, faults, craters or calderas rims. The top of this low resistive medium was only at a very few hundreds metres beneath the ground surface. The lowest resistivity values were located beneath the 1940 cone which seemed to correspond to the centre of the July 8, 2000 collapse. The thickness and the horizontal extensions did not reach 500 m (for the 50 Ωm isoline). The surface projection of this low resistive zone approximately encompasses the western O-Ana crater rim. Thus existing hydrothermal system was mainly responsible of the phreatic explosions during the Miyake-jima eruption.

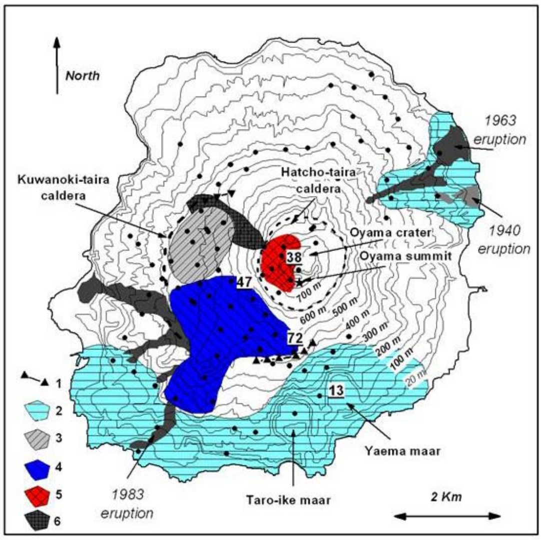

Figure 7: Main resistive structures. Black dots indicate the location of AMT soundings. 1: Limit and extent of Kuwanoki-taira caldera; 2: Stetch of seawater penetration in the Island; 3: Intra caldera tuff deposits (partly swamped by meteoric water); 4: Recent and fresh lava flows (hiding partly the SW Kuwanoki-taira caldera wall); 5: Summit hydrothermal system; 6: Location of the seismicity during 1983 crisis

Continuous AMT soundings

The horizontal magnetic and electric fields were recorded at three spots on the volcano between 1995 and 2000. One was set on the summit (OYC) and two (MYS and MYN) on the southern and northern flanks along the 1983 and 1963 fissures, respectively. The sampling rate was fixed to 60 seconds for memory storage capacity.

These stations can be used as continuous AMT stations. The apparent resistivity can be computed on a 3 days running window incremented day after day. This method permits to compute one sounding par day. For two stations (OYC and MYN) the data were good enough to detail the apparent resistivity changes. For both stations no change more than 5% were observed till 2000.

After April 2000, a slow regular change in the apparent resistivity at the two stations has appeared indicating a decrease of the apparent resistivity at a depth less than a few kilometres. These changes could be attributed to the 1983 thermal source.

The most outstanding changes were observed after June 12 when the apparent resistivity at the summit station sharply decreased by almost an order of magnitude before the occurrence of the June 26 seismic swarms. This well-documented sequence clearly show the migration of the magma toward the ground surface and the displacement outside the Island after June 27.

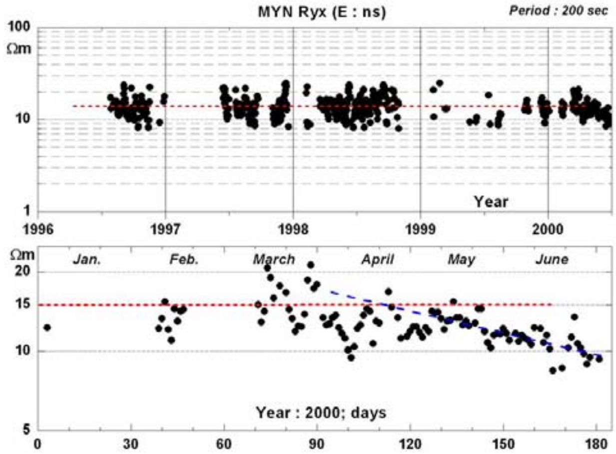

Figure 8: Upper graph: Apparent resistivity versus time of the TE mode at MYN station. Lower graph: Change in the apparent resistivity in 2000.

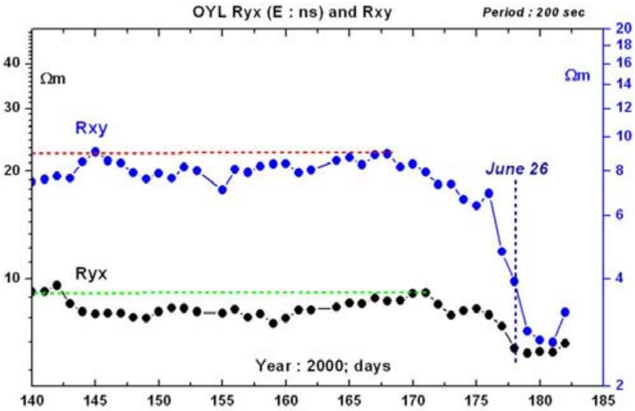

Figure 9: Changes in the apparent resistivity at OYC in TE and TM modes, from May 1' to June 30, 2000.

Continuous Schlumberger resistivity soundings

In May 1999 a continuously recording of DC apparent resistivity was installed through Hatcho-Taira caldera in the East-West direction. The equipment was set in a Schlumberger array with three injection lines of 600, 1000 and 1400 m length and of two receiving lines of 100 and 150 m length. Every 6 hours the system automatically made measurements. Unfortunately the resistivity-meter broke after October 1999. After calibration and tests, it was re-installed one week before July 8, 2000 eruption. But the equipment was destroyed in the July 8 collapse and data were lost. Only values obtained during tests made on July 3rd are available.

When the resistivity-meter was operating in 1999 the mean apparent resistivities remained almost constant around values of 260, 230 and 170 Ωm, for the 600, 1000 and 1400 m lines, respectively. Progressive variations appeared in August. Within one month apparent resistivities reached values up to 360, 230 and 180 Ωm. Finally on July 3rd 2000, apparent resistivities had drastically changed on the shortest and longest lines; mean values were about 70 and 550 Ωm, respectively (Zlotnicki et al., 2003). These results point out that between October 1999 and July 2000, the resistivity pattern, inside and outside O-Yama crater, had drastically changed. The resistivity has lowered to 20 % of the initial value on July 3rd, 2000 on the 600 m line while a resistivity has reached more than 3 times its original values on the 1400 m line. On July 3, the active hydrothermal system had mostly disappeared and groundwater was drained to larger depths caused by opened cracks forming the future caldera.

Self-potential mappings

Energy and thermal transfers in active volcanoes can play an important role in controlling their dynamic depending on the hydrothermal state. Much geothermal energy is released through the groundwater circulation, hot gas emission and thermal conduction. Therefore, it is very important to know the hydrological and thermal environments associated with volcanoes from the volcano-energetic point of view.

Recent studies reveal that self-potential (SP) anomalies (up to some hundreds of mV) are observed on volcanoes, active fissure zones and/or fumarolic areas, suggesting that the SP anomalies are closely related to heat-triggered phenomena such as thermoelectric and electrokinetic effects due to hydrothermal circulations. SP variations are based on the well-accepted hypothesis that a downward water flux produces a negative SP anomaly at the ground surface of a volcano while an upward fluid flow generates a positive one.

Therefore, SP studies can be appropriate for sensing the thermal and hydrothermal states of volcanoes. In addition, monitoring SP anomalies can be an efficient method for describing the change of thermal state and the evolution of the hydrothermal (and volcanic) activities (i.e. Zlotnicki and Nishida, 2003).

The hydrothermal activity inferred by SP mapping

The co-existence of positive and negative anomalies was also found on Miyake-jima Volcano, Japan (Nishida et al., 1996; Sasai et al., 1997). The SP anomalies corrected for a mean topographic effect (-1.1 mV/m) has revealed that a positive anomaly, about 800 mV in magnitude, developed over the summit area, while two negative ones, amounting to -250 and -100 mV, were distributed on the North and South West mountainsides, respectively. These negative anomalies were correlated with the concentrated distribution of craters connected with 1874 and 1763 fissures. Substantial precipitation (> 3 m/year) over Miyake-jima Island probably recharged highly permeable fissures and craters to generate the observed negative SP anomalies. Hot volcanic gases from relatively deep-seated magma intruded into the recharged water to drive the intense upward flow of heated water which consequently generated the positive SP anomaly on the summit area. The upward flow formed the hydrothermal aquifer of low resistivity, which maintained the fumarolic fields on the summit.

The large scale 1995 SP mapping and further surveys of Miyake-jima had revealed a powerful hydrothermal system centred on Hatcho-Tairo caldera. The associated 2.7 km maximum wide positive anomaly, up to 600 mV in amplitude (maxima-minima), suggested a thermal source located beneath the volcano summit which did not changed noticeably in the two next years. Therefore Miyake-jima was the seat of a stable hydrothermal activity pointing out that the coming eruption could be controlled firstly by a phreatic activity.

Long time SP variations across Hatcho-Taira caldera

A 1-km long SP line was set in an East-West direction through Hatcho-Taira caldera during May 1999 (Figure 6). This line was composed of eight non polarisable Pb-PbCl2 electrodes buried at least at 60 cm depth [11]. Potential measurements between electrodes were regularly made and referred to electrode E8 located on the west flat part of the caldera (Figures 6 and 8).

The SP values measured in May 1999 give information on the ground water pattern related to the local summit structure (Figure 9c). Values point out two negative anomalies relative to their external borders. This pattern imaged the meteoric water to accumulate inside or along crater or caldera rims [14]. Thermal transfers and hydrothermal circulations preferentially take place along these interfaces. On Miyake-jima volcano these negative SP anomalies were well associated with O-Ana and O-Yama crater rims.

The time variations of the potential differences can be considered in two periods, May to December 1999 and December 1999 to July 2000, corresponding to two different phases of activity of the hydrothermal system.

During the first period the SP pattern corresponds to an increase of negative potential values at electrodes close to inner part of the future collapse (Figure 9a). Electrodes E6 and E3 which had always lower values were the closest to the future caldera rims. This period corresponds to an increase of downwards water transport along the pre-existing caldera rims (see discussion). This general pattern is drastically reversed after December 1999 (Figure 9b). Till April 2000 a gradual increase of the potential, up to 50 mV, was recorded at all stations except at E5. It was corresponding to a renewal of the hydrothermal activity inside O-Yama crater. Beyond April 2000 sharp variations appeared. Negative variations were again recorded in the vicinity of the probable focus of the future collapse (electrodes E6 to E5) while positive variations accelerated to the East of the SP line. This pattern of negative, positive and then negative SP variations indicate periods in which the infiltration of water at the spot of the future caldera is sometimes counterbalanced by pulses of hydrothermal activity.

July 4, 2000 self-potential mapping of Hatcho-Taira caldera

On July 4, 2000 SP surveys were performed in one day of work inside the caldera (Zlotnicki et al., 2003). During this time a few earthquakes were recorded beneath the summit, accompanied by some collapses of O-Yama crater rims. Relative potential values were measured every 25 m along each survey line while the location was determined by a GPS (Global Positioning System) receiver with a precision on the order of 5-10 m.

Positive anomalies up to 150 mV relative to the reference R occur along O-Yama crater rim especially on the west and south borders; their elongated shapes followed the rims. The western positive anomaly spread above the fumaroles zone in existence since the 1962 eruption. The southern positive anomaly was unknown. Two large negative anomalies were recognised inside Hatcho-Taira caldera with an amplitude less than –225 mV for the western one. This negative anomaly lies over the 1940 cone which has been the seat of thermal activity during at least the past 30 years. The eastern smooth negative anomaly covers the North-East depression of O-Yama crater. These observations were opposite to those expected before an eruption in which the hydrothermal is re-activated giving rise to large phreatic explosions, like on Soufrière of Guadeloupe in 1996 and 1997 (Feuillard et al., 1983). Four days before Miyake-jima eruption the hydrothermal activity was mainly surrounded to the summit crater rims while negative anomalies were lying inside them.

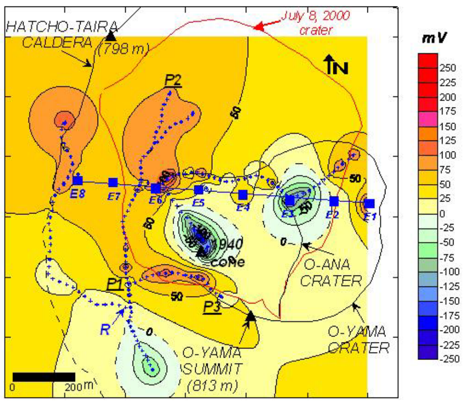

Figure 10: SP mapping made on July 4, 2000. Contours lines are every 25 mV. Surveys stations are figured by blue crosses. R represents the location of the reference electrode. Blue squares connected by a blue line represent the permanent 1 km long SP line with electrodes names.

Unrest of Miyake-jima volcano inferred by EM observations

As early as 1996 magnetic changes were observed on two stations located on the Miyake-jima summit. The smooth changes, up to 3 nT/year, were attributed to a thermal source which took place above the thermal supply at the origin of the 1983 eruption at about 4 km depth (Sasai et al., 2001). These volcano-magnetic signals sharply accelerated in the days preceding the July 8, 2000 caldera collapse (Sasai et al., 2003).

The comparison between AMT surveys made after the 1983 eruption and those performed in 1997-98 leads to assume that no drastic resistivity changes had occurred in the area of the future 2000 caldera. Only a possible enlargement of the conductive zone to the South was recognized by the 1997-98 AMT soundings. This assumption can also be assumed for the period 1997-98 to May 1999 when the DC resistivitymeter started to operate.

In 1999, The 1 km long SP line exhibits (i) negative anomalies which coincide with the East and West rims of the newly formed caldera and (ii) an increase in the hydrothermal activity after December 1999. These observations suggest that the permanent hydrothermal activity has favored the mechanical weakness of some existing structures inside Hatcho-Taira caldera, as O-Yama rims and O-Ana craters.

After April 2000, the continuous audio-magnetotelluric soundings clearly show a progressive decrease of the resistivity at a depth less than a few kilometers depth while the SP measurements indicate a stronger hydrothermal activity along the craters rims.

Two weeks before the occurrence of the seismic swarm on June 26, the resistivity sharply decreases by almost an order of magnitude indicating a rapid upward displacement of the thermal source.

These deep phenomena are accompanied and relayed by superficial changes in the hydrothermal system itself. The 1.4 km long current injection lines associated with the resistivity-meter suggest that the superficial hydrothermal system beneath the summit was disturbed after December 1999. On July 3rd, 2000 the resistivity pattern is completely changed: a part of the hydrothermal remains in the first hundreds meters depth while a high resistivity structure takes place at a few hundreds meters depth. The high resistivity values are well in accordance with the hypothesis of opened cracks leading to the formation of the caldera formation.

On July 4, the hydrothermal activity, inferred by the summit SP mapping, is essentially surrounded to O-Ana and Oyama crater rims. This effect supposes that the hydrothermal system (and the ground water) has disappeared through the opened cracks evidenced by the resistivity soundings.

Finally, between July 6 and 8, large magnetic changes on the summit record the rapid displacement of the thermal source which enters in contact with the hydrothermal system on July 8, 2000 giving rise to a phreatic explosion and the caldera formation.

After the July 8 collapse of Miyake-jima summit the ground water was again confined within unwelded blocks and was strongly reheated by a close and deeper magmatic source. The pore pressure again increased to some threshold which gave rise later to strong phreatic explosions as the July 14 and August 18, 2000 ones.

Concluding remarks

EM methods are now able to give valuable information on volcanic structures and their potential eruptive behavior as well as on the sources which take place in the plumbing system and leads to the eruptive phase.

Two main steps have now to be overcome:

- The densification of integrated EM networks on volcanoes and the development of real time monitoring and data processing,
- The extension of research in the complete frequency band of EM phenomena, from DC to high frequency sampling till several tens of kilohertz, as compared to present day studies mainly devoted to the ULF band.

ACKNOWLEDGMENT

We strongly thanks all people who have contribute to get these results, especially F. Bruère, J.F. Delarue and A. Mille,

REFERENCES

Boudon, G., Semet, M., and Vincent, P., 1987. Magma and hydrothermally driven sector collapses : The 3100 and 11500y. B.P. eruptions of La Grande Découverte (La Soufrière) volcan, Guadeloupe, French west Indies. J. Volcanol. Geotherm . Res., 33 : 317-323.

Feuillard, M ., Allègre, C.J., Brandeis, G., Gaulon, R., Le Mouël, J.L., Mercier, J.C., Pozzi, J.P., and Semet, M., 1983. The 1975-1977 crisis of La Soufrière de Guadeloupe (F.W.I.) : A still born magmatic eruption, J. Volcanol. Geotherm. Res ., 6 : 295-304.

Furaya, M., Okubo, S., Tanaka, Y., Sun, W., Watanabe, H., Oikawa, J. and T. Maekawa, 2001. Caldera formation process during the Miyakejima 2000 volcanic activity detected by spatio-temporal gravity changes. Journ. of Geography, 110, 2, 217-225.

Japan Meterological Agency, 2000. Recent seismicity in the Miyakejima and Niijima-Kozushima region, Japan- the largest earthquake swarm ever recorded. Earth Planets Space, 52, 1-8.

Kaidzu, M., Nishimura, T., Murakami, M., Ozawa, S., Sagiya, T., Yarai, H. and T. Imakiire, 2000. Crustal deformation associated with crustal activities in the northern Izu-islands area during summer. Earth Planets Space, 52, 9-17.

Nishida, Y., Matsushima, N., Goto, A., Nakayama, Y., Oyamada, A., Utsugi, M. and H. Oshima, 1996. Self-potential studies in volcanic areas (3) Miyake-jima, Esan and Usu, J. Fac.Sci., Hokkaido Univ., Ser. 7, 10, 63-77.

Pham, N.G., Boyer, D., Boudon, G., Gruszow, S. and Zlotnicki, J., 1990. Self-potential mapping on La Soufrière volcano (Guadeloupe). Relationship between SP anomalies and the structure. C. Acad., Sci., 310, II : 815-821.

Sasai, Y., J. Zlotnicki, Y. Nishida, P. Yvetot, P. Morat, H. Murakami, Y. Tanaka, Y. Ishikawa, S. Koyama, and W. Sekiguchi, Electromagnetic monitoring of Miyake-jima volcano, Izu-Bonin Arc, Japan: A preliminary report, 1997. J. Geomag. Geoelectr., 49, 1293-1316.

Sasai, Y., Zlotnicki, J., Nishida, Y., Uyeshima, M., Yvetot, P., Tanaka, Y., Watanabe, H. and Y. Takahashi, 2001. Evaluation of Electric and Magnetic Field Monitoring of Miyake-jima Volcano (Central Japan): 1995–1999, Annali di Geofisica, 44, 2, 239-260.

Y. Sasai, Uyeshima, M., Zlotnicki, J., Utada, H., Kagiyama, T., Hashimoto, T. and Y. Takahashi, 2002. Magnetic and electric field observations during the 2000 activity of Miyake-jima volcano, Central Japan, Earth Planet. Sci. Lett., 203, 769-777.

Tsukui, M. and Y. Suzuki, 1998. Eruptive history of Miyakejima volcano during the last 7000 years, (in Japanese with English abstract), Bull. Volcanol. Soc. Japan, Ser. 2, 43, 149-166.

Yukutake, T., 1990. An overview of the eruptions of Oshima volcano, Izu, 1986-1987 from the geomagnetic and geoelectric standpoints. J. Geomag. Geoelectr., 42, 141-150.

Zlotnicki J., Feuillard M., and G. Hammouya, 1994. Water circulations on la Soufrière volcano (Guadeloupe, Lesser Antilles) : May-December 1992 seismovolcanic crisis. Renew of volcanic activity ? J. Geomagn. Geoelectr., 46, 797-813.

Zlotnicki, J., Sasai, Y., Yvetot, P., Nishida Y., Uyeshima, M., Fauquet, F., Utada, H., Takahashi, Y. and G. Donnadieu, 2003. Resistivity and Self-Potential changes associated with volcanic activity : The July 8, 2000 Miyake-jima eruption (Japan), Earth Planet. Sci. Lett., 205, 3-4, 139-154.

Zlotnicki J. and Y. Nishida, 2003. Review on morphological insights of Self-Potential anomalies on volcanoes, Surveys in Geophysics, 24, 291-338.

Zlotnicki J., Vargemezis G., Mille A., Bruère F., Hammouya G., 2004. State of the hydrothermal activity of Soufrière of Guadeloupe volcano Inferred by VLF surveys, in press in J. Applied Geophys.

Jacques Zlotnicki
CNRS, Obervatoire de Physique du Globe – UMR6524
24 av des landais, 63117 Aubière, France
Email: Jacques.zlotnicki@opgc.univ-bpclermont.fr

The Use of Volcanic Hazard Information by Tokyo Metropolitan Government

Yoichi SASAI
The Disaster Prevention Specialist (Chief), Tokyo Metropolitan Government

ABSTRACT

KEYWORDS: Seven Izu Islands, Miyake-jima volcano, Izu-Oshima volcano, Hachijo-Fuji volcano, Basaltic volcano, Rhyolite monogenetic volcano

1. INTRODUCTION

There are 108 active volcanoes in the Japanese Islands, twenty one of which belong to the City of Tokyo in the central part of Japan. Tokyo Metropolitan City is one of the top three prefectures who have a number of active volcanoes; the others are Hokkaido Prefecture (18 volcanoes except for 11 ones in the northern territories of Japan) and Kagoshima Prefecture (11 ones). The volcanoes in the City of Tokyo are located in the northern Izu-Bonin Arc stretching by 1500 km to the south from the mainland Honshu. Among them, there are 9 islands with inhabitants, 5 uninhabited ones and 7 reeves above sea floor volcanoes. Tokyo is a unique capital in the world which is located above a junction of three plates, i.e. North American, Pacific and Philippine Sea Plate.

Japan Meteorological Agency (JMA) classifies these volcanoes into three groups according to its activity, which are A (very active), B (moderate) and C (less active, which has erupted in the past 20 ky). The rank A volcanoes are Izu-Oshima island (10,000 people), Miyake-jima island (3,800 people), and the rank B Iwo-jima island (an air base for the Self-Defence Force, no civilians), Izu-Torishima island (uninhabited). Several large eruptive activities occurred in these volcanic islands during the 20th century. The total number of inhabitants is about 25,000, and there are a number of tourists visiting these islands. All these islands where people live with active volcanoes are located in the northern half of the Izu-Bonin Arc, which is called the Seven Izu Islands.

The experience in the 1983 eruption of Miyake-jima volcano first motivated those in Tokyo Metropolitan Government (Tokyo MG) to accept scientists' suggestions for mitigation of volcanic hazards. During the eruption of Izu-Oshima volcano in 1986, they were obliged to manage evacuation of all the inhabitants in the island, when a few volcanologists played a leading role in their decision of such a drastic countermeasure. After the 1986 event, Tokyo MG organized a scientific committee to investigate the activities of volcanoes in the Seven Izu Islands and to evaluate their potential risk. Following the suggestions by the committee, Tokyo MG established the volcano monitoring system for the Seven Izu Islands in 1993.

Tokyo MG encountered the eruption of Miyake-jima volcano and the magma intrusion event in Kozu-shima and Nii-jima islands area in 2000 under such advance preparations. I will present here the risk management made by Tokyo MG and the influence of volcanologists on their decision-making during the three volcanic events, i.e. eruptions of Miyake-jima volcano in 1983, Izu-Oshima volcano in 1986 and Miyake-jima volcano together with the magma intrusion beneath Kozu-shima and Nii-jima islands in 2000.

2. THE 1983 ERUPTION OF MIYAKE-JIMA VOLCANO

Miyake-jima volcano erupted on October 3, 1983. This basalt volcano erupted in 1940 and 1962, which were the flank-fissure eruptions on the north-eastern slope. In the 1983 eruption, the fissure vents opened on the south-western flank and phreato-magmatic explosions took place around the southern coast of the island; the lava flow buried Ako village on the SW side of the island, while scoria fell on Tsubota village on the SE side causing severe damage to agricultural products. Only a few months before the eruption a scientific report [1] on the geological hazards (earthquake, volcanic eruption, tsunami, typhoon etc) possibly to occur in the Seven Izu Islands had been published by Tokyo MG. This report pointed out that quite similar disasters as those in 1983 did occur in the 1643 eruption when people in Ako village had to abandon their village owing to lava flow; they were obliged to live elsewhere in the southern part of the island and came back to their old village after about 100 years. The warning on the possible occurrence of a similar disaster did actually come true, which gave strong impression to those in charge of disaster prevention in Tokyo MG.

3. THE 1986 ERUPTION OF IZU-OSHIMA VOLCANO

On November 15, 1986, lava began to flow out from the crater of the central cone Miharayama in the summit caldera of Izu-Oshima volcano. This basaltic volcano had repeated several eruption cycles in the past, the latest one of which continued from 1950 till 1974. Eruptions for the past few hundreds years always took place from the crater of the central cone. However, on Nov. 21, the fissure eruption started in the caldera floor and it extended outside the caldera to the NNW direction. This large eruption compelled all the inhabitants of about 10,000 people to evacuate from the island .

The decision of the total evacuation was made in the following process:

(1) The volcano hazard information is issued officially by JMA. However, Izu-Oshima weather station was situated on the north-western mountainside, which was just at the extention of explosive fissures. JMA stuffs were obliged to leave the weather station in the evening of Nov. 21, and they could no longer obtain necessary data to issue volcanic hazard information.

(2) A few members, however, remained at Izu-Oshima volcanological observatory, Earthquake Research Institute (ERI), the University of Tokyo, near the western coast of the island, toward which lava flow was approaching. When the fissure eruptions almost terminated around 21 o'clock in the evening of Nov. 21, a number of earthquakes began to occur in the SE part of the island. On the other hand, other members of ERI tentatively escaped from the observatory heard a rumor that some new cracks appeared on the road along the SE coast of the island, which was confirmed by policemen.

(3) Fortunately, Prof. Daisuke Shimozuru, the chairman of Coordinating Committee for Prediction of Volcanic Eruptions (CCPVE), visited the island on that day. He and some of his colleagues stayed at the Izu-Oshima Town office interpreting the ongoing volcanic eruption processes to the local administrators. The urgent information on swarm earthquakes and newly opened cracks in the SE part of the island was delivered quickly to Prof. Shimozuru, who judged that phreato-magmatic explosions could occur in the SE part of the island where several thousands of people took refuge.

(4) The mayor of Izu-Oshima Town issued the evacuation order from the island at 22h 50m LT. All the inhabitants left the island safely during the midnight until next morning.

About ten thousands of refugees stayed in Tokyo for one month and then they came back home. No phreato-magmatic eruption took place in the SE part of the island, although the alignment of earthquake foci and crustal deformation revealed by leveling survey clearly indicated the intrusion of magmatic dyke(s) into the SE part of the island: The emergency countermeasure during the 1986 eruption should be evaluated as appropriate. However, its sequela remained because the total evacuation gave the local people much economic as well as mental damage. It gave strong impression to the administrators on the difficulty of the total evacuation.

4. THE VOLCANO MONITORING SYSTEM FOR THE SEVEN IZU ISLANDS BY TOKYO MG

With the 1986 event as a turning point, Tokyo MG decided to organize a research group to investigate every active volcanoes in Izu Seven Islands: This group (chairman, Prof. Daisuke Shimozuru) published a research report [2] in 1990, in which the most recent results of geophysical, geological and geochemical studies were compiled and the potential risk of the eruptive activity for each volcano was evaluated. In particular, the report claimed the possibility of eruptions in Nii-jima and Kozu-shima islands, which are rhyolite volcanoes consisting of several monogenetic lava domes. Two domes were formed in the 9th century according to historical documents, which caused catastrophic hazards by base-surge. The average interval of such dome formation turned out to be one thousand years according to new ^{14}C dating rather than 2 thousands years or more as had been estimated before. The report warned the forthcoming magma intrusion event, which actually happened in 2000.

Following suggestions by this general report, Tokyo MG established the volcano monitoring system in the Seven Izu Islands. It consists of seismic array with 3 to 5 seismometers in Miyake-jima, Hachijo-jima, Aoga-shima, Nii-jim and Kozu-shima islands and 1 seismometer in To-shima, Mikura-jim and Shike-jima islands, together with some other kinds of geophysical instruments (tilt-meter, water-level, ground temperature). The largest island Izu-Oshima was excluded from this system because this volcano has been well equipped with this kind of instruments by JMA and ERI since 1986. The seismic data are transmitted to Tokyo MG office by administrative radio waves and delivered simultaneously to JMA and ERI; in exchange Tokyo MG can obtain necessary information on earthquakes and volcanic activities in the Seven Izu Islands region from both the institutions. The seismic array covers the northern half of Izu-Bonin Arc and serves in part to monitor even the Tokai region where a large earthquake of M 8 is expected to occur in the near future.

5. THE ERUPTION OF MIYAKE-JIMA VOLCANO AND MAGMA INTRUSION EVENT BENEATH KOZU-SHIMA & NII-JIMA ISLANDS REGION IN 2000

The volcanic activity in Miyake-jima island started in the evening of June 26, 2000. Magma first moved toward the summit, but it did not extrude and then intruded beneath the western sea. The behavior of magma was well detected by seismic (Tokyo MG) and tilt-meter (NIED) arrays. Thanks to refuge training conducted every year, local people in the southern part of the island successfully evacuated to the places of refuge in the north. Four days later, CCPVE judged that the danger had gone for fissure eruptions on land, and the people returned home.

However, strong earthquakes continued to occur beneath the sea between Miyake-jima and Kozu-shima island, 20 km to the west. Most probably, the intrusion of magma from Miyake stimulated the deep-seated rhyolite magma beneath the western islands to extrude toward shallower depth. On July 1, one person was killed by land slide associated with a strong shock of M 6.5, who was the only victim during the 2000 activity. Strong swarm earthquakes continued during the period from the end of June to August; most of the inhabitants took refuge from the three islands, Kozu-shima, Nii-jima and Shikine-jima. Those in charge of disaster prevention had to prepare for the worst case of sea floor eruptions, which did not happen fortunately.

On July 8, a small-scale phreatic explosion took place in the summit caldera of Miyake-jima volcano, which produced a hole of 1 km in diameter and 200 m in depth. The sinkhole enlarged and deepened to form a new caldera with a diameter of 1.6 km until the end of August. Although eruptions occurred from a crater in the new caldera several times, total amount of ejecta was much smaller than the volume of the new caldera: Most of the vacant space beneath the volcano was produced by lateral intrusion of magma. After the summit collapse on July 8, it was most difficult to predict the next step of the volcanic activity. Moderate eruptions took place on July 14-15, Aug. 10, 13-14, and then the largest eruption occurred on Aug. 18 followed by a low-temperature pyroclastic flow on Aug. 29. In the last two eruptions, no one was killed or severely injured because of some lucky conditions. However, the total evacuation order was finally issued on Sept. 1 by the village mayor under the full support of Tokyo MG.

Although there was eventually no casualty during the period from the Aug. 18 largest eruption till the completion of total evacuation on Sept. 4, people's life was exposed to danger. There could be three reasons for that: 1) It was very difficult to forecast the Aug. 18 largest eruption. No anomalous seismicity nor inflation of the volcano were observed before the eruption. 2) JMA missed the time to announce the 'Urgent volcano information', which usually implies urgent evacuation from a volcano. 3) Tokyo MG and Miyake Village Office (Miyake VO) hesitated to issue the total evacuation order partly because of the memory of it difficulties in the 1986 eruption of Izu-Oshima volcano. Koyama [3] critically described the discussions at CCPVE meetings and the lack of countermeasure by Tokyo MG. Sasai [4] introduced and discussed the role of volcanologists during the 2000 eruption of Miyake-jima volcano, which is reproduced in the Appendix.

After the total evacuation, no destructive eruption took place, but harmful volcanic gas (SO_2) amounting to several tens of thousands tons/day was emitted from the summit crater, which had prevented people's return for the past 4 years.

6. AFTER-EFFECTS OF THE VOLCANIC EVENTS IN 2000

Various seismo-volcanic events followed in the northern part of Izu-Bonin Arc after the 2000 eruption of Miyake-jima volcano. They are enhancement of low-frequency volcanic earthquakes beneath Mt. Fuji, swarm earthquakes in Aogashima, Izu-Oshima islands, volcanic eruptions in Izu-Torishima and Iwo-jima islands. In particular, swarm earthquakes suddenly started beneath Hachijo-Fuji volcano in the middle of August 2002, which were accompanied with crustal deformation probably caused by a N-S oriented intrusive dyke. Moreover, very long-period seismic events (about 10seconds period) were frequently observed for two months, which could be explained as due to oscillation of a vertical thin magmatic plate. Hachijo-Fuji volcano is a basalt volcano located on the NW side of Hachijo-jima island having 8,000 population. This volcano is very young (active since 2000 years ago), but it has been quiescent for the past 200 years. Tokyo MG nominated this volcano as the one under careful watching.

In order to support people's return to Miyake-jima island, Tokyo MG organized two scientific committees: The one is the committee for investigation of the activity of Miyake-jima volcano (Oct., 2000 - present) and the other the committee for investigation of volcanic gas from Miyake-jima volcano (Sept., 2002 - Mar., 2003). The former has given appropriate advice in the countermeasure against the ongoing volcanic activity to the administrators of Tokyo MG and Miyake VO. The latter has the medical scientists as its leading members to assess the safety level of the SO_2 gas concentration to human health as well as to propose the countermeasure against the harmful gas.

The emission rate of SO_2 gas showed exponential decay from as high as several tens of thousands tons/day in October 2000, to several thousands tons/day in the middle of 2002. However, it turned almost constant since then. Because of dominant seasonal wind and topographic effects there are some areas where the concentration of SO_2 gas is too high. Miyake VO changed their plan for people's return: They made up their minds not to wait until the gas concentration will become low enough everywhere but to come home even under the present circumstance that there still remain some areas of high gas concentration. Miyake VO organized the committee for the safety countermeasure against volcanic hazards, in particular against the harmful SO_2 gas.

Recently, in September 2004, the town mayor of Miyake Village declared that the total evacuation order would be cancelled in February next year and that all the inhabitants could come back to the island. However, emission of harmful SO_2 gas, i.e. several thousands tons/day, still continues from the summit crater. Some areas will be prohibited to live there. Too long time has passed since the exodus: Many young/middle-aged people found new jobs in the city zone of Tokyo, which make them difficult to come back to the island. There are so many problems for the resuscitation of Miyake-jima island.

ACKNOWLEDGMENT

I greatly acknowledge Dr Tsutomu Miyazaki, the former Disaster Prevention Specialist, for his suggestions and advice. Most of the materials in this abstract are provided with the aid of some veteran colleagues at Disaster Prevention Division, to whom I am thankful.

REFERENCES

[1] Tokyo Metropolitan Government, General report on natural hazards in the islands region of Tokyo Metropolitan City, June 1983, (in Japanese), 295pp., 1983.

[2] Council for Disaster Prevention of Tokyo Metropolitan City, Research report on the characteristics of volcanic eruptions in the Seven Izu Islands, May 1990, (in Japanese), 663pp., 1990.

[3] Koyama, M., Unsuccessful risk evaluation and communication during the crisis of Miyakejima volcano in August, 2000, (in Japanese), Rep. CCPVE, 78, 125-133, 2002.

[4] Sasai, Y., Countermeasure against unforeseen volcanic hazards and role of volcanologists: The 2000 eruption of Miyake-jima volcano, (in English), Proc. International Workshop on Strategy of Volcanic Disaster Mitigation, September 24-27 2003, 28-37, 2003.

APPENDIX: Reproduction of the paper [4]

Countermeasure against Unforeseen Volcanic Hazards and Role of Volcanologists: The 2000 Eruption of Miyake-jima Volcano

Yoichi SASAI

1. Introduction

The eruption of Miyake-jima volcano had been anticipated and prepared for it because of its regular occurrence in the 20-th century, i.e. 1940, 1962 and 1983. Nevertheless, the 2000 activity was more or less unexpected for us in the following aspects: (1) It suddenly started on June 26, 2000, which was rather earlier than the expected time to occur. (2) Intrusion of magma into the western sea floor stimulated the preexisted rhyolite magma beneath Kozu-shima and Nii-jima islands, which caused severe earthquake swarm. Fortunately, no destructive eruption happened in this region 20 km west of Miyake. (3) On July 8, the summit collapse took place to produce a large sinkhole, which enlarged to form a new caldera in the following two months. The new caldera was born without catastrophic eruptions. (4) Eruptions from the new caldera ejected much amount of volcanic ash, which caused mud flow and landslide. This was a new type of volcanic hazard in Miyake-jima volcano. (5) The largest eruption on August 18 and the August 29 one with "low-temperature" pyroclastic flow spread out ejecta all over the island, which compelled all the inhabitants to evacuate from the island in early September. The big problem was that we could not predict such destructive eruptions despite with good enough monitoring system. (6) A large amount of harmful volcanic gas (SO_2) continued to be emitted from a crater in the new caldera, which has prevented people's return for the past three years.

Miyake Village Office (Miyake VO) and Tokyo Metropolitan Government (Tokyo MG) met every kind of difficulties in volcanic hazard mitigation because things always went on unexpectedly. I will describe here the risk management made by the local administration at some stages during the eruption and scientists' influence on their decision-making. For the sake of better understanding, I will give a brief summary of geophysical and geological studies in the Appendix, although most of the results were not presented during the on-going volcanic activity in 2000.

2. Advance preparations for the 2000 activity

We will first summarize the countermeasure for preventing volcanic disasters achieved by the local administration as well as the volcano monitoring system constructed by governmental institutions and universities. Miyake VO made out "The hazard map of Miyake-jima volcano" (edited by Prof. Daisuke Shimozuru) in 1994, and distributed it to all the inhabitants. Once a few years on October 3 (the day of the 1983 eruption), they had made refuge training using public buses, in which more than a thousand people (the population of Miyake Village: ca. 4000) participated. At the onset of the intrusive event on June 26, 2000, such experiences worked most effectively. Since after the 1983 eruption a conference on the disaster prevention has been regularly held among Miyake VO, Miyake Local Office of Tokyo MG, Miyake-jima Weather Station (JMA) and Miyake-jima Police Office, i.e. Four Agencies Conference, in which the cooperation among the four agencies was discussed. Such connection functioned effectively throughout the 2000 activity.

The volcano monitoring system was greatly advanced as compared with the past three eruptions. Even at the time of 1983 eruption, the geophysical instrument in operation was only one seismograph by JMA. However, in the 2000 eruption, we had seismic array, GPS, leveling, bore-hole tilt-meters, gravity, electromagnetic and geochemical observations, results of which were reported in many scientific papers. In particular, the state of the volcano was monitored in real-time on line by the seismic array (JMA, ERI, Tokyo MG), bore-hole tilt-meters (NIED), and GPS network (GSI). On October 30, 1999, Dr Miyazaki, the Disaster Prevention Specialist of Tokyo MG gave a lecture to the audience of the Four Agencies Conference in Miyake on the impendence of the coming eruption. The warning was based on his own analysis of repeat leveling data that the tilt movement of the island had recovered more than 80 % of the depression at the time of the 1983 eruption owing to the accumulation of magma at depth.

Earthquake Research Institute (ERI), the University of Tokyo, has long been working on this volcano since the 1940 eruption. However, there is no volcanological observatory on the island. ERI tried to overcome the disadvantages owing to the lack of a base of observations: They organized a contingency plan for urgent observations. Actually, ERI staffs made practice on the island in December 1999, in which communication via satellite telephones among observation sites and ERI together with the publicity work via internet media were the main subjects of the training. Thanks to such training, an information corner on Miyake-jima volcano was quickly provided in the ERI home-page on June 27, which had been one of important information sources for scientists during the 2000 eruption.

3. Intrusive stage (June 26 – July 8): Successful refuge action

On June 26, 2000, volcanic swarm earthquakes began to occur around 18h 30m LT, which accompanied abrupt ground deformation. Japan Meteorological Agency (JMA) issued the 'extraordinary volcano information' at 19h 30m, and at 19h 33m announced the 'urgent volcano information', i.e. "Warning for possible occurrence of eruption". At 20h 45m Miyake VO established the headquarters for disaster prevention; they issued an evacuation order to people in Ako area (SW part of the island) at 21h 10m, and to those in Tsubota (SE part of the island) at 21h 39m. On June 27 at 0h 15m Tokyo MG also started the headquarters as well as the local one in Miyake Local Office. The chief of the local headquarters was Mr. Aoyama, the vice-governor of Tokyo MG, who flied to the island during midnight. Action by JMA and the local administrations was quick enough: Local people also behaved smoothly during the night following the instruction manual indicated by the hazard map. About 1500 people including elderly and/or handicapped persons safely evacuated from both the areas to the refuges in the northern part of the island within a few hours. Volunteers including high school students helped supply relief goods.

Several volcanologists from universities arrived in the island early in the morning of June 27, who immediately attended at the local headquarters. They scouted around the summit and western slope of the volcano, watched the upwelling seawater due to sea-floor eruption on helicopters, and investigated surface cracks along the western coast caused by intrusion of magma beneath the ground: They functioned as eyes and ears for the Coordinating Committee for Prediction of Volcanic Eruption (CCPVE) and for the local headquarters.

During the first day, i.e. on June 27, information on the volcanic activity gathered by JMA via CCPVE was not properly transmitted to the local headquarters nor to Miyake-jima Weather Station. The university scientists on the island at that time were not official members of CCPVE, whose observations were delivered to the committee via ERI. The most urgent thing was to know if the phreato-magmatic explosion could occur on the northwestern coast. Migration of volcanic earthquake epicenters toward west off the coast had been detected by JMA, but such a "safety signal" was not directly transmitted to the local headquarters. Actually, the evacuation order to people in Igaya area (NW part of the island) was issued because these people themselves appealed to Miyake VO threatened by successive strong shocks early in the morning of June 27.

Good communication between the local headquarters and JMA was established about 24 hours after the onset of activity. JMA staffs were dispatched to give explanation on the volcano information at the local headquarters meeting. Many volcanologists arrived in the island, preparing for temporary measurements and field investigations: Every observations on the volcano by the scientists were reported to the local headquarters, which gave them permission to enter the forbidden area in the volcano and supported them providing cars and helicopters. Media reporters collected news materials at the local headquarters: Scientists were rather free from journalists.

On June 29, CCPVE announced a comment that the crisis of fissure eruptions on Miyake- jima volcano had passed. Miyake VO removed the evacuation order for each area and people returned home. On June 30, Miyake VO and Tokyo MG dismissed the headquarters for disaster prevention. However, the Disaster Prevention Division of Tokyo MG was successively involved in the countermeasure against strong swarm earthquakes in and around Kozu-shima and Nii-jima islands 20 km west of Miyake-jima island, taking account of possible devastating eruptions caused by rhyolite magma. One person was killed by a landslide (July 1), and the tourism on these islands was severely damaged. Strong earthquakes continued to occur until the end of August: Tokyo MG was obliged to encounter the operations on two separated fronts, i.e. the one on Miyake-jima and the other on Nii-jima and Kozu-shima islands.

4. Summit subsiding stage (July 8 – middle of August): Pertinent action against unexpected volcanic events

Since the beginning of July, small earthquakes began to occur again beneath the summit caldera. On July 5, JMA announced the 'volcano observation information', in which they suggested "increase of humarole activity in the summit area, or possible ejection of volcanic ash". Miyake VO decided to keep out people from the summit area. At 18h 41m, July 8, the summit collapse took place to form a new sinkhole of 1 km wide and 200 m deep. No one was harmed. On July 14 and 15 the first phreato-magmatic eruption occurred in the new caldera. Miyake VO restarted the headquarters for the volcanic disaster prevention. On July 18, CCPVE gave a comment "The new sinkhole in the summit is expanding. The volcano edifice is shrinking, which suggests the decline of magma head. But phreatic explosion may occur hereafter. Caution for mud flow by rainfall."

On July 26, heavy rain first caused a large-scale avalanche of mud and rocks. On August 10, 13 to 14, medium-scale summit eruptions took place. Most of the ejecta were hydrothermally altered volcanic ash, which resulted in mud flow repeatedly. Volcanic events and associated hazard went on within the scope of the June 18 comment by CCPVE until the August 18 largest eruption.

5. The August 18 largest eruption and exodus: Confusion in the eruption forecast

At 17h 02m, August 18, the largest eruption took place: Volcanic clouds rose as high as 15,000 m and the total volume of ejecta was 5.2 x 10^6 m^3. Volcanic ash fell all over the island; even ballistic fragments larger than 1 m in diameter reached the northwestern coast of the island; cars on the southern side of the volcano were damaged in their window glass; a few cows were killed by volcanic bombs in the village farm within 1.5 km from the caldera rim. It happened that there was no severe damage on people: Only one person was slightly injured. It was simply a rare luck.

Since the eruption took place in the evening, it was not recognized so quickly by CCPVE how destructive it was. At 17h 20m, August 18, JMA announced the 'extraordinary volcano information' to raise caution for eruptions. CCPVE examined the data and discussed the generating mechanism of the eruption on August 21 and 24. As the summary, JMA issued 'extraordinary volcano information' which includes warning for a possible coming eruption with volcanic ash and bombs as well as the mud flow due to rain. However, these messages were not the 'urgent volcanic information', which has been regarded as direct warning for refuge by administrators.

On August 20, Tokyo MG demanded the Self-Defense Forces to help people recover from damages (removal of volcanic ash, sandbagging to prevent mud flow, etc). Tokyo MG hastily set up emergency shelters along the main road encircling the island, and began to transfer aged/nursed persons to the mainland. Many people who have relatives outside the island temporarily left the island, but those who could not find such refuges had to stay in the island with apprehensions. The local administrations stood ready for evacuation of all the inhabitants. Actually, Tokyo MG began to reserve public housing for all the evacuee just after the August 18 eruption. However, the efforts were still under negotiation and the official answer to the question for possible exodus was 'No'. The behavior of Tokyo MG was severely blamed by some media and scientists.

At 4h 35m on August 29, a 'low-temperature pyroclastic flow' took place: The volcanic clouds did not rise high and fell down to the north with very slow speed of 10 km/h. The temperature was as high as 30□C: People walked through the falling ash and no one was harmed. However, Tokyo MG started up again the headquarters for disaster prevention, which has continued until now for more than 3 years. Urgently, aged persons under protective care were moved to the corresponding facillities in the mainland; pupils, middle and high school students evacuated to Akikawa High School which has a dormitory.

On August 31, CCPVE announced an official comment "Larger eruptions than those on August 18 and 29 could occur in the near future". Since the comment was not presented as the 'urgent volcano information', it was rather uncertain as a legal basis for a village mayor to issue the evacuation order. However, the governor Mr. Ishihara of Tokyo Metropolitan City decided to recommend the mayor Mr. Hasegawa of Miyake Village to do it under the full support of Tokyo MG and the Government: The decision was made at the headquarters meeting on September 1. At 7h 00m on September 2, Miyake Village mayor announced the evacuation order within 3 days to about 2500 people who remained in the island. All the evacuee tentatively stayed at the National Youth Center (Monbu-sho) in Tokyo for several days, and then moved to live at public housing distributed mainly in Tokyo until September 9. Several prefectures and cities around Tokyo Metropolitan City were supportive enough to provide the refugees with their own public housing.

6. Reasons for the lack of decision

The volcanic smoke which fell on the northern part of the island on August 29 was not rigorously what is called the ‘pyroclastic flow’ in volcanology. However, its picture taken from the sea looked just like the pyroclastic flow or the dry avalanche. The danger of the pyroclastic flow was well recognized even by local people because of the 1993 Mt. Unzen eruption: The evacuation order was accepted with little opposition probably owing to the term ‘pyroclastic flow’. If the temperature of volcanic clouds were as high as several tens of degree C, there should have been human loss: It was again nothing but lucky that no one was harmed by the August 29 eruption. During the initial stage of the 2000 activity, the refuge action by the local administration worked effectively, which was based on the precise information on volcanic activity by JMA. However, in the latter period from August 18 to early September, CCPVE and JMA seem to have fallen into suspension of judgement. The reason for this should be clarified for the future.

Koyama (2002) described discussion made at CCPVE meetings on August 21 and 24: He pointed out that the discussion was too much biased toward the physical mechanism of the August 18 eruption and that its dangerous feature to human life was not emphasized adequately. A serious thing for us was that there were no distinct precursors to all the phreato-magmatic eruptions in July and August: There was no enhancement of seismicity; tilt-meters and GPS measurements continued to show contraction of the volcano, which was regarded as due to shrinkage of the magma reservoir. It was clear that we could not forecast such phreatic and/or phreato-magmatic explosions by the present monitoring system (see Appendix). Also we could not tell if such destructive eruptions would successively occur or not. Koyama (2002) argued that JMA should have issued the ‘urgent volcano information’ even after the event on August 18 was over.

Tokyo MG was also accused that they endangered the local people on August 29 by doing nothing. Some argued that the local administration should have ordered the evacuation of all the inhabitants despite that the ‘urgent volcano information’ was not issued. However, Tokyo MG had not any more information or knowledge to verify such decision. Moreover, they have had an experience of the evacuation of all the inhabitants, i.e. at the time of the 1986 eruption of Izu-Oshima volcano: About 10,000 people urgently left Izu-Oshima island by ship in danger of possible phreato-magmatic explosions. They stayed for a month in Tokyo and returned home because no serious eruption took place. Although the recommendation for the evacuation order was based on some reliable evidences from volcanological viewpoint, the eruption did not happen: The administration inevitably imposed much mental blow and economic loss upon the local people. The memory of the 1986 eruption was one of the reasons that Tokyo MG hesitated to decide the evacuation of all the people during several days after the August 18 eruption.

7. Toward people’s return and resuscitation of Miyake-jima island

In September a few small-scale eruptions occurred with ejection of volcanic ash. There was some indication at the end of 2000 that magma column rose up to a shallow depth, but the eruption did not take place. Instead, an enormous amount of harmful volcanic gas (SO_2) began to be emitted (ca. several tens of thousands tons/day). The amount of gas emission decreased to a level of several thousands tons/day in 2003, but it is still dangerous for people’s life. The August 18 eruption should have blew away the blockade of the vent. Effective degassing seems to have prevented explosion of magma from the reservoir.

Nobody has ever imagined that the people in Miyake were obliged to live outside their home island for such a long time. However, it is beyond the scope of this article to report on the people’s efforts for life and the support by the administration. Miyake VO made up the revival plan for the future, in which the tourism is supposed to be the major means for living. The new Hatcho-Taira caldera which was born during the 2000 activity should be the main object of sight-seeing when the disaster from the harmful volcanic gas will have passed away. I believe that volcanologists can help people’s revival through efforts to educate the public on Miyake-jima volcano.

Acknowledgement

I am much indebted to Dr Tsutomu Miyazaki, who is the former Disaster Prevention Specialist at Tokyo MG. He was at the position until March 2001, who played a key role as an in-between among scientists and the local administration during the 2000 activity of Miyake- jima volcano. I was working at ERI in those days, and then occupied his position since April 2001. Most of the materials from Tokyo MG in this article are due to Dr Miyazaki.

Appendix: Magma plumbing system of Miyake-jima volcano in the 2000 activity:

Summary of geophysical and geological studies

Fig. 1 shows a schematic representation of the magma plumbing system, which resulted in some major volcanic events. I summarized it from several important papers related to geophysical and geological studies, following a brief summary by Watanabe (2003). However, there remain some unsolved problems, which are still in controversy.

First of all, there existed two magma reservoirs and two different kinds of magma participated in the 2000 activity of Miyake-jima volcano. The deep reservoir A lies at a depth of 9.5 km, where magma continued to accumulate since after the 1983 eruption. This was confirmed by repeat leveling surveys as well as by GPS measurements (Nishimura *et al*., 2002). On the other hand, a shallow reservoir B is located at a depth of 2.9 km (Nishimura *et al*., 2002). The swarm earthquakes on July 26 were surmised to be caused by upward intrusion of magma from the reservoir B (Ukawa *et al*., 2000; Sakai *et al*., 2001). However, the existence of B has never been noticed until the onset of the 2000 activity. A question arises when the reservoir B was formed. Most probably, it was the remnant of magma at the time of 1983 eruption.

The ground deformation during the activity is characterized by shrinkage and subsidence of the island. Nishimura *et al*. (2001) analyzed all the GPS data available in the northern Izu Islands to determine the sources of enormous crustal deformations in this region for the period from June to August, 2000. They consist of a single Mogi source beneath Miyake-jima volcano and an intrusive dyke plus some seismic and aseismic shear faults beneath the sea extending about 20 km to the west. The depth of the Mogi source (depressurized) was estimated as 4.2 km. However, Nishimura *et al*. (2002) reexamined the analysis and found that the overall deformation on Miyake-jima island can be better explained by depressurization at both the sources A and B than that of a single source. The horizontal position of B is 1 km to the south from the new caldera rim, while that of A is 2 km to the southwest. The deformation after September 2000 (i.e. the degassing period) is ascribed to deflation of the B reservoir alone.

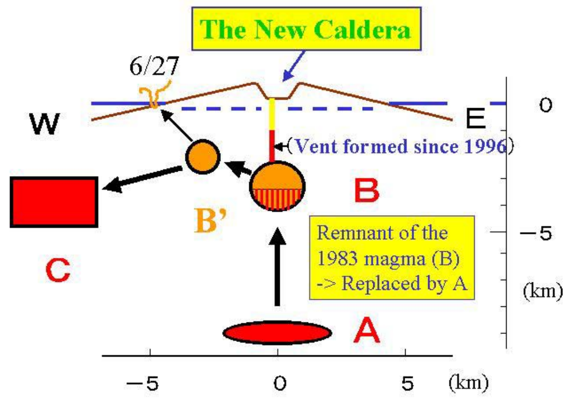

Fig. 1. A schematic representation of the magma plumbing system of Miyake-jima volcano during the 2000 activity.

The ejecta of the sea-floor eruption on June 27 and the summit eruption on July 14 and 15 have the same chemical composition as those of the 1983 eruption, which is basaltic andesite with SiO_2 = 54 wt % (Geshi *et al*., 2002b). It drastically changed to that of basaltic magma with SiO_2 = 51.5 wt % at the August 10 eruption after a month's quiescence. During the interval between July and August, the magma which filled the reservoir B should have been completely replaced by the deep-seated magma at A (Geshi *et al*., 2002b).

The magma continued to flow away into an intrusive dyke beneath the western sea (C in Fig. 1) (Nishimura *et al*., 2001). It caused collapse of the roof of the reservoir B, which resulted in the formation of a new caldera (Geshi *et al*., 2002a). Only 2 days before the summit collapse on July 8, gravity measurement was done at the summit caldera, which showed decrease of up to 150 mgal as compared with the measurement done in 1998. This can be regarded as a straightforward indication that a large vacant space had already been formed beneath the caldera (Furuya *et al*., 2001). Several magnetometers in and around the summit caldera detected significant changes since at least a few days prior to the summit collapse, which suggested uprising of non-magnetic area from depth (Sasai *et al*., 2002).

Since after the July 8 summit collapse, an abrupt inflation in the summit area followed by gradual recovery within several hours happened about once a day, which is called the tilt-step (Ukawa *et al*., 2000). It disappeared after the August 18 eruption. The tilt-step event was recorded as a very-long-perod (VLP) seismic wave of 50 seconds duration, of which source was simply a volumetric expansion at a few km depth (Kikuchi *et al*., 2001; Kumagai *et al*., 2001). The generation mechanism of the tilt-step or the VLP event is still a matter of controversy. Kumagai *et al*. (2001) proposed a vertical piston and magma chamber model, in which piston-like solid materials intermittently sink into a magma chamber to cause its inflation. Kikuchi *et al*. (2001) suggested a buried geyser model in which a reservoir of hydrothermal fluids at a shallow depth (ca. 2 km) inflates by abrupt evaporation.

Phreato-magmatic explosions occurred several times in July and August, which erupted much amount of volcanic ash. Ejecta contained some portion of fresh magma, but most of them consisted of hydrothermally altered minerals and old volcanic rocks. This feature was very different from the past eruptions in Miyake-jima volcano where lavas and fresh scoria were the major part of erupted materials. The problem is that these eruptions were accompanied by no distinct mechanical signals such as inflation or seismic activity. Moreover, even three major eruptions (July 14-15, August, 18, 29) did not affect the shrinking trend of the volcano observed by GPS measurements, which was considered to monitor the stress state of magma reservoir(s). Yamashina (2003) analyzed GPS data to detect some small amount of inflation signals prior to a few eruption events by subtracting the general trend of contraction. He reported an attempt of eruption forecast in his home page, in which he estimated the occurrence probability of eruption as 20 to 30 %. He suggested that the source for the precursory inflation was much shallower than the B reservoir.

There were two precursory phenomena to the 2000 activity: Inflation of the volcano (1984 - 2000) due to accumulation of magma at the reservoir A, and thermal demagnetization (1996 - 2000) beneath around the southern rim of the summit Hatcho-Taira caldera. The former was effectively used as the basis for the medium-term prediction, as was the case when Dr Miyazaki gave warning to the member of the Four Agency Conference in 1999. The latter is considered as the formation process of the presently active vent (Sasai *et al*., 2002).

References

Furuya, M., *et al.*, Caldera formation process during the Miyakejima 2000 volcanic activity detected by spatio-temporal gravity changes, (in Japanese with English abstract)), *J. Geogr*., **110**, 217-225, 2002.

Geshi, N., *et al*, Caldera collapse during the 2000 eruption of Miyakejima Volcano, Japan, *Bull. Volcanol*., **64**, 55-68, 2002a.

Geshi, N., *et al*., Magma plumbing system of the 2000 eruption on Miyakejima Volcano, Japan, (in Japanese with English abstract), *Bull. Volcanol. Soc. Jpn*., **47**, 419-434, 2002b.

Kikuchi, *et al*., Source process of the long-period seismic pulses associated with the 2000 eruption of Miyake-jima volcano and its implications, (in Japanese with English abstract), *J. Geogr*., **110**, 204-216, 2001.

Koyama, M., Unsuccessful risk evaluation and communication during the crisis of Miyakejima volcano in August, 2000, (in Japanese), *Rep. CCPVE*, **78**, 125-133, 2002.

Kumagai, H., *et al*., Very-long-period seismic signals and caldera formation at Miyake Island, Japan, *Science*, **293**, 687-690, 2001.

Nishimura, T., *et al*., Crustal deformation caused by magma migration in the northern Izu Islands, Japan, *Geophys. Res. Lett*., **28**, 3745-3748, 2001.

Nishimura, T., *et al*., Crustal deformation and source estimation before and after the 2000 Miyakejima eruption, (in Japanese with English abstract), *Bull. Earthq. Res. Inst., Univ. Tokyo*, **77**, 55-65, 2002.

Sakai, *et al*., Magma migration from the point of view of seismic activity in the volcanism of Miyake-jima island in 2000, (in Japanese with English abstract), *J. Geogr*., **110**, 145-155, 2001.

Sasai, Y., *et al*., Magnetic and electric field observations during the 2000 activity of Miyake- jima volcano, central Japan, *Earth Planet. Sci. Lett*., **203**,769-777, 2002.

Ukawa, M., *et al*., The 2000 Miyakejima eruption: Crustal deformation and earthquakes observed by NIED Miyakejima observation network, *Earth Planets Space*, **52**, 19-26, 2000.

Yamashina, K., Experimental prediction of the 2000 eruption of Miyakejima volcano, Japan - Discussions on inflations before major eruptive activities -, (in Japanese with English abstract), *Bull. Volcanol. Soc. Jpn*., **48**, 35-42, 2003.

Watanabe, H., Prediction research on recent volcanic eruptions: A view from geophysical observation, (in Japanese with English abstract), *Bull. Volcanol. Soc. Jpn*., **48**, 87-93, 2003.

Yoichi Sasai
The Disaster Prevention Division, Bureau of General Affairs,
Tokyo Metropolitan Government Office
Nishi-Shinjuku 2-8-1, Shinjuku-ku, Tokyo, 163-8001, Japan
email: yosasai@zag.att.ne.jp

GEOMORPHOLOGY

Reconstruction of recent behavior of active faults in the plate convergence zone, central Japan: Application of the off-fault paleoseismology to estimate the recurrence interval and the last event age.

Haruo Yamazaki

Department of Geography, Graduate School of Science, Tokyo, Metropolitan University

ABSTRACT

Since the 1995 Hyogo-ken Nanbu earthquake (M7.3: Kobe earthquake) which was caused by the displacement of an onshore active fault after the long dormant period, Japanese Government promotes the organized geological survey including trench excavation for active faults to estimate the future potential of large earthquake. However, no noticeable surface breaks appeared at the onshore shallow earthquakes such as the 2000 Tottori-ken Seibu earthquake (M7.3) and the 2004 Niigata-ken Chuetsu earthquake (M6.9). These facts suggest that the geological records obtained from the trench excavation may not correctly represent all of destructive events from the active fault. To solve this problem, new method called "off-fault paleoseismology" was applied to reveal the Holocene history of fault movement of the Fujikawa-kako fault zone (FKZ), which is situated along the onshore plate boundary in central Japan, and which shows the highest vertical slip-rate in Japan. The off-fault paleoseismology tries to uncover the ages of past fault events by means of coseismic geological evidences that are not directly related to seismogenic fault movement. Using the geological evidences on the scarp failure, emergence of marine terraces, and sudden depression of marshes, it is revealed that the FKZ has repeated its movement at 1500 years interval during the Holocene time and that the last fault event occurred at about 1500 years ago.

KEYWORDS: plate convergence zone, active fault, off-fault paleoseismology, reconstruction of fault behavior, Suruga trough, Fujikawa-kako fault zone

1. OFF-FAULT PALEOSESISMOLOGY

The 1995 Hyogo-ken Nanbu (Kobe) earthquake (M7.2), which gave the severe disaster to modern metropolis in Japan, diverted the national policy of disaster prevention from the earthquake prediction of some limited regions to the mitigation of earthquake hazard of all the country. Active faults also attracted the national concern as the source of onshore large earthquakes. Helped by the autonomous bodies and national institutes, Japanese Government started the project of active fault survey to reveal the past fault behavior that is necessary for the assessment of future activity.

This project primarily aimed to reveal the recurrence interval and the age of the last event of each major active fault in Japan by means of the geological research including the trench excavation survey. Although some trench excavations along the active faults failed to obtain the confirm geological data because of the dense land use condition, many researches successfully provided the information on the detailed behavior which is useful to estimate the probability of future fault activity.

On October of 2000, the Tottori-ken Seibu earthquake (M7.3), an onshore shallow earthquake larger than Kobe in magnitude, attacked the Japan Sea coast side in southwestern Japan. In spite of very shallow focal depth, no conspicuous surface rupture related to the under ground source fault appeared in the quake-stricken area. In the case of the Hyogo-ken Nanbu earthquake, only a part of source fault, which runs beneath Kobe city, appeared along the western coast of Awajishima Island and no surface fault break was recognized on Kobe area and the Rokko Mountains. In the case of recent Niigata-ken Chuetsu earthquake of 2004, which was onshore shallow earthquake with M6.9 and occurred along a major tectonic line, no clear surface rupture was observed along the active fault that was seismically suspected as source fault. These facts derive the doubt that geological records obtained from the trench excavation survey may not correctly represent all of the destructive events from the active fault.

"Off-fault paleoseismology" [1] is a new research method for reconstruction of fault behavior to compensate the above mentioned weak point of the trench excavation. The term "off-fault" [2] is derived from the classification of tectonic features associated with the fault movement (Table 1). MaCalpin and Nelson (1996) divided the tectonic feature into two categories as "primary" and "secondary". Primary indicates the features created by tectonic deformation and secondary indicates the features associated with the seismic shaking. They subdivided seismic-related features including each category into "on-fault" and "off-fault."

Table 1 Hierarchical classification of paleoseismic features

(Modified and simplified from MaCalpin and Nelson,1996)

	On fault	Off fault
Primary	*Geomorphic features*	
	Fault scarp	Tilted surface
	Fissures	Uplifted shorelines
	Fold	Drowned shorelines
	Moletracks	
	Pressure ridges	
	Stratigraphic features	
	Faulted strata	Tsunami deposits
	Folded (tilted) strata	
	Colluvial wedges	
	Fissure fills	
Secondary	*Geomorphic features*	
	Sand blows (liquefaction)	Sand blows (liquefaction)
	Landslides	Landslides
		Fissures
	Stratigraphic features	
	Sand dykes	Sand dykes
	Rapidly deposited lake or estuarine sediments	Turbidites

Haruo Yamazaki
Department of Geography, Graduate School of Science, Tokyo Metropolitan University,
Minami-ohsawa 1-1, Hachioji, Tokyo, 192-0397 JAPAN
Email: yamazaki@comp.metro-u.ac.jp

The category of on-fault means the geological and geomorphic phenomena observed on the surface trace of seismogenic fault. The off-fault category includes the all of the phenomena that are excluded from the on-fault. The features of primary and on–fault type have been exclusively used as the evidence for the source fault movement in trench excavation survey in Japan. Whereas off-fault paleoseismology means studies to identify the ages and source fault of specific paleo-earthquakes using analysis of geologic and geomorphic features included in the other three types on Table 1, except for the primary and on-fault type.

Although each of these features, such as landslides, liquefaction and coastal uplift are not directly related to source fault movement, a concentration of their occurrence into some specific ages and areas would provide clues to identify the precise age and source fault which caused the paleo-earthquake. Therefore, a lot of precise chronological data such as AMS ^{14}C dating and high-resolution tephrochronology is needed on the occurrence of these features.

2. ONSHORE PLATE CONVERGENCE ZONE

2.1 Collision of Izu-Bonin arc with Honshu on the Eurasian plate

Japanese Islands situated on the eastern edge of Eurasian plates have been deformed by the subduction of Pacific and Philippine Sea plates (Fig.1). In the early Pleistocene, buoyant Izu-Bonin volcanic arc developed on the eastern edge Philippine Sea plate collided with the Honshu Island on the Eurasian plate. This collision resulted in the onshore plate boundary (convergence zone) on the northern margin of Izu Peninsula.

The onshore borderland between two plates runs the relative low relief areas connecting the offshore Sagami and Suruga troughs where Philippine Sea plate is subducting beneath the Eurasian plate (Fig.2). Several Quaternary volcanoes including Mt. Fuji have erupted in this onshore boundary region.

Distinct active faults system develops in the plate boundary region surrounding the northern margin of Izu Peninsula. Thrust type dip slip faults are prominent in this region with the highest class vertical slip-rate (>5mm/yr.) in Japan.

The Quaternary system in the convergence zone is classified into basin fill type and non-basin fill type deposits based on their lithofacies, thicknesses and tectonic features. The active faults develop on the boundary between older uplifted deposits in the Honshu side and present subsiding basins in the Izu side. These subsiding areas have migrated towards the Izu side along with the migration of fault system. Yamazaki (1984, 1992)[4],[3] suggested that the active faults in the plate convergence zone are imbricate thrust faults caused in accretion process, as branched faults from the concealed plate bounding mega-thrust. This is one of the reasons why the active faults in the plate convergence zone have higher slip-rate than those in other region of Japan.

2.2 The Fujikawa-kako fault zone

The Fujikawa-kako fault zone (FKZ) is situated at the northern onshore extension of the Suruga trough where the oceanic Philippine Sea plate is driving beneath the Eurasian plate. This fault zone consists of two subparallel fault systems running in a N-S direction. The eastern system, named the Iriyamase–Ohmiya -Agoyama fault system, comprises two echelon-arranged thrust faults and a normal fault connecting the thrust faults. This system has built a conspicuous fault scarp of more than 100m in height bounding the subsiding lowland to the east and the uplifting hilly area to the west (Fig.3 and Fig4). The long-term slip-rate of the system is estimated to be 7mm/yr based on vertical offsets of the late Pleistocene volcano-clastic sediments and lavas from Mt. Fuji [3]. The western faults, called the Iriyama-Shibakawa fault system, with a vertical slip-rate of 1mm/yr, also form a distinct boundary between the hilly area to the east and the mountains to the west.

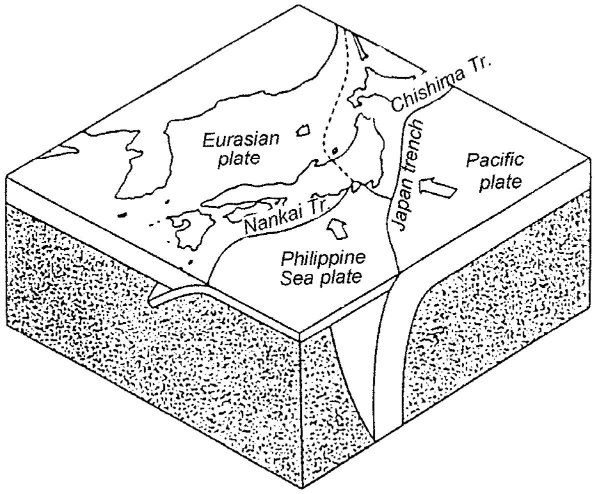

Fig.1 Schematic convergent structure of oceanic plates in and around Japan.

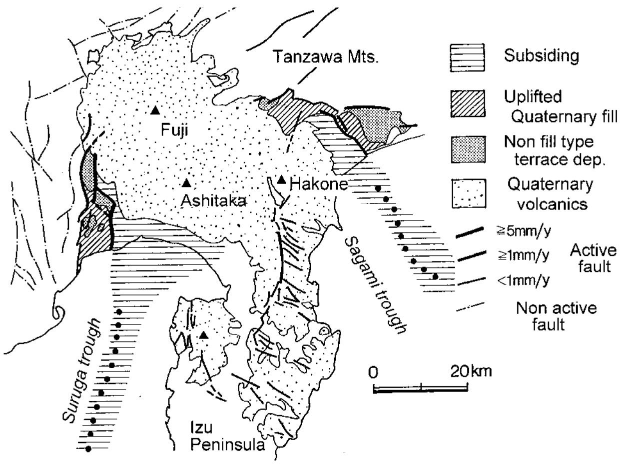

Fig.2 Distribution of active faults and the Quaternary sediments around the onshore plate convergence zone in the northern margin of Izu Peninsula. [3]

Fig.3 Prospect of the uplifting Hoshiyama hills and subsiding Fujinomiya basin on the southwestern foot of Mt. Fuji. The Iriyamase fault runs at the right edge of hilly area (Photo from uplifted Kambara hills by H. Yamazaki).

As above mentioned [3], the active faults constituting the FKZ are imbricate thrusts developed in the accretionary prism associated with the plate subduction. The thick gravels which compose the hilly and mountainous areas were thought to be originally trough fill sediments deposited in Pliocene to middle Pleistocene times. It was also suggested that the reactivation of these thrusts was closely related to the slip of the plate-bounding mega-thrust, which would cause a huge earthquake [3].

However, we have no obvious historical information on huge earthquakes that have a close relationship to the growing of these imbricate thrusts. Therefore, the reconstruction of past fault movement of the FKZ provides the most important and useful information for hazard assessment of future destructive earthquakes in the Izu-Tokai region, central Japan.

3. RECONSTRUCTION OF FAULT BEHAVIOR

After the 1995 Hyogo-ken Nanbu earthquake, the trench excavation surveys for the FKZ were planed and carried out as well as with other onshore active faults in Japan. However, it failed to reveal the recurrence of fault movement, as the fault scarp was too large to excavate the effective trench. Therefore, “off-fault paleoseismology”, a new method making up for weak points of the trench excavation survey was applied to reconstruct the precise and detailed behavior of the FKZ in Holocene time [5].

Off-fault paleoseismology is not a single survey procedure but a comprehensive method to identify the synchronicity of past geological events obtained from the various kinds of chronological surveys. Matters for investigation that are necessary to identify the past fault events are selected from the phenomena described in the conceptual system model on the crustal deformation associated with the displacement of FKZ (Fig.5). Figure 5 shows that the Kambara hills to the west side of the Iriyamase fault coseismically uplift and Fujikawa alluvial fan and Ukishima-ga-hara to the east side suddenly subsides by the fault movement. It is expected that emergence of marine terrace along the coastal area of Kambara hills, collapse of fault scarp and succeeding cumulative burial of debris in the basin fill deposits.

Geochronologic information from the trench excavations, concentrated drillings at a foot of fault scarp, Holocene marine terraces at Yui, southwestern end of Kambara hills, and archaeological site in Ukishima-ga-hara were used to reconstruct the fault behavior.

In this paper, author used the conventional ^{14}C ages rather than calibrated ages. This is because he has to use many age data from tephrochronology and archaeology that are difficult to convert to calibrated ages.

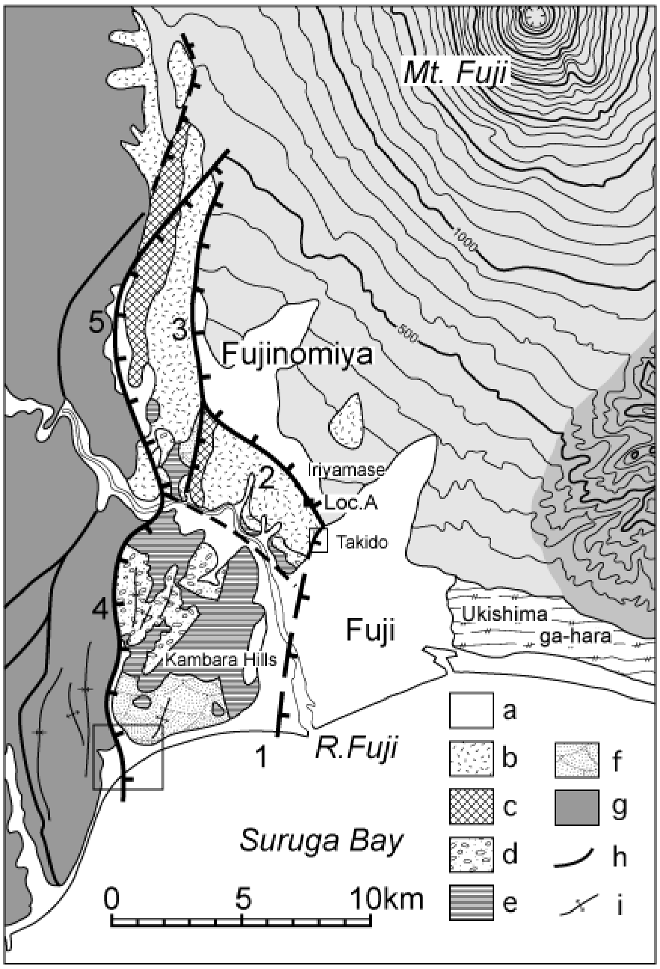

Fig.4 Geological map showing the structure of the onshore plate boundary zone at the northern extension of the Suruga trough and configuration of the Fujikawa-kako fault zone [3],[5]
Fault name: 1. Iriyamase fault, 2. Ohmiya fault, 3. Agoyama fault, 4. Iriyama thrust fault, 5. Shibakawa fault.
Legends: a. Alluvium, b. Old Fuji mudflow, c. Fuji lavas, d. Saginota gravels, e. Iwabuchi andesite, f. Kambara gravels, g. Pre-Quaternary, h.Non-active fault, i. Fold axis.

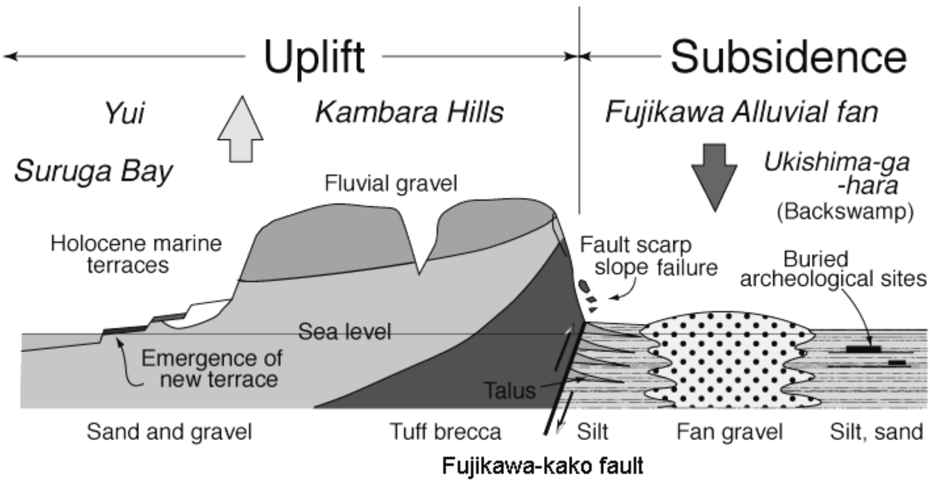

Fig.5 Schematic E-W geological section crossing Kambara hills, the Fujikawa-kako fault and Ukishima-ga-hara.

3.1 Trench excavation survey

In 1996 the Geological Survey of Japan carried out a trench excavation survey at the southeastern end of the Ohmiya fault in Iriyamase, Fuji city (Loc. A in Fig. 4). A normal fault striking sub-parallel to the main fault scarp appeared in the lowest part of the trench wall. The fault cut a tuffaceous silt layer, ca. 3.2 ka BP, and is overlain by large failure block consisting of basaltic debris derived from Old Fuji mudflow of the upper part of the fault scarp. The block contains some fragments of the Kawago-daira pumice (Kg) erupted from Amagi volcano in Izu Peninsula at 3.1 ka BP. Moreover, the debris block is overlain by Ohsawa scoria (F-Os) erupted from Mt. Fuji at ca.2.8 ka BP. This means that the failure of block from the fault scarp occurred between 3.1 and 2.8 ka BP.

3.2 Concentrated drillings at the foot of fault scarp

A steep scarp at the northeastern end of the Iriyamase fault contacts the alluvial plain at Takido, Fuji city. A drilling survey was carried out at Takido to obtain some evidence of past fault movements. Three all-core drillings each 40m in depth were arranged at 20m intervals at the foot of fault scarp [5]. Figure 6 shows the drilling logs, conventional ages of ^{14}C dating and their stratigraphical interpretation. Some debris layers with basalt blocks from the Old Fuji mudflow are intercalated intermittently in the peaty silt and fine sand sediments. Grain size and thickness of the debris layer gradually fine and thin with distance from the fault scarp. As the result of ^{14}C dating, five episodes of debris occurrence are recognized from the colluvial wedge horizons dated at 6.0-5.5 ka BP, 4.6-4.3ka BP, 4.0-3.8ka BP ca. 3.0ka BP and ca. 1.5ka BP. Cyclic facies change and nearly constant interval of debris age strongly indicate the periodic recurrence of fault movement. However, as scarp failure is a secondary feature, it is difficult to prove from debris only that the fault movements caused the slope failure.

3.3 Holocene terraces

Holocene terraces of marine and fluvial origin are developed along the coastal region of the Kambara hills. In particular, many Holocene terraces remain at Yui and Iwabuchi on the southwestern margin and eastern edge of Kambara hills, respectively. At Yui, five Holocene terraces (Yu1 to Yu5) are recognized around the mouth of the Yui River. The existence of many young terraces suggests that these terraces formed by the intermittent uplift of Kambara hills caused by the movement of the Iriyamase-Ohmiya-Agoyama fault system. The lowest Yu5 terrace seems to be of non-tectonic origin associated with artificial changes to the river. Therefore, these uplifted terraces, except for the youngest Yu5, are primary and off-fault geomorphic features. Emergence ages based on the ^{14}C dating and archaeological remains of Yu1 to Yu4 terraces are estimated to be ca. 6 ka BP, ca. 4.5 ka BP, before 1.7 ka BP, and after 2.0 ka BP, respectively.

3.4 Ukishima-ga-hara

In 1988, an archaeological survey was carried out to reveal a buried settlement site from the Yayoi Period (ca. 1.5ka BP) on the buried barrier in the west of Ukishima-ga-hara. This site was abandoned at 1.5 ka BP, just after the eruption of Ohbuchi scoria (F-ObS) from Mt. Fuji. Through a drilling survey in western Ukishima-ga-hara, Shimokawa et al. (1999) [6] found two horizons of blue silt that directly overlie the air fall Kg and ObS tephras, and thought that these sudden facies changes indicated instantaneous tectonic subsidence. From this evidence, it is recognized that coseismic crustal deformation occurred in this region at ca.3.0 ka BP and ca. 1.5 ka BP, respectively.

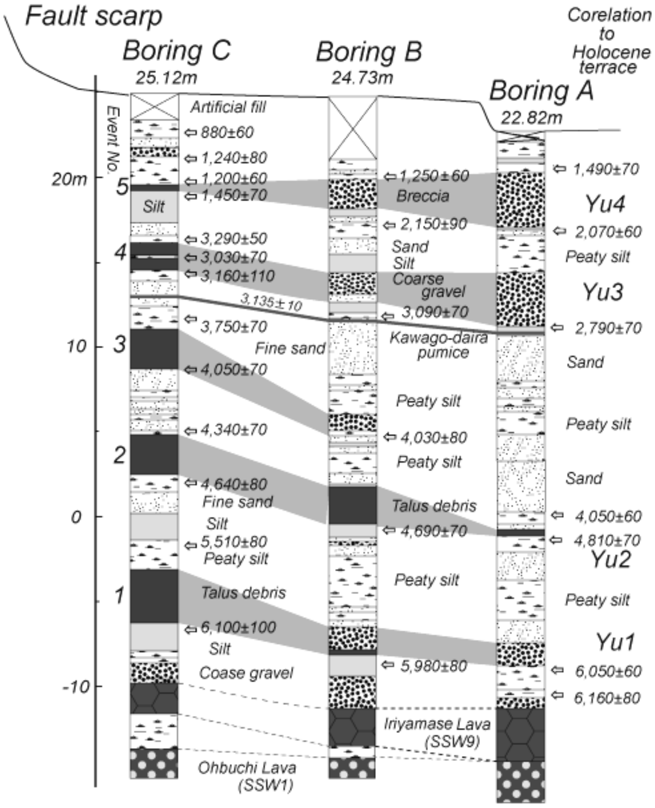

Fig. 6 Drilling logs and their geological interpretation [5].

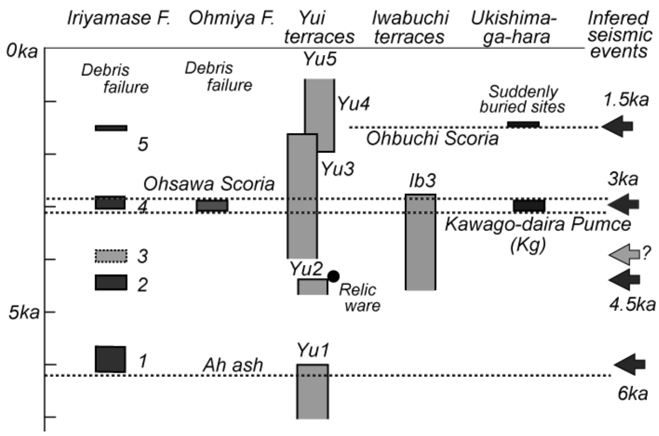

Fig. 7 Age correlation of paleoseismological features around the Fujikawa-kako fault zone [5].

3.5 Reconstruction of the fault movement

The ages of coseismic features that are recognized through various geological surveys conducted around the FKZ are shown in Fig. 7. The vertical coordinate axis in Fig. 7 shows the estimated age of each event with error bars and the horizontal axis represents research areas where coseismic feature were recognized. Intensive occurrence of coseismic features are recognized around the FKZ at about 6 ka BP, 4.5 ka BP, 3 ka BP and 1.5 ka BP.

As a scarp failure or a landslide is generally classified into the secondary category, it is difficult to identify the source fault without regard to on-fault or off-fault features. However, if some of the secondary features occurred simultaneously with primary and off-fault features, it would be possible to identify the source fault.

The primary features in paleoseismology are related to subsidence of Ukishima-ga-hara and uplift of Kambara hills (Table 1). These tectonic deformations can be explained by the coseismic fault displacement of the FKZ. Accordingly, the recurrence interval and the last fault event of the FKZ are estimated to be 1.5 ka and about 1.5 ka BP, respectively. Coseismic surface break probably reaches more than 10m because the vertical long-term slip-rate of the FKZ is estimated to be 7mm/yr.

ACNOWLEDGMENT

The author expresses his gratitude to Prof. Yoshihiro Kinugasa of the Tokyo Institute of Technology, and Dr. Kiyohide Mizuno and Dr. Koichi Shimokawa, the chief researchers of the National Institute of Advanced Industrial Science and Technology for their kind supports and suggestions to this work.

REFERENCES

[1] Y. Kinugasa, Off fault paleoseismology for Pacific margin, *EOS Transactions, AGU 1998 Western Pacific Geophysics Meeting*, **79**(24 suppl.), pp.w81, 1997.
[2]J.P. MaCalpin, and A.R. Nelson, Introduction to paleoseismology, in *Paleoseismology,* ed. J.P. MaCalpin, 1-28, Academic Press, 1996.
[3] H. Yamazaki, Tectonics of a plate collision along the northern margin of Izu Peninsula, central Japan, *Bull. Geological Survey of Japan*, **43**, pp.603-657, 1992.
[4] H. Yamazaki, Neotectonics of the South Fossa Magna in central Japan deduced from active faults, *Quaternary Research of Japan*, **23**, pp.129-136, 1984.*
[5] H. Yamazaki, K. Shimokawa, K. Mizuno, and T. Tanaka, Off-fault paleoseismology in Japan: with special reference to the Fujikawa-kako fault zone, central Japan, *Geogr. Rep. Tokyo Metropolitan Univ.*, **No.37**, pp.1-14, 2002.
[6] K. Shimokawa, H. Yamazaki, and T. Tanaka, Paleoseismological study of the Fujikawa-kako fault zone, *The seismological Society of Japan, 1999 Fall Meeting, Programme and abstracts,* pp.C36, 1999.**

* In Japanese with English abstract. ** In Japanese.

Ground Penetrating Radar measurements and developments for fracture imaging and characterization in limestone cliffs

*Stéphane Garambois (1), Colette Grégoire (2), Mathieu Jeannin (1), Jacques Deparis (1) and Denis Jongmans (1)

(1) LIRIGM, Université Joseph Fourier, Grenoble, France
(2) Department of Civil Engineering, Katholieke Universiteit Leuven, Belgium

ABSTRACT

The geometry and properties of fractures are important properties of rock masses that must be taken into account in their stability assessment for rock fall hazard. Until now, geophysical methods have been rarely used to investigate vertical cliffs, mainly regarding to the extreme conditions of material deployment. In this study, the GPR method, which is able to yield information about the internal structure of resistive rocks, was applied in several test sites. The purpose was to evaluate the potential of different acquisition configurations (vertical and 2D profiles, CMP, transmission, tomography, TE & TM modes) for better characterizing the geometry and properties of the main discontinuities (fractures) within the massif. Furthermore, the reflectivity of GPR data, which provided geometrical imaging and characterization of discontinuities, exhibits frequency variations, which can provide quantitative information on the fracture properties. The possibilities and the limitations of the reflectivity inversion were tested using the Jonscher formulation. For this, the Neighbourhood Algorithm (NA), which is an optimising technique looking for the best solutions, was used. This inversion technique was mainly tested on 100 MHz synthetic GPR signals reflected on fractures filled with air, clay or water. Most of the results were consistent, and the reliability of the method was estimated by analyses of the derived models on the parameter space. Nevertheless, the choice of a reference signal has still to be tested on synthetic data, before considering real applications.

KEYWORDS: Rock fall hazard, Ground Penetrating Radar, Fracture characterization, Neighbourhood inversion

INTRODUCTION

The growing urbanization in mountainous area implies to better understand and assess natural hazards. Among them, rock falls are frequent phenomena characterized by their suddenness and their difficulty to predict. Rock mass stability assessment is a complex problem generally addressed from surface observations: slope morphology, mass fracturing, deformation measurements (e.g. [1]). Even if such studies are essential, the lack of information concerning the geometry and properties of discontinuities within the rock mass leads to major uncertainty. Consequently there is a crucial need to precisely image and characterize these objects. Except heavy geotechnical drilling, only geophysical methods are able to obtain information about the discontinuity geometry within the studied massif. However, these techniques have rarely been applied to vertical cliffs or high natural rock slopes, probably due to practical difficulties in such extreme conditions.

In the last decade, there has been a growing literature dealing with fracture characterization using GPR. At a lower scale and/or in easier field conditions, the GPR method was successfully applied to comparable geological problems such as fault and fracture 2D mapping in resistive rocks ([2], [3], [4] & [5]). For imaging sub horizontal fractures as well as sub vertical faults, a 3D radar technique was applied in a gneiss quarry [6]. Similarly, the distribution and continuity of cracks from GPR data acquired on the vertical wall of a welded tuff rock was detected [7]. A strike-direction-finding scheme using GPR data was developed [8] and tested from three different acquisition modes for the same survey line in a granite quarry. The computed reflectors azimuths were found to be well correlated with those of observed fractures and joints. In limestone, 2D and 3D GPR measurements showed that open fractures, joints or discontinuities filled with clay or water are clearly visible when an appropriate wavelength is used ([9], [10]). A semi-quantitative evaluation method based on the amount of backscattered GPR energy was defined as an index of rock quality [11].

Recently, GPR measurements and seismic tomography were performed [12] on a 12 m high limestone cliff with GPR antennas and some geophones set on the cliff. The results indicate that simple vertical GPR profiles performed on the cliff were efficient to detect and image sub vertical discontinuities as far as 10 m deep. The latter were well correlated with fractures deduced from surface observations. In contrast, seismic tomography (seismic sources and geophones deployed on the surface and on the cliff) was found not efficient to detect and characterize these discontinuities. It provided a rough image of the consolidation state mass. For tunnel stability, it has been showed [13] that GPR data supplied information about the number and location of discontinuities in the investigated zone, while seismic methods provided estimates of the distribution of the mean elastic properties.

Compared to previous studies, the aim of our work takes a step forward to the use of multi-configuration GPR experiments on real rock-fall problem cases. First, experiments consisted in evaluating the potential of 2D, CMP, transmission, tomography and different mode acquisition profiles to characterize the geometry and properties of the fracture set. Various test sites in limestone and sandstone formations were investigated. The analysis of these experiments [14] clearly shows that GPR images gave valuable 2D or 3D images (some were validated with boreholes) of the discontinuities geometry and in some cases quantitative information on fractures using CMP analysis. In this paper, only a few investigations performed on one test site will be presented. In a second part, we present theoretical and numerical studies conducted to get more systematically quantitative information on fracture properties (thickness, filling material) from GPR reflectivity. This study is based on the frequency content analysis of the reflectivity. The possibilities and limitations of the reflectivity inversion technique in function of the fracture properties and the used frequency were established [15]. However, the inversion technique was based on a grid search of the parameters. In this paper, a more efficient search technique, the neighbourhood algorithm, was applied to invert the amplitude and phase of the reflection coefficient. Synthetic examples of this ongoing research will be presented here.

MULTICONFIGURATION GPR MEASUREMENTS

Calcareous cliffs surrounding the urban area of Grenoble city (Isère, France) exhibit a cumulative length of 120 km and can reach 400 m high. They are part of the Chartreuse and Vercors subalpine massifs made of sedimentary rocks from upper Jurassic and lower Cretaceous age (limestone and marls). In these massifs, most of the cliffs are located in Tithonian and Urgonian limestone beds which dip slightly inwards. Because of the cliff morphology, this region has been submitted to extensive rock fall risk (ranging from block fall to major events), which has been studied considering a probabilistic approach [16]. As mentioned in the introduction, various test sites presenting different properties (scale, filling properties, rock formation) were investigated, but only one will be presented hereafter.

The presented site is an unstable rock mass of approximately 3000 cubic meters, located at the top of a 400-m high cliff in the Vercors massif (Fig. 1b).

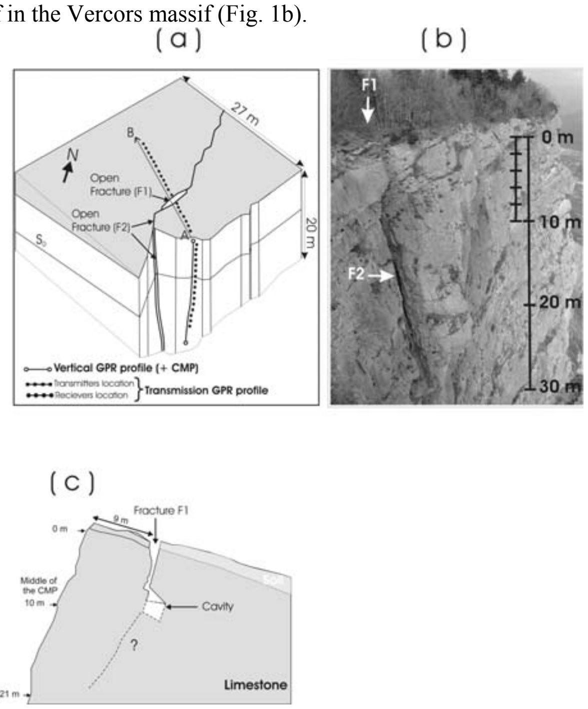

Figure 1. Schematic representation of the test site including i) the location of the main fractures (F1 & F2) and ii) the different GPR configurations. The AB direction represents the orthogonal of the vertical GPR profiles. (b) Photography of the studied rock scale. (c) Schematic view of the main fracture.

The cliff is made of hard Urgonian limestone and the horizontal plateau is recovered by soil and vegetation. Three discontinuity sets were measured: the bedding plane (N40°E/45°W), dipping gently inwards the massif and two sub vertical fractures sets (N50°E/70°SE and N170°E/70°E). The rock flake is limited on two sides by two open fractures (F1 and F2) belonging to each discontinuity set (Fig. 1a). These two fractures are clearly visible on the cliff and on the horizontal plateau. Fracture F1 is widely open on the surface of the plateau and can reach an aperture of 1 meter. The second fracture, denoted F2, delimits the western part of the rock mass. The eastern limit of the rock column is not well defined. Fig. 1c displays a schematic section of the cliff morphology and the geometry of the open fracture F1, which was investigated down to a cavity, whose top is located at 7 m depth. For practical and safety reasons, the different GPR tested configurations were limited to vertical multifrequency GPR profiles, a vertical CMP profile and a 100 MHz transmission experiment.

GPR measurements were conducted using a RAMAC/GPR unit system (MALÅ Geosciences), which was adapted to these extreme conditions. Indeed, as the main fracture networks are almost vertical, only profiles where at least one antenna was directly positioned on the cliff surface were able to image the possible interfaces constituted by these main discontinuities. For this reason, and to optimize the coupling between the rock surface and the antennas, an operator has to climb down the cliff with the antennas and suitable cables.

Multifrequency vertical profiles

Vertical multifrequency GPR measurements were recorded along a 21 m high profile located on the cliff wall. These TE mode multifrequency profiles were acquired using unshielded antennas of 100 MHz, 200 MHz and 400 MHz. The data processing sequence was limited to band-pass filtering, top mute of direct air arrivals followed by a zero-phase band-pass filter, whose characteristics depend on antenna frequency. Finally, to amplify late reflected events, which are more attenuated, an AGC was used. Filtered data are presented in Fig. 2a for the 100 MHz antenna ([10-200] MHz band-pass filter), in Fig. 2b for the 200 MHz antenna ([10-350] MHz band-pass filter) and in Fig. 2c for the 400 MHz antenna ([10-550] MHz band-pass filter). Data were not migrated, as the studied medium obviously exhibits 3D characteristics, i.e., a correct migration process should have required at least a 2D velocity field, which is difficult to obtain in this extreme context.

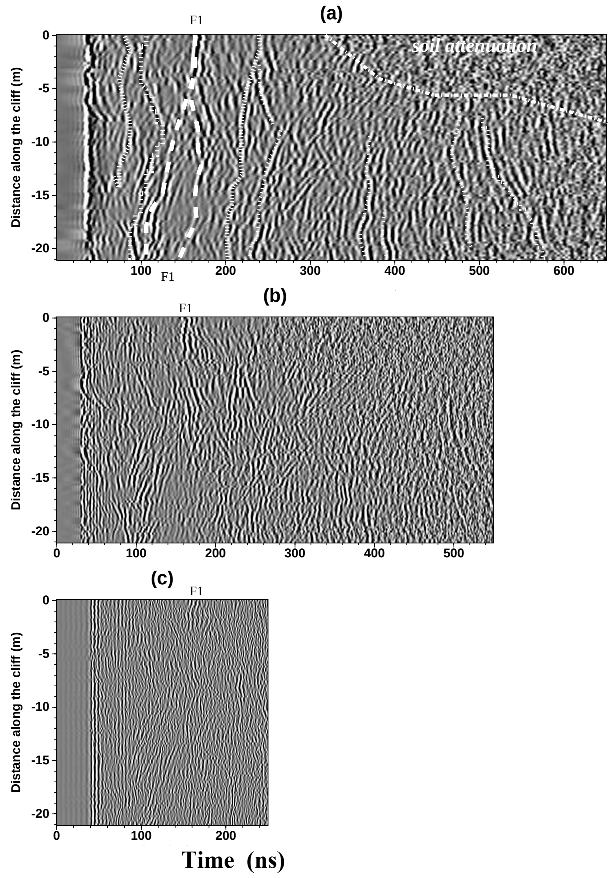

Figure 2. Multifrequency filtered (but unmigrated) time sections for vertical acquisitions. (a) 100 MHz, (b) 200 MHz, (c) 400 MHz.

These figures display numerous reflected waves. As awaited, the 100 MHz antenna allows to penetrate deeper in the rock mass than the others antennas, but with a significant loss in resolution. In contrary, the 400 MHz frequency image shows a higher number of better resolved discontinuities, but limited to the first 200 ns. With a limestone velocity of 12 cm/ns, the 400 MHz antenna is able to detect fractures as thin as 7.5 cm ($\lambda/4$). On the three images, the conductive soil cover leads to a loss of wave penetration at the surface of the plateau, particularly when the distance from the cliff increases. It is noticeable that the reflectivity properties of a given reflector both vary as a function of distance on the cliff, but also of frequency. The main fracture observed at the surface (Fig. 1c, F1) appears clearly around 160 ms on the three images and can be followed inside the rock mass. The top and the bottom of the fracture F1 are underlined on the 100 MHz profile with superimposed dashed curves, showing a strong dip toward the cliff wall. From this image, it appears that the cavity extends inside the massif all along the profile. Other fractures appear on the images, which were not identified by surface observations and are picked with dotted curves.

Vertical CMP profile

In order to get the velocity profile inside the massif, a Common Mid-Point profile (CMP) was performed at 10 m from the top of the cliff using 200 MHz antennas. The filtered CMP section ([30-220] MHz band-pass filter + AGC time equalization) is displayed in Fig. 3a and shows a top direct air-wave with a velocity of 30 cm/ns, a linear wave propagating directly in the limestone from the transmitter to the receiver with a velocity of 12 cm/ns, as well as numerous reflected events.

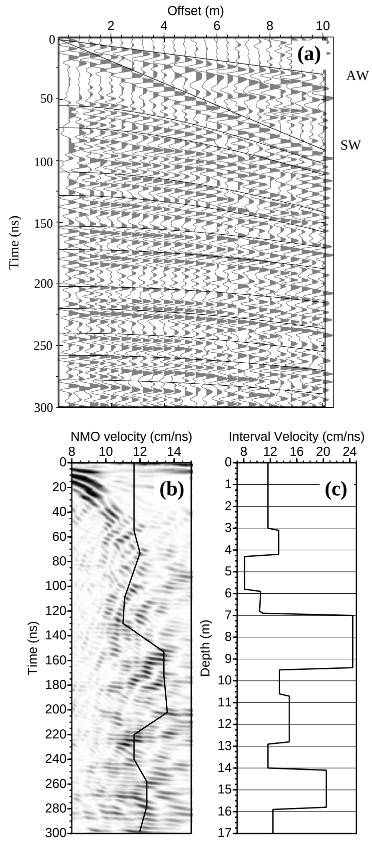

Figure 3. (a) CMP data showing different EM waves and the corresponding hyperbolae picking. (b) Semblance analysis of reflected events and deduced NMO velocity profile, (c) Interval velocity profile deduced from the NMO velocities.

NMO velocity was analyzed using the semblance maxima approach (Fig. 3b) and refined using hyperbolae superimposition to reflected events (Fig. 3a). These processes allowed to obtain a high-resolution NMO velocity profile as a function of time, which was converted to the interval velocity profile versus depth (Fig. 3c) using the Dix formula ([17]). The latter, shows high 1D velocity variations inside the rock mass. Considering 12 cm/ns as a mean velocity in cracked limestone, a low velocity zone is visible between 4.5 to 7 m, probably linked to a decrease in fracture density (if the fractures are opened and unfilled) or a change in filling properties (clays). It also exhibits two dramatic increases in velocity up to 24 cm/ns at 7 m and 14 m. As the GPR velocity is proportional to the air fraction in rocks, this result suggests two large opened fractures of 2.8 and 1.8 m thick were detected. The first one, between 7 m and 9.8 m from the cliff wall corresponds exactly to the open cavity shown on Fig. 1c. The second high velocity zone between 14.2 and 16 meters correspond to another open fracture, which was not observed from the surface (but *a posteriori* with surface electrical tomography performed on the plateau). The fact that the obtained velocity in at least one open fracture does not reach 30 cm/ns (air velocity) may come from two approximates: the Dix formula is only valid for a perfect stratified media and with moderate velocity variations. These results clearly show the potential of CMP data to characterize the properties of wide open fractures (aperture superior to half a wavelength), when reflected events from two faces of the fractures are separated.

Transmission experiment

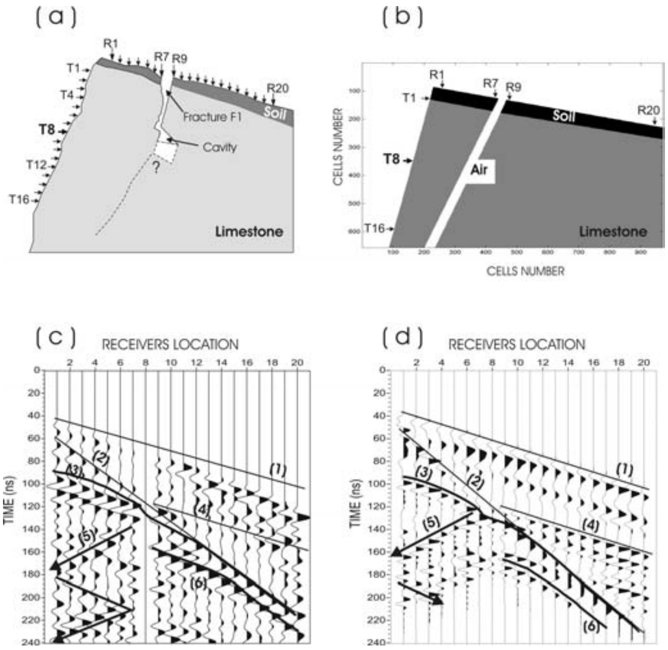

Figure 4. Transmission studies, including (a) layout of the field experiment and location of the main fractures, (b) geological model used in the GPR transmission FDTD modelling, (c) real transmission radargram obtained for transmitter T8 and (d) synthetic transmission radargram obtained for transmitter T8 for model (b).

GPR transmission measurements were conducted with the 100 MHz bistatic antennas using the layout displayed on Fig. 4a.For each transmitter location, 20 traces were recorded. The wide open fracture F1 is located between receivers R7 and R9, at 9 meters from the edge of the cliff. Fig. 4c shows an example of the complexity of an experimental radar section obtained for the transmitter T8.

In parallel, a 2D synthetic model (Fig. 4b) allows the identification of the main observed radar waves. The synthetic model is composed of an open fracture with a larger cavity, a homogeneous limestone material (11 cm/ns) and a 1 m thick soil covers (7.5 cm/ns). The derived synthetic radar section (Fig. 4d) is quite similar to the measured radargram, showing the direct transmitted air wave “1”, the wave propagating in the air up to the plateau and diffracted in the soil (“2”) and the direct transmitted wave within the rock “3”. Numerical modelling permitted to identify event “4” as the wave propagating in limestone along the surface of the cliff wall (merged with the direct transmitted wave within the massif), and which is diffracted in the air at the corner of the cliff.

As expected, this wave presents a 40 ns time delay with respect to the direct air wave "1". Then a reflected wave (denoted "5"), which is present until the receiver R7, results from the presence of the wide open fracture F1. Multiple reflections, between the fracture and the cliff are visible. The last wave ("6") is only recorded after receiver R9 and results from diffraction by the cavity. This study shows the complexity of transmission experiments, but also underlined all the information they contain.

To go further, the waves transmitted directly inside the massif were picked for all transmitter-receiver couples and the derived travel times were inverted both for the real and synthetic cases using existing software ([18]). The obtained results ([14]) showed the sensitivity of resulting images (real and synthetic) after inversion on the starting model (before inversion), because of the complex geometry of the fracture zone. The 2D velocity image appeared smoothed and an open fracture zone with higher velocity is not well constrained, showing highest velocities close to 16 cm/ns (instead of 30 cm/ns).

FRACTURE CHARACTERIZATION

The electromagnetic behaviour of a medium can be described by the effective permittivity (ε_e). This constitutive parameter, which takes into account the permittivity and the conductivity of the medium, is complex and frequency dependent. As the radar signal exhibits a broad frequency range, it is important to account for this frequency dependence. The Jonscher formulation including 3 real parameters (n, χ_r and ε_∞) is used in this study to describe this frequency dependence ([19], [20]):

$$\varepsilon_e(\omega) = \varepsilon_0 \chi_r \left(\frac{\omega}{\omega_r}\right)^{n-1} \left(1 - i\cot\frac{n\pi}{2}\right) + \varepsilon_\infty . \qquad (1)$$

The values 1 and 0 for n and χ_r respectively correspond to a perfect dielectric material. A low value for n and a high value for χ_r characterise a high dispersive (conductive) material. ε_∞ corresponds to the real part of the effective permittivity for high frequencies.

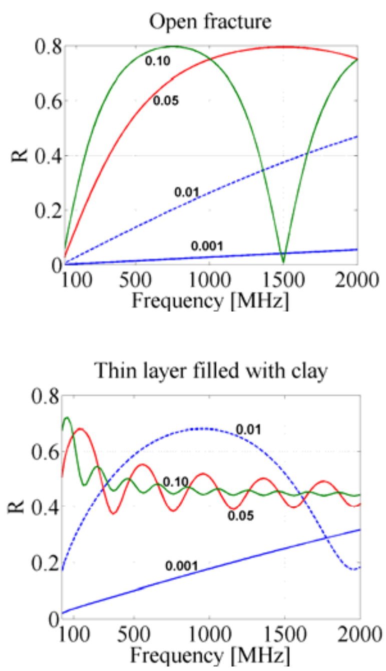

Figure 5. Theoretical reflection coefficient corresponding to an open fracture filled with air and clay for various apertures.

The reflection due to a discontinuity is related to i) the contrast of properties between the material filling the discontinuity and the surrounding medium, ii) the opening, iii) the incidence and iv) the frequency ([20]). For example, Fig. 5 shows the theoretical reflection coefficient amplitude as a function of frequency of a fracture filled with air (top) and with clay (bottom). The curves correspond to different fracture openings, ranging from 0.001 m to 0.1 m. The purpose of this study is to use the amplitude and phase dependences of the reflectivity to recover the fracture properties. For this, an automatic inversion process has been tested on synthetic data based on the Neighbourhood algorithm [21] (NA).

This inversion scheme is based on the search of an ensemble of models that preferentially samples the good data fitting regions within the parameter space. The search in this space is performed using the nearest neighbour regions defined under a suitable distance norm. The search of models is first initialised by a random number and the algorithm requires the solving of a large number of forward problems. In our case, the method was adapted to the inversion of fracture properties from the radar reflection variations with frequency. The inversion can be completed on the reflection coefficient magnitude only or on the real part and imaginary part of the reflection coefficient. In all cases, the algorithm is very fast to investigate the all space.

Inversion of synthetic signals

The inversion process was first tested on synthetic signals corresponding to open and clayey fractures. For each inversion, several runs corresponding to different random numbers were completed to get reliable results. The Jonscher parameters (n, χ_r, ε_∞) for air and clay in the synthetic models were (1, 0, 1) and (0.25, 30, 55), respectively. In the case of the open fracture, different apertures were tested from 5 cm to 200 cm in the frequency interval [80-120 MHz], where λ_{air} is around 3 m. Results for the lowest RMS values are summarised in Table 1 for an opening of 5 cm. When completed on the real and imaginary part of the reflection coefficient, the inversion leads to good results for χ_r, ε_{inf} and d. The parameter n is undetermined when the parameter χ_r is zero or close to zero, due to the mathematical form of the Jonscher law. The error on the thickness is lower than 5% for the smallest RMS errors. On the contrary, inversion of the reflectivity magnitude alone (not shown here) gives parameters different from the theoretical ones, even with low errors.

	Air	Clay
d	5.0-5.2 cm	4.7-5.8 cm
ε_{inf}	1 – 1.35	40-61
n	0.45-0.67	0.18-0.33
χ_r	0-0.06	21.5-46.5

Table 1. Synthesis of inversion results for 5 cm thick fractures filled with air or clay.

For the clay filling, where λ_{clay} is around 32 cm at 100 MHz, the considered openings were 5 cm, 10 cm and 20 cm. The inversion completed on the real and imaginary part of the reflection coefficient leads to satisfying results for openings of 10 cm and 20 cm. For those openings, the error on the thickness is lower than 5% for the smallest RMS errors. Good results were also obtained for the Jonscher parameters (or for the real part of the effective permittivity (ε_e') and the real part of the effective conductivity (σ_e') at 100 MHz). Results for the lowest RMS values are summarised in table 1 for an opening of 5 cm. In that case, the error on the thickness is larger (but still lower than 20%) for the smallest RMS errors. It is due to the limitation of the method for thin fractures (here λ/6) filled with a high-loss dielectric material. When the thickness is well estimated, the calculated values of the Jonscher parameters can be different than the theoretical values, but the estimation of ε_e' and σ_e' at 100 MHz remains realistic for those parameters.

The analysis of the full set of solutions as a function of the RMS is quite interesting to estimate the reliability of the results. The representation of each Jonscher parameter versus the aperture in the clay case (Fig. 6) and in the air case (Fig. 7) shows if the solution is constrained or not in the parameters space. Note that for the air case, a 5 % Gaussian noise was added to the data. These two figures shows that the solution was well constrained and that no second minima can be found in the parameter space.

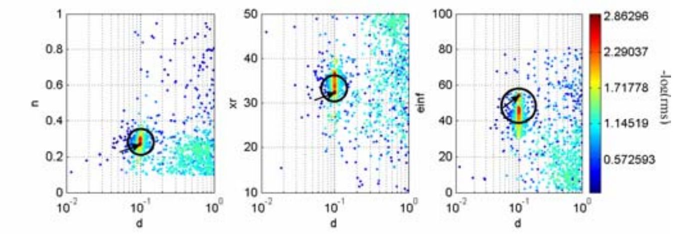

Figure 6. Inversion results for a 10 cm-thick fracture filled with clay ($n = 0.25$, $\chi_r = 30$, $\varepsilon_{inf} = 55$). 5050 models were generated with the NA inversion. The circles indicate the areas where the error is minimal.

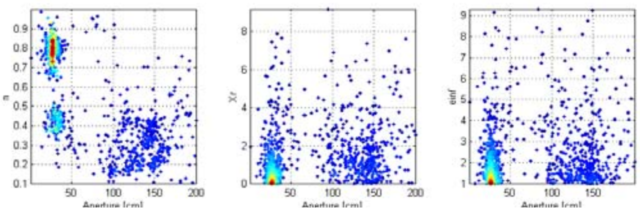

Figure 7. Inversion results for a 30 cm-thick fracture filled with air. A 5 % Gaussian noise which was added to the synthetic data.

The main conclusions of this systematic study can be sum up as follow : i) the inversion give better results when both amplitude and phase of the reflectivity are considered; ii) problems arise when aperture is not far from $\lambda/2$ and its multiples; iii) better results obtained with a limited number of parameters, i.e., when aperture of filling material is known.

To conclude this part, we must emphasize that in practice, the reflection coefficient can not be determined directly from field data because the GPR source signal is unknown. A reference signal is thus required to proceed to a sort of deconvolution of the reflected signal in the frequency domain. To evaluate this problem, the ongoing research uses a 2D EM waves modelling in order to calculate reference signals. The choice of the reference signal is crucial (reflection on a known fracture, transmitted signal within the massif, direct soil direct wave in the CMP with the problem of the source pattern). Using the reflection as reference signal, an open fracture of 35 cm was modelled. Satisfying results were obtained for the opening (33.5 cm instead of 35 cm) and for the permittivity. The value found for χ_r was very close to zero. Using the transmitted signal as reference, an open fracture of 20 cm was modelled. An opening of 25 cm was derived instead of 20 cm. More tests need to be completed in future with several reference signals (different apertures when a reflected wave is taken as reference) and for fractures with different properties before considering applications on real data. This last purpose will be first tested on a test site were boreholes were drilled, i.e., fracture properties are known.

DISCUSSION, CONCLUSIONS

Different GPR layouts were tested on different cliffs to evaluate the potential of such measurements to detect, image and characterize the fracture network for rock fall hazard assessment. One of these sites was a prone-fall rock mass showing open fractures on the cliff and on the plateau. As the top of the plateau is covered with a conductive weathered layer and the fractures were near vertical, all measurements were made on the cliff with people abseiling. With such an experimental configuration, a maximum penetration of 30 m was obtained in the limestone with 100 MHz antenna.

Vertical profiles were performed with different frequency antenna showing near vertical reflectors, the majority being related to fractures observed at the outcrop. Reflectivity variations were observed as a function of location on the cliff and on frequency. On another site, an additional horizontal profile was made, allowing the definition of the 3D fracture geometry within the rock mass [14]. Evolution of radar wave velocity as a function of horizontal distance was obtained by CMP profiles and the velocity value curve differs considerably from one site to another. The presented velocity profile benefited from numerous reflected events, and permitted to characterize two open fractures.

Transmission experiments between the vertical cliff and the plateau were conducted and successfully modelled using a 2D EM wave modelling code, allowing the recognition of the main wave types. A radar tomography was tested, giving radar velocity images of the cliff edge. However, these images are too smoothed for accurately detecting and characterizing the fracture network within the mass. On the contrary, the total wave field (including reflected and scattered waves) appeared to be very sensitive to the presence of the main fractures and cavities.

Reflectivity variations as a function of traces (vertically**),** but also as a function of frequency**,** clearly suggest that the GPR data are sensitive to the properties of the fractures (filling, aperture). To evaluate the potential of these variations for characterization, a direct search method (the NA algorithm) was applied for inverting synthetic reflection coefficient as a function of frequency to determine the fracture properties (thickness and filling material). In this case, the derived model is generally unique. Tests on synthetic signals for fractures filled with air or clay have shown the efficiency of the method when the real and imaginary parts of the reflectivity were inverted. More tests need to be completed with several frequency ranges. For applications in the field, the problem of defining a reference signal needs to be solved and several possibilities are currently tested (the use of the transmitted wave or of another reflected wave). In the near future, this inversion method will be applied on field data recorded along a vertical cliff in order to characterise the detected fractures.

To conclude this study, we would like to point out that other GPR observables can be used to better characterize the massif. For example, studies of reflectivity variations as a function of the mode acquisition (TE and TM) or reflectivity AVO (Amplitude versus Offset) and PVO (Phase versus Offset) analyses derived from CMP data can be performed to help in characterization. A 1D full-waveform inversion of these events can also be considered. Finally, it is noticeable that lot of information contained in the transmission radargrams have been omitted for interpretation (attenuation, reflected and diffracted waves on fractures and edges, dispersion) and should be used in the future by using a more sophisticated interpretation algorithm (full-waveform inversion for example).

ACKNOWLEDGMENTS

All data were processed using Seismic Unix. The authors acknowledge the contribution from Dr. A Giannopoulos who made the 2D modelling code available for everyone (a free version of the software GprMax2D can be downloaded from the address: http://www.see.ed.ac.uk/~agianno/GprMax/). This work was partially supported by the “Pole Grenoblois des Risques Naturels” through a funding from the Conseil General de l’Isère (France) and by the Parc Régional de Chartreuse. We thank all people who helped us during the field experiments and particularly Michel Sintès for

providing us topographic data. LIRIGM is part of the RNVO network.

REFERENCES

[1] Hoek E. and Bray J. W., 1981, Rock slope engineering, Elsevier Science, Cambridge.
[2] Benson A.K., 1995, Application of ground penetrating radar in assessing some geological hazards: examples of ground water contamination, faults, cavities, *Journal of Applied Geophysics*, 33, 177-193.
[3] Stevens K.M., Lodha G.S., Holloway A.L., and Soonawala N.M., 1995, The application of ground penetrating radar for mapping fractures in plutonic rocks within the Whiteshell Research Area, Pinawa, Manitoba, Canada., *Journal of Applied Geophysics*, 33, 125-141.
[4] Demanet D., Renardy F., Vanneste K., Jongmans D., Camelbeek T. and Meghraoui M., 2001. The use of geophysical prospecting for imaging active fault in the Roer Graben, Belgium. Geophysics, 66, pp. 78-89.
[5] Rashed M., Kawamura D., Nemoto H., Miyata T. and Nakagawa K., 2003, Ground penetrating radar investigations across the Uemachi fault, Osaka, Japan, *Journal of Applied Geophysics*, 53, 63-75.
[6] Grasmueck M., 1996, 3-D ground penetrating radar applied to fracture imaging in gneiss. Geophysics, 61, p. 1050-1064.
[7] Toshioka T., Tsuchida T., and Sasahara K., 1995, Application of GPR to detect and mapping cracks in rock slopes, Journal of Applied Geophysics, 33, 119-124.
[8] Seol S.Y., Kim J.-H., Song Y., and Chung S.-H., 2001, Finding the strike direction of fractures using GPR, *Geophysical Prospecting*, 49, 300-308.
[9] Pettinelli E., Beaubien S., and Tommasi P., 1996, GPR investigation to evaluate the geometry of rock slides and buckling in a limestone formation in northern Italy, *European Journal of Environmental and Engineering Geophysics*, 1, 271-286.
[10] Pipan M., Forte E., Guangyou F. & I. Finetti, 2003, High-resolution GPR imaging and joint characterisation in limestones, *Near Surface Geophysics*, 1, 39-55.
[11] Orlando L., 2003, Semiquantitative evaluation of massive rock quality using ground penetrating radar, *Journal of Applied Geophysics*, 52, 1-9.
[12] Dussauge-Pesser C., Wathelet M., Jongmans D., Hantz D., Couturier B. and Sintes M., 2003, Investigation of a fractured limestone cliff (Chartreuse Massif, France) using seismic tomography and ground penetrating radar, *Near Surface Geophysics*, 1, 161-170.
[13] Cardarelli E., Marrone C. and Orlando L., 2003, Evaluation of tunnel stability using integrated geophysical methods, *Journal of Applied Geophysics*, 52, 93-102.
[14] Jeannin M., Garambois S., Grégoire C. and D. Jongmans, 2004, multiconfiguration GPR measurements for geometrical fracture characterization in limestone cliffs (Alps), submitted to Geophysics.
[15] Grégoire C., Halleux L. and Lukas V., 2003, GPR capabilities for the detection and characterisation of open fractures in a salt mine. Near Surface Geophysics, 1, p. 139-147.
[16] Dussauge-Pesser C., Helmstetter A., Grasso J.-R., Hantz D., Jeannin M. And A. Giraud, 2002, Probabilistic approach to rock fall hazard assessment: potential of historical analysis, *Natural Hazards and Earth System Sciences*, 2, 1-13.
[17] Dix C.H., 1955, Seismic velocities from surface measurements, *Geophysics*, 20, 68-86.
[18] Demanet D. 2000. Tomographie 2D et 3D a partir de measures geophysiques en surface et en forage. *PhD thesis*, University of Liege.
[19] Jonscher A.K., 1977, The Universal dielectric response. Nature, 267, p. 673–679.
[20] Hollender F. and Tillard S., 1998, Modelling of ground penetrating radar wave propagation and reflection. Geophysics, 63, p. 1933-1942.
[21] Sambridge M., 1999, Geophysical inversion with a neighbourhood algorithm- I. Searching a parameter space. Geophys. J. Int., 138, p. 479-494.

Stéphane Garambois
LIRIGM – Maison des Géosciences
Université Joseph Fourier, BP 53
38041 Grenoble Cedex 9, France
email: Stephane.Garambois@ujf-grenoble.fr

Shallow landslide mechanism and its susceptibility evaluation from geological view point

Masahiro Chigira [(1)]

(1) Disaster Prevention Research Institute, Kyoto University

ABSTRACT

This paper summarizes rain-induced shallow landslide mechanisms and its susceptibility evaluation from geological view point, particularly weathering profile and water infiltration behavior within weathering profiles. Rainstorms have been causing numerous numbers of shallow landslides, which used to be supposed not to be closely connected to geologic conditions. However, our experience tells us that there are specific geologies preferable to shallow landslides. This paper deals with non-welded ignimbrite, vapor-phase crystallized ignimbrite, granite, and granodiorite.

KEYWORDS: rainstorm, landslide, weathering profile, water filtration, ignimbrite, granite, granodiorite

1. IGNIMBRITE

Pyroclastics are widely distributed in tectonically active regions with volcanism. A pyroclastic flow deposit (i.e., ignimbrite), one of the most common pyroclastics, has been prone to landslides during heavy rainfalls. Shirasu, a typical non-welded and unconsolidated ignimbrite (age 24,500 years before the present), has been subject to shallow landslides on many occasions, resulting in numerous casualties in Kagoshima Prefecture in southern Japan. Ignimbrite that has been consolidated by vapor-phase crystallization, which hereafter will be referred to as vapor-phase-consolidated ignimbrite, when it occurs in the outer zones of welded ignimbrite, is not as easily weathered as Shirasu, and reportedly has not been subject to landslides caused by heavy rainfall. In addition, the weathering profile of vapor-phase-consolidated ignimbrite has not been studied before. However, a rainstorm in August 1998 in northern Japan triggered numerous landslides in a region of vapor-phase consolidated ignimbrite.

1.1 Non-welded ignimbrite

The mechanism underlying rain-induced shallow landslides of non-welded ignimbrite is found to be a special type of weathering profile and the behavior of water infiltrating through that profile, according to our study of Ito ignimbrite in southern Kyushu, Japan. Rhyolitic volcanic glass, the primary component of ignimbrite, is first hydrated and dissolved, forming halloysite. Halloysite near ground surface is then transported through the ignimbrite by infiltrating water and becomes clogged in interstices to form clay bands. Suction monitoring across a weathering profile indicated that downward infiltration of water is disrupted once by a zone of less-permeable clay bands and again at the weathering front. This disruption at the front is caused by a capillary barrier effect caused by the structure where finer, weathered material overlies coarser, fresh material. This results in a well-defined weathering front, particularly beneath a slope where water flux is parallel to the front, whereas the front is transitional beneath a ridge top where the front is nearly horizontal and the water flux is normal to the front. Infiltrating water from rain increases the weight of weathered material and decreases the suction within the material, which is the final trigger of a shallow landslide of non-welded ignimbrite (Fig. 1, [1]); long-term weathering, which proceeds on the order of years, provides slide material.

1.2 Vapor-phase crystallized ignimbrite

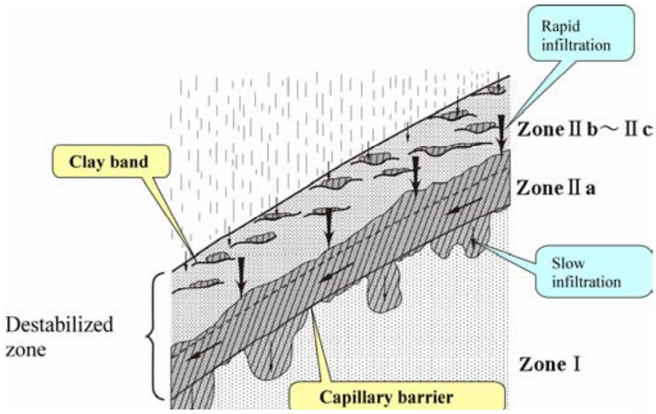

Fig. 1 Schematic sketch of water infiltration and destabilization of a slope.

Ignimbrite, which is consolidated by vapor-phase crystallization, is weathered in humid regions to form a special type of weathering profile that consists of a hydrated zone, an exfoliated zone, and a disintegrated zone from the depth to the ground surface, with each zone having a basal front [2]. The ignimbrite is hydrated first and loses a significant amount of phosphorous at the hydration front. The ignimbrite further loses its alkali and alkali earth components at the top of the hydrated zone by reacting with reactive water from the exfoliated zone, then the leached layers are exfoliated and become part of the exfoliated zone, and then they soften significantly. At the top of the exfoliated zone, rock is disintegrated so completely that rock texture disappears. Water from rainstorms infiltrates down to the exfoliation front, but penetrates only slightly further downward, thus saturating the weathered rock in the exfoliated and disintegrated zones and leading to a landslide with a slip surface within the exfoliated zone.

2. GRANITIC ROCKS

2.1 Micro-sheeted granite and granodiorite

Certain types of granite and granodiorite in mountainous areas are microscopically sheeted to a depth of 50 meters due to unloading under the stress field that reflects slope morphology. Micro-sheets generally strike parallel to major slope surfaces and gently dip downslope, forming cataclinal overdip slopes. The cataclinal overdip slope accelerates creep movement of micro-sheeted granitoid, which in turn loosens and disintegrates granite via the widening or neoformation of cracks, probably in combination with stress release, temperature change, and changes in water content near the ground surface. The surface portion of micro-sheeted granitoid is thus loosened with a well-defined basal front, which finally slides in response to heavy rain (Fig. 2, [3]). Innumerable landslides of this type occurred in Hiroshima Prefecture, western Japan, following the heavy rainstorm of 29 June 1999 as well as in Kannung, Korea by the rainstorm of typhoon Rusa in 2002. Following such landslides, the weathering of micro-sheeted granite exposed on the landslide scar recommences, setting the stage for the next landslide. Micro-sheeted granodiorite is known for the Shibisan granodiorite in Kyushu and for the Kabasan granodiorite in Ibaraki, where many landslides are known to have occurred or inferred from the data obtained by air-born laser scanning technique.

2.1 Granite and granodiorite without micro-sheeting

Some granite and granodiorite are weathered without micro-sheeting, although it is not known what factor is controlling the difference. Weathered granite without micro-sheeting is loosened at slope surface and this loosened layer easily slide during rainstorm, but weathered granodiorite without micro-sheeting is rather cohesive and is not loosened at the surface part resulting in less landslides occurs (Fig. 3, [4]).

REFERENCES

[1] M. Chigira and O. Yokoyama, Weathering profile of non-welded ignimbrite and the water infiltration behavior within it in relation to the generation of shallow landslides. Submitted to *Engineering Geology*.

[2] M. Chigira, M., M. Nakamoto, and E. Nakata, Weathering mechanisms and their effects on the landsliding of ignimbrite subject to vapor-phase crystallization in the Shirakawa pyroclastic flow, northern Japan. *Engineering Geology*, 66, pp. 111-125., 2002.

[3] M. Chigira, Micro-sheeting of granite and its relationship with landsliding specifically after the heavy rainstorm in June 1999, Hiroshima Prefecture, Japan. *Engineering Geology*. 59, pp. 219-231, 2001.

[4] K. Yairi, K. Suwa, Y. Masuoka, Landslides by the rainstorm of July 1972 Obara Village and Fujioka Villate, Nishikamo, Aichi Prefecture. Yano, K. ed. Report of the Grant-in Aid for Scientific Research from the Japanese Ministry of Education, Science, Culture and Sports. pp. 92-103, 1972. (in Japanese)

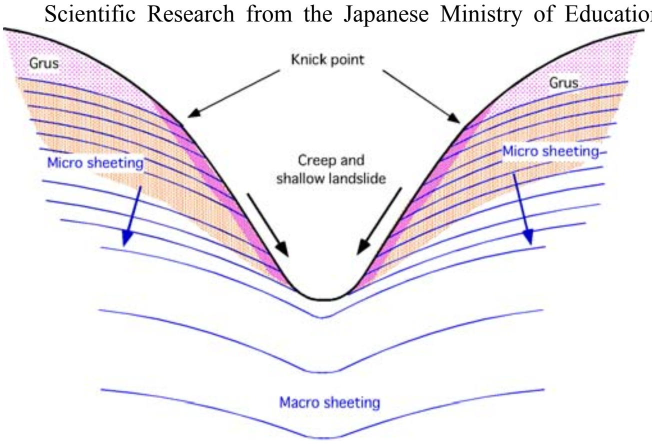

Fig. 2 Schematic sketch showing the development of micro-sheeting and landslide.

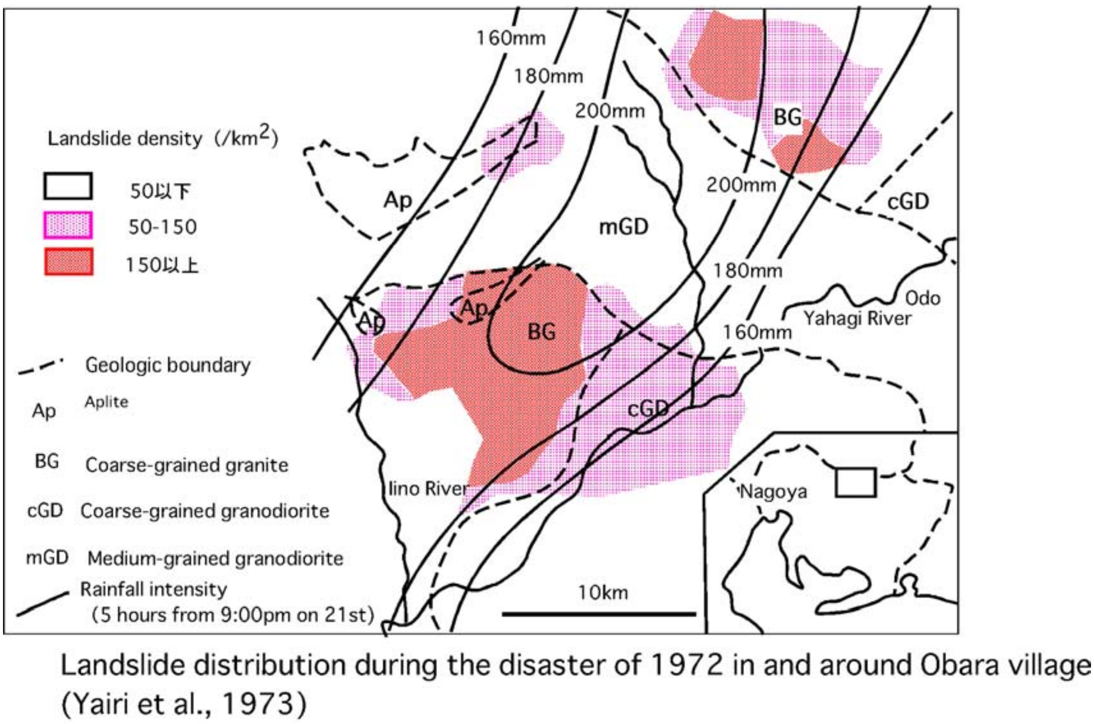

Fig. 3 Landslide distribution during the heavy rain of 1972 Nishimikawa disaster (Yairi, et al., 1972).

Masahiro Chigira
Disaster Prevention Research Institute, Kyoto University
Gokasho, Uji 611-0011 Japan,
email: chigira@slope.dpri.kyoto-u.ac.jp

Multi-scale rock slope failure initiation mechanisms: results from multi-parametric field and modeling studies conducted on the Upper Tinée valley (French Alps) over the past 10 years

*Yves Guglielmi [(1)], Frederic Cappa[(1)], S.Binet[(2)], Florence Bigot-Cormier[(1)], Emmanuel Tric [(1)]

(1) Geosciences Azur Laboratory, CNRS-Nice University, 250 A.Einstein street, 06560 Valbonne, France
(2) Geosciences laboratory, University of Franche-Comté, 16 Gray street, 25003 Besançon, France

ABSTRACT

This paper summarizes part of the results from a multi-parametric study that was conducted for several years on a 70 km long valley located in the Southern French Alps. The valley slopes display several different gravitational features from the valley floor up to the mountain crest. Large landslides (volumes exceeding 5 $10^6 m^3$) with well individualized failure surfaces are located at the slopes foots and pluri-kilometric tensile cracks characterize the slopes tops. A perched saturated-with-water zone located within the cracks is drained towards the slope foot through the landslides. Annual precipitation infiltration induces hydro-mechanical effects up to 400m deep inside the slopes. Those effects mainly participate to the rock strength decrease and the shear plane development with time. Dating of failure surfaces revealed at least 3 main destabilizations of slopes at 11, 7.1 and 2.3 10^3 yr that are not easy to correlate with climatic or tectonic events on the area. This result illustrates the major role played by progressive failure propagation mechanisms during periods between two catastrophic events.

KEYWORDS: Large moving rock mass, hydromechanics, triggering factors, cosmogenic dating, numerical models

INTRODUCTION

Massive natural rock slopes destabilization involves several complex mechanisms relating to geological, mechanical and hydrological processes for which no clear trigger can be asserted [1]. This paper summarizes part of the results from a multi-parametric study that was conducted for several years on a 70 km long valley located in the Southern French Alps. This valley was chosen because it was found representative to study rock slope destabilization under climatic factors and moderate seismic activity.

GEOMORPHOLOGICAL ANALYSES

The Tinée valley is situated at the northwestern edge of the Argentera-Mercantour metamorphic unit (Southern French Alps, Fig. 1A). East side of the valley is made of metamorphic basement with a N150-60°E foliation average trend. Close to the surface of the slope, within a 100 m thick shallow zone, foliation is dipping gently (less than 20°) either to the NE or to the SW [2]. Metamorphic rocks are weathered on a thickness ranging from 50 m to 200 m depending on the zones of the valley. Three sets of faults can be distinguished, trending N010°E-N030°E, N080°E-N090°E and N110°E-N140°E with a dip angles close to 90° (Fig. 1A and B). The valley slopes display several different gravitational features that can roughly be grouped in two main zone types, a tilted zone which is located at the foot of the slope between the elevation of the valley floor and the mid-slope elevation and a sagging zone that is located between the mid-slope elevation and the mountain crest (Fig. 1A). In the tilted zone, metamorphic rocks are strongly toppled and affected by landslides with volumes ranging between 5 and 50 $10^6 m^3$ (about 29 landslides are documented in the valley). This zone contains some currently active large landslides like the "La Clapière" landslide which is located less than 1km downstream from the Saint-Etienne de Tinée village and whose behavior is typical of rock masses movements in the zone (Fig. 1B). The top of the La Clapière landslide is a 120 m high scarp that extends over a width of 800 m at elevation 1600 m. The depth of the failure surface may not exceed 100 m to 200 m (Fig. 1). The landslide itself is divided into three main compartments limited by pre-existing faults. The main central volume is bounded by the main failure surface. It moves downward with 45 to 90 mm.yr-1 velocity and N010°E and N115°E motions. The upper northeastern compartment (5 million m^3 volumes) behaves like a block landslide sliding along its own failure surface and overlapping the main landslide with downward 100 and 380 $mm.yr^{-1}$ motions. The upper northwestern compartment is bounded to the south by the 150 m high scarp of the main landslide failure surface and to the north by a 50 m high scarp. This compartment behaves like a fractured rock mass with active tension cracks and motions ranging between 20 and 70 $mm.yr^{-1}$. It is not certain that this compartment should be included in a failure surface at the present time. The tilted zone is nested in the larger sagging zone which has been active (Fig. 1A and B). This zone is characterized by extensional deformation structures like large tension cracks with a pluri-kilometric length and several meters high downhill scarps. These landforms involve displacements along penetrative preexisting tectonic joints consistent with gravitational movements. Tension cracks correspond to a meter-scale horizontal opening of the superficial part of the faults that induce a 10 to 50 m deep trench. Scarps correspond to shear displacements with a vertical throw ranging from 1 and 50 m. Gravitational features of this zone extend deep inside the slope if we consider their pluri-kilometric extension and they follow major tectonic faults trends rather than the valley slope main direction (Fig. 1B).

HYDRO-MECANICAL PROCESSES WITHIN SLOPES

- Geometrical coupling between hydrogeology and gravitational structures

Slope hydrogeology can be regarded like 3 nested discontinuous fractured reservoirs [3]. Water flows into fractures whose openings depend on the depth and mainly on the gravitational structures of the slope. Rock matrix (gneisses) can be considered as impervious. First zone is the lower tilted zone which is drained through the landslides that can be taken as highly permeable fractured reservoirs where displacements induce the formation of large pores inside opened fractures, breccias and blocks. The landslides are drained at there foot by perennial springs (springs S18, S7, S1 on Fig. 1A) with discharges comprised between 0.95 and 2.35 $l.s^{-1}$. Second zone is the upper sagging zone which is a highly fractured area where tension cracks create highly permeable linear drains. Many of the cracks are filled with colluvial deposits which constitute small reservoirs with an interstitial porosity. These tiny reservoirs are interconnected via the tension crack network. Typically, the filling has a 4 to 20 m wide triangular geometry and, depending on the places, it can be completely dry or it can be drained by perennial springs (springs S3-6, S9-14, S16, S19-20, Fig. 1A). In the first case, water infiltrating in the colluvial deposits is drained deeper in the slope through the underlying tectonic fault. In the second case, water is partially or totally trapped in the filling. The interconnection of the fillings creates a perched perennial saturated zone that could explain the presence of springs rising in the upper part of the slope in the Tinée valley slope and in the adjacent valleys (Fig. 1A and B).

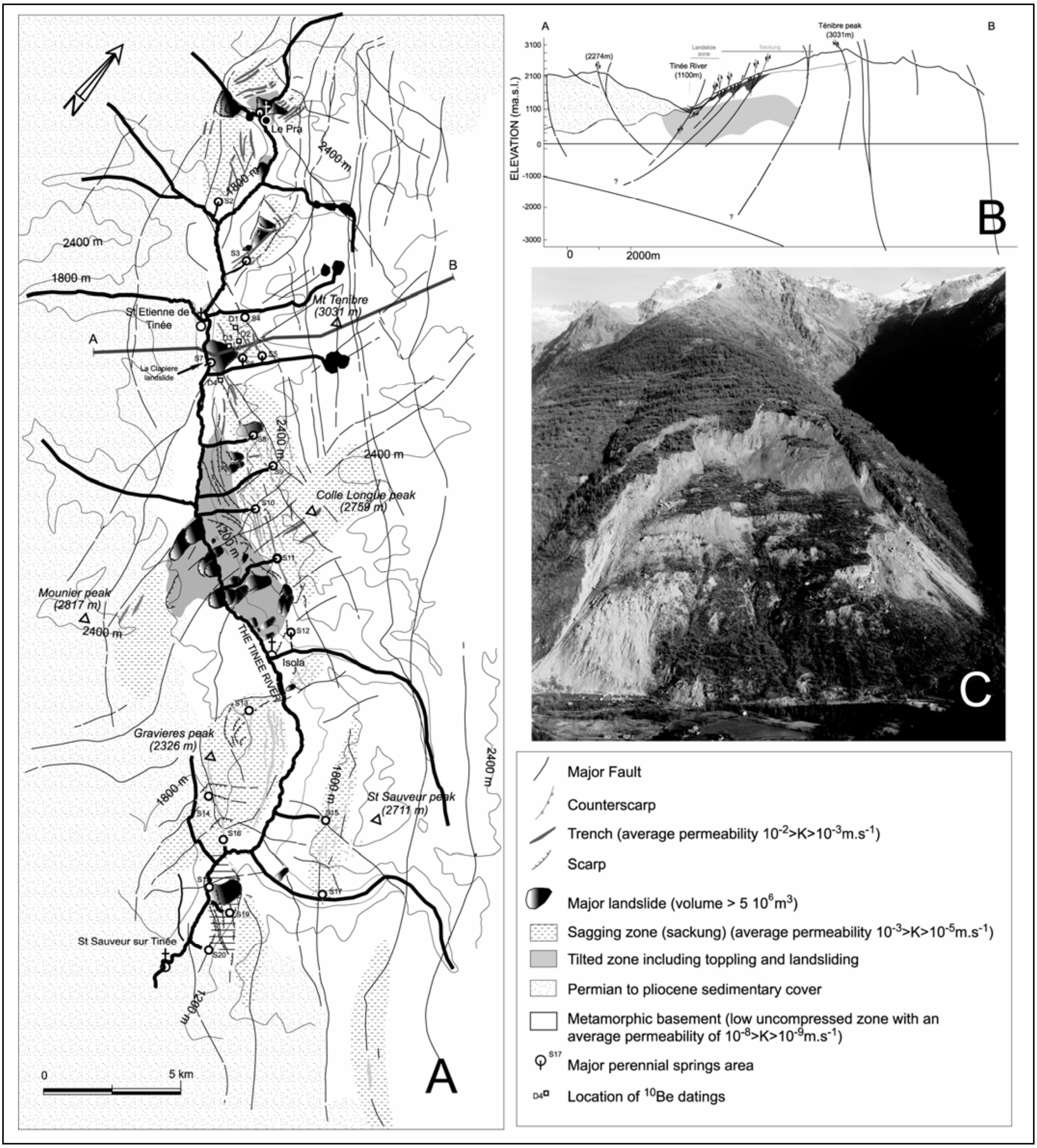

Figure 1. Hydro-geomorphological map (A) and cross section (B) of the Tinée valley; Photo of the La Clapière active landslide (C)

All these springs discharge display large variation depending on their location in the valley but their flow-rates are more important that the tilted zone springs ones ranging between 5 and 10 $l.s^{-1}$. Third zone is the low uncompressed deep part of the slope that was only explored through galleries and deep wells within the area. This zone is fractured by major tectonic joints and can be considered as a relatively low-permeability fissured reservoir (Fig.1B). There is a continuity between the joints and the tensile cracks mapped in the uncompressed toppled zone. Small discharges were measured within fractures located in that zone with flow-rate values less than 0.1 $l.s^{-1}$.

- Temporal coupling between infiltration yields and slope deformations taking the example of the la Clapière slope

In order to characterize long term coupling, we compared historic Tinée river flood (RTM database) to landslide annual velocities (CETE database) since 1920 (Fig. 2A). It appears that the activation of the La Clapière, currently active movement, begins around the years 1950-1955. From 1951 to 1987 there is a constant non linear velocity increase up to a 6 $m.y^{-1}$ peak. After 1987, there is a small decrease of velocities that show annual variations ranging between 4 and 2 $m.y^{-1}$ values. During the 1920-1999 period, there are 7 Tinée major flood events that correspond to major precipitation events that caused numerous damages to the valley landscape.

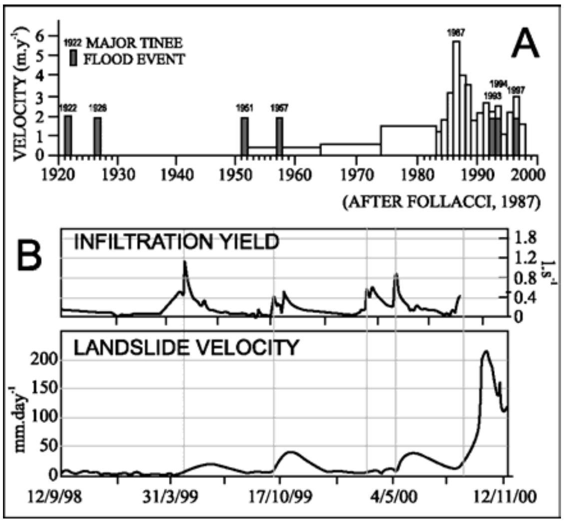

Figure 2. (A) Long-term comparison between La Clapière landslide velocity and Tinée river major flood events (after [4] modified) - (B) Correlation between infiltration and velocity variations at the year scale.

It clearly appears that La Clapière movement activation fits with 1951 and 1957 major floods. It also appears that 1922 and 1926 flood events did not cause any slope destabilization and that 1987 maximum velocity does not correspond with any major flood event. For the 1987 to actual period, speeds fluctuations roughly fit with annual precipitation fluctuations [5]. At the year scale and for recent years (since 1998), a reconstitution of infiltration yields were performed using hydrogeochemistry of springs waters [3]. There are two main infiltration peaks that correlate with long duration moderate precipitation amounts (for ex. 426 mm/30 days during 3/99 period) or with short duration high precipitation amounts (for ex. 122 mm/2 days during 18-22/10/99 period). For a 0.6 km^2 infiltration area, such amounts correspond to precipitation yields respectively ranging between 0.7 and 2.8 $l.s^{-1}$. Landslide velocities curves show accelerations that range between 0.02 and 0.25 $m.day^{-1}$ (Fig. 2B) synchronous to the infiltration peaks periods. Acceleration periods begin when there are spring S5 chemical peaks events and roughly reach a maximum value when there are spring 1 chemical peaks events (Fig. 2B). Accelerations curves have an asymmetric shape with a rapid rise synchronous with the increasing part of the infiltration yield curve (main groundwater flood infiltration) and a slow decrease synchronous to the decreasing and the drying up part of the infiltration yield curve (slope drying up). Duration of acceleration periods is about the same as infiltration periods.

DATING THE EVENTS FROM 10^3 YEARS TO PRESENT USING ^{10}Be AND ^{14}C

A reconstitution attempt of the Tinée valley history from 20 kyr to present was performed by combining various dating methods [6]: ^{10}Be, ^{14}C and geomorphologic approach. A local deglaciation rate of about 0.2 to 0.25 $m.yr^{-1}$ can be estimated. Since the glacier front was at Saint-Sauveur (elevation: 500 m) 20 10^3years ago, this implies that it reached Saint-Etienne de Tinée (elevation: 1100 m) roughly 17 10^3 yr ago. This is consistent with ^{10}Be age of 18970 ± 4543 ^{10}Be-yr obtained at an elevation of 1600m just above Saint-Etienne de Tinée and with a ^{14}C age of 13300 ± 139 yr obtained on a travertine at 1100m in the valley. The main glacier from the Tinée valley disappeared a long time before the lateral ones where deglaciation took place less than 13 10^3 yr ago.

The first destabilization is dated at about 11 10^3 yr. It was sampled at point D4 located at the bottom of a major scarp that bounds a large sagging zone immediately downward the La Clapière landslide (Fig. 1A). This destabilization could be linked to decompression of the slope following this late deglaciation. Since the main scarp dated extends up to the Tinée valley eastern crest, this decompression could be the first destabilization of the whole slope. A second main destabilization phase is dated at about 7.1 kyr. It was sampled at points D1 (6.747 10^3 yr, fig.1A) and D2 (7.257 10^3 yr) located within the middle part of La Clapière slope. This second gravitational event is roughly synchronous to the so called “climatic optimum”, a period of forest cover development on the valley slopes. It could be interpreted as a period of high precipitation rate propitious to landslide triggering as it was recognized in other European areas [7]. Last evidenced destabilization before the historic one occurred 2.3 ± 0.5 ^{10}Be 10^3 yr ago. It was sampled on a scarp that is the lateral continuation of the currently active La Clapière landslide upper scarp. No characterized climatic event is related to this destabilization phase. It could be the consequence of a catastrophic event on a Tinée valley scale or the effect of rock slope strength decreasing as a consequence of a long multi-phase destabilization history.

TOWARDS A HYDRO-GEOMECHANICAL MODEL OF SLOPE FAILURE INITIATION

Numerical methods were used to provide approximate solutions to such complex rock slope stability problems. A huge literature grew, dealing with modeling the effects of all kind of landslide triggering factors. In this study, we focused on two mains processes, slope strength decreasing and fluid hydro-mechanical effects. We considered a vertical cross-section oriented NE-SW perpendicular to the topographic surface and extending from the slope crest (2600 m a.s.l) to the Tinée valley (1100 m a.s.l).

- Modeling of strength decreasing

We have used a two-dimensional finite-element code (ADELI, [8]) using a Lagrangian description of the geological medium [9]. The model use quadrilateral elements of constant strain, while using an adaptative remeshing method [10] to accurately follow strain localization phenomena. Material behaves as strain-softening or strain-hardening elastic plastic materials according to the Drucker Prager law. The strain-softening/hardening parameter depends both on the internal friction angle and on the dilatancy angle. The reference parameters values were taken from field measurements [11] and from laboratory tests: Young’s Modulus, E = 6.4 MPa, cohesion, c = 210 kPa, angle of internal friction, ϕ = 29°, Poisson’s ratio, v = 0.3 and density, ρ =2400 kg/m^3. From the five parameters given previously, two have been tested systematically: the cohesion

(c) and the friction angle (ϕ) in order to model the strength degradation of the slope.
All the converged static solutions display three plastic deformation zones. The first zone which is 200m thick extends from the slope foot up to 1400 meters elevations. The second zone extends from 1400 m to 1800 m elevations and it is about 100 m thick. The third zone is at the top of the slope (Fig. 3A). When the couple (c, ϕ) is lowered, the divergence of the numerical experiment result in a strong plastic deformation initiated at the foot of the slope. Then, this plastic deformation leads to the destabilisation of the massif by a regressive evolution of the plastic zone towards the top of the slope. This deformation propagates up to 1800 m, which is currently the top of the currently active “La Clapière” landslide. This deformation concerns only a depth of around 100 – 200 m.

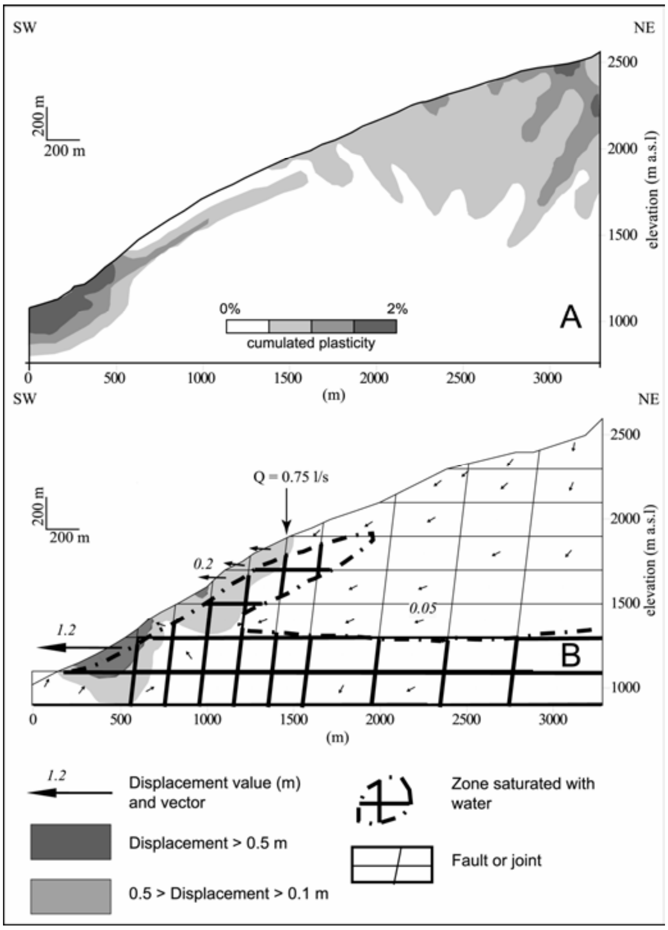

Figure 3. (A) Strength decrease model with ADELI - (B) Coupled hydro-mechanical modelling with UDEC

- Modeling hydro-mechanical processes

We performed parametric simulations with UDEC code in order to estimate water infiltration influence during the initial 1951-1987 behavior of the slope and during the actual post 1987 seasonal behavior of the slope. In the test shown in Fig. 3B, only preexisting fractures were taken into account. UDEC code allows large finite displacements/deformations of a fractured rock mass under pressure loading [9]. We considered the same vertical cross-section as the one modeled previously with ADELI code where 9 discrete penetrative vertical fractures represent the major faults mapped on the site were added. So as to hydraulically connect faults between them and to approximate foliation planes geometry, horizontal joints were included in the model. We used the same mechanical boundary conditions and matrix mechanical parameters that for the ADELI model. Impervious hydraulic boundary conditions were set. Rock matrix mechanical behavior is taken as linearly elastic and isotropic. Faults are assumed to behave according to an elasto-plastic law with the Mohr-Coulomb failure criterion. Fault hydraulical parameters were deduced from field measurements [11].

A perched saturated zone is simulated affecting a local zero permeability at faults segments corresponding to the basal boundary of this zone (dashed line between 1500 m and 2000 m elevation - Fig. 3B). Flow in the faults was set to be compressible. Gravity acceleration was applied. We performed a static hydromechanical calculation with steady-state flow. The cross-section is first consolidated to gravity until stress and displacements are numerically stabilized. Then, initial groundwater conditions were simulated in the basal saturated zone. No interstitial pressure was set in the perched saturated zone. A 0.75 l.s-1 effective infiltration is simulated in the slope at 1900 m elevation (Fig. 3B). On the cross-section, we plot maximum displacements induced by the hydraulic loading.
Pressures increase from 0 to 1 MPa in the perched aquifer. In the basal aquifer, a 0.5 MPa piezometric bump extends from 300 to 1500 m along the x-axis. The maximum calculated values of displacement vector are located between the foot of the slope at 1100 m and the middle part of the slope at 1900 m. This strain zone extends from 50 m to 400 m inside the slope. Displacements values vary between 0.1 m and 1.3 m in that zone. Water pressures are situated in two distinct zones which hydraulically communicate with each other: a basal 500 m thick saturated zone with interstitial pressures ranging between 0 MPa and 5 MPa, and a perched 200 m thick saturated zone with interstitial pressure ranging between 0 MPa and 2 MPa. In the middle part of the slope there is swelling with vectors’ dip towards the top linked with mechanical opening of fractures under pressure elevation in the perched saturated zone. In the upper part of the slope there is a lowering (sackung) with vertical vectors’dip.

CONCLUSION

The Tinée valley current landslides are “only” one more reactivation of larger and older slope movements. The oldest known movements correspond to large scale sagging of the upper part of the slope up to the mountain crest. Such movements could be linked to the last deglaciation event where the controlling mechanism involves the release of strain energy leading to the generation and reactivation of tensile extensional features [1]. Nevertheless, such rebound effect can induce deep seated gravitational deformations in the case of a high magnitude glacial retreat like it was measured in the northern French Alps [12] or in Canada for example (Kinakin et al., 2004). This was not the case of the Tinée valley which was located at the southern boundary of the ice front. Thus, some tectonic effects like the high-deformation rate at the Mediterranean margin located 50 km southwards of the valley [13] can also be taken into consideration.
Following destabilizations are obviously influenced by this first event which strongly modified rock slope strength and hydrogeology. Destabilized volumes are smaller and are located towards the foot of the slope. They can be linked to strength decrease of the rock slope and one predominant mechanism is then hydro-mechanical effects of water flow within fractures. We show in this study that tensile features are filled with local material of the slope and that they constitute perched reservoirs at the boundaries of the toppled rock columns. Hydrostatic pressures are concentrated in the middle and upper parts of the slope where a relatively low infiltration yield (mean inter-annual value for example) can cause sufficient hydrostatic pressures elevation in the cracks to increase rock columns destabilization. Tilting at the column surface and failure propagation deep in the slope can be generated roughly from the theoretical bottom of the perched aquifer down to the slope foot. At La Clapière such a failure through tilt could have worked until 1987 when it is taken [5, 14] that a general failure surface was

created. When a major failure surface is generated, a large mass slides downslope. The slope drainage becomes more active through this failure surface and there is a general lowering of the hydrostatic pressures in the slope. The perched aquifers is partly drained by the landslide and, at the reverse, waters coming from this aquifer impose pressures elevations in the landslide failure surface upper segments which are closer to failure than lower parts (where stress state is high and segment dip is low or 0). In regions with moderate seismicity, such typical rock slope gravitational structures [15, 16] can then be activated in a few tens of years under precipitations induced periodic hydromechanical effects.

ACKNOWLEDGMENT

This work was funded by the French Ministry of Education and Research within the frame of PNRN2002-2003 and ACI CATNAT SAMOA scientific programs.

REFERENCES

[1] E. Eberhart, D. Stead, J.S. Coggan, Numerical analysis of initiation and progressive failure in natural rock slopes – the 1991 Randa rockslide, *International Journal of Rock Mechanics and Mining Sciences*, 41, pp. 69-87, 2004.

[2] Y. Gunzburger, B. Laumonier, Origine tectonique du pli supportant le glissement de terrain de la Clapière (Nord-Ouest du massif de l'Argentera-Mercantour, Alpes du Sud, France) d'après l'analyse de la fracturation, *Comptes Rendus Géosciences*, 334, 6, pp. 415-422, 2002.

[3] F. Cappa, Y. Guglielmi, V. Merrien-Soukatchoff, J. Mudry, C. Bertrand, A. Charmoille, Hydrochemical modeling of a large moving rock slope interred from slope levelling coupled to spring long-term hydrochemical monitoring : example of the La Clapière landslide (Southern Alps, France), *Journal of Hydrology*, 291, pp. 67-90, 2004.

[4] J.P Follacci, Les mouvements du versant de La Clapière à Saint-Etienne-de-Tinée (Alpes-Maritimes), *Bulletin des laboratoires des ponts et Chaussées*, 220, 150/151, pp. 107-109, 1987.

[5] J.P. Follacci, " Seize ans de surveillance du glissement de La Clapière (Alpes Maritimes). ", *Bulletin de Liaisin des Lab. Des ponts et Ch.*, 220, 35-51, 1999.

[6] F. Bigot-Cormier, R. Braucher, Y. Guglielmi, D.L. Bourlès, M. Dubar, J.F Stéphan, Chronological constraints of la Clapiere landslide (44°15N, 6°56E, France): Geomorphology and cosmonuclide approaches. *Earth and planetary science letters*, submitted.

[7] W. Margielewski, J. Urban, Crevice-type caves as initial forms of rock landslide development, *Geomorphology*, 54, pp. 325-338, 2003.

[8] R. Hassani, D. Jongmans and J. Chéry, " Study of plate deformation and stress in subduction processes using two-dimensional numerical models ". *J. G. R.*, 102, 17,951-17,965, 1997.

[9] P.A. Cundall, A Generalized Distinct Element Program for Modelling Jointed Rock, Peter Cundall Associates, US Army, European Research office, *London Report PCAR-1-80*, 1980.

[10] R. Hassani, Modélisation numérique de la deformation des systèmes géologiques, *Ph.D. thesis*, University of Montpellier II.

[11] Y. Gunzburger, Apports de l'analyse de la fracturation et de la modélisation numérique à l'étude du versant instable de la Clapière (Saint-Etienne-De-Tinée, Alpes-Maritimes), Diplôme d'Etudes Approfondies, DEAPAE3S Nancy (2001), 82 pages.

[12] J.M. Vengeon, Déformation et rupture des versants en terrain métamorphique anisotrope. *PhD Thesis*, University Joseph Fourier – Grenoble 1, 1998, 186 p.

[13] F. Bigot-Cormier, F. Sage, M. Sosson, J. Deverchère, M. Ferrandini, P. Guennoc, M. Popoff and J.F. Stephan, Déformations pliocènes de la marge nord-Ligure (France): les conséquences d'un chevauchement crustal sub-alpin, *Bull. Soc. Géol. Fr*, t. 175, n°2, pp.197-211, 2004.

[14] C. Vibert, Apport de l'auscultation de versants instables à l'analyse de leur comportement, les glissements de Lax-le-Roustit (Aveyron) et Saint-Etienne-de-Tinée, France, *PhD Thesis*, Ecole des Mines de Paris, 1987.

[15] F. Agliardi, G. Crosta, A. Zanchi, Structural constraints on deep-seated slope deformation kinematics, *Engineering Geology*, 59 (2001) 83-102.

[16] M.J. Bovis and S.G. Evans, Extensive deformations of rock slopes in southern Coast Mountains, southwest British Columbia, Canada, *Engineering Geology*, 44 (1996) 163-182.

Yves Guglielmi
Geosciences Azur, CNRS-UNSA, 250 A.Einstein street, 06560 Valbonne, Email: guglielmi@geoazur.unice.fr

Monitoring of debris flow event at the Ohya collapse in the upper reach of the Abe River, Japan

*Satoshi Tsuchiya [(1)] and Fumitoshi Imaizumi [(2)]

(1) Faculty of Agriculture, Shizuoka University, (2) Disaster Prevention Research Institute, Kyoto University

ABSTRACT

The knowledge of debris-flow initiation and development is important for the improvement of warning systems and structural measures. However, only few observations have been made in initiation areas of debris flows. We aim to consider and discuss the behaviors of debris flow in the initiation area based on the observed data. A monitoring system composed of video cameras, ultrasonic sensors and water pressure sensors installed in the Ichinosawa catchment of the Ohya collapse in the upper reach of Abe River, Shizuoka prefecture in Japan.

As a result of observations, video image analysis suggests that the flows appearing in the main flow phase can be classified into two types: flows which consists mainly of muddy water, and flows which consists mainly of cobbles and boulders. The comparison of data obtained by ultrasonic sensors and water pressure sensors show that the former flow has abundant interstitial water throughout all its layers, whereas the latter flow has unsaturated layer in its upper part. The concentration of solids in debris flows differs from flow to flow, causing both erosion and deposition, and also presents changes in their concentration of solids.

KEYWORDS: Debris flow, Ohya collapse, flow behavior, monitoring, initiation area

1. INTRODUCTION

Debris flows in mountainous catchment cause severe natural hazards. The knowledge of debris-flow initiation and development is important for the improvement of warning systems and structural measures. However, only few observations (Takahashi, 1991) have been made in initiation areas. Many detailed field observations of debris flows have been carried out in many countries of the world, e.g., Japan (Suwa et al., 2000; Ikeda and Hara 2003), and Italy (Arattano, 1999). In many cases, the channel slopes in the initiation areas of debris flows are over than 25 degrees (Pareschi 2002).

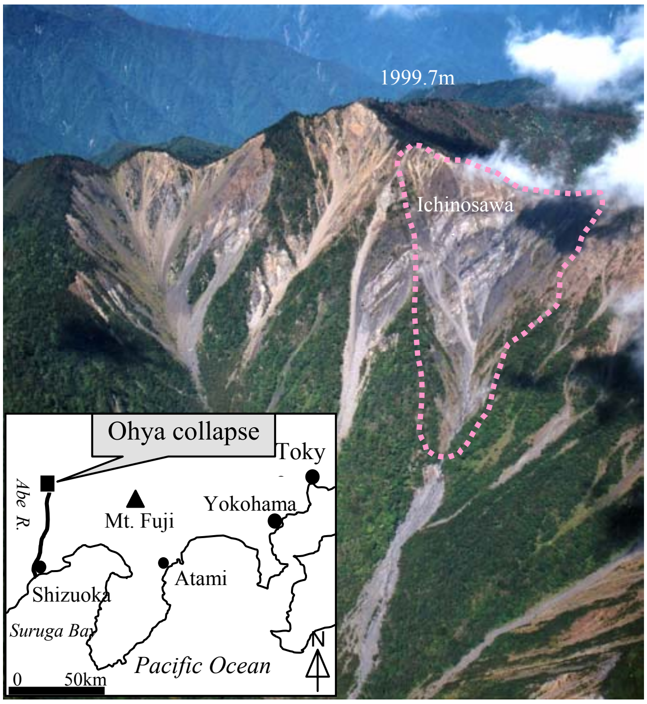

Figure 1. Location of the Ohya collapse and view of the Ichinosawa catchment.

Figure 2. View of accumulated deposits and the observation site on the Ichinosawa catchment in the Ohya collapse

Watanabe (1994), based on experimental data, suggested that debris flows with an unsaturated layer in their upper part should occur in steep channels ranging from 17 degrees to 29 degrees. There is a grate possibility that debris flows, for example the unsaturated flow suggested by Watanabe (1994), may occur in the initiation area. Therefore, field-monitoring data of debris flow in the initiation area is really important.

The aim of this paper is to consider and present a behavior of debris flow in an initiation area. We present the field settings and monitoring data of the debris flows occurred in the Ichinosawa catchment of the Ohya collapse, Shizuoka prefecture in Japan, and discuss the behaviors of debris flow in the initiation area based on the observed data. The debris flows observed in the Ichinosawa catchment have both high concentrations of solids and high discharge variations, and there is a possibility that these flows are different from the mature debris flows that are commonly observed in the transit area. This paper treats such developing flows as debris flow.

2. STUDY SITE

2.1 Outline of Ichinosawa catchment

The study site, as shown in **Figure 1** is the Ichinosawa catchment located on the Ohya collapse at the source of the Abe River in Shizuoka prefecture, Japan. The Ohya collapse is one of Japan's gigantic one (Tsuchiya, et. al., 1996) with a total debris volume of approximately 120 million m^3. The total length of the main channel is approximately 650 m and the watershed, south facing, has an area of 0.22 km^2. Most of the slope in the site is covered by outcropping rocks, occupying 70% of the channel area; whereas vegetation-covered areas (forest, shrubs and tussock) are occupy 30%.

Satoshi Tsuchiya
Faculty of Agriculture, Shizuoka University,
836 Ohya, Shizuoka-shi, 422-8529 JAPAN,
Email: afstuti@agr.shizuoka.ac.jp

The bedrock geology of the study area is the old Tertiary strata represented by highly fractured shale and alternation of strata composed of sandstone and shale. The shale is characterized by its highly shattered state and provides a large amount of silty material, whereas the sandstone is well jointed and provides many boulders.

2.2 Debris deposits on channel bed

Unconsolidated debris material, sand to boulder sized, has accumulated on the channel bed, and many talus slopes are generated on the foot of the slope as shown in **Figure 2**. Large boulders with an intermediate diameter of 2 to 3 meters are also common in the debris deposits in the channel. The thickness of debris deposits reaches several meters in some sections. The production of material from the bare steep slope and its transportation by debris flow change the distribution of the debris deposit area. The typical channel gradients of the debris deposit area are from 28 to 37 degrees, and are from 36 to 38.5 degrees for talus slopes.

2. MONITORING SYSTEM

The monitoring system was installed in the early spring of 1998 and includes video cameras, water pressure sensors, and a rain gauge (Imaizumi et. al., 2003). Other observation instruments, i.e., ultrasonic sensors and a capacitive water depth probe, were installed after 1999. The locations of the monitoring system set up in the catchment are shown in **Figure 1** and **Figure 2**.

2.1 Video cameras

The interval-shooting camera captures images for 0.75 seconds at an interval of 3 minutes in April 2001, before that 5 minutes, and the continuous shooting video camera captures images non-stop (**Figure 3**). It is triggered by the cutting of the wire sensor installed at cross section of the channel. The video camera captured a debris-flow event that occurred on 12 July 2003.

2.2 Ultrasonic sensor, water pressure sensor and rain gauges

The ultrasonic sensor having a measuring range of from 120 to 600 cm with an accuracy of 0.4% was set up for measuring the level of the debris-flow surface and making a debris flow hydrograph (**Figure 3**). The water pressure sensors, semiconductor type pressure sensors, rating the pressure range of 49kPa with an accuracy of 3% were set up to measure hydrostatic pressure on the channel bed. The sensors were installed in holes dug in the bedrock of the channel and were fixed by mortar in addition to being covered by cobbles to prevent the affect of hydrodynamic pressure. The ultrasonic sensor and water pressure sensor were set up at the same cross section as shown in **Figure 4**, and the logging interval was set for 1 minute. A rain gauge, a tipping bucket-type rain gauge with 0.5 mm per tipping, was installed at the observation site in order to obtain precise rainfall data regarding the upper Ichinosawa catchment. It records rainfall every 1 minute.

3. MONITORING DATA

Depend on the recorded video images, Several sequences of debris-flow surges occur in a series of rainfall-event and the normal stream flows, which have no muddiness according to the video image and show no abrupt increases in flow depth, appear between each sequence of surges. The typical debris flow in the upper Ichinosawa catchment consists of three phases: precedent flow, main flow, and subsequent flow. The precedent flow, which is confirmed as a black flow by the video image because of a high concentration of silty shale, appears before the arrival of surges, and an intense increase in water depth cannot be found during this phase.

3.1 Types of flow

Flows that appear in main flow phase can be classified into two types: flows which consist mainly of muddy water (Type-1, hereafter) and flows which consist mainly of cobles and boulders (Type-2, hereafter). A large proportion of the main flows belong to the Type-1, which is characterized by its black surface due to a high concentration of silty shale.

A video image of the Type-1 flow is presented in **Figure 5(a)** and its schematic diagram is presented in **Figure 5(b)**. Cobbles and

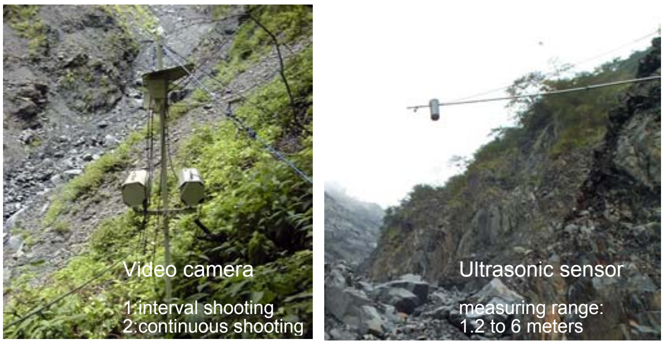

Figure 3. Video cameras (left) and ultrasonic sensor (right)

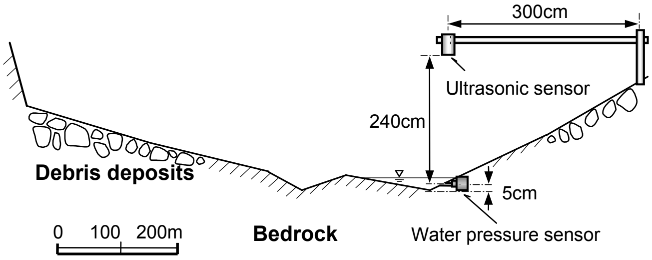

Figure 4. Cross sectional profile of observation site (7 August 2000)

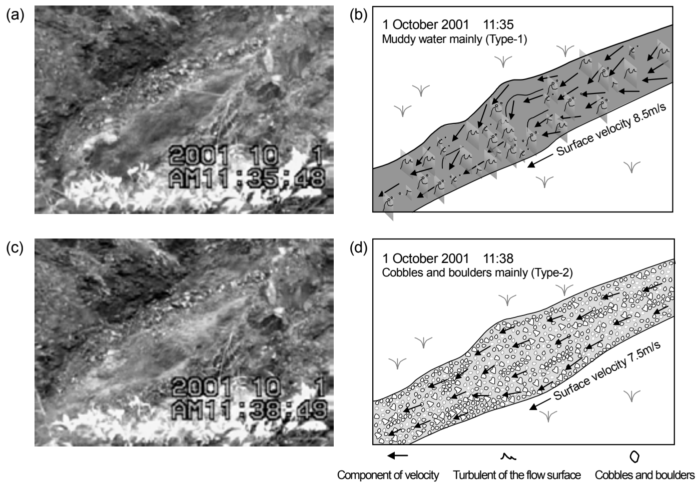

Figure 5. Video images and schematic diagrams of flow types.
Flow consists mainly of muddy water
(a) Video image, (b) Schematic diagrams
Flow consists mainly of cobbles and boulders
(c) Video image, (d) Schematic diagrams

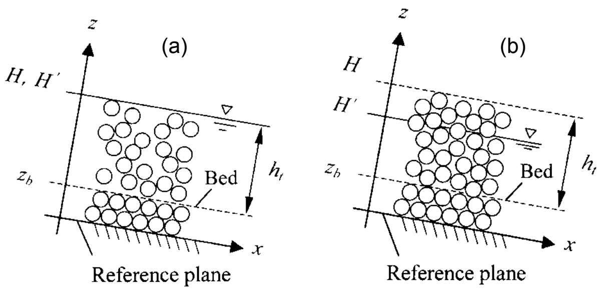

Figure 6. Schematic diagrams of longitudinal distributions of debris flow
(a) Internal water height is the same as debris flow surface
(b) Internal water height is lower than debris flow surface

boulders are occasionally present on the surface, and video images show the flow as turbulence. A Video image of the Type-2 flow is presented in **Figure 5(c)** and its schematic diagram is presented in the **Figure 5(d)**. The Type-2 flow is predominantly composed of cobbles and boulders, and muddy water is hardly present in the matrix of flow surface.

The interior structure of the Type-2 flow may be illustrated (Miyamoto, 2002) as seen in **Figure 6(b)** because of the lack of interstitial water on its flow surface, whereas the Type-1 flow can be illustrated as seen in **Figure 6(a)** because of the abundance of interstitial water on its flow surface. The velocity of the Type-2 flow is slower than that of the Type-1 flow, their flow depth being equal. Video image analysis suggests that the Type-2 flow is characterized by laminar flow, and rotary motion of particles is not seen.

3.2 Interior structure of flows

The monitoring data measured by ultrasonic sensor and water pressure sensor, which were installed in the same cross section, have allowed the analysis of the interior structure of the debris flow. **Figure 7** indicates the debris-flow events that occurred on 7 August 2000; flow depth was measured by ultrasonic sensor and water level by water pressure sensor.

Analysis of the video image shows that a little surface runoff appeared in the channel before the appearance of debris flow as illustrated by term A in **Figure 7**, then Type-2 flow appeared at 14:55 causing rapid increase in discharge. Several surges, which can be classified mainly as the Type-2, caused rapid and violent variation in discharge, and this continued for 20 minutes as illustrated by term B.

The typical Type-1 flow, which has a high concentration of silty shale, was confirmed at 15:15, and continued flowing for about thirty-five minutes as illustrated by term C as far as the analysis of the video image at a 5-minutes interval. However, there is a possibility that short-time Type-2 flow appeared during the term C. After the term C, the discharge began to decrease and muddiness disappeared gradually during as term D shown in **Figure 7**.

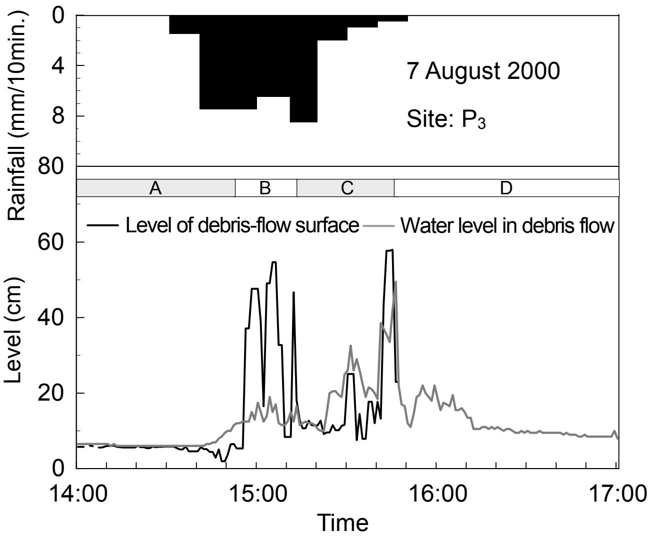

Figure 7. Changes in the level of debris-flow surface and the water level in debris flow

Term A: the phase before the main flow.

Term B: the phase in which Type-2 flow was predominant.

Term C: the phase in which Type-1 flow was predominant.

Term D: absence of the data of the ultrasonic sensor

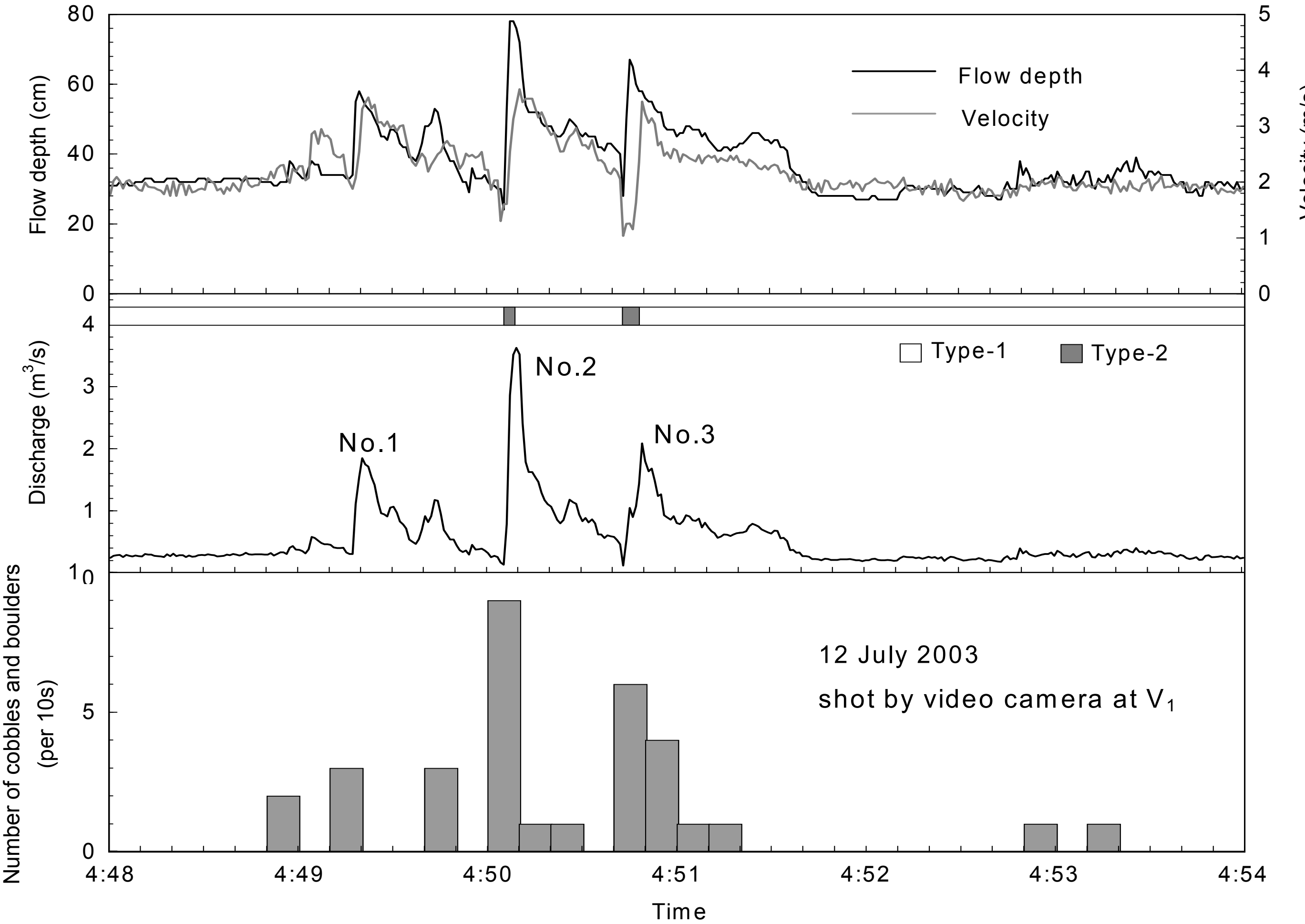

Figure 8. Flow depth, velocity, discharge, and number of cobbles and boulders (>15cm) in debris flow, which occurred on 12 July 2003, obtained by video image analysis.

Turing term B, changes in water level occurred within a narrower range from 11.5cm to 17.5cm in comparison with the level of the debris-flow surface, which exhibited violent and abrupt changes ranging from 12.5cm to 55cm. The discrepancy in the level of the debris-flow surface and the water level suggests that the flow during term B has unsaturated layer in its upper part, such as that seen in **Figure 6(b)**. In contrast, changes in water level corresponded to that of debris-flow surface during term C, suggesting that the flow in this case has abundant interstitial water throughout all of its layers, such as seen in **Figure 6(a)**.

3.3 Debris flow on 12 July 2003

The continuous video image recorded on 12 July 2003 allowed analysis of the alteration of flow type, Type-1 and Type-2, during the debris-flow event. Flow depth, flow velocity, and discharge obtained by analysis of the video image are illustrated in **Figure 8**. The video image analysis allows obtaining surface velocity; the mean velocity illustrated in **Figure 8** was estimated by multiplying surface velocity by 0.6, applying the constitutive equation of movable beds suggested by Takahashi (1977). The discharge was calculated by multiplying the cross sectional area of the debris flow by mean velocity. **Figure 8** illustrates the event consisting of three main surges, No.1, No.2, and No.3, and several other secondary small surges.

The surge No.1 had no Type-2 phase, and several cobbles and boulders transported by highly concentrated muddy water are found in the front of the surge. On the other hand, surges No.2 and No.3 have Type-2 phases at their fronts correspond to the description of debris flow that was observed in the initiation area (Berti, 1999), such as accumulation of cobbles and boulders in its front that can be described as the Type-2, and followed by the turbulent flow that is described as Type-1. The accumulation of cobbles and boulders are also typical characteristics in the transit and deposition area (Suwa, 1988). The number of cobbles and boulders, whose diameters were over 15 cm, is illustrated in the lower section of **Figure 8**. Although surge No.3 has a lower discharge in comparison with that of surge No.2, it had a long duration in the manner of the Type-2 flow and transported many cobbles and boulders.

3.4 Flow depth and velocity

Comparison of flow depth and velocity is illustrated in **Figure 9**, using data presented in upper section of **Figure 8**. The distributions of the Type-1 plots are around an approximate curve whose equation is presented in **Figure 9**. The power of the curve is given as 0.714, indicating that the velocity of the Type-1 flow nearly equal Manning's equation whose power is 2/3. The velocity of the Type-2 flow is lower in comparison with that of the Type-1, and it has scattered distributions whose R^2 is calculated as 0.234. In the front of surge No.3, the video image shows that the Type-1 flow passes over the Type-2 flow due to higher velocity.

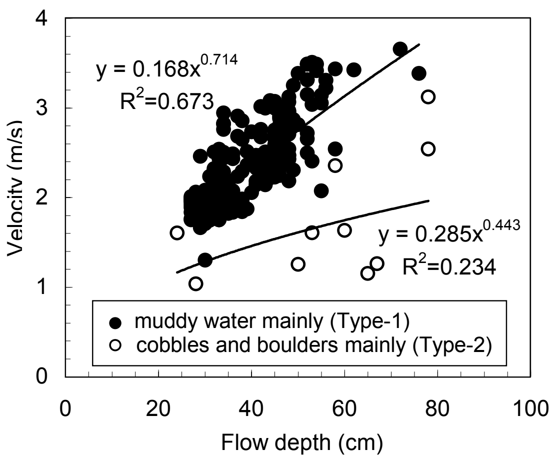

Figure 9. Comparison of flow depth and velocity, debris flow on 12 July 2003.

4. CONCLUSIONS

As a result of observation in the upper Ichinosawa catchment, debris-flow behavior in the initiation area are presented, and following conclusions are drawn. (1) Video image analysis suggests that the flows appearing in the main flow phase can be classified into two types: the flow which consists mainly of muddy water, and the flow which consists mainly of cobbles and boulders. The former flow has abundant interstitial water throughout its all layers, whereas latter flow has an upper layer where continuous interstitial water is absent. (2) Video image analysis provides only surficial information. However, comparison of the ultrasonic sensor data and the water pressure sensor data provides information regarding interior structure. This can be useful for estimating the interior structure of debris flows.

REFERENCES

[1] Arattano, M., On the use of seismic detectors as monitoring and warning system for debris flows. Natural Hazards, 20, pp.197-213.

[2] Berti, M., Genevois, R., Simoni, A., Tecca, P. R., Field observations of a debris flow event in the Dolomites, Geomorphology, 29,pp. 265-274, 1999.

[3] Ikeda, A., Hara, Y., Flow properties of debris flows on the Kitamata Valley of the Name River, Japan. Proceedings of Debris-flow Hazard Mitigation, vol.2, pp. 851-862, 2003.

[4] Imaizumi, F., Tsuchiya, S., Ohsaka, O., Observation of the formation and dynamic process of debris flows in a mountainous debris torrent. Journal of the Japan Society of Erosion Control Engineering, 55(3), pp.50-55, 2002. (in Japanese with English abstract)

[5] Miyamoto, K., Two dimensional numerical simulation of landslide mass movement, Journal of the Japan Society of Erosion Control Engineering, 55(2), pp.5-13, 2002. (in Japanese with English abstract).

[6] Pareschi, M.T., Santacroce, R., Sulpizio, R., Zanchetta, G., Volcaniclastic debris flows in the Clanio Vally (Campania, Italy) insights for the assessment of hazard potential, Geomorphology, 43, pp.219-231, 2002.

[7] Suwa, H., Focusing mechanism of large boulders to a debris-flow front, Transactions, Japanese Geomorphological Union, 9(3), pp.151-177, 1988.

[8] Takahashi, T., A mechanism of occurrence of mud-debris flows and their characteristics in motion, Annuals Disaster Prevention Research Institute, Kyoto Univ., 20(B-2), pp.405-435, 1977. (in Japanese with English abstract).

[9] Takahashi, T., Debris flow, IAHR Monograph. A.A. Balkema, Rotterdam, 165 pp., 1991.

[10] Tsuchiya, S., Kimura, M., Ohsaka, O., Tarumi, M. 1996. Debris transport on the steep gully of the mountainous large-scale Ohya collapse, Shizuoka prefecture, Japan. Proceedings of INTERPRAEVENT 1996, Bd. 1, pp. 273-281.

[11] Watanabe, S., Influence of the mixing ratio of water to sediment on the threshold slope of debris flow: a laboratory experiment. Transactions, Japanese Geomorphological Union, 15(4), pp.349-369, 1994. (in Japanese with English abstract).

Long-term behavior and assessment of the hazard associated to slow-moving clay-rich earthflows

Malet Jean-Philippe [1, 2],* and Maquaire Olivier [1,3]

(1) School and Observatory of Earth Science, Institute of Global Physics, Strasbourg, (2) Faculty of Geoscience, University of Utrecht, (3) LETG-Geophen, University of Caen-Basse Normandie.

ABSTRACT

Clayey flow-like landslides are characterized by their capability to suddenly change behaviour; from slow-moving slides to fast-moving flows. Fundamental points to assess the hazard associated to these specific type of landslide are to understand the physical processes controlling their short- and long-term behaviour, and develop a methodology to correctly delineate the area exposed to debris flow downstream. In this paper, research carried out on the Super-Sauze earthflow, one of the persistently active clayey landslide in the South French Alps, since 10 years, are synthesized.

KEYWORDS: slow-moving landslide, earthflow, hydrology, physically-based modelling, runout modelling, clay-shale

1. INTRODUCTION

Landslides on clay-shale slopes of the French South Alps are, in most cases, complex catastrophic failures in which the initial structural slides transform into slow moving earthflows (0.01 to 0.40 m.day^{-1}). For specific hydrogeological conditions, these earthflows can transform into muddy debris flows characterized by high velocities (1 m.s^{-1} to 15 m.s^{-1}) and runout distances. Due to their sediment volume and their high mobility, debris flow induced by landslides are far much dangerous than these resulting from continuous erosive processes. A fundamental point to correctly delineate the area exposed to debris flows on the alluvial fans is therefore to understand why and how some earthflows transform into debris flow while most of them experiences a significant creep behaviour [1], then decelerates and finally stop flowing after achieving a new hydro-mechanical equilibrium.

In the "Terres Noires" region, between Nice at the South, and Grenoble at the North, several large clayey earthflows have initiated more or less mobile mudflows or muddy debris-flows in the recent years [2], with volumes ranging from 5,000 m^3 to over than 60,000 m^3 [3]. These landslides offer an unique chance to understand, at the field scale, the triggering mechanism of debris flow in cohesive material and to develop hazard assessment methodologies [4].

To define the short- and long-term behaviour of these earthflows, an approach combining geomorphology, hydrology, geotechnics geophysics, and rheology is adopted to model the landslide hydrology (prefailure stage), the debris flow initiation (failure stage) and its runout (postfailure stage). In this paper, the objective are to characterize the hydrological and mechanical conditions leading to debris flow initiation in such cohesive material, and to simulate hazard scenarios. A full description of the work carried out on this topic is detailed in several references [5, 6, 7, 8].

2. FIELD SETTING AND DATA COLLECTION

2.1 Earthflows in clay-shale of Southeast France

Deep-seated earthflows are the most typical landslides involving weathered clay-shale in the French South Alps [9]. Their movements may result from sliding and flowing, either singly or in combination. Such multiple-mode slope movements exhibit a rapid or slower intermittent movement influenced by slope morphology, rock mass fabric, and hydrology [10].

In the Barcelonette Basin, about 100 km north of Nice, three large earthflows (*Poche*, *Super-Sauze* and *La Valette*) have occurred and are still very active. The horizontal length of the earthflows reaches 1100 m at *Poche*, 820 m at *Super-Sauze*, and 1800 m at *La Valette*. The accumulation zone presents an average slope of 20° for *Poche*, 25° for *Super-Sauze*, and 28° for *La Valette*. The total volume is estimated at 700,000 to 900,000 m^3 for Poche, 750,000 m^3 for Super-Sauze and over 3,500,000 m^3 for *La Valette*. Over the period 1992-2002, the displacements reached 130 m for *Poche*, 145 m for *La Valette*, and 160 m for *Super-Sauze*. It is worth noting that the maximal annual displacements are reached for the wettest years of this period, showing the hydro-climatic control of these landslides.

Among these earthflows, the *Super-Sauze* earthflow is surveyed by the *School and Observatory of Earth Sciences, Institute of Global Physics (Strasbourg, France)* since 1991. It affects a 75 ha area of badlands cut in clay-shale. The earthflow has a characteristic morphology of blocks of marls that fail the main scarp (2105 m) by plane ruptures, accumulate, progressively deform and result in a heterogeneous flow-like tongue (Fig. 1a). Uphill, the main scarp, inclined at approximately 70°, cuts into moraine deposits and subjacent *in-situ* black marls steep slopes about 100 m high. Immediately below the main scarp, the so-called 'upper-shelf' appears as a block field, with black marls panels and dihedrons more or less buried in a very heterogeneous formation. The reworked material then transforms into a flow over a distance of almost 500 m. The intermediate slopes on this section range up 20 to 25°. The toe of the moving mass is presently at an altitude of 1740 m.

The paleotopography, a succession of more or less parallel crests and gullies, plays an essential role in the behaviour of the flow by delimiting preferential water and material pathways and creating sections with differing kinematical, mechanical and hydrological characteristics. The earthflow is bordered by two lateral gullies with perennial run-off and characterized by a central intra-flowing gully with intermittent run-off (Fig. 1b). Water flows in the gullies and in the landslide body vary greatly with the season, as can be observed by the presence of dry or saturated cracks (Fig. 1c, 1d).

Rainfall is the main triggering factor of the earthflow motion, and it produces an intermittent and delayed recharge of the groundwater [6]. The earthflow has been active since 1970's [11]. The long-term kinematics are characterized by continuous movements with a seasonal trend. Its continued motion is likely given a Factor of Safety that is often below unity [7].

2.2 Constraints and investigation strategies

Observations and on-site measurements of the meteorological characteristics, the hydrology and displacements at the earthflow began in 1991 [5, 12]. A geophysical and geotechnical investigation (dynamic penetration tests, percussion drillings, pressuremeter tests, inclinometer survey) combined with a photogrammetric analyses was initiated in 1996 along five cross-sections in order to determine the structure of the accumulated mass [8].

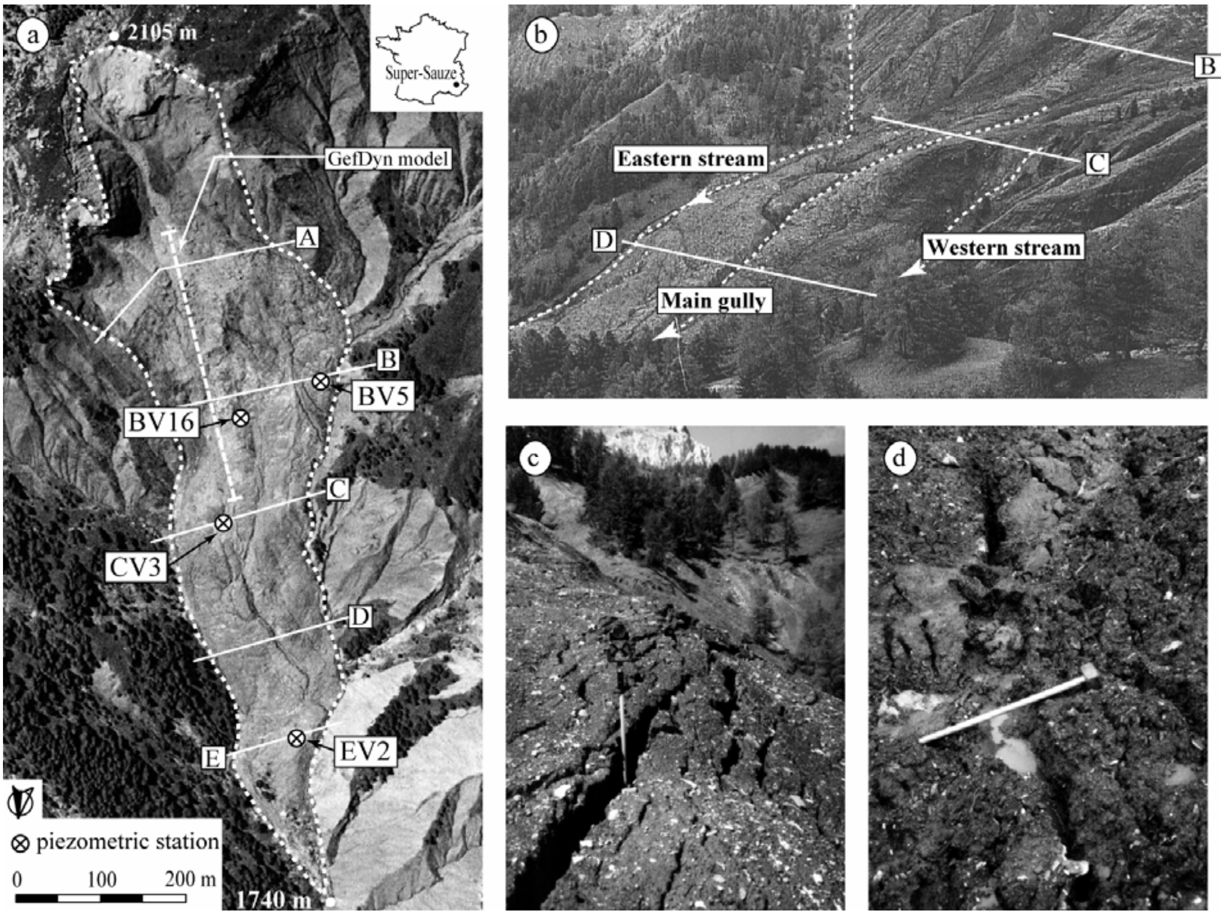

Figure 1. Morphology of the Super-Sauze earthflow. (a) Aerial ortho-photograph of the earthflow. (b) Morphological track of the earthflow and location of the drainage streams. (c), (d) Dry (August 2000) and saturated tension cracks (May 2001) in the upper part of the earthflow.

A water balance station to monitor pressure heads, combined with several *Time-Domain-Reflectrometry* sensors to monitor soil moisture over depth, has been installed in 1997. Around fifty open standpipe piezometers with manual recordings, filtered at different levels, were installed on five cross-sections to define the geometry of the water reservoir. Among them, four piezometric recorders were installed to monitor pore pressure (Fig. 1a). Cross-correlation of all information in a distributed database has allowed the construction of a hydrological and mechanical concept of the earthflow [13].

Other investigations were carried out in order to analyse the hydro-mechanical properties of the earthflow: an on-going survey of surface movements by high-precision differential GPS [6]; the installation of an extensometric device [6]; experiments of rainfall simulations to identify the respective balance of infiltration or runoff water, depending on soil surface characteristics [14]; the test of specific geophysical tools like SASW [15] or network noise measurements, or the installation of electrodes of spontaneous potentials, combined to an hydro-geochemical survey of the groundwater, to describe the fluxes of water within the landslide body.

To develop physically-based hydro-mechanical models for these earthflows, we need to define their internal structure, their hydrology and mechanics, and their kinematics.

3. INTERNAL STRUCTURE OF THE EARTHFLOW

The paleotopography comprises a series of crest quasi-intact in the accumulation zone. Some emerge over the earthflow on the B cross-section; others are intact to few metres below the surface. The earthflow reaches a maximum of 20 m in the eastern part of cross-section C. Thereafter the thickness diminishes progressively towards the downstream area.

The earthflow consists of a heterogeneous tongue with a high silty-sand matrix mixed with moraine debris. Its vertical structure consists of two superimposed units [16]. The upper unit, 5 to 9 m thick, is a very wet viscous muddy formation, which can be sub-divided into two sub-units (C1a and C1b), depending on the shape of the paleotopography and the seasonal position of the groundwater table (Fig. 2a, 2b). This unit is very active from a hydrological and mechanical view point. The lower unit, with a maximum thickness of 10 m, is a stiff compact, relatively impervious and apparently stable formation. The reader will find a detailed description of the soil hydro-mechanical characteristics in the following references [7, 17].

If the geophysics indicates the same succession of layers [8], the joint electric-TDEM interpretation (Fig. 2c) enabled us to demonstrate a thin transition zone (0.7-0.9 m) undetected by geotechnical prospection [5, 16]. This zone is the highly conductive with resistivities which showed little contrast (2-3 Ω.m) and anisotropic factors from 0.35 to 1.0. These resistivity figures correspond to those present in samples of pure water. Furthermore the measurements were not disturbed by any mineralogy-induced polarisation. This being so this horizon must be saturated and would correspond to a shear surface between the active unit and the stabilized mass.

This compartmentalization in connection with gullies and crests is also evident because of the surface displacements [6, 9]. The hydrodynamic and mechanical behaviour of the compartments varies with the seasons and the climatic conditions [5, 6].

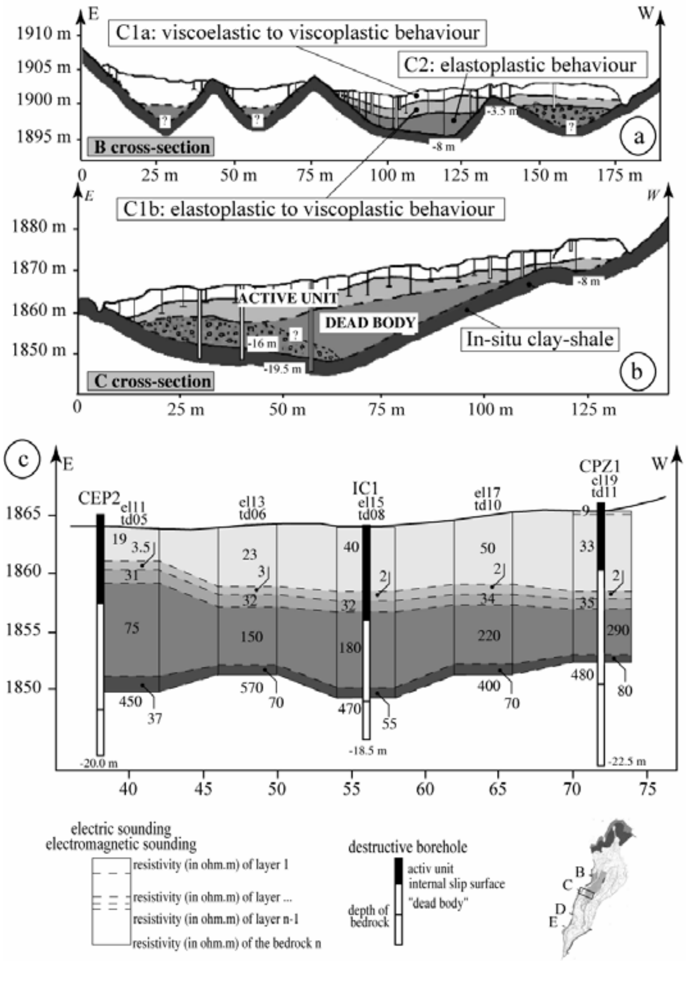

Figure 2. Internal structure of the earthflow. (a), (b):Geotechnical structure on the B and C cross-sections, (c): Geophysical structure derived from a joint interpretation of electrical and TDEM soundings pairs.

4. HYDROLOGY OF THE EARTHFLOW

4.1 Inferences from field data

The hydroclimatic time series (rain, either liquid or solid, temperature, net radiation, soil water content, soil suction, pressure head, groundwater level) over the period 1997-2001 and the results of an extended hydrological investigation were used to define a hydrological concept [17, 18].

The water reservoir consists of C1a et C1b units, and the eastward and westward streams may be considered as lateral boundaries of the landslide system. The thickness of the reservoir averages 7-8 m on cross-sections A and C, and 4 m on cross-sections B, D and E. The total volume of the reservoir is estimated at 300,000 m^3. The observed range of hydraulic conductivity values classifies the material as semi-permeable. In the unsaturated zone, the hydraulic conductivity values vary greatly according to the presence of fissures from 10^{-4} $m.s^{-1}$ to 10^{-8} $m.s^{-1}$. Furthermore Lugeon tests carried out *in-situ* indicates a permeability of 10^{-10} $m.s^{-1}$. For the purposes of our modelling study, this allows us to assume the lower unit of the earthflow and the underlying *in-situ* intact material as impermeable.

Inputs (rainfall, snowfall) and outputs (surface water, evaporation) of the saturated zone represent the mass balance of the hydrological system. The long-term yearly cumulated precipitation is usually 750 to 900 mm (with about 200 to 250 mm as snowfall), but the maximum daily or monthly value can vary greatly and produce significant groundwater fluctuations [17]. The earthflow is characterized by high groundwater levels whose fluctuations are correlated with rainfall and snowmelt. The piezometric behaviour shows high pore pressure variations (up to 20-25 kPa corresponding to an average fluctuation of the groundwater level of about 2.5 m) with sudden recharge following snowmelt. Pore pressures may remain high for a long time due to the medium permeability of the reworked marls and the presence of the relatively impermeable layer underneath. Water level fluctuations of different intensity are related to changes in permeability and geometry of the earthflow. In the unsaturated zone, the range of matrix pressure heads varies between saturation and an average of + 150 kPa. For specific climatic situations, soil suction may reach more than 40 kPa in summer, or even 80 kPa when the soil freezes. Accordingly, the soil moisture content varies considerably, ranging from 8 to 35% per volume.

Water is transported to depth quickly with an immediate drop in pressure potentials after rainfall. Moreover, in the top layer of the landslide body, saturation always remains temporary (1/4 h to 2 h) after a rainfall. Because these data relate to low hydraulic conductivities in the soil matrix, rapid drops in matrix pressure head appear to be connected both to matrix fluxes in the nearly saturated material and to fissure fluxes [17, 18].

4.2 Hydrological concept for clayey earthflows

In such as way, the following conceptual hydrological model for clayey earthflows has been proposed [13, 17, 18]:

- above a certain groundwater threshold level (0.6-1m), groundwater fluctuations are invariably rapid (less than a few hours),of moderate magnitude (0.1 to 0.4m) and relatively short duration (within days) following liquid rainfall. Peaks following snowmelt have a longer duration;
- the decline of the groundwater levels below this threshold strongly depends on the season, with faster drainage in summer;
- the hydrological regime is influenced by two important recharge events, one at the end of spring and one at the beginning of autumn;
- no deep alimentation occurs within the landslide body.

The rapid piezometric responses are attributed to matrix fluxes in nearly saturated materials, combined to fissure fluxes through a superficial (0.3-1m) system of interconnected cracks. The depth of this crack system is similar to the boundary between the unsaturated and saturated zones. These considerations are schematised into a hydrological concept with three layers: a layer with a continuous permeable crack system ($C1a_1$) overlies two layers marked by different hydraulic conductivity values ($C1a_2$, C1b) due to compaction. The groundwater table is mainly located in the C1b and $C1a_2$ layers. The lower unit (C2) and *in-situ* marls are not considered in the model. A similar concept has been proposed in the Alverà landslide [19, 20].

4.3 Physically-based hydrological modelling

This hydrological concept has been incorporated into a numerical model by adaptating the spatially distributed physically based model STARWARS developed by Van Beek [21] for the simulation of catchment hydrology. The hydrological model is built around a core model resolving the dynamic equation for saturated and unsaturated transient flows in the vertical and horizontal directions, and additional sub-models describing specific hydrological processes, like snowpack/snowmelt or fissure flow. The hydrological model consists of three permeable reservoirs (three layers) and an underlying impervious bedrock. A complete mathematical description of the model can be found in the references [17, 21]. The calibration and validation procedure are described in the reference [17].

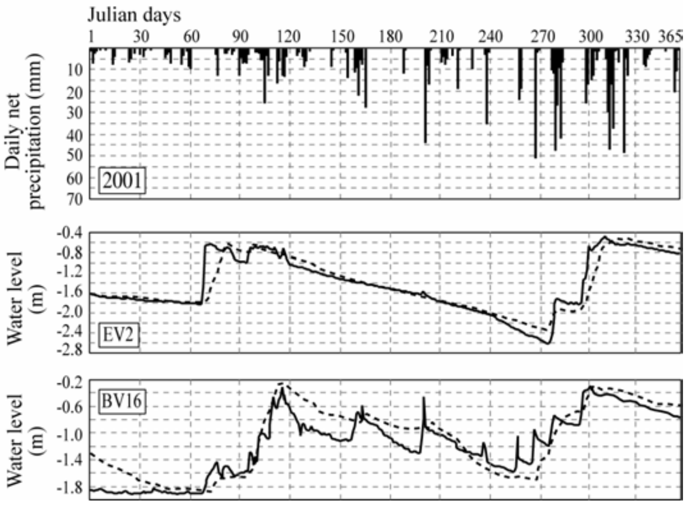

Figure 3. Hydrological modelling of the earthflow. Observed and best-fit simulated groundwater levels over year 2001 at two locations.

Figure 3 shows the simulation results for two piezometers. The response pattern is reproduced well, although some recorded peaks are underestimated or missed. This underestimation is less important because these short-lived high groundwater levels do not influence the kinematics of the earthflow [6].

5. MECHANICS OF THE EARTHFLOW

5.1 Inferences from field data

Five years (1997-2001) of continuous displacements and pore water pressures monitoring have demonstrated that the earthflow accelerations are the result of the undrained reactivation of the reworked material; the induced displacements being characterised by a high variable rate [9]. Two acceleration periods are observed: one in Spring and one in Autumn.

From the velocity profiles computed from inclinometer measurements, it appeared that the earthflow exhibits a complex style of movement, associating strong displacements along an internal slip surface, located within the reworked landslide body, superimposed by a viscoplastic body (with a shear rate estimated at 10^{-10} m.s^{-1} assuming a 5-m thick unit) and a rigid body on top (Fig. 2a, b) [9, 16]. Indeed, velocity monitoring reveal that stress field change, induced by pore pressure fluctuations, involve the slip surface but also stress the importance of deformability and viscous properties of the landslide body. This implies the use and the implementation of viscoplastic creeping laws in the numerical codes to account for the dependence of the mobilized strength on the displacement rate [22, 23].

5.2 Geomechanical concept for clayey earthflows

From the field data, it appeared that two thresholds of pore pressures trigger the acceleration of the movement; above it, the velocity increases non-linearly. The “spring movements” are initiated as soon as the water level ranges between -0.8 and -0.7 m below the ground surface; the “autumn movements” are triggered by a higher threshold value (between -0.6 and -0.5 m below the ground surface). This higher level is probably explained by strength regain due to an increase in undrained cohesion by consolidation in summer [24].

The long-term behaviour is characterized by continuous movements with a seasonal trend. The earthflows may be active for decades or more as is justified by the very low Factor of Safety of the landslide body (mean ϕ'_r=20°, mean slope angle β=25°) very often below 1 [7]). Once a threshold pore pressure distribution is attained, the rate of movement increases. Also, while pore pressures decrease, velocity decreases too, but no stop of the movement is observed. This may be explained considering that both the residual strength parameters and the applied shear stresses are constant with time.

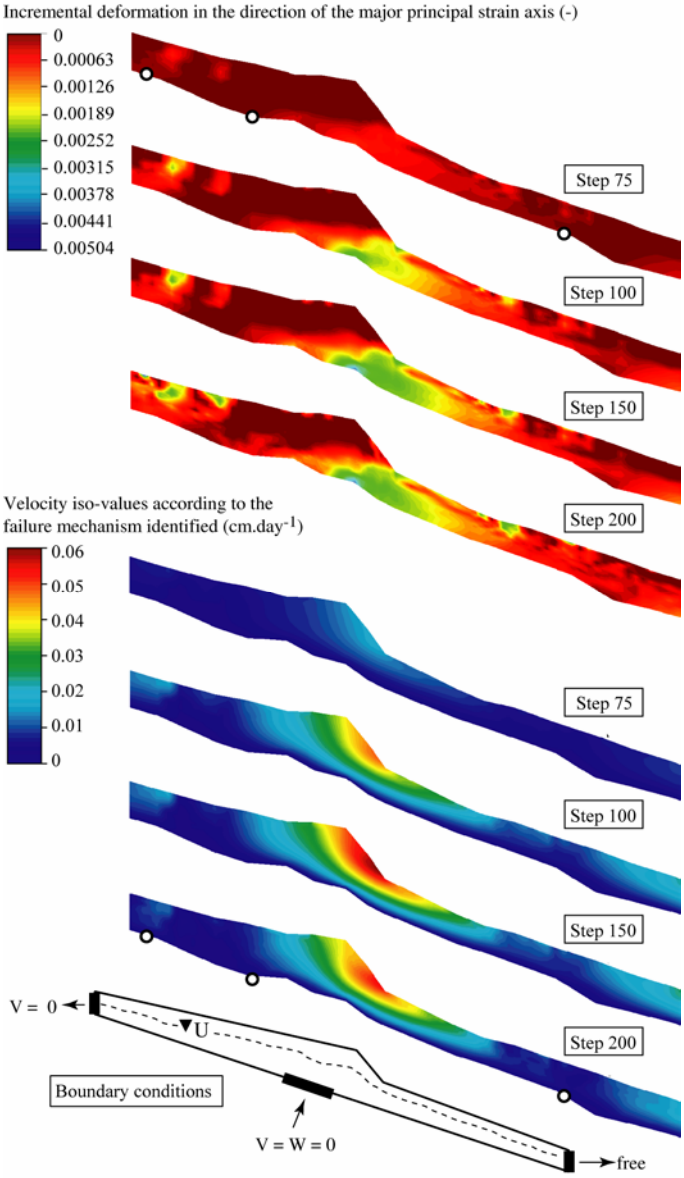

Figure 4. Hydro-mechanical modelling of the earthflow with the pore water pressures variations observed in the field over the period 01/01/1999-19/07/1999 (200 days). The circles indicate the positions of nodes in which the pore water (U) variation with time is imposed.

This scheme corresponds to the seasonal long-term dynamics of the earthflow. It can be well represented by elasto-plastic laws with a viscous component implemented in analytical models [9] or in numerical model [13]. Figure 4 shows the simulation of the effects of hydrologic variation on the mechanical behaviour of the earthflow. This was carried out through the use of the 2D finite-element program GefDyn© 2-D, assuming a Hujeux-elasto-plastic model, along a longitudinal cross-section in the upper part of the earthflow (Fig. 1a). The range of simulated velocities is in accordance with the observations. As an evidence, the manner in which the progressive soil plastification (hardening) is taken into account in the Hujeux model, is appropriate to simulate the behaviour of the earthflow. Moreover, both observations and numerical calculations show that conditions in the upper part of the earthflow for average pore water pressures are close to failure. The beginning of a movement (slump type) is simulated (Fig. 4). An excess of water caused by a combination of snowmelt and rainfall, or changes in the geometry of the landslide body by internal deformation, may build excess pore pressure leading to crisis of the earthflow [26, 27].

6. CONDITIONS LEADING TO CRISIS OF THE EARTHFLOW

6.1 Inferences from field data

Small volume muddy debris flows (7000 m^3), of velocities ranging from 3 to 4 $m.s^{-1}$, have been released from the upper part of the earthflow at several time (1997, 1999, 2001). From a rheological viewpoint, the debris flow material exhibits a viscoplastic behaviour over the range of shear rates under consideration, and this is well represented by a Herschel-Bulkley constitutive equation [28]. Herschel-Bulkley parameters (τ_c, K) increase with the total solid fraction ϕ. In such a way, modelling the propagation of these debris flows necessitates the use of propagation models based on a viscoplastic rheology, such as the Cemagref-1D program.

6.2 Physically-based propagation modelling

The performance of the runout model to replicate field observations has been evaluated by analysing the mobility of several debris flow events initiated in the upper part of the earthflow. The methodology, as well as the calibration and validation procedure are described in the following references [4, 28].

Results indicate that the code matches the observed geometry fairly well for the flow thickness and the runout distance. The relative error is less than 31% for the deposit thickness and less than 15% for the runout distance. This error is acceptable according to the relative error associated to the determination of the rheological parameters. Therefore, as a good concordance between model predictions and reality has been observed, the Cemagref 1-D code can be used to forecast the mobility of the failed debris and assess the hazard.

7. ASSESSMENT OF DEBRIS FLOW HAZARD

To prepare a hazard zonation (runout distance, deposit depth), we estimated the volume of debris necessary to reach the alluvial fan, and verified if these volumes could be released from the earthflow. The methodology consists of performing several numerical simulations with the Cemagref 1-D code by (1) using the rheological and hydraulic parameters used in the debris flow mobility analysis, (2) by changing the volume of released sediment and (3) by changing the total solid fraction (ϕ=0.40, ϕ=0.45 and ϕ=0.50). A peak discharge of 7 $m^3.s^{-1}$ and a triangular hydrograph of 120 min are used in the simulations. These values correspond to a decennial flow discharge recurrence. We adjusted the volume of input debris with the assumption that the deposits must be at least 0.50 m thick. Figure 5a shows the results of the scenario analysis.

For total solid fractions consistent with those generally observed in muddy debris flows, the minimal volume of sediment (mixture of debris and water) necessary to reach the apex ranges between 30,000 and 50,000 m^3 (Fig. 5a). Figure 5b shows the geometry of the events. The simulated velocities are consistent with those generally observed for muddy debris flows in the French Alps and lie in the range between 2 and 2.5 $m.s^{-1}$.

Assuming a total solid fraction of ϕ=0.45, the volume of debris that has to fail in the debris source area ranges between 21,000 and 29,000 m^3. Seepage analysis has been used to estimate the volume of debris that can be released for several hydro-climatic conditions. Results of the parametric analyses [28] show that hydrogeological conditions able to initiate failures of 21,000 to 29,000 m^3 are attained for a cumulative input of water of 65 mm (on a 3-day long period) corresponding to a 25-years return period rainfall.

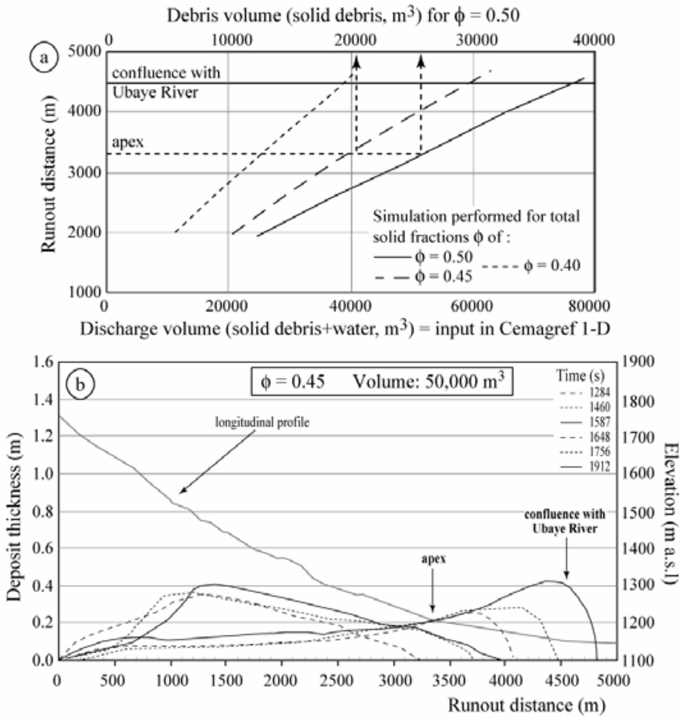

Figure 5. Hazard assessment for the Sauze alluvial fan. (a): Estimation of the debris volume necessary to reach the apex of the torrent and the Ubaye river confluence for different total solid fraction; (b): Computed debris-flow geometry to stop at the Ubaye river confluence.

CONCLUSION

Large clayey landslides often show their complex nature being able of sudden changes in behaviour (from sliding to flowing) or in velocities (from less than 0.01 $m.day^{-1}$ over more than 1 $m.s^{-1}$). As a consequence, such phenomenon provides an opportunity to develop a flow-like landslide assessment approach that incorporates prefailure, failure and postfailure stages. Such methodologies are vital to estimate realistic hazard scenarios for watersheds affected by landslides. Moreover, the Super-Sauze case history outlines significantly the importance of field observations to usefully calibrate the numerical models. It should be stressed that numerical models are only one of the tools available to the expert in charge of hazard assessment. Although the models do not claim to simulate all behaviour, nevertheless they do provide a means establishing the influence of certain parameters and thereby reducing the subjectivity of assessments. Further research on landslide hydrology, mechanics and propagation should be undertaken in the future, using the different landslide databases now available.

ACKNOWLEDGMENT

This research was supported by the European Community in the framework of the FP4 NEWTECH Project (*New Technologies for Landslide Hazard Assessment*) and FP5 ALARM Project *(Assessment of Landslide Risk and Mitigation in Mountain Areas)*, by Centre National de la Recherche Scientifique (CNRS) within the framework of INSU-PNRN (Project ECLAT: Ecoulement, initiation et Contribution des Laves Torrentielles dans les bassins marneux) and the French Ministry of Research within the ACI-CatNat Project MOTE (MOdélisation, Transformation, Ecoulement des coulées boueuses dans les marnes).

example of the Super-Sauze earthflow. *Comptes-Rendus Geosciences*, 12p. [submitted].

REFERENCES

[1] L. Picarelli, *Transition from slide to earthflow and the reverse.* In K. Sassa, (ed), Transition from slide to flow. Mechanisms and remedial measures, Proceedings of the IAEG Conference, Trabzon, 2001.

[2] G. Le Mignon, R. Cojean, R., *Rôle de l'eau dans la mobilisation de glissement-coulées (Barcelonnette, France)*. In J. Rybar, J. Stemberk, P. Wagner (eds), Proceedings of the 1st European Conference on Landslides, Prague, 2003.

[3] R. van Beek, Th.W.J. van Asch, *The mobility characteristics of the La Valette landslide*. In K. Senneset (ed), Proceedings of the 7th International Symposium on Landslides, Trondheim, 1996.

[4] J.-P. Malet, O. Maquaire, J. Locat, A. Remaître, Assessing debris flow hazards associated with slow-moving landslides: methodology and numerical analyses. *Landslides*, 1, pp. 83-90, 2004.

[5] J.-C. Flageollet, J.-P. Malet, O. Maquaire, The 3D structure of the Super-Sauze earthflow: a first stage towards modelling its behaviour. *Physics and Chemistry of the Earth*, 25, pp. 785-791, 2000.

[6] J.-P. Malet, O. Maquaire, E. Calais, The use of Global Positioning System for the continuous monitoring of landslides. Application to the Super-Sauze earthflow, *Geomorphology*, 43, pp. 33-54, 2002.

[7] O. Maquaire, J.-P. Malet, A. Remaître, J. Locat, S. Klotz, J. Guillon, Instability conditions of marly hillslopes, towards landsliding or gullying? The case of the Barcelonnette basin, South East France, *Engineering Geology,* 70, pp. 109-130, 2003.

[8] M. Schmutz, Y. Albouy, R. Guérin, O. Maquaire, J. Vassal, M. Descloîtres, J.-J. Schott, Contribution of electrical and TDEM methods employed separately and combined to Super-Sauze earthflow knowledge, *Surveys in Geophysics*, 21, pp. 371-390, 2000.

[9] J.-P. Malet, O. Maquaire, *Black marl earthflows mobility and long-term seasonal dynamic in southeastern France.* In L. Picarelli, (ed.), Proceedings of the Conference on Fast Slope Movements: Prediction and Prevention for Risk Mitigation, Sorrento, 2003.

[10] O. Hungr, S.G. Evans, M. Bovis, J.N. Hutchinson, A review of the classification of landslides of the flow type*. Environmental and Engineering Geoscience*, 7, pp. 221-238, 2001.

[11] D. Weber, A. Herrmann, Reconstitution de l'évolution géomorphologique de versants instables par photogrammétrie numérique: l'exemple du glissement de terrain de Super-Sauze, *Bulletin de la Société Géologique de France*, 171, pp. 637-648, 2000.

[12] J.-C. Flageollet, J.-P. Malet, O. Maquaire, M. Schmutz, *Chapter 14. Integrated investigations on landslides: example of the Super-Sauze earthflow*. In R. Casale, C. Margottini (eds), Natural Disasters and Sustainable Development, Springer-Verlag, Berlin, 2004.

[13] J.-P. Malet, *Flow-like landslides in clay-shale outcrops of Southeast France. Morphology, behaviour and hydro-mechanical modelling*. PhD Thesis in Earth Science, University of Strasbourg I, 2003 [in French].

[14] J.-P. Malet, A.-V. Auzet, O. Maquaire, B. Ambroise, L. Descroix, M. Esteves, J.-P. Vandervaere, E. Truchet, Soil surface characteristics influence on infiltration in black marls: application to the Super-Sauze earthflow, *Earth Surface Processes and Landforms*, 28, pp. 547-564, 2003.

[15] G. Grandjean, C. Pennetier, A. Bitri, O. Meric, J.-P. Malet, Characterization of the internal structure and the hydric state of clayey-marly landslides through geophysical tomography: example of the Super-Sauze earthflow. *Comptes-Rendus Geosciences*, 12p. [submitted].

[16] O. Maquaire, J.-C. Flageollet, J.-P. Malet, M. Schmutz, D. Weber, S. Klotz, Y. Albouy, M. Descloîtres, M. Dietrich, R. Guérin, J.-J. Schott., Une approche multidisciplinaire pour la connaissance d'un glissement-coulée dans les marnes noires. *Revue Française de Géotechnique,* 95/96, pp. 15-31, 2001.

[17] J.-P. Malet, Th.W.J. van Asch, R. Van Beek, O. Maquaire, Forecasting the behaviour of complex landslides with a spatially distributed hydrological model, *Natural Hazard and Earth system Science*, 21p. [in press].

[18] J.-P. Malet, O. Maquaire, Th.W.J. van Asch, *Hydrological behaviour of earthflows developed in clay-shale: investigation, concept and modelling.* In L. Picarelli (ed), The Occurrence and Mechanisms of Flows in Natural Slopes and Earthfills, Patron Editore, Bologna, 2004.

[19] M.G. Angeli, J. Buma., P. Gasparetto, A. Pasuto, A combined hillslope hydrology/stability model for low gradient clay slopes in the Italian Dolomites, *Engineering Geology,* 49, 1-13, 1998.

[20] T. Bonomi, A. Cavallin, Three-dimensional hydrogeological modelling application to the Alverà mudslide (Cortina d'Ampezzo, Italy), *Geomorphology*, 30, pp. 189-199, 1999.

[21] R. van Beek, *The impact of land use and climatic change on slope stability in the Alcoy region, Spain*. PhD Thesis in Earth Science, University of Utrecht, 2002.

[22] L. Vulliet, K. Hutter, Viscous-type sliding laws for landslides. *Canadian Geotechnical Journal*, 25, 467-477, 1988.

[23] Th.W.J. van Asch, P. van Genuchten, A comparison between theoretical and measured creep profiles of landslides, *Geomorphology*, 3, 45-55, 1991.

[24] Th.W.J. van Asch, T. Bogaard, *A study on the displacements of a landslide near Salins-les-Bains, Eastern France*. In D. Moore, O. Hungr (eds), Proceedings of the 8th International Congress for Engineering Geology and the Environment, Vancouver, 1998.

[25] Th.W.J. van Asch, J.-P. Malet, A. Remaître, O. Maquaire O, *Numerical modelling of the run-out of a muddy debris-flow. The effect of rheology on velocity and deposit thickness along the run-out track*. In A. Lacerda M. Ehrlich, S.A.B. Fontoura, A. Sayão A (eds.), Proceedings of the 9th International Symposium on landslides, Rio de Janeiro, 2004.

[27] Th.W.J. van Asch, J.-P. Malet, R. van Beek, Theoretical considerations about the role of landslide geometry and kinematic deformation for the liquefaction of landslides, *Engineering Geology*, 12p. [submitted].

[28] J.-P. Malet, D. Laigle, A. Remaître, O. Maquaire, Triggering conditions and mobility of debris flows associated to complex earthflow*s, Geomorphology*, 21p. [in press].

Dr. Jean-Philippe Malet
Faculty of Geosciences, UCEL, University of Utrecht
Po.Box 80.115, 3583 TC Utrecht, NETHERLANDS
Email: j.malet@geog.uu.nl

HYDROGEOLOGY

Hydrological Modelling and Forecasting: application of geospatial information systems

Kaoru Takara

Disaster Prevention Research Institute, Kyoto University, Uji 611-0011, Japan

ABSTRACT

This paper describes current situation of hydrological modeling and forecasting, mainly focusing on application of geospatial information systems such as DEM, thematic maps and remote sensing images. Grid-cell-based distributed hydrological models are introduced to indicate distribution of water on the ground surface and in the subsurface layer over the catchment area, as well as sediment yield at each grid-cell from a catchment covered by volcanic ash soils.

The principal model for each grid-cell is the kinematic wave model with surface permeable layer, which deals with surface overland flow and subsurface saturated and unsaturated flows. The inclination of each grid-cell is based on DEM information with spatial resolution of 50 to 250 m. The roughness coefficient is given to each grid-cell by the land cover based on digital land use maps or remote sensing images. Digitized channel networks and hydraulic techniques are used for flood routing.

The catchments demonstrated are the Yodo River in Japan and the Brantas River in East Java, Indonesia. The application to an upstream well-forested sub-basin of the Yodo with an area of 100 km2 indicates the effect and limitation of so-called “green dam”, which is assumed to be in well-vegetated mountainous catchments, especially in the cases of very heavy rainfall with recurrence intervals of 50 to 200 years. The grid-cell-based hydrological model can describes the whole Yodo River catchment (8,200 km2) and consider human intervention to river regimes by incorporating a number of artificial reservoir operation system models. A sediment runoff model is also developed in the same framework by conceptualizing sediment yield processes on each grid-cell covered with volcanic ash and applied to the Lesti River (640 km2), a tributary of the Brantas River.

Kaoru Takara
Disaster Prevention Research Institute, Kyoto University,
Uji 611-0011, Japan
takara@mbox.kudpc.kyoto-u.ac.jp

Evolution of human-induced "natural hazards" in urban geosphere due to the change of groundwater environment -an example from Tokyo Metropolitan Area-

Tomochika Tokunaga

Department of Geosystem Engineering, University of Tokyo

ABSTRACT

Underground environments at the Tokyo Metropolitan Area have dramatically changed in accordance with the change of groundwater condition in the area. This presentation summarizes the temporal changes of the underground environments at the Tokyo Metropolitan Area from 1920s until present, focusing on the change of groundwater level of the confined aquifers and associated change of human usage of urban geosphere. The evolution of "natural hazards" which have been caused mainly by the change of groundwater usage is also shown. Several new approaches to improve surface environments using "surplus" groundwater are also presented.

KEYWORDS: underground environments, urban geosphere, Tokyo Metropolitan area, groundwater, underground infrastructure

1. INTRODUCTION

Tokyo, the capital of Japan, is situated in the southwestern part of the Kanto plain, the largest flat plain in Japan (Fig. 1). The underground environments at the Tokyo Metropolitan Area have been changing dramatically in accordance with the change of groundwater condition and with the continuous increase and heavy usage of underground space. Because of the complex interaction between the change of groundwater environments and human activities for the underground usage, we have experienced a variety of human-induced "natural hazards". This paper describes the temporal change of groundwater environments and associated hazards at the Tokyo Metropolitan Area. Several projects and approaches which try to simultaneously solve the presently faced problem of underground facilities and improve the urban environments are also presented.

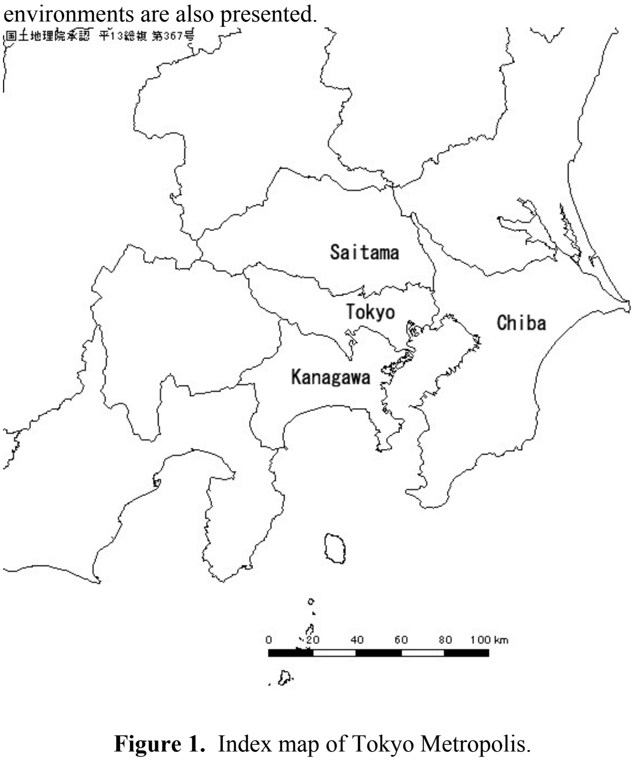

Figure 1. Index map of Tokyo Metropolis.

2. GEOLOGY AND GROUNDWATER SYSTEM IN THE TOKYO METROPOLITAN AREA

In Tokyo area, Late Pliocene and younger sediments and sedimentary rocks unconformably overlies the Miocene basement rocks. The shallower part of the sediments constitutes the confined aquifer-aquitard system. According to the Institute of Civil Engineering of Tokyo Metropolitan Government (ICE-TMG) [1], this confined aquifer-aquitard system is bounded at its bottom by relatively thick mudstone layer, and the top of this mudstone becomes shallower towards southwest. It is situated at more than 600 m depth in the northeast of Tokyo while it is about 100 m depth at the southwestern part of Tokyo (Fig. 2). Below the aquifer bottom, the Plio-Pleistocene sediments extend more than 2000 m thick and it mainly consists of alternating sandstones and mudstones, which comprises a reservoir system of methane gas dissolved in water.

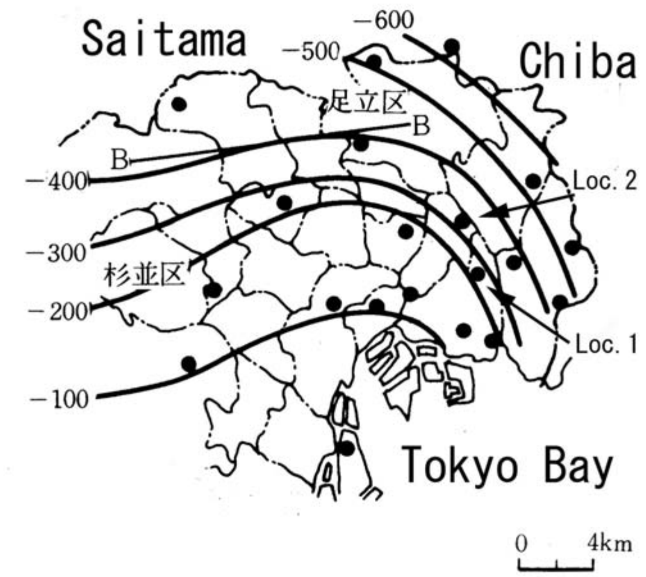

Figure 2. Contour map showing the depth distribution of the bottom of the aquifer-aquitard system at Tokyo [1].

In addition to the above mentioned confined aquifer system, there exists an unconfined aquifer in the area. Kawashima [2] reported the temporal change of water level of unconfined aquifers and showed that the water levels are more or less stable at least from 1970s to present (Fig. 3).

Fig. 4 shows the examples of the change of groundwater potentials of confined aquifers together with the extraction rate of fresh groundwater (white bars) and formation waters (black bars). The formation waters were extracted for mining methane gas dissolved in water and it had been one of the main causes for severe ground subsidence in this area [3].

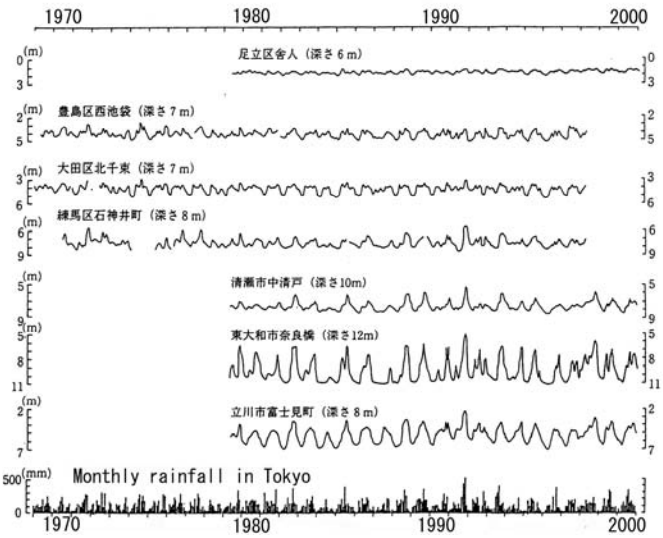

Figure 3. Examples of the change of unconfined water table (monthly mean data) at Tokyo. Water table depths are measured from the ground surface. [2]

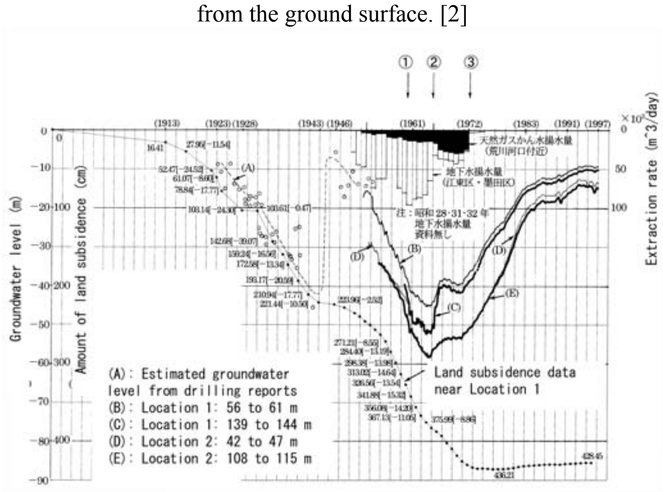

Figure 4. Examples of the change of confined groundwater potential in Tokyo from 1881 until 1997 [3]. Localities of the wells are shown in Figure 2. White bars indicate the extraction rate of groundwater and black bars the extraction rate of formation waters. The events shown are: ① Southern part of the alluvial lowlands in Tokyo was designated by the Industrial Water Law (IWL) as a restricted area where no new wells were to be installed for industrial usage, ② Pumping of groundwater for industrial usage in southern part of the alluvial lowlands was restricted by IWL, and ③Extraction of methane gas dissolved in water was suspended in the southern part of the alluvial lowlands by means of purchasing the mining rights by Tokyo Metropolitan Government.

3. HAZARDS CAUSED BY THE SIGNIFICANT DROP OF WATER TABLE

As shown in Fig. 4, the groundwater level of the confined aquifer had dropped to about 50 m below ground surface in the early 1970s. Because of the significant decline of the groundwater level, severe land subsidence appeared as a direct result of over-exploitation of groundwater (Fig. 5). Also, several confined aquifers had changed to become unconfined conditions (Fig. 6) and introduced the oxygen-deficient air mass under the ground. The oxygen-deficient air migrated along the aquifer during underground construction by pneumatic caisson method and caused deaths of people staying in basement floor (Fig. 7).

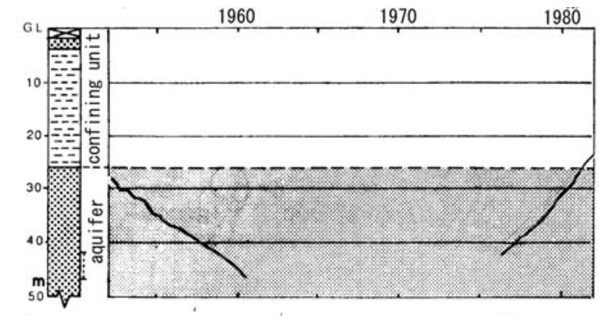

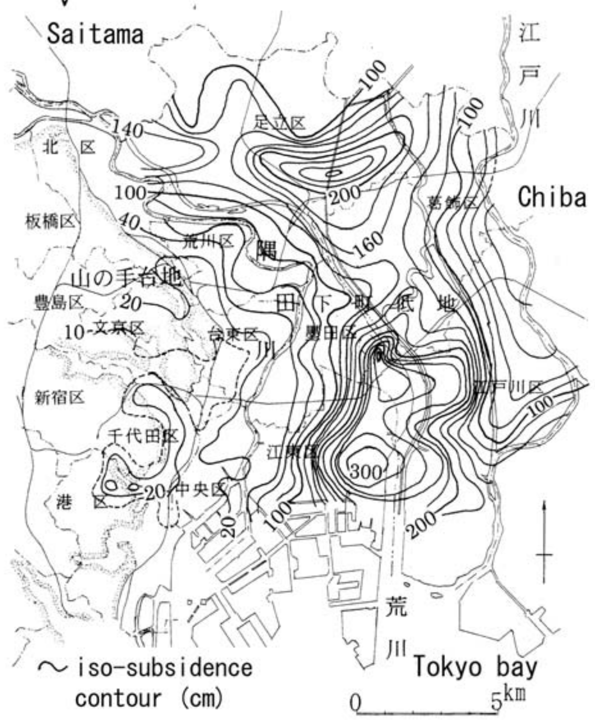

Figure 5. Contour map showing the subsidence between 1938 and 1977 (40 years) at lowland Tokyo [3].

Figure 6. Change of groundwater level at Loc. 2 (42 to 47 m) [4]. Note the unconfined condition of the aquifer between 1950s and 1970s.

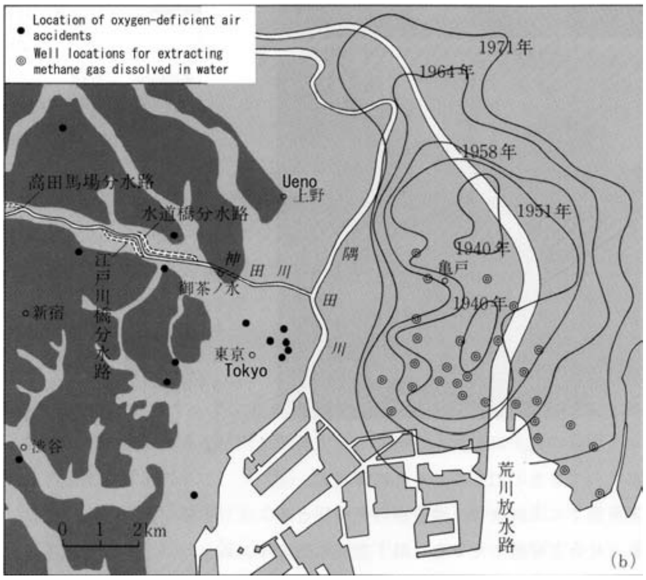

Figure 7. A map showing the distribution of the oxygen-deficient air accidents. Dots indicate the location of oxygen-deficient air accidents, and double circles the location of wells for extracting methane gas dissolved in water. Contour shows the extent of below zero meter region at 1940, 1951, 1958, 1964, and 1971 [5].

4. REGULATION OF GROUNDWATE USE TO CEASE LAND SUBSIDENCE

Because of the serious problems related to the over-extraction of groundwater, the local government and Japanese national government decided to regulate the groundwater extraction to the absolute minimum. From January 1961 until April 1974, the Japanese national government and the Tokyo Metropolitan government with its surrounding three prefecture governments implemented the following groundwater regulation laws. The national government has restricted groundwater withdrawal for industrial use since 1961 by the Industrial Water Law (IWL) (in 1961, southern part of alluvial lowland was designated as a restricted area where no new wells were to be installed for industrial usage; in 1966, pumping of groundwater for industrial usage in southern part was restricted; in 1971, pumping of groundwater for industrial usage in the northern part was restricted), and for air conditional use since 1963 by the Law Controlling Pumping of Groundwater for Use in Building. In 1972, extraction of methane gas dissolved in water was suspended in the Tokyo area by means of purchase of the mining rights by Tokyo Metropolitan Government.

After implementing the above mentioned regulations, groundwater potentials have recovered quickly, as shown in Fig. 4, far better than expected. The rapid recovery of groundwater levels have been considered to be due to the relatively high recharge rate (2 to 3 mm per day) in this region[6,7].

5. PROBLEMS OF UNDERGROUND INFRASTRUCTURES DUE TO THE RECOVERY OF GROUNDWATER LEVEL

Even though the land subsidence in Tokyo area has ceased and groundwater level has recovered, it has caused new types of damages to the underground infrastructures which have been constructed during the drawdown period of groundwater level in the region. The following shows an example of the problem.

Tokyo underground station was designed at 1965 and has been operated from 1972. At the time of its design, the groundwater level at the location was 35 m below the ground level, however, it has continuously recovered and reached to be 15 m below the ground level in 1998. The detailed investigation for the possible damage to the station revealed that the buoyant water pressure was quite high, and critical groundwater level for the severe damage was estimated to be 14.3 m below ground [8]. The East Japan Railway Company decided to conduct countermeasure construction work to the station by applying ground anchor technique (Fig. 8), which makes it possible to support the underground station until groundwater level be 12.8 m below ground [9]. Similar problems have been reported in Tokyo area (Ueno underground station [9]) and rebuilding operation close to Osaka station in Osaka prefecture [10]. Hirose et al. [11] summarized the published data on infrastructure damages caused by the recovery of groundwater level in Tokyo area.

Groundwater levels of confined aquifers have still been recovering (see Fig. 4), and accurate prediction of the rate of recovery and of the final groundwater level is necessary to plan the maintenance operations for the underground infrastructures.

6. EFFICIENT USAGE OF “SURPLUS” GROUNDWATER

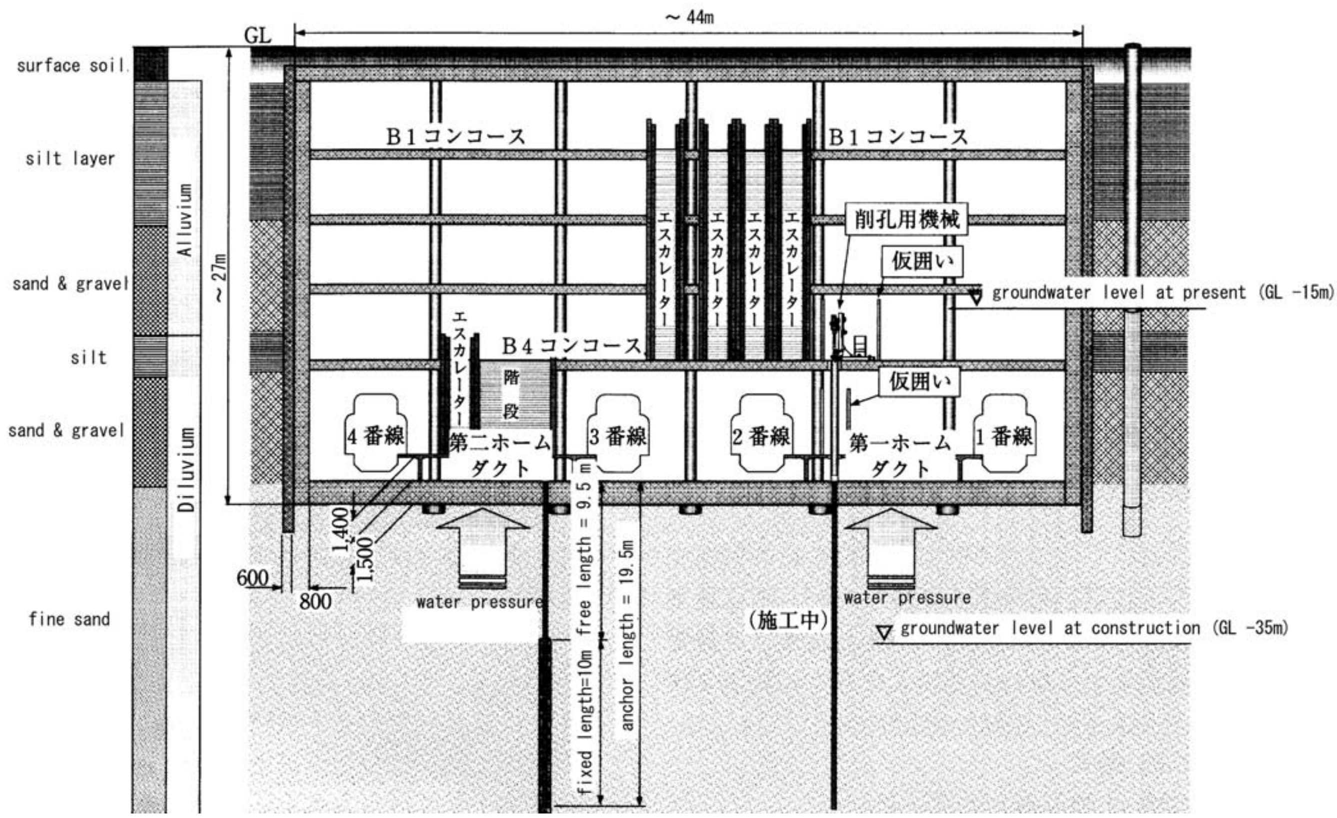

Figure 8. Schematic diagram showing the situation at the Tokyo underground station and the image of the countermeasure construction work to the recovery of groundwater level [9].

TO IMPROVE ENVIRONMENTS

Because of the recovery of groundwater level, the amount of leakage water into the underground structures has been increased. Usually, the leaked water is damped to the sewer. However, several plans for efficiently using the leakage water into the structuresare presented to improve the surface water environments and some of them have been implemented.

Here shows one example which has been done by the East Japan Railway Company, the Tokyo Metropolitan Government, and the Kokubunji City [8].

The Kokubunji tunnel of the Musashino line was constructed and has been operated since 1973. This tunnel is oriented perpendicular to the general groundwater flow direction of the area, and was experienced groundwater related problems at 1974 and 1991, respectively, due to the rapid increase of groundwater level and seepage by heavy rain. To prevent the rapid increase of groundwater level, twenty-four drain pipes were set and controlled the groundwater level. From 2002, the drained groundwater has been used to restore a local small pond and to increase the flow rate of the river to improve the local surface environments (Fig. 9).

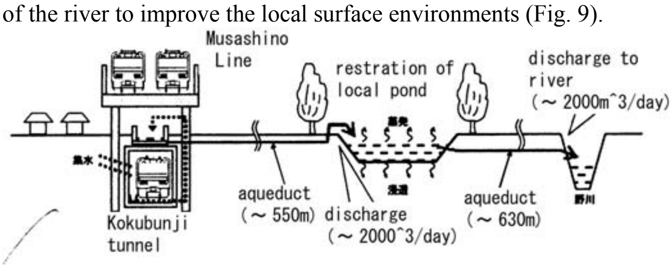

Figure 9. An example of efficient usage of leaked water into the tunnel (the Kokubunji tunnel) [8]

Recently, Kajino et al. [12] presented an idea to use "surplus" groundwater for cooling the pavement in the urban area to reduce heat-island phenomenon. Their idea comes from the fact that the groundwater temperature usually is very close to the annual mean temperature of the area and is much lower than the pavement temperature in summer. Considering that there exists "surplus" groundwater in the urban area and heat exchange can be done by applying cooler groundwater to the permeable pavement, it might be possible to control and improve the urban summer environments.

Similar and other ideas to efficiently use the groundwater to improve the urban environments and at the same time reduce the damage to the infrastructure are necessary to achieve the sustainable development of the urban areas.

7. CONCLUSIONS

This paper summarized the temporal changes of the underground environments and related "natural hazards" at the Tokyo Metropolitan Area. It is possible to divide the evolution into three stages, i.e., deterioration of underground and surface environments due to over exploitation of groundwater (first stage), regulation of groundwater extraction to the absolute minimum and the recovery of groundwater potentials (second stage), and damaging underground infrastructures by buoyant force and increase of groundwater seepage due to the recovery of groundwater potentials (third stage). Recent activities to use "surplus" water to improve the urban environments and to reduce the damage to underground infrastructures were shown. These activities should be expanded to achieve the sustainable development of the urban cities.

ACKNOWLEDGMENT

I would like to thank the members of the Committee of Groundwater Problems in the Field of Engineering Geology which has been established in the Japan Society of Engineering Geology for their helpful discussions.

REFERENCES

[1] Institute of Civil Engineering of Tokyo Metropolitan Government (ICE-TMG), *Synthetic Ground Chart in Tokyo Metropolis*, Gihodo Pub., Tokyo, 1977. (in Japanese)

[2] S. Kawashima, Temporal change of groundwater lelve in Tokyo Metropolis, *Found. Eng. Equip.*, **29**(11), pp. 77-79, 2001. (in Japanese)

[3] T. Endo, S. Kawashima, and M. Kawai, Historical review of development of land subsidence and its cease in Shitamachi Lowland, Tokyo, *J. Japan Soc. Eng. Geol.*, **42**, pp. 74-87, 2001. (in Japanese with English abstract)

[4] T. Endo and M. Ishii, Hydrogeology and subjects caused by recovering of groundwater level in Tokyo. *J. Japan Soc. Eng. Geol.*, **25**, pp. 111-120, 1984. (in Japanese with English abstract)

[5] K. Kojima, Urban environments looking from underground. *In*: K. Nakamura, K., Koike, and K. Takeuchi (*eds.*), *Nature in Japan 3, Kanto*, pp. 111-124, Iwanami Pub., Tokyo, 1994.. (in Japanese)

[6] J. Shimada, The mechanism of unsaturated flow through a volcanic ash layer under humid climatic conditions. *Hydrol. Proc.*, **2**, 43-59, 1988.

[7] J. Shimada, C. Tang, T. Tanaka, Y. Yang, Y. Sakura, X. Song, and C. Liu, Irrigation caused groundwater drawdown beneath the North China Plain, *Proc. Int. Groundwater Conf., Darwin, Australia*, pp. 1-7, 2002.

[8] M. Shimizu, Groundwater problems related to construction of underground structures, *Proc. 2004 Symp., Japan Soc. Eng. Geol*., pp. 26-33, 2004. (in Japanese)

[9] N. Kurasawa, Examples of countermeasure constructions to overcome groundwater pressure due to the recovery of groundwater level –Ueno underground station and Tokyo underground station-. *Found. Eng. Equip.*, **29**(11), pp. 72-76, 2001. (in Japanese)

[10] T. Hashimoto, Groundwater problems in Osaka plain. *Proc. 2004 Symp., Japan Soc. Eng. Geol*., pp. 1-7, 2004. (in Japanese)

[11] M. Hirose, T. Kawagoe, and H. Kiya, A relation of a groundwater level change for construction and underground structures, *Proc. 2004 Ann. Meet., Japan Soc. Eng. Geol.*, pp. 419-422, 2004. (in Japanese)

[12] N. Kajino, T. Tokunaga, G. Mogi, K. Mogi, S. Yasumoti, and K. Bando, Research on the pavement cooling system using groundwater. *Proc. 2004 Ann. Meet., Japan Soc. Eng. Geol.*, pp. 109-112., 2004. (in Japanese)

Tomochika Tokunaga
Department of Geosystem Engineering, University of Tokyo,
7-3-1 Hongo, Bunkyo-ku, Tokyo 113-8656 JAPAN,
email: tokunaga@geosys.t.u-tokyo.ac.jp

CEMAGREF'S FLOOD FORECASTING METHODOLOGIES IN THE FRENCH FLOOD ALERT SYSTEM

Marine Riffard* and Cécile Loumagne

Cemagref, Hydrology Unit, Antony Regional Centre - Parc de Tourvoie – BP44 – 92163 Antony Cedex
e-mail : marine.riffard@cemagref.fr

ABSTRACT

A RESEARCH INSTITUTE FOR HYDROSYTEMS AND RISKS MANAGEMENT

Cemagref is a French public research institute focused on environmental sciences for the sustainable management of land and water. Cemagref has 10 regional centers and 25 research units organised into four scientific departments:

- Water resources (uses and hazards)
- Aquatic ecosystem (quality and pollution)
- Landscape management
- Ecotechnologies and agrosystems

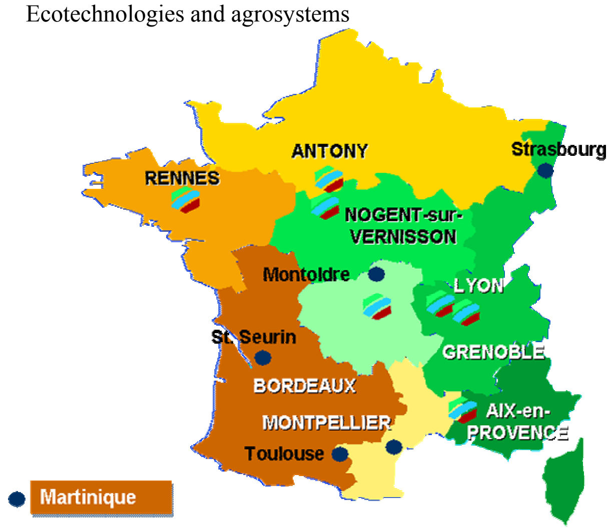

*Figure 1. **Cemagref's regional centers***

Its research usually addresses complex systems and their interaction with human society based on an interdisciplinary approach covering environmental and life sciences, human and social sciences, physics, mathematics, chemistry and earth sciences.

Cemagref has a staff of 1000 permanent employees (researchers and engineers), about 180 PhD students, 40 Post Docs and 150 long-term trainees.

The Water resources department: uses and hazards

In this department research aims at finding tools and operational methods to improve the management of freshwater systems. It focuses on how hydrosystems behave to identify, predict, and control the impact of both natural processes and human activity on the dynamics of rivers and basins. Research subjects address the challenging issues of improving water resource management, and preventing natural disasters throughout seven areas of interest:

- Natural hazards in mountainous areas
- Water flow within catchments and river systems
- Irrigated agriculture - environmental impacts
- Water uses – governance and management tools
- Hydraulic works safety
- Pollutants in rural catchments – modeling and mitigation
- Water delivery systems - modeling and automation

The Hydrology Research Unit

The Hydrology team, located at Antony (near Paris), is part of the Water Resources department. The team also manages the Orgeval experimental research basin located at 70 km East of Paris. The are 8 permanent employees in the team, 5 PhD students and 2 Post Docs.

Its aim is to produce methods and models that can be used by managers and those in charge of public policy-making on natural risks in order to strengthen research on prevention. In order to reach this objective there is a need in improving knowledge of the water resource as a basis for designing water management schemes along with the identification and control of the water-related risks for a better understanding of processes and events (flood prediction and control, hydrometeorological events….).

Modeling plays a key role in the scientific approach, and also in the evolution of predictive tools. Research activities in the team are based on the development of Rainfall-Runoff (R-R) models, methodologies for applications in water resources management and engineering along with the management of the Orgeval research basin.

Model developments

Rainfall-Runoff models have numerous applications in water resources management and engineering. They can be used for flood forecasting, low flow forecasting, flood estimation, impact detection, dam management or design... Keen to address part of these issues the hydrologic team at Antony has developed four research areas of interest (Figure 2):

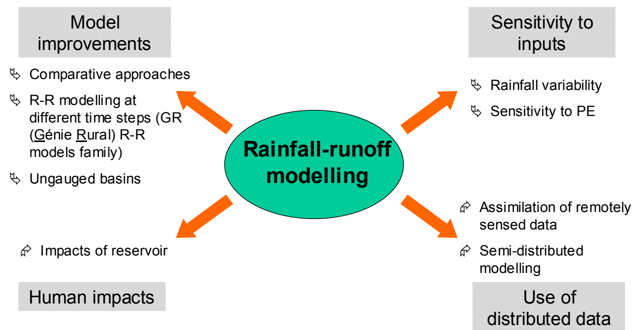

*Figure 2. **Model development activity in the Hydrology Unit***

Hydrology is a science based on observations up to now, no one has produced a significant rainfall-runoff model that does not need observations for calibration of various parameters or at least for the elaboration of hydrological state parameters. Observations are also needed to evaluate the performance of a model. Constitution of a general database is thus of great importance since it aims at improving rainfall-runoff modeling in a systematic way. The basic unit considered relevant to the study of hydrologic processes is the river basin. It is then at this scale and with an extended database of basins that modeling tests have been performed with simple R-R models in order to address different issues in water resources management. Cemagref has developed four models running at different time steps: GR1A the annual model, GR2M the monthly one, GR4J the daily one and GR5H the hourly one. This was carried out in comparison with more than forty other R-R model structures.

Management of the Orgeval experimental research basin

*Figure 3. **The Orgeval experimental and research basin***

The Orgeval experimental basin (104 km^{2}) is studied and followed by Cemagref since 1962. It is located in Seine et Marne within the Seine basin near Paris, France (Figure 3). It is an agricultural catchment with more than 80% of agricultural lands and with approximately 70% of drained soils. Since 1962, the equipment has been continuously improved following technology and allowing studies in a lot of different areas such as remote sensing, water quality, modeling, erosion or drainage.

Over this basin the hydrological behavior is quite well-known. As forty years of continuous data time series (flows, rainfalls, meteorological data, water quality data, soil moisture, agricultural practices, changes in land cover) are available, the analysis of changes in cultural practices or impact of forest and drainage on stream flow are possible. Today, the Orgeval is a basin unique in France, with its availability of more than forty years of time series. The information concerning the location and the map of the basin, the current equipment along with the data series is available on a web site dedicated to the basin : http://www.antony.cemagref.fr/webQHAN/Site orgeval/Page accueil francais.htm

A lot of collaborations with other French or American institutes as CNRS, CETP, ENPC, NASA, JPL, or with French or American Universities, have been realized. The basin is also integrated in different national and European research programs. Collaborations with other countries are welcome.

THE FRENCH FLOOD FORECASTING CONTEXT

For the 1991-1995 period, the European Environment Agency estimated the cost of flood damages in the European Union at 99 billion € [1]. In France there are lots of recent examples of important floods on French rivers. It is known that 5-7% of the land and 10% of the population are concerned with flood problems, more than 80% of natural catastrophes are due to floods and 75% of catastrophes costs are due to flood damages.

If floods are natural phenomena that will continue to occur in the future, human and economic losses can be alleviated if reliable forecasts are made available with enough lead-time. Adequate forecasting methodologies reduce flood-associated risks and allow in some cases to avoid expensive structural alternatives such as dikes or reservoirs. The implementation of modern flood forecasting methodologies faces both economical problems (cost efficiency of forecasting systems and associated data acquisition networks) and technical problems (lead-time, robustness and precision of forecasts). However, these two aspects have rarely been taken into account together. If operational hydrology and meteorology have made huge progress over the last decades, most of the research efforts have been dedicated to rainfall-runoff models [2] that are not often integrated in flood forecasting systems[1][3]. While research activities have focused on the newest available technologies, to understand how these may contribute to forecast improvement, no real attention has been devoted to the actual integrated system of flood forecast (Figure 4 and Figure 5).

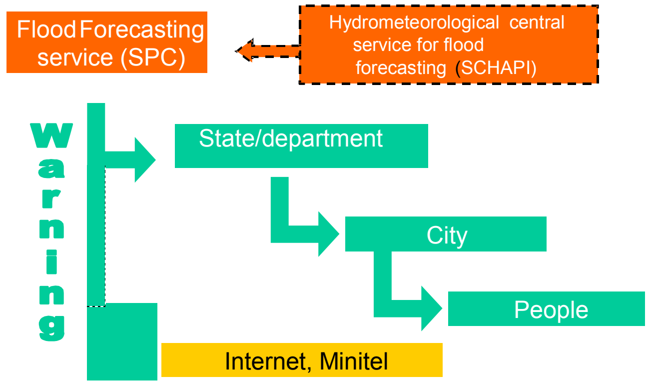

Figure 4. French flood alert system

Flood forecasts are performed by 22 regional flood forecasting services (SPC) in charge of flow monitoring on the different French river basins with the help of the Hydrometeorological Central Service (SHAPI) that provides them with new technical and scientific methodologies. Then, the Prefecture, at the state and department level, and the city council are in charge of warning the population.

Short term forecasts are most often used for flood warning and for real-time operation of water resources systems (e;g. reservoirs). But before flood warning the flood forecasting system is divided in three steps :

- Data acquisition
- Modeling
- Stream flow forecast

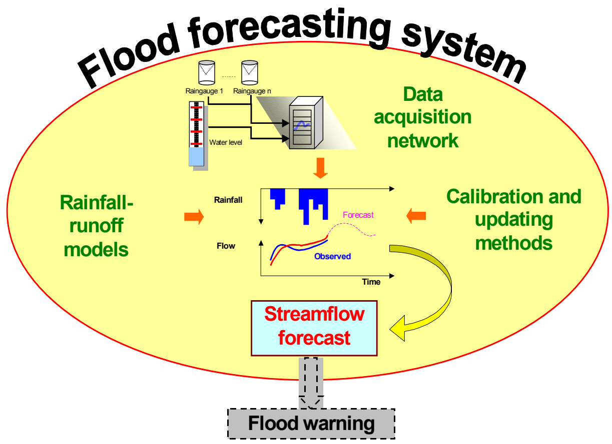

*Figure 5. **Short term flood forecasting***

[1] In the following, we will distinguish *rainfall-runoff models* (i.e. the mathematical representation of the rainfall-runoff transformation) and *flood forecasting systems* (which encompass the model, the data acquisition network and the methods used to calibrate and update model parameters).

Data acquisition

- The meteorological network :

This network is managed by Météo France, the French Institute for meteorological data. They provide the SPCs with all kinds of meteorological data:

classical rainfall (rain gauges), radar images, satellite images and meteorological forecasts.

- The hydrological network :

SPCs manage their own network of flow gauging stations. But they can also use other public networks: DDE (Departmental Equipment Service), DIREN (Regional Environment Service), and SNS (Seine Navigation Services).

Modeling

There is a wide gap between theoretical and actual modeling capabilities in flood forecasting services. Although strong efforts have been made to implement efficient forecasting systems in some basins (for example transnational basins such as the Rhine basin), many of existing services, all across France, still use methods such as upstream-downstream linear relationships that provide forecast of very limited lead-time (as flood waves rapidly propagate in channels) and sometimes of limited accuracy. The reasons for this situation lie in the lack of funds to invest in precipitation and flow monitoring networks, the lack of experience to identify the appropriate model in the jungle of existing ones, and the lack of physical data to feed complex models [2, 4]. Indeed, we have to recognize that while modern technology offers huge possibilities, operational services cannot afford their generalized use. Where floods threaten only small- or medium-size communities, available financial means are always limited.

Still today each SPC service applies its own model, and there are great differences between the methods and the models used. That’s why an Hydro Meteorological Central Service (SHAPI) has been created in June 2003 to solve this problem. This service has to propose tools for forecasting and has to coordinate the different services working on the same basin during extreme events.

Stream flow Forecast

The difficulty of predicting floods in a reliable way originates partly from a certain lack of accuracy of hydrological models, particularly during unusual hydrologic events. Because models are far from being perfect, hydrologists need to put the model in better compliance with the current observation prior to using it in forecasting mode. Methods have thus been developed to improve hydrologic forecasting. The fundamental idea is that if the model predictions diverge from the observations at a given time, there is little chance that future estimations will approach the correct values.

The improvement then, comes from a correction of the trajectory of the model based on observations preceding the forecast. This operation has been termed updating in hydrology. Updating is a way to take advantage of additional information on the studied system for modelling. Such a procedure is necessary when this additional information is not a classical input of the model. After applying different updating methodologies to the models, if the stream flow forecast is near or over the alert level, it is sent to the Prefecture (state and department level). The Prefecture decides then to warn the city council and the riverside population if necessary.

CEMAGREF’S METHODOLOGIES FOR FLOOD FORECASTING

Rainfall-Runoff modeling

Today flood forecasting is still mostly viewed as a single problem of propagation, and hydraulic models are used to propagate flood waves in the river channel. However, we know that for flood forecasting, rainfall-runoff modeling is a much needed complement to hydraulics, as it can bring a solution to some of the drawbacks of hydraulic models:

- by making the link between rainfall and streamflow, rainfall-runoff models lengthen considerably the forecasting lead time (they add the time necessary for water to join the stream);
- by including a production function, they are able to estimate which part of gross rainfall will contribute to streamflow;
- They can be applied in small upland catchments

These models generally do not need much data because their parameters can be estimated numerically by calibration against streamflow records even when only short streamflow time-series are available. Then it can be run with longer rainfall time-series (generally of larger availability) to determine the required flood estimate or with synthetic series generated by a stochastic rainfall model. The limit of such a method may arise from the difficulty of the rainfall-runoff model to simulate flood peaks with good accuracy or from the uncertainties brought by the rainfall model. Several authors have already proposed the application of rainfall-runoff models in the context of flood estimation [5, 6, 7, 8]. Although extensive work has been done on the issue of flood estimation [9], this new direction is still at a research stage and needs further developments.

At Cemagref in the Hydrology Unit, research is based on the development of rainfall-runoff models to be used in forecasting mode. One of them, the GR4J model, a lumped conceptual model, running at the daily step is shown in Figure 6.

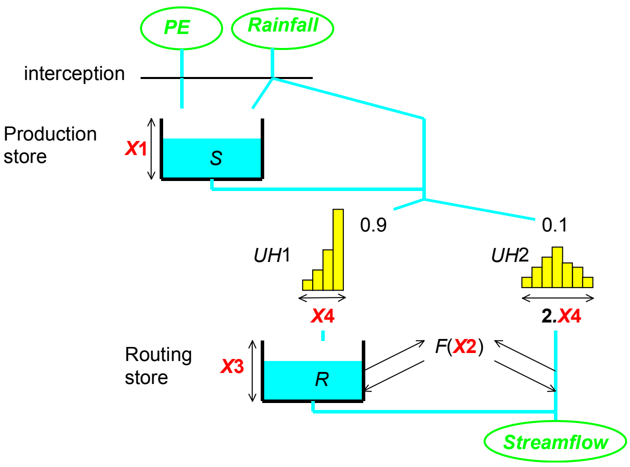

Figure 6. **The GR4J rainfall-runoff model**

Monthly, annual and hourly models are also in development at Cemagref in comparison with other well-known R-R models such as IHACRES, HBV or TOPMODEL [10,11,12].

However using rainfall-runoff modeling in a flood forecasting context is not a trivial exercise and a precise methodology must be followed [3]. First, model parameters must be optimized against existing data. When applied, the model requires the use of an updating methodology, which helps bringing simulated flow as close as possible to observed flow at the time of forecast. Last, the model must be run using a rainfall scenario until the lead-time, typically a few hours or a few days ahead.

The updating methodologies

The updating problem is a tricky question and several updating procedures were proposed in the literature. In the case of rainfall-runoff modeling, the two model inputs are rainfall and potential evapotranspiration that feed the model that calculates runoff, i.e. the target variable. In a forecasting context, the knowledge of streamflow when issuing the forecast can be most valuable, in that we can compare at that time what gives the model with what is actually observed in the stream. Minimizing the model error before issuing the forecast, i.e. using additional information on the catchment gives better chance to make more reliable forecasts.

There are several ways for model updating, depending on what is judged by the modeler to be the major cause of model error (uncertainty in data, in model structure or in model parameter values). O'Connell & Clarke [13] and, more recently, Refsgaard [14] reported on four different methodologies used for R-R model updating. Updating can be made by:

- correcting the input data (rainfall),
- correcting model output,
- correcting model state variables (levels in stores),
- correcting model parameters.

Three of these methodologies have been set up at Cemagref:

The first methodology was proposed by Yang and Michel [3] in the field of flood forecasting. The model's inability to produce correct stream flow values generally translates into parameter uncertainty. Parameter calibration is the means by which a model structure adjusts to a given set of data. Therefore, parameter updating seems to be a natural way to amend the current error in stream flow value.

Consequently, a specific methodology of parameter updating was chosen as the starting point from which stream flow and soil moisture assimilation could best be coped with (Figure 7). This methodology consists of adjusting the parameter of the model over a certain number of days preceding the date when a forecast is desired, so that over that period the calculated values (either discharge or discharge and soil moisture) fit better with the observed ones. Oudin *et al,* [15], present the implementation of this methodology over 4 selected areas in France and Portugal, with a comparison of the results obtained with classic procedures using only recent stream flow and the new approach introducing gradually the soil moisture information.

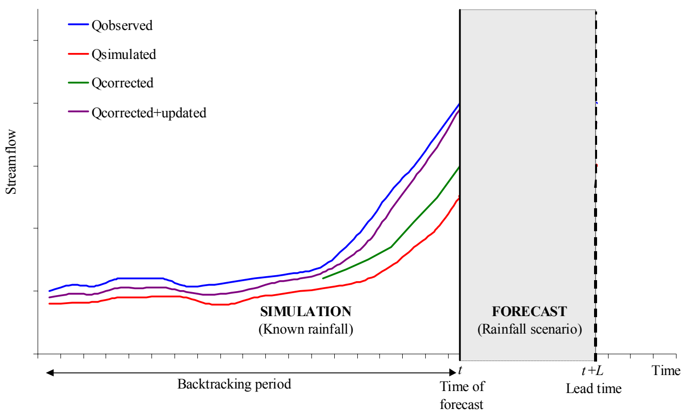

Figure 7: Parameter updating

The second methodology is based on a sequential assimilation algorithm, with state updating (Quesney *et al,* [16], François *et al,* [17]) (Figure 8). The aim of the sequential assimilation is to improve the performances of a hydrological model by controlling its evolution and by limiting the divergence between the model and available observations.

The most widespread method of sequential correction is that proposed by Kalman [18]. For about ten years, thanks to numerical calculation advances, the Kalman filter has been subject of applications in environmental sciences. The Kalman filter consists of calculating this correction term taking into account the estimated errors on model and observations, and locally linearising the model: the correction will be done by using linear equations, and the more the observations are accurate, the more the *a posteriori* internal state (after correction) are close to them. Aubert *et al*, [19], applied this methodology on 2 different catchments in France. The efficiency of the assimilation procedure in flood prediction is discussed focusing on the contribution of soil moisture data.

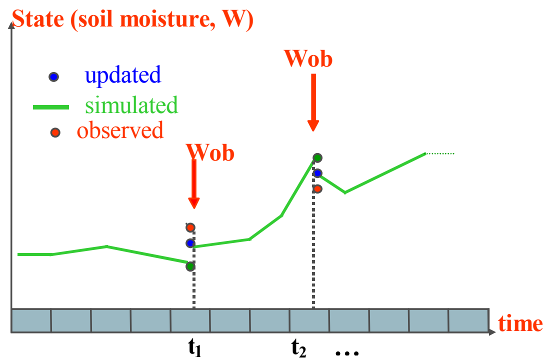

Figure 8: State Updating

The third methodology describes the estimation of a catchment wetness index from measured or simulated distributed soil moisture data along with the assimilation of remote sensing data into hydrological models. It is based on input updating where internal variables are forced to fit the inputs. In the implementation presented in Ragab *et al* [20] the estimation of catchment wetness index is calculated from model simulations and is used as an input for the hydrological model in order to substitute soil moisture accounting procedures of the models in forcing mode. The catchment wetness index is estimated by averaging the wetness indices at a catchment scale in a hydrological distributed model. The model can be calibrated against the wetness index obtained from observations such as remote sensing data or TDR data. Then the continuous time series of soil moisture data calculated by the model can be used as input in rainfall-runoff models.

These methodologies are derived from climatic domains were they are much more used than in surface hydrology. The updating procedures proposed in the literature were seldom comparatively assessed, maybe because such algorithms are still tricky to implement. Although some experiments were proposed to assess the efficiency of forecasting systems [14, 21], we do not have at the moment clear indications on the robustness of these procedures. Similarly, there has been no methodology yet proposed to compute forecast uncertainties in the context of model updating.

CONCLUSION

The approaches based on rainfall-runoff modeling such as developed at Cemagref are promising but still lack extensive validation and there is a need to compare their results with those of more classical methods. The theoretical aspects of model uncertainties and coupling of rainfall and hydrological models must also be more deeply investigated. However, these approaches have been implemented in operational services in collaboration with the French consultancy SAFEGE to develop and implement an operational real-time flood forecasting tool for the Oise and the Aisne Rivers [22] with the following characteristics:
- real-time import of rainfall and streamflow data from measurement stations,
- the possibility to correct manually the data or to add information from field observers,
- ease of use with graphical outputs that can be quickly interpreted in terms of warning thresholds.
- possible export of results for quick use in the warning chain.

The Service de Navigation de la Seine (SNS), in charge of issuing forecasts, is presently assessing the reliability of the software in real conditions.

Early warning of extreme events becomes today more and more feasible and reliable with hydrological forecasting systems that can help authorities to warn people. For example, the forecast of flash flood events may give a few hours for people to evacuate risky zones or to save some of their goods. Such warning would also benefit to civil protection services to organize evacuations and rescue actions. On large catchments, floods can be forecasted a few days ahead. Such a delay can leave time to build up temporary protection that could help to protect endangered locations and avoid damages. So the development / improvement of flood forecasting systems will contribute to improve the safety of citizens and their quality of life by reducing the risks linked to such natural events.

KEYWORDS: flood forecasting, flood alert, modeling, rainfall-runoff models

ACKNOWLEDMENT

The authors would like to thank Cemagref's team for its support and its help and specially Charles Perrin for the care he took reading this abstract. They would like to thank also N. Kocher and F. Lacroix for their suggestions and useful documents.

REFERENCES

[1]European Environment Agency, Sustainable water use in Europe. Part 3: Extreme hydrological events: floods and droughts. 2001, Copenhagen: *EEA*. **84**.

[2]Beven, K.J., Changing ideas in hydrology - the case of physically-based models. *Journal of Hydrology*, 1989. **105**: p. 157-172.

[3]Yang, X. and C. Michel, Flood forecasting with a watershed model: a new method of parameter updating. *Hydrological Sciences Journal,* 2000. **45(4)**: p. 537-546.

[4]Beven, K.J., Prophecy, reality and uncertainty in distributed hydrological modelling. *Advances in Water Resources*, 1993. 16: p. **41-51**.

[5]Cameron, D.S. et al. (1999): Flood frequency estimation by continuous simulation for a gauged upland catchment (with uncertainty). *Journal of Hydrology*, **219**, 169-187.

[6]Fontaine, T.A. (1995): Rainfall-runoff model accuracy for an extreme flood. *Journal of Hydraulic Engineering*, 121(4), 365-374.

[7]Institute of Hydrology (1999): Flood *Estimation Handbook, Institute of Hydrology,* Wallingford, UK.

[8]Lamb, R. (1999): Calibration of a conceptual rainfall-runoff model for flood frequency estimation by continuous simulation. *Water Resources Research*, **35(10)**, 3103-3114.

[9]Perrin, C., Michel, C. (2002): Robustness of two flood estimation methods with data availability. *In: Proceedings of the International Conference on Flood Estimation,* Manfred et al. (Editor), Berne, Switzerland.

[10]Schreider, S.Y., Whetton, P.H., Jakeman, A.J., Pittock, A.B. and Li, J., 1997. Runoff modelling for snow-affected catchments in the australian alpine region, Eastern Victoria. *Journal of Hydrology*, 200(**1-4**): 1-23

[11]Bergström, S., 1975. The development of a snow routine for the HBV-2 model. *Nordic hydrology*, **6**: 73-92.

[12]Beven, K.J. and Kirkby, M.J., 1979. A physically based, variable contributing area model of basin hydrology. *Hydrological Sciences Bulletin,* **24(1)**: 43-69.

[13]O'Connell P.E., Clarke RT. (1981). Adaptive hydrological forecasting a review. *Hydrol.Sci. Bull,* **26(2)**, 179-205.

[14]Refsgaard, J.C., Validation and intercomparison of different updating procedures for real-time forecasting. *Nordic Hydrology, 1997*. **28**(65-84).

[15]Oudin L., Weisse A., Loumagne C., Le Hegarat-Mascle S., 2003, Assimilation of soil moisture into Hydrological models for flood forecasting a variational approach. *Canadian Journal of Remote sensing* **29(6***),* pp 679-686

[16]Quesney, A., C. François, C. Ottlé, S. LeHégarat, C. Loumagne and Normand, M., 2000. Sequential assimilation of SAR/ERS data in a surface hydric model coupled to a global hydrological model with an extend Kalman filter. *Remote sensing and Hydrology 2000, IASH Red Book Publication* **n°267**, edited by Brubaker, Ritchie, Rango, pp. 495-497

[17]François, C., Quesney, A. and Ottlé, C., 2003. Sequential assimilation of SAR/ERS1 data into a coupled land surface-hydrological model using an Extended Kalman Filter. *Journal of Hydrometeorology,* **4 (2),** 473-487.

[18]Kalman R.E. (1960). A new approach to linear filtering and prediction problems. *J.Basic Eng.,* **vol 82 D**, 35-45

[19]Aubert D., Loumagne C., Oudin L., 2003, Sequential assimilation of soil moisture and streamflow data in a conceptual rainfall-runoff model. *Journal of Hydrology* **280**, pp 145-161.

[20] Ragab R., Perrin C., Littlewood I, Bromley J., France M., Prediction of runoff to surface reservoirs using the remotely sensed catchment wetness index., *Fifth International Workshop of Remote Sensing in Hydrology, IASH, 2-5 October,* Montpellier, France, Proceedings in CDROM, 1-12.

[21]WMO, Simulated real-time intercomparison of hydrological models. 1992, World Meteorological Organization: Geneva.

[22]Perrin C., Loumagne C., Andreassian,V., Michel C., Real time flood forecasting with rainfall-runoff models on the Oise River Basin, France. *AGU- EGS, Joint Assembly*, Acropolis Nice, France 7-11 April 2003.in CDROM *'Geophysicae research abstract'*, **Vol 5,** 2003.

Groundwater Pollution and Role of Organisms

Mio Takeuchi

Institute for Geo-Resource and Environment, National Institute of Advanced Industrial Science and Technology

KEYWORDS: geo-pollution, arsenic, marine organisms, organoarsenicals, trichloroethylene, methane, methanotrophs, bioremediation

1. INTRODUCTION

Groundwater pollution is a worldwide issue. In Japan, NO_3-N, NO_2-N, As, Pb, F, B and volatile organic halocarbons (VOCs) such as tetrachloroethylene (PCE) and trichloroethylene (TCE), are the most commonly found contaminants. Here we introduce interactions between organisms and two major groundwater contaminants, arsenic and VOCs.

2. ARSENIC AND MARINE ORGANISMS

2.1 Background

Groundwater monitoring by the Ministry of the Environment has revealed that of 3520 wells tested in 2002, arsenic was detected in 321 of them (9.1%) ([1]). Of these, 53 wells (1.5%) had concentrations exceeding the environmental standard (0.01 mg L^{-1}). Not only did arsenic concentrations in contaminated groundwater often exceed the environmental standard, but so did that in soil ([2]). Most of this arsenic pollution, however, is not anthropogenic in origin. Rather, it is derived from naturally-concentrated arsenic in the subsurface as is also seen in other countries such as India, Bangladesh and China. Arsenic is related to volcanic activity. Therefore, high concentrations are found in geothermal water and mine drainage. Groundwater contamination is also often found in Holocene to Pleistocene lacustrine and marine sediments. One of the primary sources of arsenic in such sediments appears to be erosion of volcanic rocks. In some areas, however, the origin of arsenic still remains unknown. Since marine clay sediments tend to exhibit higher concentrations of arsenic than fresh water sediments, arsenic concentrated by marine organisms should be considered as a possible source of arsenic in marine sediments. Several marine organisms, such as plankton, fish and seaweed, are known to concentrate arsenic in various organic forms. Total arsenic concentrations in these marine organisms are reported to be 0.8-14.5 mg kg^{-1} wet weight for macro-algae and 0.1-106.6 mg kg^{-1} wet weight for marine animals ([3]). These biologically concentrated organo-arsenicals may contribute to the accumulation of arsenic in marine sediment once they settled to the bottom in coastal areas. We determined the distribution of organo-arsenicals in coastal marine sediments to better understand the role of marine organisms in the geochemical cycle of arsenic.

2.2 Distribution of organo-arsenicals in coastal marine sediment

Six surface sediment samples (Sts. 1, 2, 3, 5, 6, 7) and one core sample (St. 4) were taken from the Otsuchi Bay, Iwate, Japan 2002 (Fig. 1) ([4]).

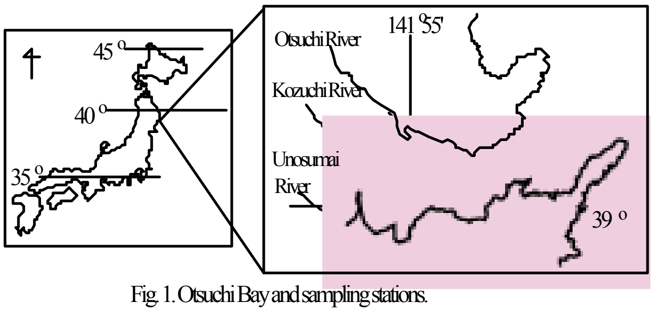

Fig. 1. Otsuchi Bay and sampling stations.

Sediment was extracted with methanol-water and served for high performance liquid chromatography (HPLC)-inductively coupled plasma mass spectrometry (ICP-MS, ICPM-8500, SHIMADZU, Kyoto, Japan) analysis for the determination of organo-arsenicals. Columns used were CAPCELLPAK C_{18} MG (SHISEIDO, Tokyo, Japan) and PRP-X100 (Hamilton, NV, USA).

By HPLC-ICP-MS analysis, we detected monomethyl arsonic acid (MMA), dimethylarsinic acid (DMA), arsenobetaine (AsB), trimethylarsine oxide (TMAO), and arsenocholine (AC) together with some other unknown arsenic species which are considered to be arsenosugars. AsB which is mainly formed by marine animals was the dominant organo-arsenical in the surface sediments of St. 1, 2, 5, and 6. Total concentrations of organo-arsenicals ranged from 10.6 to 47.5 μg As kg^{-1} dry sediment (Fig. 2). This is the first evidence for the pathway of arsenic from marine organisms to marine sediment.

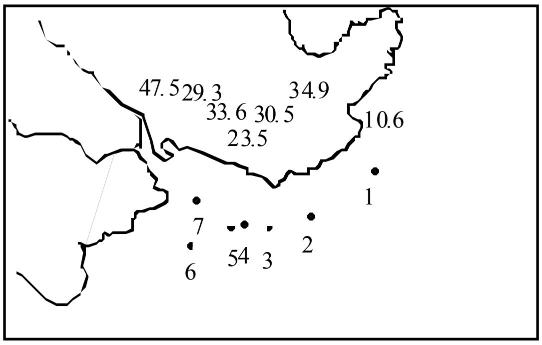

Fig. 2. Concentrations of total organo- surface sediment (μg As kg^{-1} dry sediment).

Core analysis revealed a decrease of organo-arsenicals with depth (Fig. 3). AsB, AC, and unknown species were not detected below 13.5 cm. With the sedimentation rate of 0.18 cm $year^{-1}$ obtained in this study, organo-arsenicals could almost be degraded in approximately 60 years.

However, concentrations of organo-arsenicals were less than 1% of the total arsenic concentrations measured by digestion procedure. Fe, a good coprecipitator of arsenic, has been known to be removed from a water column at the river mouth with the increase in salinity, as iron oxide-organic matter colloids ([5]). Arsenic is expected to be trapped and sedimented near the mouth of the river with iron-organic matter colloids. It should be also noted that Mukuromi Contact Metasomatic Gold Deposits exist in the upper stream of the Unosumai River. Gold has been found there along with loellingite ($FeAs_2$, [6]). Although the mine has been closed since 1943, a transportation of small particles containing arsenic may be occurring there.

Further study is needed to evaluate their contribution to total arsenic in sediment.

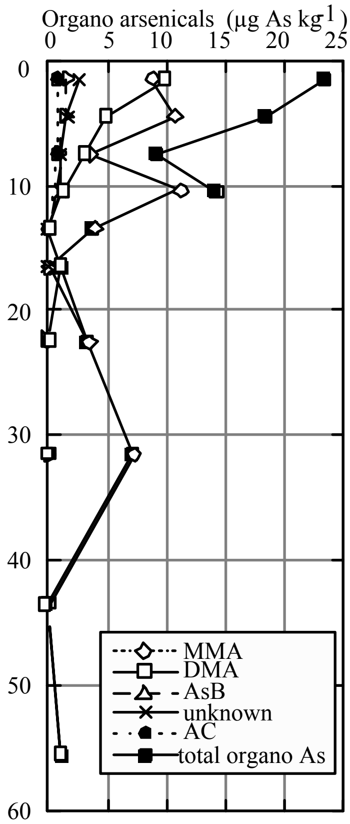

Fig. 3. Vertical profile of organo-arsenicals at St. 4 (µg As kg-1 dry sediment).

3. VOCs AND MICROORGANISMS

3.1 Background

VOCs such as PCE and TCE are widely detected in groundwater. All such contamination is due to human activity. Groundwater monitoring by the Ministry of the Environment revealed that of 4414 wells tested in 2002, TCE was detected in 125 of them (2.8%) ([1]). Of these wells, 10 (0.2%) exceeded the environmental standard of TCE (0.01 mg L^{-1}).

These VOCs are known to be degraded by various microorganisms, including both aerobic bacteria (toluene-, methane-, and ammonia-oxidizing bacteria) and anaerobic bacteria (Sulfate reducing bacteria, methanogens, *Dehalococcoides*).

In the city of Mobara, located in the south Kanto gas field, groundwater of the first aquifer (unconfined aquifer) used to be contaminated with TCE. However, the contaminant disappeared faster than in other contaminated sites (Nirei, personal communication). In this area, methane gas seeps even from the surface soil. It led us to suspect that the groundwater of this area contains high concentrations of methane and hence, methane-oxidizing bacteria (methanotrophs) capable of co-metabolizing TCE may be present. We suggested that methanotrophs in the contaminated groundwater speeded up the decrease of the contaminant. Therefore, we examined chemical and microbial characteristics of the groundwater from Mobara.

3.2 Methanotrophs in groundwater of a gas field

Chemical and microbial characteristics were compared in the groundwater from the first aquifer of Mobara and the TCE-contaminated site in the city of Abiko which is in the outside of the gas field. The maximum number of methanotrophs reached 9.9 x 10^6 MPN mL^{-1} in Mobara while it was 1.4 x 10^3 MPN mL^{-1} in Abiko. The fraction of total bacteria consisting of methanotrophs in Mobara exceeded 10% in four samples and reached 100% in two samples. The maximum dissolved methane concentration observed in Mobara water was 3.1 mM, which was more than the saturated concentration (1.6 mM, under 100% methane, atmospheric pressure, salinity=0, and 17 ^oC). The concentration of DO (0-0.8 mg L^{-1}) and ORP (-133 – +97 mV) of the first aquifer of Mobara indicated a microaerobic condition. Phosphate, which is not often detected in groundwater, was found at < 1.6 ppm in Mobara.

Table 1. Characteristics of groundwater of Mobara and Abiko. The range of values observed at four wells (n=8) is shown for Mobara ([7]).

	Mobara	Abiko
Temperature (^oC)	15.9-16.8	14.3
pH	6.48-7.97	6.14
Electric Conductivity (mS cm^{-1})	0.460-1.469	0.223
ORP (mV)	-133-+97	174
DO (mg L^{-1})	0-0.8	4.3
CH_4 (mM)	0.2-3.1	9.8 x10^{-5}
NO_3^- (ppm)	0.5-2.1	5.9
PO_4^{3-} (ppm)	ND[a]-1.6	ND
Methanotrophs (MPN mL^{-1})	1.6 x 10^3-9.9 x 10^6	1.4 x 10^3
Total bacterial number (cells mL^{-1})	2.5 x 10^5-3.0 x 10^8	3.2 x 10^5
The proportion of methanotrophs to total bacterial number (%)	0.8-100	0.4

[a] Not detected, lower detection limit; 0.05

The potential of the indigenous methanotrophs in the groundwater of Mobara and Abiko to degrade TCE was examined. Groundwater was incubated with nutrients (nitrate, phosphate, and methane) and TCE. In Mobara-groundwater, methane was consumed after 10 days (Fig. 4a). At this point, methane was re-injected to the same concentration as the initial. After the re-injection, methane was again totally consumed in six days. The TCE concentration decreased to 52% after three days of incubation as the methane was consumed and decreased to lower than the detection limit (<5 µg L^{-1}) after 16 days from the start of the incubation. In Abiko-groundwater, after 29 days of incubation, 25% of the methane decreased whereas TCE remained (Fig. 4b). Thus the groundwater of Mobara was proved to have high potential activity of methanotrophs and ability to degrade TCE.

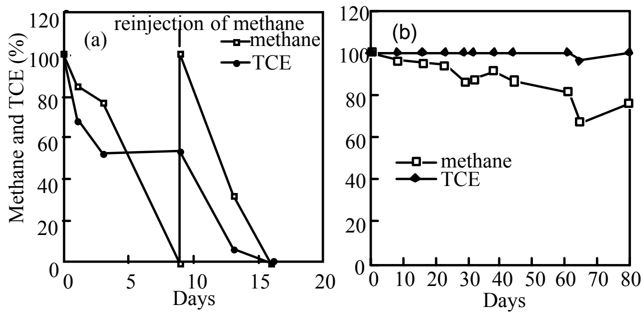

Fig. 4 Concentrations of methane (circle) and TCE (square) in groundwater of (a) Mobara and (b) Abiko incubated under initial conditions of 20% methane, 220 µg L^{-1} of TCE, 10 mM of nitrate and 4 mM of phosphate. The mean value of the

duplicates is shown.

Methanotrophs require methane, oxygen, nitrate and phosphate as major substrates. Because Mobara-groundwater contained more methane and phosphate than Abiko-groundwater, and Abiko-groundwater contained higher concentrations of oxygen and nitrate than Mobara-groundwater, an injection of Mobara-groundwater into a contaminated aquifer of Abiko would result in appropriate conditions for methanotrophs. This would further stimulate methanotrophic activity. Therefore, Mobara-groundwater was injected into the contaminated aquifer in Abiko through a pit. At the monitoring well 2 m downgradient of the pit, the concentration of TCE was 128 μg L^{-1} before the injection, and the average concentration was 86 μg L^{-1} in the period of control water injection, while it decreased to less than the detection limit (<12.5 μg L^{-1}) in the period of Mobara-groundwater injection. After the Mobara-groundwater injection, the TCE concentrations at the monitoring well remained below the detection limit for about one week and gradually increased (Fig. 5).

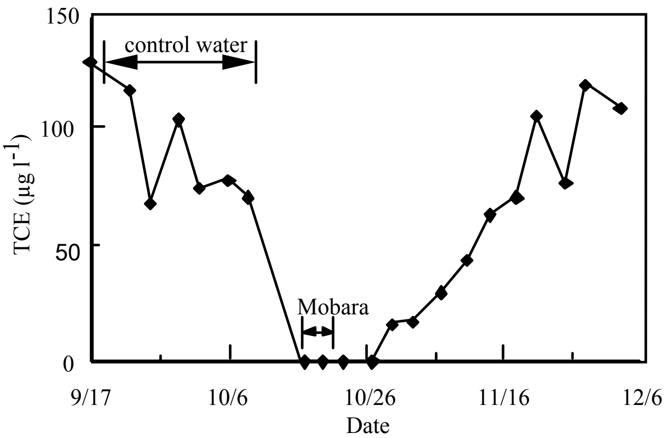

Fig. 5. Trichloroethylene concentration at monitoring well. Arrows show the period of time when control water and Mobara-groundwater were predicted to run through the monitoring well according to the calculated groundwater velocity.

Thus, methane-rich groundwater from a natural gas field area was shown to be valuable not only chemically but also microbially for use in bioremediation of a TCE-contaminated site.

This remediation technique was also evaluated at a cis-dichloroethylene (c-DCE) contaminated site in Chikura, Chiba. At this site, the second aquifer was contaminated, and the groundwater of the third aquifer was rich in methane. Therefore, the groundwater from the third aquifer was introduced into the second aquifer. As shown in Fig. 6, at the monitoring well 2 m downgradient of the injection point, we observed about 50% decrease in c-DCE concentration while only 10% decrease with the same rate of control water injection. Along with the decrease in c-DCE, the concentration of dissolved methane also dropped by one order of magnitude when the groundwater from the third aquifer was injected (Fig. 5). The methanotrophic population also increased to 2.9 x 10^4 MPN ml^{-1}. Kinetic analysis of methane uptake by bacterial populations in groundwater revealed that methanotrophs with low affinity for methane (high Km, <57,600 ppmv) have increased.

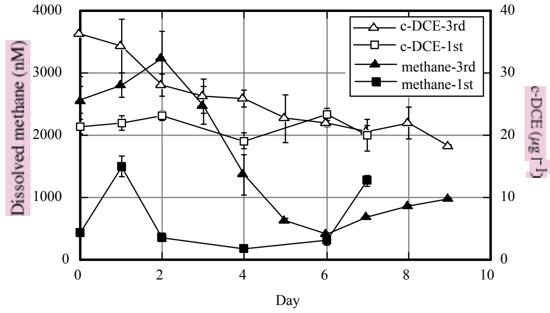

Fig. 6. cis-DCE (open mark) and dissolved methane (filled mark) concentrations in the monitoring well when groundwater from the third aquifer (triangle) or control water (square) was injected after the extraction was started. Error bars show the standard deviation of triplicates.

ACKNOWLEDGMENTS

We are grateful for the kind assistance by the staff of the Otsuchi Marine Research Center in sampling. We appreciate the cooperation of the Chikura Town Welfare Department for this study.

REFERENCES

[1] Ministry of the Environment, Japan, Groundwater quality monitoring results, 2002.

[2] K. Marumo, M. Takeuchi, T. Ebashi, and H. Nirei, Regional geochemistry of soil and sediment of Anesaki (1:50,000), Geological Survey of Japan, AIST, 2003.

[3] J. S. Edmonds and K. A. Francesconi, Arsenic in Seafoods - Human Health-Aspects and Regulations. *Mar. Poll. Bull.* **26**(12), 665-674, 1993.

[4] A. Terada, M. Takeuchi, K. Nanba, A. Takahashi, T. Kuroiwa, T. Komai, H. Nirei, Distribution of arsenic compounds in coastal marine sediment, *The Proceedings of the 13th Symposium on Geo-environments and Geo-techniques*, 529-531.

[5] E. A. Boyle, J. M. Edmond, and E. R. Sholkovitz, The mechanism of iron removal in estuaries. *Geochim. Cosmochim. Acta* **41**, 1313-1324, 1997.

[6] T. Takeuchi, M. Shimada, M. Nambu, and K. Okada, Sulfurian loellingite from the Mukuromi contact metasomatic gold deposits, Iwate Prefecture, Japan. *Bulletin of the Research Institute of Mineral Dressing and Metallurgy Tohoku University* **13**(2), 123-130, 1958.

[7] M. Takeuchi, K. Nanba, M. Yoshida, H. Nirei, and K. Furuya, Natural groundwater of a gas field utilizable for a bioremediation of trichloroethylene-contamination. *Env. Geol.* **45**, 891-898, 2004.

Mio Takeuchi
Institute for Geo-Resource and Environment,
National Institute of Advanced Industrial Science and Technology
16-1 AIST West, Onogawa,Tsukuba,Japan,305-8569
email: takeuchi-mio@aist.go.jp

Preferential Flow through Fractures in Weathered Bedrock and Slope Stability: Numerical Modeling

*Daizo Tsutsumi (1), Masaharu Fujita (1), and Roy C. Sidle (1)

(1) Disaster Prevention Research Institute, Kyoto University

ABSTRACT

Numerical experiments were conducted to assess the effect of preferential flow through pipes and cracks within weathered bedrock on slope stability, using hydrological model in which water flows within both the matrix and macropores. The hillslope consists of soil and weathered bedrock layers. Hydraulic properties were assigned to the weathered bedrock as well as the soil layer, and the regolith flow calculations were conducted within the slopes. Results demonstrated that the preferential flow pathway rapidly transported rainwater to the deeper layer of the slope, and if the outlets of the preferential flow pathway remained within the slope, the pressure head increased around these points. This increase in pressure head caused a decrease in the factor of safety at the deeper layer of the slope.

KEYWORDS: fractures, weathered bedrock, slope stability, landslide, Richards' equation, Manning's equation

1. INTRODUCTION

Many field studies have documented the existence of lateral preferential flow networks in hillslopes (e.g., [1], [2], and [3]). Water flow through preferential flow paths can contribute significantly to the rapid transfer of storm water (e.g., [4], [5], and [6]) as well as subsurface soil erosion (e.g., [7], [8], and [9]). Therefore, preferential flow is recognized as an important hydrologic and geomorphic control at the hillslope scale. Moreover, several observational studies have pointed out that the preferential flow has a close relationship to trigger mechanism of landslides ([6], [10], and [11]). Actually, some laboratory experiments and numerical simulations confirmed that clogging of the preferential flow pathway or the preferential flow network which concentrates soil water decreased stability of the slope due to rising pore water pressure ([12], [13], and [14]).

As a recent example which exhibit the relationship between the preferential flow and the slope stability, we might focus on a landslide occurred in Minamata, Southern Kyusyu, Japan, on 20 July 2003. Although antecedent 10-day rainfall was only 70 mm at Minamata prior to the disaster, moderately deep slope failure (maximum depth was 10-15 m) occurred during the highest rainfall intensity. Probable scenario of this slope failure is that pore water pressure developed at the base of weathered andesite (above tuff-breccia) due to rapid rainwater infiltration through the fractures and interstices of the weathered andesite [15].

Authors have developed a calculation method modeling the preferential flow through soil pipes or macropores developed within the soil matrix based on the hydraulic theory [14], and confirmed its applicability by simulating bench-scale experiments. In this study, numerical experiments on rainwater infiltration and subsequent stability changing process within a slope consist of soil layer and weathered bedrock layer including fractures and interstices were conducted by the calculation method. Through the numerical experiments, trigger mechanism of deep landslide reaching to the underlying weathered bedrock was considered, rather than the shallow landslide in which only soil layer failed.

2. NUMERICAL MODELING

2.1 Soil water flow considering preferential flow

Water flow within the matrix were calculated by Richards' equation,

$$C(\psi)\frac{\partial \psi}{\partial t} = \nabla \cdot \{K(\psi)[\nabla(\psi + z)]\} \tag{1}$$

where, t[sec] is time, ψ[m] is pressure potential□$C(\psi)$ [m^{-1}] is the specific soil water capacity, $K(\psi)$ [m/sec] is the hydraulic conductivity, z [m] is positive upwards.

If the matrix surrounding the preferential flow pathways (such as soil pipes of fractures) was unsaturated ($\psi < 0$), no flow within the preferential flow pathways exists. On the other hand, if the matrix surrounding the pathways was saturated ($\psi \geq 0$), the preferential flow was calculated by following equations, classified into two types (partially filled flow and fully filled flow) according to the pressure potential ψ of the surrounding matrix.

a) Partially filled flow ($\psi = 0$)

$$S_p{}'(u) = \frac{dQ_p(u)}{du} + \frac{dA_p(u)}{dt} \tag{2}$$

$$Q_p(u) = \frac{1}{n_m} R(u)^{2/3} \left(\sin\alpha(u)\right)^{1/2} A_p(u) \tag{3}$$

b) Filled flow ($\psi > 0$)

$$S_p{}'(u) = \frac{dQ_p(u)}{du} \tag{4}$$

$$Q_p(u) = \frac{1}{n_m} R^{2/3} \left(\frac{d\phi(u)}{du}\right)^{1/2} A \tag{5}$$

where, u [m] is axis indicating flow direction, $S'_p(u)$ [m^3/sec/m] is seepage rate per unit length of preferential flow pathway from surrounding matrix, $Q_p(u)$ [m^3/sec] is preferential flow rate, $A_p(u)$ [m^2] is a cross sectional area of flow within the flow pathway, A [m^2] is a cross sectional area of the flow pathway, n_m [m$^{-1/3}$s] is Manning's roughness factor, R [m] is hydraulic radius, $\alpha(u)$ [degree] is gradient of the flow pathway, and $\phi(u)$ [m] is hydraulic potential within the flow pathway. Equations (2) and (4) are the equations of continuity, and equations (3) and (5) are Manning's equations.

In the numerical calculations, equation (1) was solved by finite element method (FEM) assuming the seepage rate from the surrounding matrix to the preferential flow pathways, and resulting pressure potential distribution was used for the preferential flow type classification, calculations of the preferential flow cross sectional area and preferential flow rate by equations (2) and (3) in the case of the partially filled flow, or the preferential flow rate calculation by equation (5) in the case of the filled flow. The obtained seepage rates by equation (4) were again used for the FEM calculation, and this procedure was repeated until convergent solutions for the pressure potential distribution and the preferential flow rates were obtained.

2.2 Slope stability analysis

Two-dimensional distribution of localized factor of safety was calculated by following equation, substituting the obtained pressure potentials by the matrix water flow calculations given previously.

$$F_s = \frac{c + \left[\gamma_s \left(z_{\max} - z\right)\cos\alpha - \gamma_w \psi\right]\tan\phi_s}{\gamma_s \left(z_{\max} - z\right)\sin\alpha} \tag{6}$$

where, c[kgf/m^2] is cohesion, ϕ_s [degree] is friction angle, $z_{\max}$ [m] is depth of layer, γ_s, γ_w [kgf/m^3] are weight per unit volume of matrix and water, respectively. According to a previous study [12]□these parameters were fixed as c = 35 kgf/m^2, ϕ_s = 25°, γ_s = 2500 kgf/m^3, γ_w = 1000 kgf/ m^3.

2.3 Conditions for numerical experiments

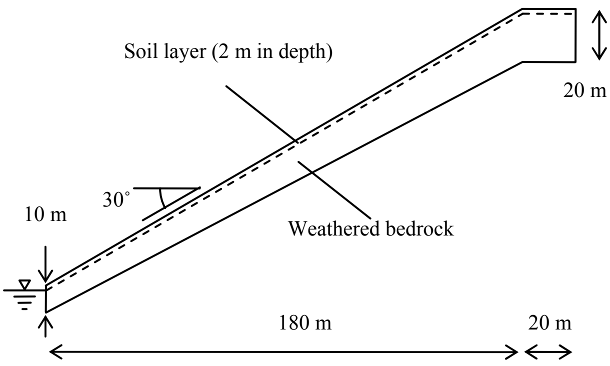

Figure 1 Side view of the assumed problem domain

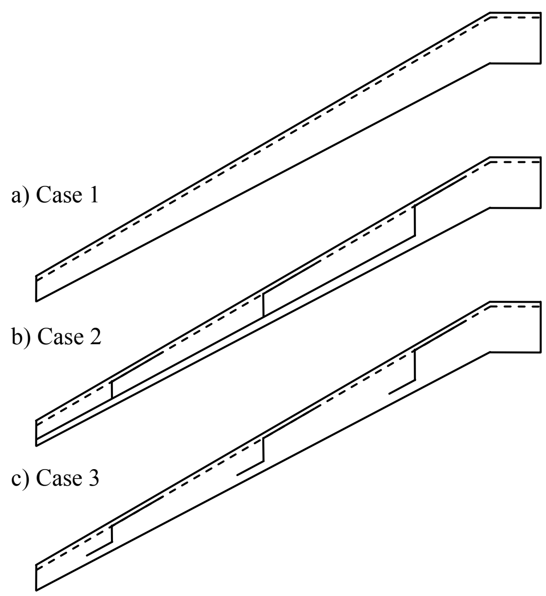

Figure 2 Assumed preferential flow pathways (Case 1: no-preferential flow pathway, Case 2: Soil Pipes and fractures opening to outside of the domain, Case 3: Soil pipes and fractures whose outlet located within the matrix)

Problem domain was assumed as 200 m in length (180 m for slope part, and 20 m for flat part), 10 to 20 m in depth (minimum at downslope end, and maximum at upslope end), 2 m in width, and 30° in slope gradient. Soil layer was assumed 2 m in depth from the surface, and weathered bedrock was underlying below it (Figure 1).

The numerical experiments were conducted for three cases of the preferential flow pathways (Cases 1, 2, and 3). In Case 1, no preferential flow pathway was assumed, that was simple matrix flow calculation (Figure 2a). In Case 2, three lateral soil pipes (diameter d = 5.0 cm) were placed at a boundary between the soil and weathered bedrock layers, and these pipes were connected to the vertical fractures whose shape was approximated to that of the soil pipes. These vertical fractures were connected to a lateral fracture near the bottom of weathered bedrock layer, whose outlet was opening to the outside of the slope at the downslope end (Figure 2b). In Case 3, same preferential flow pathways were assumed but the lateral fracture near the bottom of the weathered bedrock layer was discontinuously broken into three lateral fractures, and downstream end of those lateral fractures were remained inside of the weathered bedrock layer (Figure 2c). All preferential flow pathways were set on a vertical plane which across the center of the slope width.

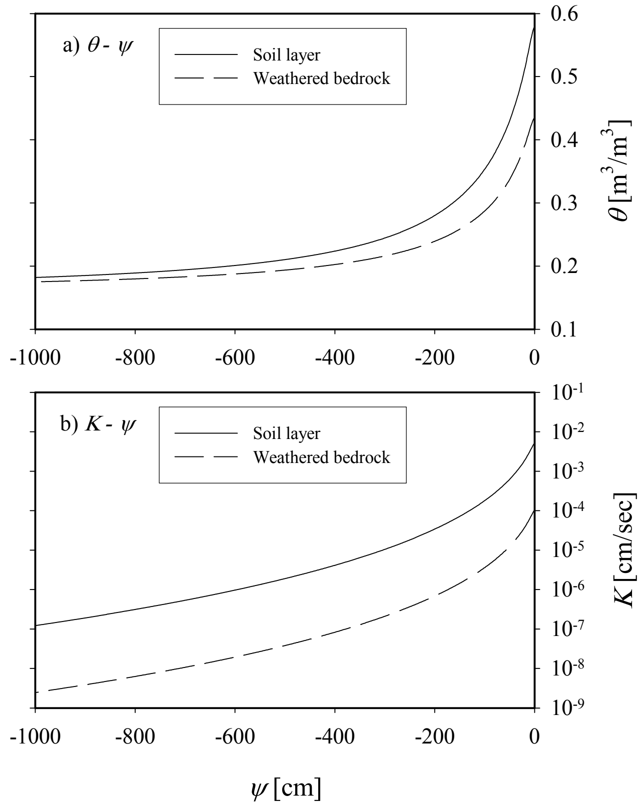

Figure 3 Assumed hydraulic properties of the soil and weathered bedrock layers (a: θ - ψ curve, b: K - ψ curve)

To represent $C(\psi)$ and $K(\psi)$, the lognormal model was employed [16]. To the soil layer, parameters for moderate sandy soil (K_s = 0.005 cm/s, θ_r = 0.162, θ_s = 0.578, ψ_m = -86.2 cm, σ = 0.639) were given. According to a recent study, it was demonstrated that water infiltrated into bedrock which had been treated to be impermeable, and general calculation method of water infiltration would be applicable especially to the weathered bedrock [17]. In the present study, parameters (K_s = 0.0001 cm/s, θ_r = 0.162, θ_s = 0.434, ψ_m = -86.2 cm, σ = 0.639) estimated by a method shown in the study [17] were given to the weathered bedrock layer, and the water flow within the composite problem domain consists of the soil and weathered bedrock layers was simulated. The hydraulic properties (θ - ψ, K - ψ relationships) of the soil and weathered bedrock layers used for the numerical calculation were shown in Figure 3.

To the surface of the soil layer, the rainfall pattern which was observed at Minamata on 20 July 2003 was applied. A constant water level was assumed at the downslope end boundary, and to the boundary above the water level seepage face condition was imposed. To other boundaries (upslope end, bottom, and sides of the problem domain), no-flux boundary condition was imposed. At the beginning of the calculation, a static pressure distribution was assumed under the water level set at the downslope end, and a linearly decreased pressure distribution along the z axis above the water level was assumed. For the numerical modeling, the problem domain was divided into 2880 finite elements, and the pressure potentials at 735 nodes were calculated.

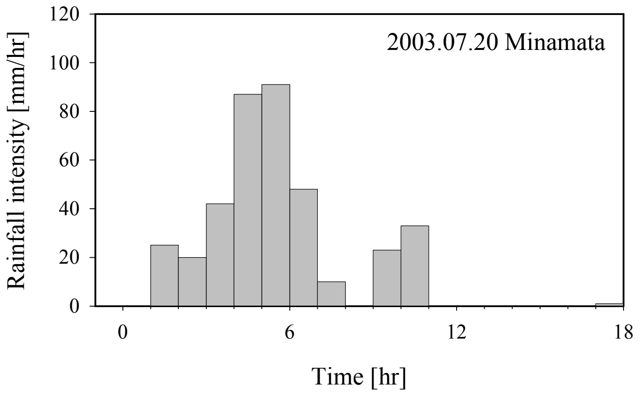

Figure 4 Rainfall pattern applied to the numerical modeling (observed at Minamata on 20 July 2003)

3. RESULTS AND DISCCUTION

3.1 Distribution of soil water pressure

Changing distributions of soil water pressure on a vertical plane which across the center of the slope width for cases 1,2, and 3 are shown in Figures 5, 6, and 7, respectively. In Figure 5 (Case 1), the soil layer through downslope end to upslope end was evenly saturated, and over-saturated area was developed at lower part of the weathered bedrock layer (x < 60 m). In Figure 6 (Case 2), the saturated area were heterogeneously distributed within the soil layer, and unsaturated part still existed in spite of peak rainfall intensity at t = 6.0 hr. The development of over-saturated area in the weathered bedrock layer was restricted by drainage effect of preferential flow through the pipes and fractures. In Figure 7 (Case 3), the saturated area were heterogeneously distributed within the soil layer similar to Case 2, but the over-saturated area was developed at lower part of the weathered bedrock layer similar to Case 1. Mid-slope part (70 < x < 90 m) in the weathered bedrock layer was also over-saturated. This over-saturation in Case 3 was closely related to the location of the outlets of the preferential flow pathways.

3.2 Distribution of factor of safety

Distributions of the factor of safety F_s on a vertical plane across the center of the slope width, at 3 hr after the highest rainfall intensity (t = 9.0 hr) are shown in Figure 8. In Figure 8a (Case 1), corresponding to the distribution of pressure potential shown in Figure 5, small F_s distributed in lower part of the weathered bedrock layer, as well as the entire surface soil layer. This distribution of small F_s indicates that not only the deeper weathered bedrock layer, but also the shallower surface soil layer are exposed to landslide hazards. In Figure 8b (Case 2), the small F_s distributed to the limited area at the bottom of the weathered bedrock layer and some parts of the surface soil layer. This indicated that the slope was comparatively stable. In Figure 8c (Case 3), the small F_s distributed to larger area in the weathered bedrock and some part of the surface soil layer. Around the outlets of the preferential flow pathways (x = 20, 80 m), F_s was obviously small, especially it was smaller than 0.6 (smallest of all cases) at lower part of the weathered bedrock (10 < x < 20 m).

3.3 Comparison of total discharge

Total discharge rates (= drainage from downslope end boundary + surface flow + preferential flow discharge) divided by surface area of the slope for cases 1, 2, and 3 are shown in Figure 9. In addition to these three cases, a numerical simulation for a case that the bedrock was regarded as an impermeable layer (water flow

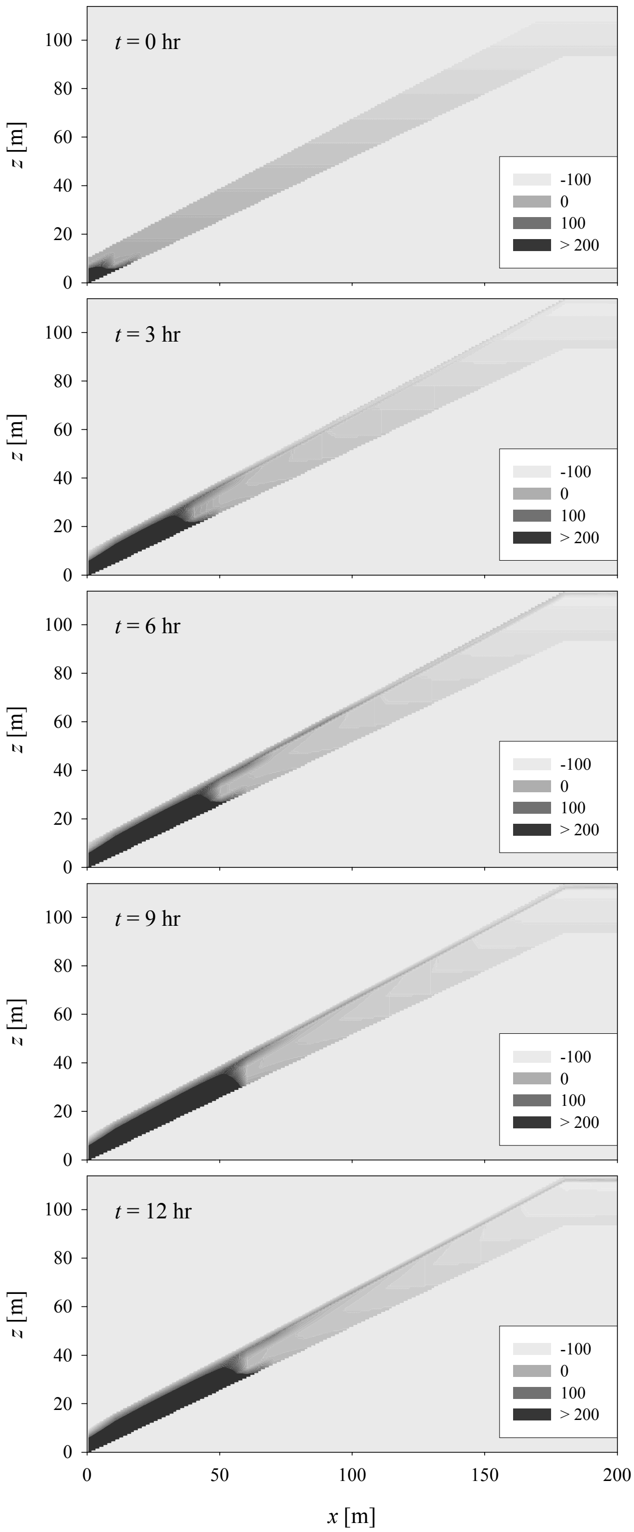

Figure 5 Changing distribution of pressure potential ψ [cmH_2O] on a vertical plane across the center of the slope width for Case 1.

calculation only in soil layer) was conducted, and the result of total discharge rate is also shown in Figure 9. From the comparison between Case 1 and the case of soil layer calculation, total flow rate of Case 1 was smaller than that of the case of soil layer calculation during high rainfall intensity. This indicates that the difference between these flow rates was retained within the weathered bedrock layer. During no rainfall periods, the total discharge rates of these two cases were almost identical. The total discharge rate of Case 2 quickly replied to the initial rainfall, and its peak was smaller than those of the previous two cases. During no rainfall periods, the total

Figure 6 Changing distribution of pressure potential ψ [cmH_2O] on a vertical plane across the center of the slope width for Case 2.

discharge rate of Case 2 was maintained higher than those of the previous two cases. The total discharge rate of Case 3 showed intermediate tendency between Cases 1 and 2. These results indicated that the weathered bedrock layer has a capability in retaining the infiltrated water, and the preferential flow pathways within the weathered bedrock layer have an effect averaging the hydrographs.

4. CONCLUSION

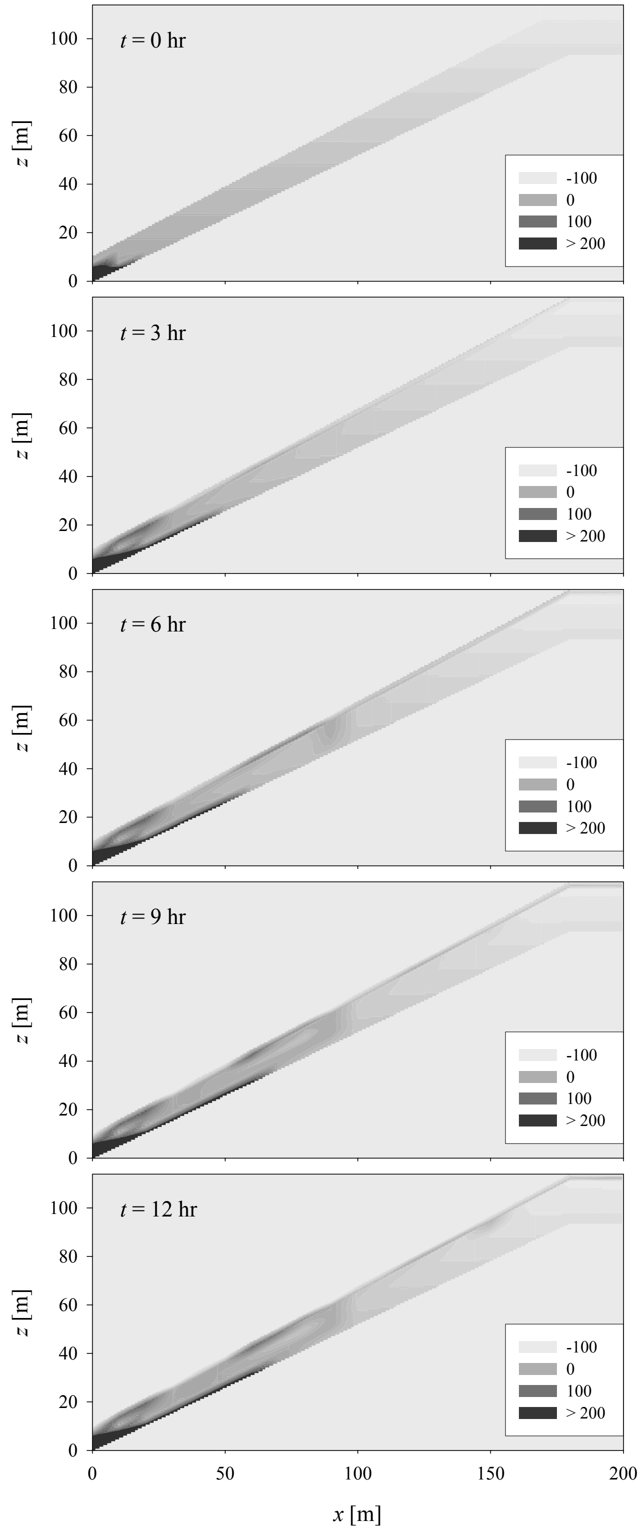

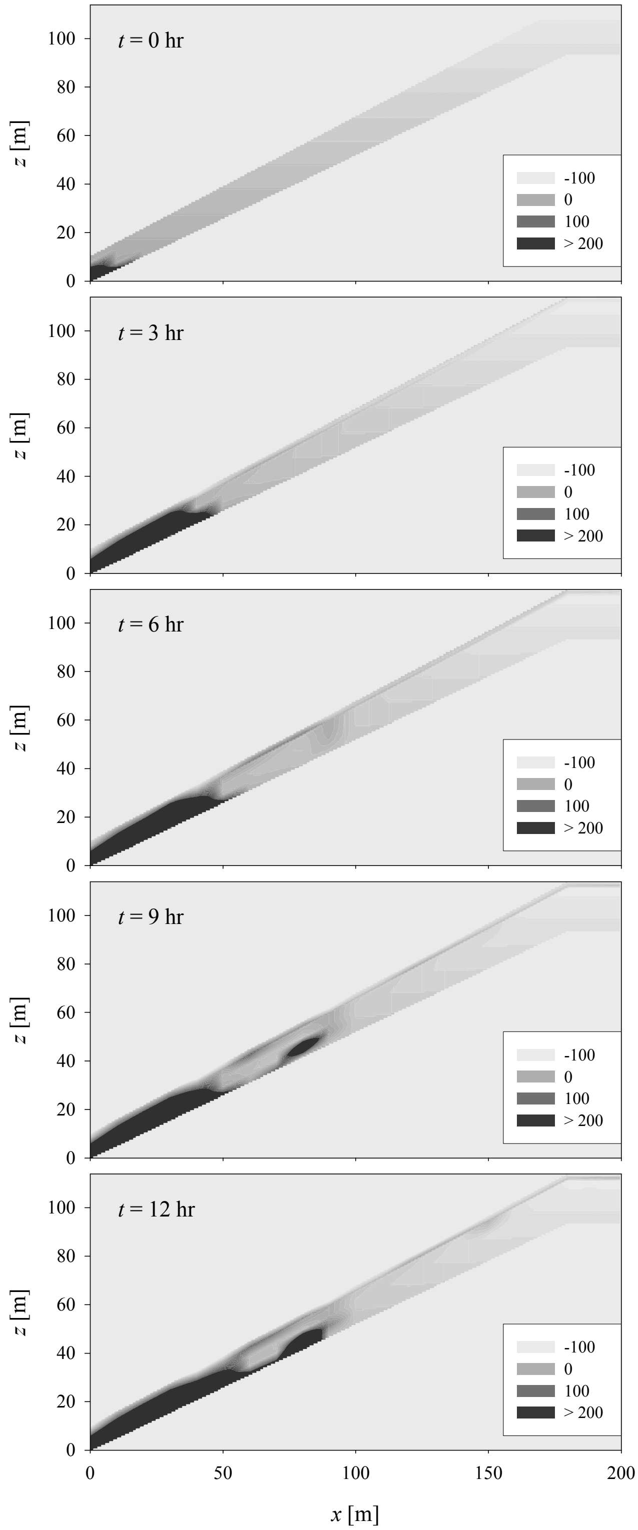

Figure 7 Changing distribution of pressure potential ψ [cmH_2O] on a vertical plane across the center of the slope width for Case 3.

From the results of the numerical experiments in this study, several relationships between the preferential flow, slope stability, and runoff process was suggested; (1) in the case that preferential flow pathways opening to outside of a slope, the drainage effect of preferential flow restricts increase in pressure potential and keeps the slope stable, (2) in the case that outlets of preferential flow pathways located within a slope, infiltrated rainwater quickly flows down to deeper layer of the slope, increases pressure potential, and makes the slope instable, (3) rainwater infiltrates and is retained within weathered bedrocks, (4) preferential flow has an effect averaging the hydrographs.

Several probable trigger mechanisms of landslides suggested from the numerical experiments are; (1) rainwater infiltrates into the weathered bedrock layer without preferential flow pathways, and makes the lower part of the slope instable, (2) rainwater quickly flows down through the vertical preferential flow pathways within the bedrock layer, and makes parts around the outlet of the preferential flow pathways quite instable, (3) due to high rainfall intensity, eroded soils within the subsurface soil layer flow into the preferential flow pathways together with the rainwater, clog the pathways at the bottom part, and this leads to the pressure potential increase and instability of the slope.

Although effect of preferential flow on the timing of the landslide occurrence was not clarified in this paper, additional numerical experiments (results were not shown) indicated that the timing of slope instability became delay or forward according to size of the preferential flow pathways. This suggested that the preferential flow within the weathered bedrock might account for the landslide occurrence during the highest rainfall intensity.

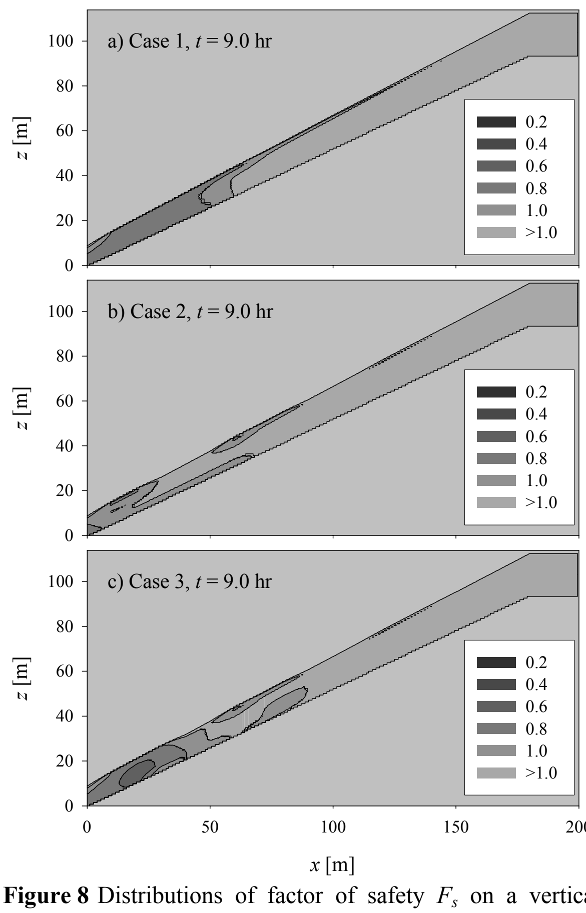

Figure 8 Distributions of factor of safety F_s on a vertical plane across the center of the slope width, at t = 9.0 hr.

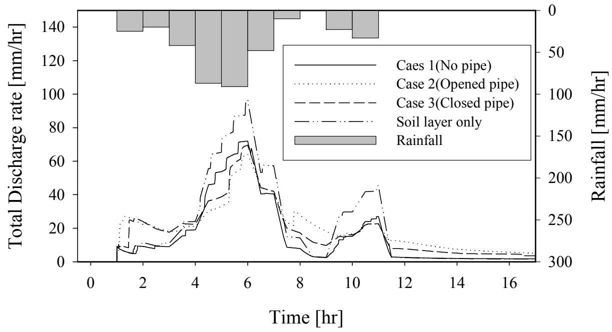

Figure 9 Hydrographs for three cases (Case 1, 2, and 3) with a case in which weathered bedrock was regarded as an impermeable layer.

REFERENCES

[1] Y. Tsuboyama, R. C. Sidle, S. Noguchi, and I. Hosoda, Flow and solute transport through the soil matrix and macropores of a hillslope segment, *Water Res. Res.*, 30, pp. 879-890, 1994.

[2] R. C. Sidle, S. Noguchi, Y. Tsuboyama, and K. Laursen, A conceptual model of preferential flow system in forested hillslopes: evidence of self-organization, *Hydrological Processes*, 15, pp. 1675-1692, 2001.

[3] J. Holden and T. P. Burt, Piping and pipeflow in a deep peat catchment, *Catena*, 48, pp. 163-199, 2002.

[4] M. P. Mosely, Subsurface flow velocities through selected forest soils, South Island, New Zealand, *J. Hydrology*, 55, pp. 65-92, 1982.

[5] R. C. Sidle, Y. Tsuboyama, S. Noguchi, I. Hosoda, M. Fujieda, and T. Shimizu, Seasonal hydrologic response at various spatial scales in a small forested catchment, Hitachi Ohta, Japan, *J. Hydrology*, 168, pp. 227-250, 1995.

[6] R. C. Sidle, Y. Tsuboyama, S. Noguchi, I. Hosoda, M. Fujieda, and T. Shimizu, Stormflow generation in steep forested headwaters: a linked hydrogeomorphic paradigm, *Hydrological Processes*, 14, pp. 369-385, 2000.

[7] Y. Onda, Seepage erosion and its implication to the formation of amphitheatre valley head: a case study at Obara, Japan, *Earth Surf. Processes and Landforms*, 19, pp. 627-640, 1994.

[8] R. B. Bryan and J. A. A. Jones, The significance of soil piping process: inventory and prospect, *Geomorphology*, 20, pp. 209-218, 1997.

[9] T. Terajima, T. Sakamoto, Y. Nakai, and K. Kitamura, Suspended Sediment discharge in subsurface flow from the head hollow of a small forested watershed, northern Japan, *Earth Surf. Processes and Landforms*, 22, pp. 987-1000, 1997.

[10] T. C. Pierson, Soil pipes and slope stability, *Quaternary J. Eng. Geology*, 16, pp. 1-11, 1983.

[11] T. Ohta, Y. Tsukamoto, and H. Noguchi, A consideration of relationship between pipeflow and landslide, *Proceedings of Ann. Meeting of Japan Soc. Erosion Control Eng.*, pp. 92-93, 1981. [In Japanese. The title is tentative translation from the original Japanese title by the authors of this paper.]

[12] T. Uchida and T. Mizuyama, Effects of pipeflow on the changes in safety factor in slopes: A numerical modeling approach, *J. Japan Soc. Erosion Control Eng.*, 55(2), pp. 14-23, 2002.

[13] Y. Tada, T. Okumura, and T Kubota, Examination of the influence of soil pipes on slope failure, *J. Japan Soc. Erosion Control Eng.*, 55(3), pp. 12-20, 2002.

[14] D. Tsutsumi, R. C. Sidle, M. Fujita, and T. Mizuyama, Numerical experiments to assess the influence of pipeflow on slope stability, *Ann. J. Hydr. Eng. JSCE*, 48, pp.337-342, 2004.

[15] R. C. Sidle and M. Chigira, Landslides and debris flows strike Kyushu, Japan, *EOS trans. AGU*, 85 (15), pp. 145, 151, 2004.

[16] K. Kosugi, Lognormal distribution model for unsaturated soil hydraulic properties, *Water Res. Res.*, 32, pp. 2697-2703, 1996.

[17] S. Katsura, K. Kosugi, N. Yamamoto, and T. Mizuyama,

Investigation of water infiltration processes within weathered granite layer, *Proceedings of Ann. meeting of Japan Soc. Erosion Control Eng.*, pp. 478-479, 2004. [In Japanese. The title is tentative translation from the original Japanese title by the authors of this paper.]

Daizo Tsutsumi
Disaster Prevention Research Institute, Kyoto University,
Gokasyo, Uji, Kyoto, 611-0011 JAPAN,
email: tsutsumi@sabom.dpri.kyoto-u.ac.jp